



THE HONG KONG
POLYTECHNIC UNIVERSITY

香港理工大學

Pao Yue-kong Library

包玉剛圖書館

Copyright Undertaking

This thesis is protected by copyright, with all rights reserved.

By reading and using the thesis, the reader understands and agrees to the following terms:

1. The reader will abide by the rules and legal ordinances governing copyright regarding the use of the thesis.
2. The reader will use the thesis for the purpose of research or private study only and not for distribution or further reproduction or any other purpose.
3. The reader agrees to indemnify and hold the University harmless from and against any loss, damage, cost, liability or expenses arising from copyright infringement or unauthorized usage.

IMPORTANT

If you have reasons to believe that any materials in this thesis are deemed not suitable to be distributed in this form, or a copyright owner having difficulty with the material being included in our database, please contact lbsys@polyu.edu.hk providing details. The Library will look into your claim and consider taking remedial action upon receipt of the written requests.

Pao Yue-kong Library, The Hong Kong Polytechnic University, Hung Hom, Kowloon, Hong Kong

<http://www.lib.polyu.edu.hk>

THE HONG KONG POLYTECHNIC UNIVERSITY
INSTITUTE OF TEXTILES AND CLOTHING

**STUDIES OF FUNCTIONAL
SHAPE MEMORY FIBERS**

MENG Qinghao

A Thesis Submitted
in Partial Fulfillment of the Requirements
for the degree of Doctor of Philosophy

May 2010

CERTIFICATE OF ORIGINALITY

I hereby declare that the thesis entitled “**Studies of Functional Shape Memory Fibers**” which is submitted to The Hong Kong Polytechnic University, Hong Kong for the award of Doctor of Philosophy is my own work and that, to the best of my knowledge and belief, it reproduces no material previously published or written, except where due acknowledgement has been made in the text. The matter embodied in this dissertation has not been submitted for the award of any other degree or diploma.

_____ (Signature)

Meng Qinghao _____ (Name of student)

ABSTRACT

Shape memory polymers (SMPs) can rapidly change their shapes from a temporary shape to the original (or permanent) shape under appropriate thermal stimulation. They have been widely used in the forms of solution, emulsion, film, bulk and foam. Recently, shape memory fibers (SMFs) prepared by different spinning methods were developed and studied. This project is intended to study the SMFs with novel functions, i.e., SMFs with thermal-responsive inner diameters, SMFs with temperature-regulating effect, SMFs with electro-active effect and SMFs with potential biological applications.

In this project, first, a T_m type shape memory polyurethane (SMPU) was synthesized and corresponding SMFs were fabricated. The switching transition temperature of the SMF was the soft segment phase melting temperature at 47°C. The mechanical properties, shape memory effect, and thermal properties of the SMF were studied. The partially crystallized soft segment phase provided the SMF with partial elasticity at ambient temperature and the ability to fix the temporary shape once the fiber was cooled to ambient temperature. The SMF could recover its original length by reheating the fiber to a temperature above 47°C. The SMF had a tenacity of about 1.0 cN/dtex, and strain at break 562~660%. The shape fixity ratio reached 84% and the recovery ratio was up to 95%.

The influences of heat treatments on the SMF properties were studied. Low temperature heat treatment increased breaking elongation and shape fixity ratios, while decreased boiling water shrinkage, tenacity and shape recovery ratios. High temperature heat treatment benefited the improvement of hard segment

phase stability. High temperature heat treatment increased both the shape recovery ratios and fixity ratios. The SMF was expected to be treated at a high temperature. Unfortunately, the heat treatment at a very temperature could not be conducted because the SMF became too tacky and soft due to the melting of the soft segment phase.

Shape memory hollow fibers could have special properties in comparison with cylindrical SMFs and could have many special applications. A shape memory hollow fiber with the thermal-responsive inner diameter was fabricated and the properties of the hollow fiber were studied. The hollow fiber had a switching temperature 41°C, a tenacity of about 1.14 cN/dtex, and strain at break 682%. The shape fixity ratio of the shape memory hollow fiber was above 80% and the recovery ratio above 90%. The inner diameter of the hollow fiber could be noticeably changed; and after being heated above the soft segment phase melting temperature, the hollow fiber inner cavity could recover its original diameter.

By employing poly(ethylene glycol) (PEG) as the soft segment of the SMF, a temperature-regulating fiber with shape memory effect was prepared. The PEG-based polyurethane fibers showed temperature-regulating effect and shape memory effect simultaneously. The fiber's phase change behaviors and crystalline morphology were investigated using polarizing optical microscopy (POM) and differential scanning calorimetry (DSC). The prepared fiber had a tenacity of 0.7 cN/dtex, breaking elongation 488%, latent heat storage about 100 J/g, shape fixity ratio more than 85.8%, and shape fixity ratio above 95.4%. Presently, the degree of supercooling of the PEG-based SMF was still too high

and the mechanical properties of the fiber were not satisfied. Furthermore, due to the significant melt transition at the low temperature, the fiber did not have good spinnability.

Usually the shape memory effect is induced by directly heating the SMP to a temperature above the switching temperature. Electro-responsive shape memory effect of the SMFs may be achieved by Joule heating if the SMF is filled with conductive CNTs. To obtain electro-active shape memory effect by Joule heating, multiwalled carbon nanotubes (MWCNTs) were incorporated into SMFs by in-situ polymerization. Electro-responsive shape memory effect was observed on the SMFs. It was also found that the MWCNTs improved the recovery stress of SMFs markedly because of the interaction between the MWCNTs and SMPU, especially with the hard segments.

The medical applications of the SMF for responsive medical devices are of great interests due to its combination of tailor-able transition temperatures, large deformation, high recoverability, and elastic properties. A T_g type SMF with the switching transition at around body temperature was fabricated. The T_g type SMF was used because of the easy adjustment of glass transition temperature (switching temperature) by varying the soft segment length and content. The biological properties of the SMF were evaluated in terms of cytotoxicity, haemolysis, sensitization and dermal irritant. Based on the test results, the shape memory fiber/fabric was not considered cytotoxic, haemolytic, sensitive and irritant.

PUBLICATIONS

PATENTS

1. Hu, J. L., Meng, Q. H., Zhu Y., Lv, J. & Zhuo, H. T., Shape Memory Fibers Prepared via Wet, Reaction, Dry, Melt and Electro Spinning, US Patent, Application No.: 11/907,012, Publication No. US-2009-2293606-A, Publication Date: 04/09/2009. Entering the second country P. R. China and India on Oct. 09, 2008.
2. Hu, J. L., Meng, Q. H., Zhu, Y., Lv, J. & Zhuo, H. T., Methods for Preparing Shape Memory Polyurethanes for Textile Products, US provisional patent application No.: 61/163,483.
3. Hu, J. L. & Meng, Q. H., A Temperature-regulating Fiber and the Method of Making Thereof, US provisional patent, application No.: 61/142,271.
4. Hu, J. L., Han, J. P., Lv, J., Meng, Q. H., Zhu, Y., Liu, Y. & Lin, Q. M., Shape Memory Garments and Accessories, US Patent, submitted.
5. Hu, J. L., Nie, K. M., Meng, Q. H., & Zheng, G. H., Multifunction Finishing Liquids Containing Dendrimers and the Application of the Liquids in Textile Finishing, US Patent Application No. 11/748,892.

REFERRED JOURNAL PAPERS

1. Meng, H. & Hu, J. L., A Review of Light, Electro and Magnetic-active Polymeric Materials on Smart Textiles Applications. Smart Materials and Structures, 2010, Submitted.
2. Meng, Q. H. & Hu, J. L., A Brief Review of Stimulus-active Polymers Responsive to Thermal, Light, Magnetic, Electric, and Water/solvent

-
- Stimuli, *Journal of Intelligent Material Systems and Structures*, 2010, 21, 859-885.
3. Hu, J., Meng, Q. H., Zhu, Y., Liu, Y., Lv, J., Ji, F. L. & Liu, B. et. al., A Review of Stimuli-responsive Polymers for Smart Textile Applications, *Carbohydrate Polymers*, 2010, In press.
 4. Meng, Q. H. & Hu, J. L., A Review of Shape Memory Polymer Composites and Blends, *Composites Part A*. 2009, 40, 1661-1672.
 5. Meng, Q. H., Hu, J. L. & Zhu, Y., Study of the PCL Based Shape Memory Segmented Polyurethane Fiber, *Journal of Applied Polymer Science*. 2007, 106, 2515-2523.
 6. Meng, Q. H. & Hu, J.L., The Influence of Heat Treatment on Properties of Shape Memory Fibers: I. Crystallinity, Hydrogen Bonding and Shape Memory Effect, *Journal of Applied Polymer Science*. 2008, 109, 2616-2623.
 7. Meng, Q. H., Hu, J. L. & Yeung, L., The Influence of Heat Treatment on the Properties of Shape Memory Fibers. II. Tensile Properties, Dimensional stability, Recovery Force Relaxation, and Thermomechanical Cyclic Properties, *Journal of Applied Polymer Science*. 2008, 111, 1156-1164.
 8. Meng, Q. H. & Hu, J. L., Self-organizing Alignment of Carbon Nanotube in Shape Memory Segmented Fiber Prepared by *in-situ* Polymerization and Melt Spinning, *Composites Part A*. 2008, 39, 314-321.
 9. Meng, Q. H. & Hu, J. L., Study on Poly(ϵ -caprolactone)-based Shape Memory Copolymer Fiber Prepared by Bulk Polymerization and Melt Spinning, *Polymers for Advanced Technologies*. 2008, 19, 131-136.

10. Meng, Q. H., Hu, J. L. & Yeung, L. Y., An Electro-active Shape Memory Fibre by Incorporating Multi-walled Carbon Nanotubes, *Smart Materials and Structures*. 2007, 16, 830-836.
11. Meng, Q. H, Hu, J.L., Shen, L., Hu, Y. & Han, J., A Smart Hollow Filament with Thermal Sensitive Internal Diameter, *Journal of Applied Polymer Science*. 2009, 113, 2440-2449.
12. Meng, Q. H. & Hu, J. L., A Temperature-regulating Fiber Made of PEG-Based Smart Copolymer, *Solar Energy Materials and Solar Cells*. 2008, 9, 1245-1252.
13. Meng, Q. H., Hu, J. L., Zhu, Y., Lv, J. & Liu, B. H., Biological Evaluations of a Smart Shape Memory Fabric, *Textile Research Journal*, 2009, 76, 1522-1533.
14. Meng, Q. H., Hu, J. L., Ho, K. C., Ji, F. L. & Chen S. J., The Shape Memory Properties of Biodegradable Chitosan/poly (L-lactide) Composites, *Journal of Polymers and the Environment*. 2009, 17, 212-214.

CONFERENCE PAPER

1. Meng, Q. H. & Hu, J. L., Study on Multiwalled Carbon Nanotube/Shape Memory Polyurethane Film, The 86th Textile Institute World Conference, 18-21 November 2008, Hong Kong.

BOOK CHAPTERs

1. Hu, J. L., and Meng, Q. H., Chapter 7: *Functional Shape Memory Textiles* in *Functional Textiles for Improved Performance Protection and Health* (edited by Prof. G. Sun), To be published by Woodhead Publishing.

2. Hu, J. L., and Meng, Q. H., Chapter 6: *Adaptive Polymeric Composites in Adaptive and Functional Polymers, Textiles and their Applications* (edited by Prof. J. Hu), Imperial College Press, ISBN-10: 1848164750, ISBN-13: 978-1848164758, Pub. date: Scheduled Fall 2010.
3. Hu, J. L., and Meng, Q. H., Section 10.1: *Structure, synthesis, property and applications of dendrimer macromolecules* in *Adaptive and Functional Polymers, Textiles and their Applications* (edited by Prof. J. Hu), Imperial College Press, ISBN-10: 1848164750, ISBN-13: 978-1848164758, Pub. date: Scheduled Fall 2010.
4. Hu, J. L., and Meng, Q. H., Section 10.2: *Structure, synthesis, property and applications of hyperbranched macromolecules* in *Adaptive and Functional Polymers* (edited by Prof. J. Hu), *Textiles and their Applications*, Imperial College Press, ISBN-10: 1848164750, ISBN-13: 978-1848164758, Pub. date: Scheduled Fall 2010.

ACKNOWLEDGEMENT

I am greatly indebted to my supervisor Professor Jinlian Hu, Professor of the Institute of Textiles and Clothing, The Hong Kong Polytechnic University. Without her help, support, guidance and valuable suggestions, it is impossible to join this interesting project and finish the doctoral dissertation. Working under her supervision has been a rich experience and will always be a pleasant memory. I appreciate her encouragement, support, direction, inspiration, enlightening guidance and kindness.

I would like to acknowledge the labmates that worked in Prof. Hu's group with me in the past several years. Special thanks to Dr. Yong Zhu, Dr. Jing Lv, Ms. Yan Liu, Mr. Kenneth Yeung, Mr. Fenglong Ji, and Mr. Yijun Liu for their unconditional help. I also want to extend my warmest thanks to Mr. Yang Hu, Mr. Jianping Han and Mr. Wenguo Li for their valuable assistance. I will cherish the academic benefit and faithful friendship forever.

I would like to thank my parents for their strong supports which lead me to finish all my degrees. They have lost a lot for my educations.

TABLE OF CONTENTS

ABSTRACT	I
PUBLICATIONS	IV
ACKNOWLEDGEMENT	VIII
TABLE OF CONTENTS	IX
LIST OF ABBREVIATIONS	XIV
LIST OF FIGURES	XIX
LIST OF TABLES	XXIV
CHAPTER 1 INTRODUCTION.....	1
1.1 Introduction of shape memory materials	1
1.2 Mechanism of shape memory effect.....	3
1.2.1 Shape memory polymers	3
1.2.2 Shape memory metals.....	5
1.3 Shape memory materials for smart textile applications	6
1.3.1 Breathable films.....	7
1.3.2 Shape memory foams	8
1.3.3 Shape memory finishing.....	9
1.3.4 Shape memory metallic wires	15
1.4 Objectives of the project.....	18
1.4.1 To study general shape memory fibers (SMFs)	18
1.4.2 To study SMFs with thermal-responsive inner diameters.....	19
1.4.3 To study SMFs with temperature-regulating effect.....	19
1.4.4 To study SMFs with electro-responsive effect.....	20
1.4.5 To study SMFs for potential biological applications	20
1.5 Significance of the project.....	21
1.6 Outline of the thesis.....	22
CHAPTER 2 LITERATURE REVIEW.....	25
2.1 Shape memory polymers of different types.....	25
2.2 Shape memory polyurethanes (SMPUs)	32
2.3 SMPUs in film forms.....	33
2.4 Phase change materials based on SMPUs	34
2.5 Multiwalled CNT (MWCNT)/SMPU composites.....	36
2.6 Biomedical applications of SMPUs.....	38

CHAPTER 3 EXPERIMENTAL	41
3.1 Material and equipment.....	41
3.2 Preparation of T_m type SMFs	44
3.2.1 Synthesis of T_m type SMPUs.....	44
3.2.2 Preparation of SMFs.....	45
3.2.3 Heat treatments	45
3.3 Preparation of T_m type SMPU hollow fibers.....	46
3.3.1 Synthesis of T_m type SMPUs.....	46
3.3.2 Preparation of SMPU hollow fibers	46
3.4 Preparation of temperature-regulating SMFs	47
3.4.1 Synthesis of temperature-regulating SMPUs	47
3.4.2 Preparation of temperature-regulating SMFs	48
3.5 Preparation of MWCNT/SMPU fibers.....	48
3.5.1 Modification of MWCNTs	48
3.5.2 Synthesis of MWCNT/SMPU composites	49
3.5.3 Preparation of MWCNT/SMPU fibers.....	50
3.6 Preparation of SMFs for biological evaluation	50
3.6.1 Synthesis of T_g type SMPUs	50
3.6.2 Preparation of T_g type SMFs	50
3.6.3 Fabrication of shape memory fabrics	51
3.7 Preparation of SMPU films	51
3.8 Characterization techniques.....	51
3.8.1 Molecular weight test	51
3.8.2 FTIR spectrometry.....	52
3.8.3 Melt flow index	52
3.8.4 Capillary rheological measurement.....	53
3.8.5 Mechanical property test	53
3.8.6 Thermomechanical cyclic tensile test.....	53
3.8.7 Shape memory effect test of SMFs	57
3.8.8 Shape memory effect test of shape memory fabrics.....	57
3.8.9 Stress relaxation test	59
3.8.10 Shape recovery stress test.....	60
3.8.11 Thermal-responsive inner diameter test	60
3.8.12 Differential scanning calorimetry	61

3.8.13 Wide angle X-ray diffraction test	62
3.8.14 Dynamic mechanical analysis	62
3.8.15 Atomic force microscopy	62
3.8.16 Polarizing optical microscopy	63
3.8.17 Scanning electron microscopy.....	63
3.8.18 Small angle x-ray scattering	63
3.8.19 FTIR dichroism	64
3.9 Biological evaluations of SMFs	65
3.9.1 Cytotoxicity test.....	65
3.7.2 Haemolysis test.....	66
3.9.3 Sensitization test.....	67
3.9.4 Dermal irritant test.....	67
CHAPTER 4 STUDIES OF GENERAL SMFs	69
4.1 FTIR analysis.....	69
4.2 Shape recovery of SMP rods	72
4.3 Capillary rheological properties	74
4.4 Morphology of SMFs	78
4.5 Mechanical properties	80
4.6 Shape memory properties	81
4.7 Thermal properties.....	85
4.8 Summary.....	87
CHAPTER 5 STUDIES OF THE HEAT TREATMENT OF SMFs	88
5.1 Thermal properties.....	88
5.2 Dynamic mechanical properties	90
5.3 Crystalline structures	91
5.4 Hydrogen bonding analysis	96
5.5 Tenacity	98
5.6 Breaking elongation.....	99
5.7 Boiling water shrinkage.....	100
5.8 Stress relaxation.....	102
5.9 Shape memory properties	103
5.10 Mechanism of the heat treatment	106
5.11 Summary.....	108

CHAPTER 6 SMFs WITH THERMAL-RESPONSIVE INNER DIAMETERS	110
6.1 Mechanical properties	110
6.2 Thermal properties	112
6.3 Crystalline structures	114
6.4 Shape memory properties	116
6.5 Thermally-tunable inner diameter	118
6.6 Summary	120
CHAPTER 7 SMFs WITH TEMPERATURE-REGULATING EFFECTS	122
7.1 Mechanical properties	122
7.2 Crystalline structures	124
7.3 Thermal properties	125
7.4 Shape memory properties	128
7.5 Microstructures	129
7.6 Summary	131
CHAPTER 8 SMFs WITH ELECTRO-ACTIVE EFFECT	133
8.1 Spinnability	133
8.2 Micromorphology	135
8.4 Stress storage properties	142
8.5 Shape recovery stress	144
8.6 Summary	146
CHAPTER 9 SMFs FOR BIOLOGICAL APPLICATIONS	147
9.1 Morphology	148
9.2 Thermal properties	149
9.3 Molecular orientation	150
9.4 Dynamic mechanical properties	154
9.5 Mechanical properties	155
9.6 Shape memory properties	157
9.7 Cytotoxicity	161
9.8 Haemolysis	163
9.9 Sensitization	164
9.10 Dermal irritation	166
9.11 Summary	168

CHAPTER 10 CONCLUSIONS AND SUGGESTIONS FOR FUTURE WORK 170

10.1 Conclusions 170

 10.1.1 Studies of general SMFs..... 170

 10.1.2 Studies of the heat treatment of SMFs 170

 10.1.3 Studies of SMFs with thermal-responsive inner diameters 171

 10.1.4 Studies of SMFs with temperature-regulating effects 172

 10.1.5 Studies of SMFs with electro-active effect 172

 10.1.6 Studies of SMFs for biomedical applications..... 173

10.2 Suggestions for future work 174

 10.2.1 Large scale production 174

 10.2.2 Two-way SMFs 175

 10.2.3 Multi-stimuli-responsive SMFs..... 176

 10.2.4 Medical applications..... 178

LIST OF ABBREVIATIONS

AFM	Atomic force microscopy
BDO	1,4-butanediol
CDA	Cellulose diacetate
CNT	Carbon nanotube
DMA	Dynamic mechanical analysis
DMAc	N,N-dimethylacetamide
DMF	N,N-dimethylformamide
DMPA	Dimethylolpropionic acid
DSC	Differential scanning calorimetry
EG	Ethylene glycol
FTIR	Fourier transform infrared spectroscopy
FWHM	Full width at half maximum
HPLC	High performance liquid chromatography
IPDI	Isophorone diisocyanate
IPN	Interpenetrating polymer network
LCST	Lower critical solution temperature
MDI	4,4-diphenylmethane diisocyanate
MEKO	Methyl ethyl ketoxime
MFI	Melt flow index
MWCNT	Multiwalled carbon nanotube
PBA	Poly(butylene adipate) diol
PCL	Poly(ϵ -caprolactone)
PCM	Phase change material

PEG	Polyethylene glycol
POM	Polarizing optical microscopy
PPG	Poly (propylene glycols)
PPy	Polypyrrole
PTMG	Poly(oxytetramethylene)glycol
SAXS	Small-angle X-ray scattering
SEM	Scanning electron microscopy
SMA	Shape memory metallic alloy
SMF	Shape memory polyurethane fiber
SMP	Shape memory polymer
SMPU	Shape memory polyurethane
TEM	Transmission electron microscopy
TRSMF	Temperature-regulating shape memory fiber
TRHF	Thermal-responsive hollow fiber
WVP	Water vapor permeability
XRD	X-ray diffraction

LIST OF SYMBOLS

Symbol	Definition	Unit
ΔH	Enthalpy data	J/g
2θ	Bragg's angle	$^{\circ}$
A_{\parallel}	Relative intensity ratios of the selected bands of the infrared spectra obtained with the polarizer parallel to the fiber direction	
A_{\perp}	Relative intensity ratios of the selected bands of the infrared spectra obtained with the polarizer perpendicular to the fiber direction	
A_a	The area of the X-ray diffraction curve due to scattering from amorphous phases	count
A_c	The area of the X-ray diffraction curve due to scattering from the crystalline phases	count
A_{NC}	Absorption of negative control group	
A_{PC}	Absorption of positive control group	
A_{TS}	Absorption of test group	
D	Dichroic ratio	
D_0	Dichroic value of perfectly oriented sample	
E'	Elastic modulus	Pa, cN/dtex
E_{η_a}	Visco-flow activation energy	KJ/mol
L	The length of capillary	cm
$L_{(hkl)}$	Average crystallite size	nm
M_n	Number average molecular weight	Dalton
M_w	Weight average molecular weight	Dalton

n	Non-Newton index	
Q	Volumetric flow rate	ml/s
R	The radius of capillary	cm
$R_f(N)$	Fixity ratio at the N^{th} cycle	%
$R_r(N)$	Recovery ratio at the N^{th} cycle	%
$R_{r\text{-tot}}$	Total recovery ratio after the N^{th} cycle	%
$\text{Tan } \delta$	Loss tangent	
T_c	Crystallizing temperature	$^{\circ}\text{C}$
T_g	Glass transition temperature	$^{\circ}\text{C}$
T_{low}	A temperature below T_{trans}	$^{\circ}\text{C}$
T_m	Melting transition temperate	$^{\circ}\text{C}$
T_{perm}	A higher phase transition temperature	$^{\circ}\text{C}$
T_{trans}	A lower phase transition temperature	$^{\circ}\text{C}$
X_c	Percent crystallinity	%
α	The angle between the transition moment direction and polymer chain axis	$^{\circ}$
β	Full width at half maximum	radians
γ	Apparent shear rate	S^{-1}
ΔP	Pressure drop	Pa
$\Delta \eta$	Structural viscosity index	
ϵ_m	The maximum strain in the cyclic tensile tests	%
$\epsilon_p(N)$	The residual strain after recovery in the N^{th} cycle	%
ϵ_u	The strain after unloading at T_{low}	%

η	Apparent viscosity	Pa.s
λ	The applied X-ray wave length	Å
σ_m	The maximum stress at the maximum strain ϵ_m .	MPa, cN/dtex
τ	Apparent shear stress	Pa

LIST OF FIGURES

Figure 1.1 Schematic representation of stimuli-responsive shape memory effect.....	2
Figure 1.2 The schematic representation of (a) one-way shape memory effect and (b) two-way shape memory effect.....	2
Figure 1.3 The molecular mechanism of thermal-responsive shape memory effect.....	4
Figure 1.4 Mechanism of smart water vapor permeability of SMPs; the 3-demansional crosslinking structure represents the network of the SMP; the big balls represent the crosslinking points; and the small balls represent water molecules.	8
Figure 1.5 The textile products made of shape memory foams	9
Figure 1.6 Wrinkle free effect of fabrics treated with water-born SMPU .	12
Figure 1.7 Crease retention of fabrics treated with SMP (crease shape was produced by ironing)	13
Figure 1.8 The pattern after 2 times washing	13
Figure 1.9 SEM images of untreated wool and treated wool fibers	14
Figure 1.10 Improved dimensional stability of SMP treated wool garments	14
Figure 1.11 Shape memory of a fabric with SMA wires	15
Figure 1.12 A shape memory dress with SMA wires	16
Figure 1.13 Smart garment with SMA wires	17
Figure 2.1 (A) lightly crosslinked SMPs containing pendent ureidopyrimidinone side-groups. The moiesties in the red circle show the quadruple hydrogen bonding interaction. B) shape memory mechanism of the SMPs with thermo-reversible H-bonding. Colored side-groups represent H-bonding groups in the hot (hollow) and cold (filled) states, and the darker lines represent the lightly crosslinked covalent network.	28
Figure 3.1 The schematic representation of the heat treatment process.....	46
Figure 3.2 Cross-sectional shape of the nozzle hole in the spinneret (unit: mm)	47

Figure 3.3 Schematic for preparing the MWCNTs	49
Figure 3.4 The thermomechanical cyclic tensile testing process of SMFs	54
Figure 3.5 (a) Cyclic tensile testing path under drawing at high temperature and thermal recovery; (b) Cyclic tensile testing path under drawing at low temperature and thermal recovery	55
Figure 3.6 (a) Schematic stress-strain curves under drawing at high temperature and thermal recovery; (b) Schematic stress-strain curves under drawing at low temperature and thermal recovery	56
Figure 3.7 The bagging and recovery process of the shape memory fabric	59
Figure 4.1 The change of –NCO FTIR intensity with increasing curing time	70
Figure 4.2 PCL-based SMPU chips	73
Figure 4.3 The shape recovery of the SMPU rod	73
Figure 4.4 The relation between apparent viscosity η_a and shear rate γ at different temperature of the SMPU	75
Figure 4.5 The relation between $Lg\sigma$ and $Lg\gamma$ of the SMPU	77
Figure 4.6 The relation between $lg\eta$ and $\gamma^{1/2}$ at different temperature of SMPUs prepared	78
Figure 4.7 PCL-based SMFs prepared by melt spinning	79
Figure 4.8 The cross-section of the prepared SMF (embedded in nylon filaments)	79
Figure 4.9 The surface image of the prepared SMFs	80
Figure 4.10 Cyclic tensile curves of the SMF under drawing at high temperature and thermal recovery	82
Figure 4.11 The molecular mechanism of the shape memory effect of the SMF	83
Figure 4.12 Cyclic tensile curves of the SMF under drawing at low temperature and thermal recovery	84
Figure 4.13 DSC analysis of the SMF	86
Figure 5.1 DSC thermograms of PCL, as the as-spun SMF and SMFs after heat treatment	89

Figure 5.2 The elastic modulus and loss tangent of the SMF-125°C	91
Figure 5.3 Wide-angle X-ray scattering patterns of the PCL, as-spun SMF and SMFs after heat treatment.....	92
Figure 5.4 Carbonyl absorption in the FTIR spectra of pure PCL-4000 and SMFs as the function of increasing heat treatment temperature	97
Figure 5.5 Influence of heat treatments on SMF tenacity	99
Figure 5.6 Influence of heat treatments on SMF breaking elongation.....	100
Figure 5.7 Influence of heat treatments on SMF boiling water shrinkage	101
Figure 5.8 Stress relaxation of SMFs	103
Figure 5.9 Thermomechanical cyclic tensile testing strain-stress curves of the SMFs.....	104
Figure 5.10 Schematic representation of molecular disorientation and phase changes of SMFs induced by heat treatment.....	107
Figure 6.1 Cross-section image of the prepared hollow fiber	111
Figure 6.2 Static stress-strain curves of the TRHF.....	111
Figure 6.3 The DSC curves of the pure PCL and the TRHF.....	113
Figure 6.4 XRD patterns of pure PCL and the TRHF	114
Figure 6.5 The cyclic tensile testing result of the TRHF (a) set maximum elongation 300%, b) set maximum elongation 600%)	117
Figure 6.6 Thermally adjustable inner cavity of the TRHF (Deformed by longitude stretching) (a, original shape; b, deformed shape, c, recovered shape).....	119
Figure 6.7 Thermally adjustable internal cavity of the TRHF (Deformed by transverse pressing) (a, original shape; b, deformed shape, c, recovered shape).....	120
Figure 7.1 SEM surface image of TRSMF.....	123
Figure 7.2 Stress-strain curves of the TRSMF	123
Figure 7.3 POM images of (a) Pure PEG at room, (b) TRSMF at the ambient temperature	125
Figure 7.4 The DSC curves of pure PEG and TRSMF (solid line: heating; dot line cooling) ((a) pure PEG, (b) TRSMF)	126

Figure 7.5 The cyclic tensile testing curves of TRSMF	128
Figure 7.6 AFM images of the bulk polymer (left: height image, right: phase image)	131
Figure 8.1 Influence of MWCNT on the fiber surface quality; (a): 0 wt%, (b): 1.0 wt%, (c): 3.0 wt%, (d): 5.0 wt%, (e): 7.0 wt% of MWCNT134	
Figure 8.2 SEM images of MWCNT	135
Figure 8.3 In-plane surface images of traditional MWCNT/SMPU films after etching using DMF (a: 0.25 wt% MWCNTs, b: 1.0 wt% MWCNTs, c: 2.0 wt% MWCNTs, d: 3.0 wt% MWCNTs).	136
Figure 8.4 SEM images of the fracture surface of the fibers with (a) 0 wt%, (b) 1.0 wt%, (c) 3.0 wt%, (d) 5.0 wt%, (e) 7.0 wt% MWCNT content	137
Figure 8.5 Schematic representation of MWCNT alignment in the SMF during blending and spinning (The thin lines represent chains of polyols, the circles represent aggregated hard segment groups, and the thick hollow lines represent MWCNTs.).....	139
Figure 8.6 The electro-active shape recovery effect of MWCNT/SMFs rod	141
Figure 8.7 The electro-active shape memory effect of MWCNT/SMFs ((a) the original length, (b) the length after elongation, (c) the length after recovery).....	142
Figure 8.8 Stress relaxation of SMFs with different MWCNT contents (with partial enlarged details).....	144
Figure 8.9 Shape recovery stress of MWCNT/SMFs with different MWCNT contents	145
Figure 9.1 PBA-based SMP solution for wet spinning	148
Figure 9.2 PBA -based SMFs prepared by wet spinning	148
Figure 9.3 The image of the prepared shape memory multifilament	149
Figure 9.4 The DSC of the SMF	150
Figure 9.5 The SAXS pattern of the SMF	151
Figure 9.6 The SAXS pattern of the SMPU film	151

Figure 9.7 The infrared spectra of the shape memory film with the polarizer in an arbitrary direction and the direction perpendicular to the arbitrary direction	152
Figure 9.8 The infrared spectra of the SMF with the polarizer parallel and perpendicular to the fiber direction	153
Figure 9.9 The LogE' - temperature curve and Tan δ - temperature curve of the SMF, E' (cN/dtex).....	154
Figure 9.10 The Log E' - temperature curve and Tan δ - temperature curve of the SMPU film, E'(cN/dtex).....	155
Figure 9.11 Dumb-bell shape specimens of SMPU film.....	156
Figure 9.12 The tensile properties of the SMF multifilament and SMPU film	157
Figure 9.13 The thermomechanical cyclic tensile testing curves of the SMF	158
Figure 9.14 The bag recovery curve of the shape memory fabric (a: the shapes of the bag during the shape recovery testing process; b: the height change of the bag during the shape recovery as a function of time).....	159
Figure 9.15 The schematic representation of the molecular mechanism of the shape memory effect of the SMF	161
Figure 10.1 The lab-scale flow chart.....	174
Figure 10.2 The newly designed flow chart	175
Figure 10.3 The backside of Nike “Sphere React Shirt” with a smart vent structure (Reprinted with permission of Nike company)	177

LIST OF TABLES

Table 3.1 Raw materials used in the synthesis of SMPUs	41
Table 3.2 The main equipment used in the project	42
Table 4.1 Band assignment and domain origin	72
Table 4.2 The non-Newton index of the SMPU.....	77
Table 4.3 The structural viscosity index of the SMPU at different temperatures	78
Table 4.4 Cyclic tensile properties of the SMF under drawing at high temperature and thermal recovery	82
Table 4.5 Cyclic tensile properties of the SMF under drawing at low temperature and thermal recovery	85
Table 4.6 Results of DSC analysis of the SMF	86
Table 5.1 Thermal properties of the PCL, as-spun SMF and SMFs after heat treatment	89
Table 5.2 The results of peak separation and calculated crystallinity	93
Table 5.3 The lattice parameters of the SMFs.....	95
Table 5.4 Thermomechanical cyclic tensile testing result of SMFs.....	105
Table 6.1 Thermal transition temperature and crystallinity of pure PCL and TRHF	113
Table 6.2 The lattice parameters of the TRHF	116
Table 6.3 Shape fixity and recovery ratios of TRHF	118
Table 7.1 Thermal transition temperature, enthalpy and crystallinity of pure PEG and TRSMF.....	127
Table 7.2 Detailed shape fixity ratios and recovery ratios of TRSMF.....	128
Table 9.1 The biological reactivity rated on a scale of 0 to 4	162
Table 9.2 Agar diffusion test results	163
Table 9.3 Haemolytic index	164
Table 9.4 Scoring criteria for skin reactions	165

Table 9.5 Guinea pig closed patch sensitization test results of control group (induction: 25 hilltop chamber moist with saline; challenge: 1 square inch test article using a 25 mm hilltop chamber moist with saline) .	165
Table 9.6 Guinea pig closed patch sensitization test results of the test group (dosage: 1 square inch test article using a 25 mm hilltop chamber moist with saline)	166
Table 9.7 Scoring criteria for skin reactions (rabbit)	167
Table 9.8 Dermal irritation response categories in the rabbit	167
Table 9.9 Primary skin irritation summary of scores for skin irritation (dose = 25 mm x 25 mm (moist with physiological saline))	168

CHAPTER 1 INTRODUCTION

This chapter first briefly introduces shape memory materials which include shape memory polymers and shape memory metallic alloys. Then the applications of shape memory materials in the forms of film, foam, finishing coating, and fiber (wire) are summarized. Following the introduction, the objectives and significance of the present study are presented.

1.1 Introduction of shape memory materials

Stimuli-responsive shape memory materials can change their shapes from a temporary shape to the original (or permanent) shape under appropriate stimuli such as heat [1], electricity [2], light [3], magnetic field [4] and moisture [5]. Figure 1.1 shows a schematic representation of the shape memory effect. For materials to be of shape memory, their shape change must be rapid and can finish within a narrow band. If the shape change between original shape and temporary shape can be achieved by the applied environment stimuli without employing external force as shown in Figure 1.2, the shape memory effect is two-way shape memory effect (see Figure 1.2 (b),). Otherwise, if external stress such as direct stretching and bending has to be used to achieve the temporary deformation, the shape memory effect is one-way shape memory effect (see Figure 1.2a). In the one-way shape memory effect, to obtain a secondary shape, an external force has to be employed. In the two-way shape memory effect without using external force but using the reversal stimulation, for example in the circumstance of two-way shape memory alloys, the alloy will shrink or elongate by increasing or decreasing the temperature.

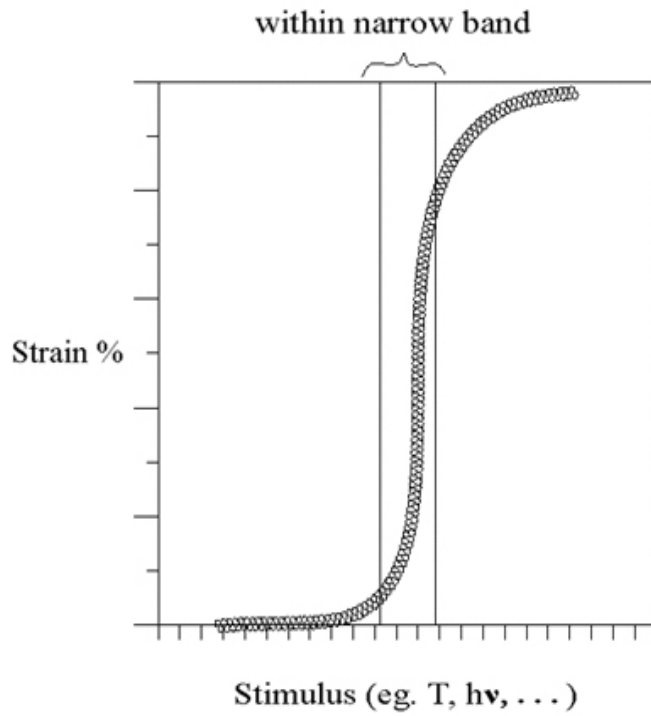


Figure 1.1 Schematic representation of stimuli-responsive shape memory effect [6]

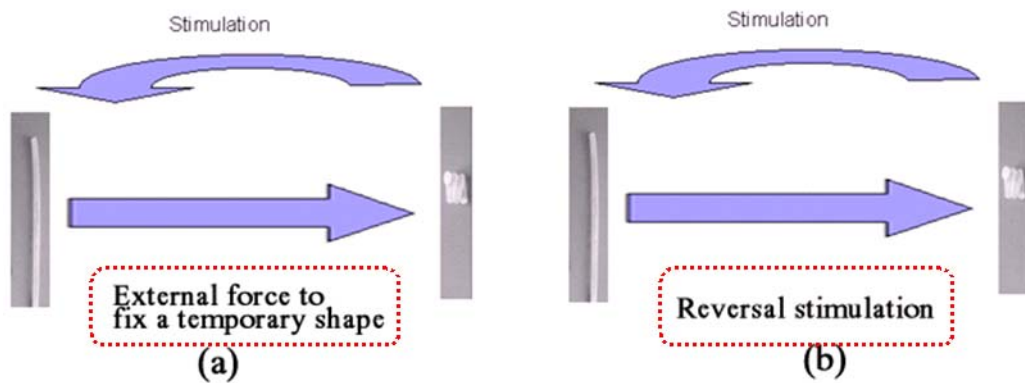


Figure 1.2 The schematic representation of (a) one-way shape memory effect and (b) two-way shape memory effect

Thermal-responsive shape memory materials can “remember” their original shape and rapidly change their shape from a temporary shape to their original (or permanent) shape under thermal stimulation [7-15]. Thermal-responsive shape memory materials include thermal-responsive shape memory polymer (SMP) and shape memory metallic alloy (SMA).

Thermal-responsive shape memory materials have been used in smart textiles and apparels [16], intelligent medical devices [17-19], heat shrinkable packages [20], sensor and actuators [21, 22], smart water vapor permeability materials [23], self-deployable structures in spacecraft [24], micro-systems [25, 26], damping materials [27], self-peeling reversible adhesive [28], vehicle components [29], toys [30], hair treatment [31, 32], and chemical feeding in chemical reactions [33, 34]. The medical applications of thermal-responsive shape memory materials have been studied extensively and intensively [33, 34], which include laser or magnetic-responsive devices for cardiovascular stents [35-38], aneurysm coils for treatment of intracranial aneurysm [39], biodegradable intelligent surgery sutures [40, 41], orthodontic appliances [42-44], self-deploying neuronal electrodes [45], dialysis needle adapters [46], and drug control release devices [47, 48].

1.2 Mechanism of shape memory effect

1.2.1 Shape memory polymers

The shape memory effect of SMPs is not a specific property of a single polymer. It is resulting from the structure and morphology of the polymer and is influenced by the programmed testing conditions. Many polymer systems [13,

14, 49-51] have been reported to possess thermal-responsive shape memory effect.

Figure 1.3 shows the molecular mechanism of shape memory effect of SMPs. SMPs usually have a physical crosslinking structure, crystalline/amorphous hard phase, or chemical crosslinking structure and a low temperature transition (switching transition) of a crystalline, amorphous or liquid crystal phase. SMPs are processed or thermally set to have an “original” shape. Generally, in the permanent shape, the internal stress is zero or very low. If the SMP is subject to deformation, the internal stress can be stored in the crosslinking structure by cooling the polymer below its switching transition temperature. By heating the polymer above the switching transition temperature, the SMP recovers its permanent shape as a result of releasing the internal stress stored in the crosslinking structure.

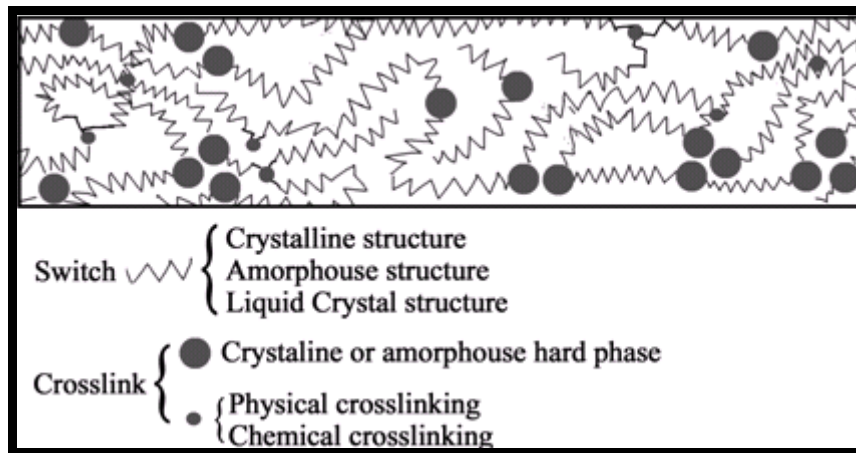


Figure 1.3 The molecular mechanism of thermal-responsive shape memory effect

The network to store the internal stress which will be used as the shape recovery driving force may be a physical crosslinking structure, crystalline/amorphous hard phase, or chemical crosslinking structure [14, 51-55]. The ‘molecular switch’ to resist the release of internal stress may be a crystalline, amorphous or liquid crystal phase [56-59]. From the application view, the prerequisite for thermal-responsive polymers as shape memory materials is that the thermal transition temperature needs to be above the temperature of the environment in which they are being applied.

Over SMAs and shape memory ceramics, SMPs have the advantages of light weight, low cost, good processability, high deformability, high shape recoverability, soft handle and tailor-able switching temperature [9, 14, 30, 49, 51, 52, 54, 57, 60-74].

1.2.2 Shape memory metals

Different from SMPs, the shape memory properties of SMAs arises from the crystal lattice change of a specific martensite variant to the parent single crystal phase. Nickel-titanium (NiTi), copper-aluminum-nickel alloys and copper-zinc-aluminum-nickel are the three main kinds of SMAs. During the shape recovery cycles, SMAs show two phases: an austenite phase with a body centered cubic structure at high temperature, and a martensite phase with tetragonal, orthorhombic or monoclinic crystal lattice at low temperature. NiTi alloys change from austenite to martensite upon cooling and change from martensite to austenite when heating. The phase transformation from austenite to martensite upon cooling is not by diffusion of atoms, but by shear lattice distortion. Upon cooling, the austenite transforms to martensite, which results in the formation of

several martensitic variants, up to 24 for NiTi. At a temperature below martensite transformation finish temperature, deformation stress changes the variants of other martensite phase into a specific variant of martensite phase, which leads to the macroscopic shape change of the SMA. The recoverable deformation strain of SMAs is usually below 10%; otherwise, the deformation will cause the slippage of the lattice, which is unrecoverable. If the SMA is heated to a temperature above the start temperature of the austenite phase, the specific martensite variant transforms to the lattice of original austenite phase, leading to the one-way shape recovery of SMA.

The two-way shape memory effect can be imparted to SMAs by training so that SMAs can remember two different shapes at a low temperature and a high temperature respectively. The two-way shape memory effect is due to the residual stress in the SMAs after specific training processes by specific heat treatment, and thermomechanical cycles. The recoverable strain and recovery stress of two-way shape memory effect are much lower compared with those of one-way shape memory effect.

1.3 Shape memory materials for smart textile applications

During the past few decades smart functional textiles have been developing rapidly. Textiles with novel functions such as luminescent textiles [75], textiles display [76], emotion sensing dress [77], and self-cleaning textiles [78] have been developed. Shape memory materials which can sense the environmental temperature and respond to the temperature variation inspire researchers to develop smart textiles with self-regulating structures and characteristics. Taking the advantage of this property, shape memory materials have been used in

textiles for breathable films, memory foam products, shape memory finishing coating and shape memory fibers (wires)

1.3.1 Breathable films

The SMPs for breathable films have a switching temperature around the human body temperature. Water vapor permeability of SMP films changes corresponding to the wearer's temperature variation. The mechanism of the thermal-responsive water vapor permeability is illustrated in Figure 1.4. At a temperature above the glass transition temperature of the SMP, the free volume of the film increases significantly, which enables the transfer of heat and vapor from perspiration to the environment. Thus, a comfortable feeling can be obtained. When the temperature is below the glass transition temperature, the free volume of the SMP film decreases to prevent air and water molecules to pass through. Consequently, the SMP film keeps the body warm. SMP films may be coated, laminated or interlined in traditional fabrics [79, 80]. Hu [23, 81-84], Jeong [85, 86] and Chen et al. [87] demonstrated that the water vapor permeability of the shape memory polyurethane (SMPU) films can be improved by employing hydrophilic segments such as dimethylpropionic acid, diol terminated poly (ethylene oxide) [85, 86] and decreasing density of the chemical cross-bonding [87] of the polyurethane.

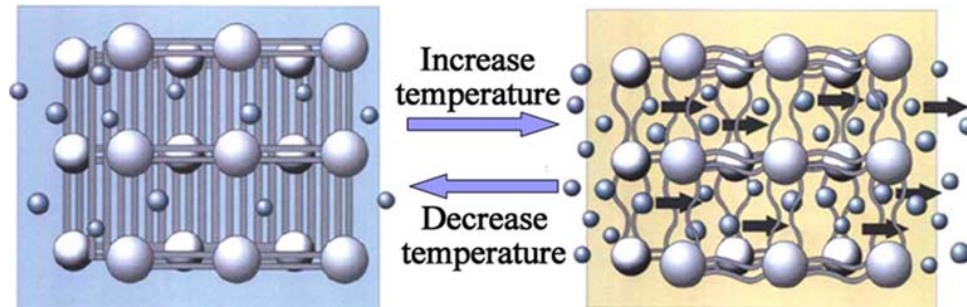


Figure 1.4 Mechanism of smart water vapor permeability of SMPs; the 3-dimensional crosslinking structure represents the network of the SMP; the big balls represent the crosslinking points; and the small balls represent water molecules. [88]

1.3.2 Shape memory foams

SMP foams can be used for aerospace applications [89, 90], weight reducing [91, 92], drug delivery [19, 93], and measuring tools of complex cavities [93]. For textile applications, SMP forms have been used as stuffing of pillows. Figure 1.5 shows some textile products using memory foams. The memory pillow is filled with low resilience polyurethane memory foams developed by Bayer. The memory pillow can adjust its shape to the contour of the neck and shoulder at the body temperature. SMP foams can also be used as memory foam mattresses. The shape memory mattress benefits users' legs, back, shoulders, and joints, because the product can provide comfort support for the user's body. SMP foams have also been used to prepare insole, which can effectively improve shoe fitting. Wearing high-heeled shoes can cause a lot of problems to ladies, such as callus, painful bunions, and spine deformity [94-97]. Dr. Scholl's Company produces Dr. Scholl's® Memory Fit™ (Work) Customizing Insoles (Figure 1.5) [98] using memory foams in forefoot or from heel to toe. The insole can adjust to everybody's unique footprint with every step and can tackle the above problems efficiently.

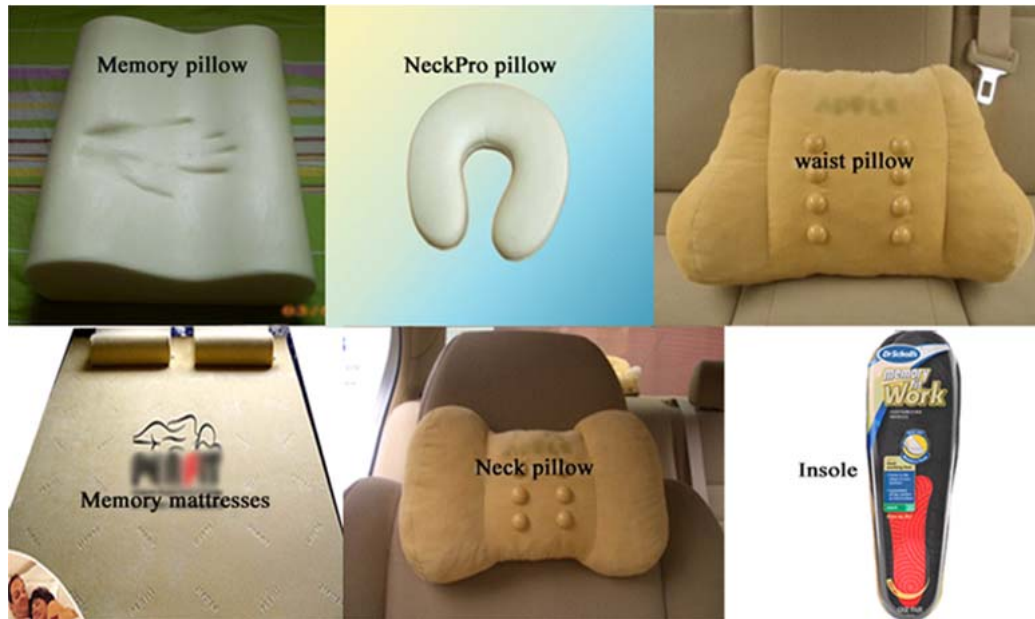
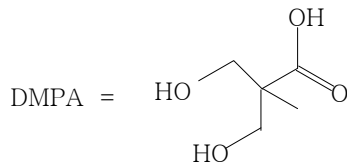
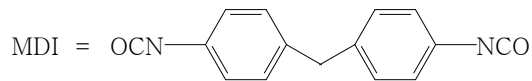
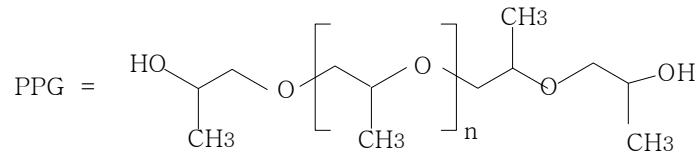
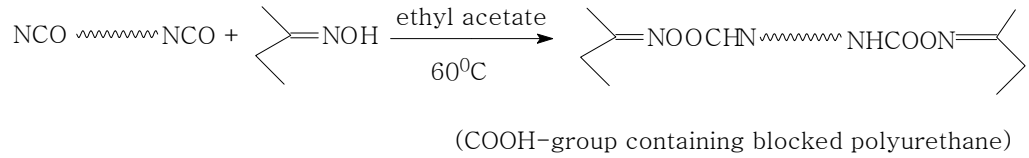
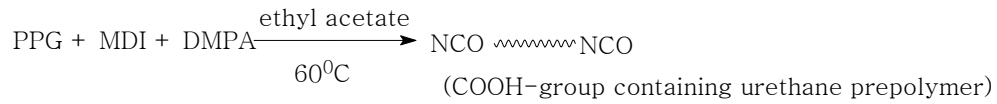


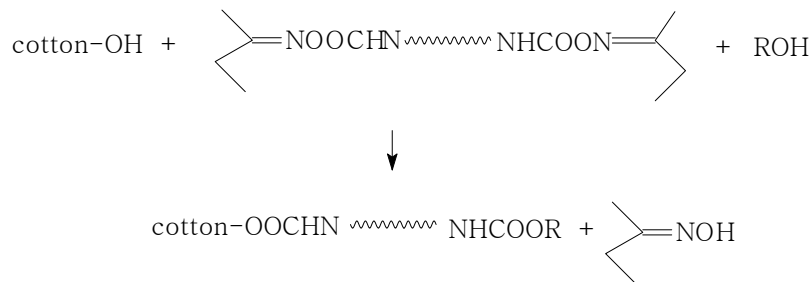
Figure 1.5 The textile products made of shape memory foams

1.3.3 Shape memory finishing

SMPs can be applied in textile sector by garment finishing to impart the shape memory effect of SMP into textiles. Wan and Stylios [99] studied the shape memory fishing of cotton fabric with a SMPU solution. The finishing solution was produced by dissolving SMPU chips in dimethylacetamide solvent. The finishing was carried out by the conventional method. The shape memory effect could be trained from being flat at high temperature to an bent shape at low temperature [100]. Hu et al. [101-103] treated cotton and wool fabrics using water-born SMPU emulsion. The water-born emulsion was prepared by solution polymerization as shown in



Equation 1.1 Synthesis of end-capped SMPU oligomers



Equation 1.2 Reaction of SMPU oligomers with cotton

The SMPU treated cotton fabrics showed wrinkle-free effect due to the shape recovery effect of the SMPs [106]. Fabrics, especially cotton materials develop wrinkles easily under low stress during wearing or storage due to the debonding and slippage of hydrogen bonds. As shown in Figure 1.6, the cotton

fabric treated by SMPU can recover its original flat shape within a short span of time by blowing steam. However, the unfinished cotton fabric cannot recover flat appearance because of its low wrinkle resistance. At present most of the current methods of wrinkle free finishing are done using DMDHEU (dimethyloldihydroxyethylene urea) which contains formaldehyde. The advantage of using SMPs for finishing when compared to DMDHEU is that the treated fabric does not release formaldehyde. Compared with another kind of wrinkle-free finishing by polycarboxylic acid containing finishing agents such as BTCA (1,2,3,4-butane tetra- carboxylic acid), SMPU finishing will not markedly affect the mechanical strength and whiteness index of the fabric. To some extent SMPU finishing on cotton increases the mechanical strength fabrics. Repeated washing experiments show that the wrinkle-free effect of SMPU emulsion treated fabric can last for hundreds of laundering cycles.

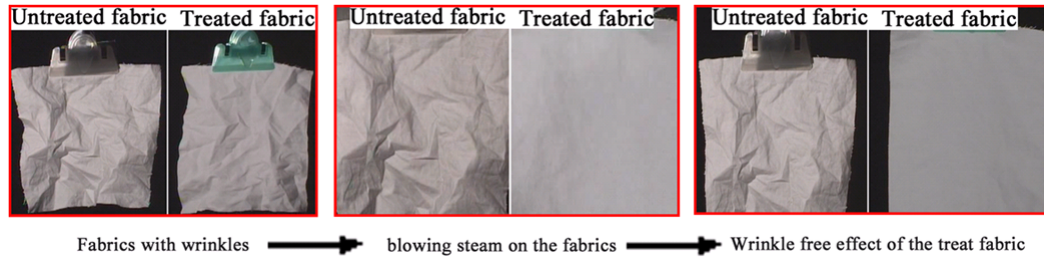


Figure 1.6 Wrinkle free effect of fabrics treated with water-born SMPU [107]

Cotton fabrics treated with SMPU emulsion have greater crease and pattern retention ability due to the excellent shape fixability of SMPs. The crease or pattern design on textiles adding to aesthetics appeal can be maintained for a long time. Figure 1.7 shows the crease retention effect on cotton fabric treated with SMPs. In Figure 1.7, both the treated cotton fabric and untreated fabric have a crease shape in the centre set at the beginning by ironing. After hot water washing under a temperature of around 60°C, the crease shape on the untreated fabric disappears while the crease shape on the treated fabric is maintained. Figure 1.8 shows a designed pattern with good pattern retention of a finished knitted fabric. The finished fabric is endowed with good shape fixability of the SMPU after the finishing process. The shape on the fabric can be maintained because of the good shape fixity of the treated fabric. Even after many laundering cycles the pattern is retained.

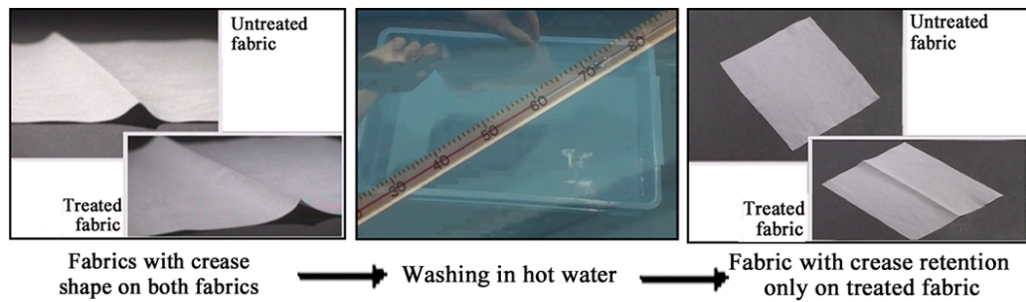


Figure 1.7 Crease retention of fabrics treated with SMP (crease shape was produced by ironing) [107]



Figure 1.8 The pattern after 2 times washing [107]

Wool fabrics were also treated with the SMPU emulsion by the similar reaction mechanism as described previously for cotton fabric. The SEM images of the treated wool fibers are presented in Figure 1.9. The wool garment treated with SMP emulsion has better dimensional stability than that of untreated garment because SMPU covers wool fiber scales and as a result reduces the wool directional frictional effect after finishing process. As shown in Figure 1.10, the

untreated wool garment shrinks to a small size, while the treated garment maintains its size after laundering. In addition, wool fabrics and sweaters have serious felting phenomenon with the entanglement of scales by directional friction. The treated wool fabric has significantly reduced the felting effect when coated with SMPU resin. Repeated washing experiments have shown that the dimensional stability and the anti-felting effect can be maintained, which may be attributed to the chemical cross-linking bonding between the SMPU and the fabric matrix.

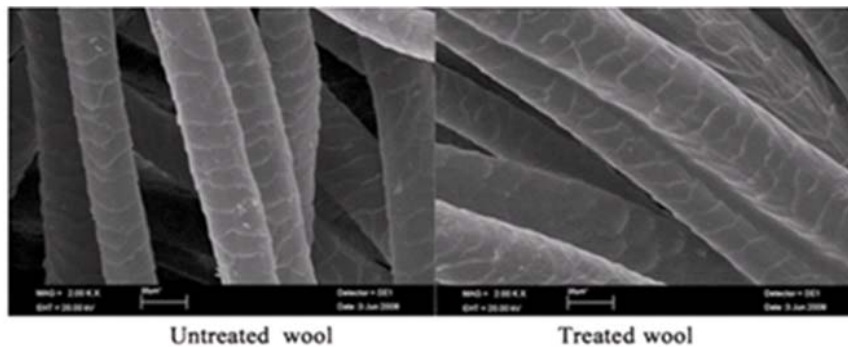


Figure 1.9 SEM images of untreated wool and treated wool fibers [108]



Figure 1.10 Improved dimensional stability of SMP treated wool garments [109]

1.3.4 Shape memory metallic wires

Stylios and Wan [100] demonstrated the shape recovery of a fabric with trained SMA wires with two-way shape memory effect. The trained SMA wires were blended with two kinds of polymer yarns. The shape of the fabric changed from a flat shape to a curled shape in 50 seconds if the fabric was heated to a temperature at 50°C which was slightly above the austenite transformation starting temperature. By cooling the fabric from above 50°C to room temperature, the fabric recovered from the curl state to its original flat state. Figure 1.11 [110] presents another shape memory fabric with two-way SMA wires. The fabric is flat originally as shown in Figure 1.11a. By heating, the fabric rolls up as shown in Figure 1.11b. Then, cooling the fabric to room temperature leads to the fabric recovery to the flat shape as shown in Figure 1.11c.

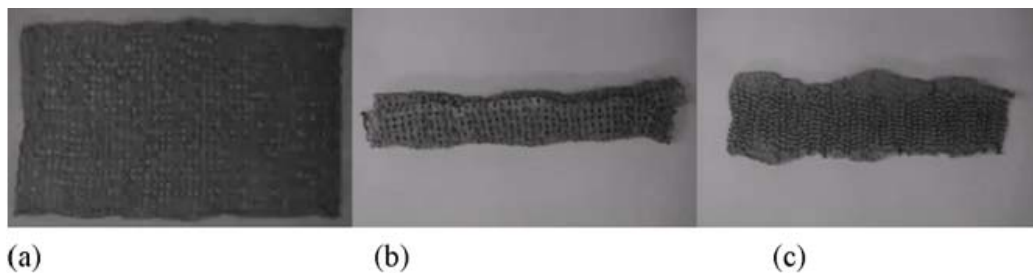


Figure 1.11 Shape memory of a fabric with SMA wires [110]

Various clothing and accessories have been designed using SMA wires for aesthetic interactive effect and functional effect. Italian design house based in Florence, Corpo Nove, designed “lazy shirt” fabric joined with SMA wires and

nylon fibers. During high outside temperature, the shirts sleeve can wind up from wrist to elbow in a short time. when the temperature becomes lower, the sleeve automatically returns to original shape [111].

Figure 1.12 [110] shows another interesting design of smart dress using two-way SMA wires. The under section of the dress is made of fabric embedded with SMA wires. As shown in Figure 1.12, the under section of the dress shrinks if the dress is heated by using a hair dryer. At a low temperature without hot air blowing, the under section can recover.

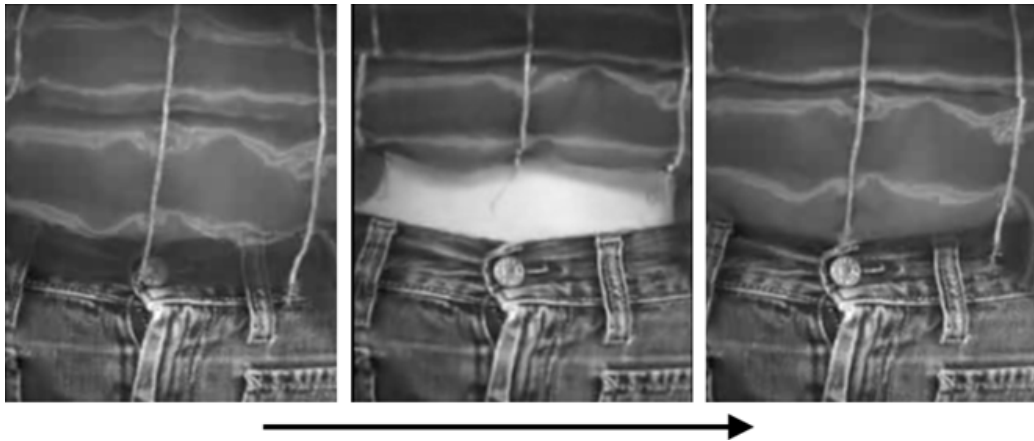


Figure 1.12 A shape memory dress with SMA wires [110]

SMAs are intermetallic alloys which are electro-conductive. They can be heated by using electrical current via Joule heating. Shape change driven by electrical current is more easy and efficient than that by direct heating. Figure 1.13 [112] shows a garment incorporated with SMA wires. The designed gaps on the garment can open and close as a result of increasing and decreasing temperature

of the SMA wires by Joule heating. The power is supplied by the power source embedded within the garment.



Figure 1.13 Smart garment with SMA wires [112]

Though SMA wires can be used in textiles to develop smart textiles with thermal-active shape memory effect, there are many problems associated with the intrinsic properties of metallic alloy. First, because of the different mechanical and surface properties of SMA wires and traditional fabrics, SMA wires have a tendency to protruding out. Complicated structures of textiles are difficult to accomplish. Second, due to the low extensibility and high stiffness of SMA wires, knitting of SMA wires is not easy to conduct. Another problem is that if not designed properly, the SMA wires in shape memory fabrics significantly affect the soft handle of fabrics.

In comparison with SMA wires, shape memory polymeric fibers have better compatibility with human bodies. Textiles made of SMFs can give the look and feeling similar to conventional clothing fabrics. Furthermore, SMFs are much cheaper in comparison with SMA wires.

1.4 Objectives of the project

Though SMFs have been developed, the functions of the present SMFs are quite simple featured with uniaxial shrinkage by direct heating stimulations [58, 113-115]. Based on the previous research, the main objective the present project is to develop and study the SMFs with novel functions: SMFs with thermal-responsive inner diameters, SMFs with temperature-regulating effect, SMFs with electro-active effect and SMFs with potential biological applications.

1.4.1 To study general shape memory fibers (SMFs)

The first objective of the present project is to develop a SMF and study the properties of the SMF. Though there has been much research on the SMPs as films, foams, and finishing coating in recent two decades [14, 60-63, 70, 116-119], the studies on SMFs are still quite few [58, 115]. In principle, shape memory polyurethane fibers can be prepared by using (i) dry, (ii) wet, (iii) chemical, or (iv) melt spinning technology. Melt spinning is most advantageous in terms of health, safety, environmental and economy concerns, because it does not involve the use of harmful solvents such as DMF (N,N-Dimethylformamide) or DMAc (N,N-Dimethylacetamide) and no coagulation bath. Thus, a SMF was prepared by melt spinning.

To eliminate internal stress and structure deficiency caused by the spinning processes, SMFs are subject to heat treatments. The influences of heat treatments on the properties of the SMFs are studied, which include thermal properties, molecular orientation, crystalline properties, hydrogen bonding,

tensile properties, dimensional stability, recovery stress relaxation and thermomechanical cyclic properties.

1.4.2 To study SMFs with thermal-responsive inner diameters

Shape memory hollow fibers have many special properties in comparison with cylindrical ones and may have many special applications. First, changes of the hollow fiber inner diameter affect the physical properties of the textile products. If this kind of shape memory hollow fiber is used in fabrics, the thermal-responsive heat transfer of the fabric will change according to the environment and body temperature. Second, the shape memory hollow fiber may be used as the stuffing of pillows and mattresses which can adjust to body contours for comfortable feeling. If unloaded, after some time, they recover their original shapes. Furthermore, this kind of hollow fibers with thermal-responsive inner diameter may be used in smart filtration, drug controlled release and liquid transportation [120]. Thus, the second object of the present study is to develop and study the properties of shape memory hollow fibers.

1.4.3 To study SMFs with temperature-regulating effect

Poly (ethylene glycol) PEG is a typical solid-liquid phase change polymeric material. It may be employed as the soft segment of SMFs to prepare polyurethanes with temperature-regulating effect. Since the shape memory effect of SMF is also because of the so-called micro-phase-separated heterogeneous structure which is composed of the hard segment phase and soft segment phase. The temperature-regulating fibers may also show shape memory

effect. The temperature-regulating effect and shape memory properties of the PEG-based SMFs are to be studied.

1.4.4 To study SMFs with electro-responsive effect

Usually the shape memory effect of SMFs is induced by directly heating the fiber to a temperature above the switching temperature. Electro-responsive shape memory effect of SMFs may be achieved by Joule heating after the SMFs are filled with conductive carbon nanotubes (CNTs). The electro-active effect and shape memory properties, especially shape recovery stress, of the CNT/SMPU fibers are to be studied.

1.4.5 To study SMFs for potential biological applications

The medical applications of the SMF for responsive medical devices are of great interest to scientists and engineers due to their combination wide range of tunable stiffness, tailor-able transition temperatures, fast actuation, large deformation, high shape recovery, and elastic properties. Furthermore, because of the soft structure and permeability of shape memory fabrics, which are more compatible with human bodies in comparison with films or bulks, shape memory fabrics in the special forms may have promising applications as biomedical materials. Therefore, SMFs and fabrics with suitable switching temperature at around body temperature are to be studied and the biological properties of the fabric are to be evaluated.

1.5 Significance of the project

SMFs have promising applications in the textile and clothing industry as they provide inspiration to create intelligent textiles with a self-regulating structure and performance in response to thermal stimulation. SMFs with novel properties such as thermo-sensitive inner diameter, electro-active effect, temperature-regulating effect and body temperature transition can have more potential applications not only in textile areas but also maybe in wound dressing, scaffolding materials, pressure garment, high performance sensors, actuators and microgrippers.

Shape memory hollow fibers may be used in fabrics for smart heat transfer according to the environment and body temperature. They may be also used as the stuffing of pillows and mattresses which can adjust to body contours, for comfortable feeling. Furthermore, this kind of hollow fibers with thermal sensitive internal diameter may be used in smart filtration, drug-controlled release, and liquid transportation.

Usually, the shape memory effect of SMFs is induced by directly heating the SMF to a temperature above the switching temperature. In many practical applications, electrical power is more convenient to trigger the shape recovery process than by an external heater. This is especially important if the SMF is to be used as smart actuators or sensors in smart textiles or other products. CNT reinforcement may also be an effective method to improve the recovery stress of SMFs, since low recovery stress has been a fatal disadvantage of SMFs in comparison with SMAs.

In comparison with their bulk counterparts, SMFs may have high mechanical properties and shape recovery force because of molecular orientation. In comparison with spandex and polyester fiber, shape memory fabrics may have better capabilities for 3-D textile due to their good shape fixity. Furthermore, the fabrics made of shape memory fibers may fit wearers well and bring comforting feeling to wearers resulting from the good deformability, retention capacity and partial elasticity of SMFs. It would be better if the shape recovery of the SMFs can be triggered by human body temperature. The evaluation of animal responses to the fiber is important in determining the fiber capacity for a clinical situation. Specific requirements may differ according to the nature of applications. In this project, the biological evaluations of the SMF/fabric are to be conducted.

1.6 Outline of the thesis

This thesis studies the properties of the SMFs and SMFs with novel functions, i.e., thermal-responsive inner diameters, temperature-regulating effect, and electro-active shape memory effect. The biological evaluation of the SMFs with a human body switching transition temperature is also conducted for potential biomedical applications.

Chapter 1 states the general background of shape memory materials and the research of shape memory materials for textile applications such as breathable fabrics, shape memory finishing, shape memory foams and SMA wires. Significance and objectives of the present study are presented.

In Chapter 2, comprehensive literature pertaining to SMPs of different types is

generally reviewed. One of the representative SMPs, i.e., SMPU, which has been used widely, is introduced. The research on phase change materials, CNT/SMP composites and biological applications SMPs is described.

Chapter 3 includes sample preparations and characterizations of the corresponding samples. SMPUs are synthesized by solution and bulk polymerization and SMFs are prepared by wet and melt spinning methods. In addition, the preparation of other related samples are presented in the chapter such as shape memory films, shape memory fabrics, shape memory hollow fibers, SMFs with temperature-regulating effect, and MWCNT/SMPU fibers. The characterization techniques used in this study are illustrated.

In Chapter 4, the properties of the prepared SMPU are studied. The properties of the prepared SMF with a melting transition as the switch are presented.

In Chapter 5, the influences of heat treatments on the SMF properties are studied, which include thermal properties, crystalline properties, hydrogen bonding, tensile properties, dimensional stability, recovery stress relaxation, thermomechanical cyclic properties and shape memory behavior.

Chapter 6 introduces the shape memory hollow fiber with thermal-responsive inner diameters. The properties of the prepared shape memory hollow fiber are studied.

Chapter 7 describes a temperature-regulating SMF with PEG as the soft segment. The fiber's phase change behaviors, crystalline morphology, and shape memory effect are studied.

Chapter 8 introduces an electro-active MWCNT/SMF by incorporating MWCNTs into SMFs. The influence of MWCNTs on the spinnability, shape recovery stress and electro-active effect of the SMF was studied.

Chapter 9 presents SMFs with a body temperature switching transition for potential biomedical applications. The properties of the SMFs are studied. Not focusing on one specific application, the biological evaluations of the SMF are conducted in terms of cytotoxicity, haemolysis, sensitization and dermal irritant.

Chapter 10 presents the conclusions of the study followed by suggestions of future work.

CHAPTER 2 LITERATURE REVIEW

Comprehensive literature pertaining to SMPs is generally reviewed here. SMPs of different types are introduced. One of the typical SMPs, i.e., SMPU, is highlighted. The research on polyurethane based phase change materials and CNT/SMPU composites is presented. The biological applications of SMPs are summarized.

2.1 Shape memory polymers of different types

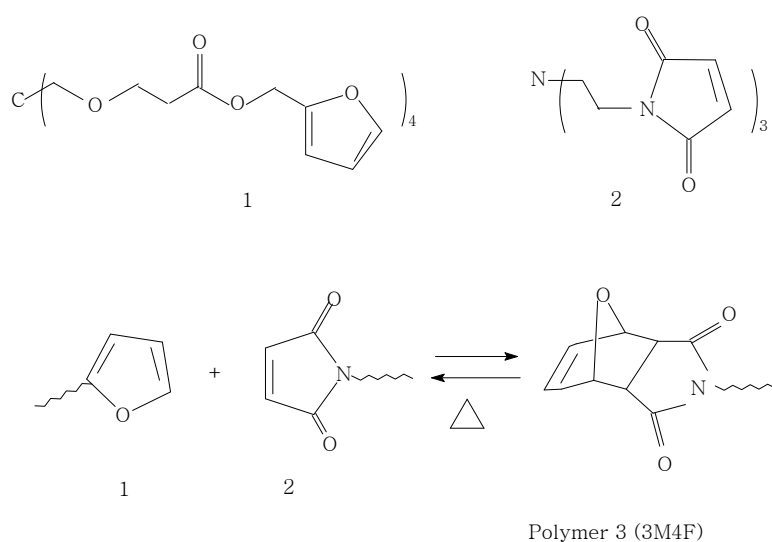
In the past decade, a few review papers regarding SMPs have been published [7-15]. According to the switching mechanisms, SMPs can be divided into following categories.

2.1.1 Shape memory effect based on conventional glass or melting transition

The research in SMPs based on conventional glass or melting transition has been conducted intensively [121-129]. With glass or melting transition as the switch, many polymer systems have been reported to possess shape memory effect. According to Liu, et al. [51], SMPs based on conventional glass or melting transition fall into four classes, class I: covalently crosslinked glassy thermoset networks as SMPs (glass transition as a switch); class II: covalently crosslinked semi-crystalline networks as SMPs (melting transition as a switch); class III : physically crosslinked glassy copolymers as SMPs (glass transition or melting transition as a switch); and class IV: physically crosslinked semi-crystalline block copolymers as SMPs (glass transition or melting transition as a switch)

2.1.2 Shape memory effect based on thermally reversible reaction

The second thermal reversibly associating structure which can be used as switches of SMPs is thermally reversible reaction. The thermally reversible reaction as shown in Equation 2.1 is a thermally reversible Diels-Alder cycloaddition of a multi-diene (multi-furan) and a multidienophile (multi-maleimide) [130, 131]. Monomer 1 contains four furan moieties on each molecule, and monomer 2 includes three maleimide moieties on each molecule. The thermal reversibility can be accomplished by the retro-Diels-Alder reaction. Ishida et al. [132] prepared a reversible polymer network consisting of furan-terminated telechelic polyesters of poly(1,4-butylenesuccinate- co-1,3-propylene succinate) reacted by Diels-Alder (DA) addition with a trifunctional maleimide. The mechanical properties of the polymer network are adjustable by changing temperature as a result of depolymerization-repolymerization and melt-recrystallization processes. These materials have good potentials as SMPs though the shape memory effect was not studied.



Equation 2.1 A thermally reversible crosslinked structure [132]

2.1.3 Shape memory effect based on supermolecular structures

Supermolecular structures containing donors and acceptors can be used as switches of SMPs. At a temperature above and below the specific temperature, the donors and acceptors are in a connective or separate state. Li et al. [133] employed a thermal reversible associating quadruple H-bonding structure as the switch for SMPs. The SMP consists of a lightly crosslinked network which is bonded to reversibly associating UPy (ureidopyrimidinone) moiety. The molecule structure of the SMP network is presented in Figure 2.1(A). The UPy moiety forms quadruple hydrogen bonding interaction as shown in Figure 2.1(A) in the red circle. The shape memory mechanism with thermal reversible hydrogen bonding as the switch is shown in Figure 2.1(B). As shown in Figure 2.1(B), during the fixity process, the thermal reversible hydrogen bonding forms new net points, which “pin” the elastomer elastic recovery. As a result, the deformed shape is fixed. Upon heating to a high temperature, the net points formed by hydrogen bonding break. The materials recover its original shape as a result of entropy elasticity. Hu et al. [134, 135] also incorporated self-complementary quadruple hydrogen bonding units into SMPU and studied the shape memory effect. Other thermal reversible supermolecular interactions such as ion-ion and ion-dipole may also be used as the switch of SMPs.

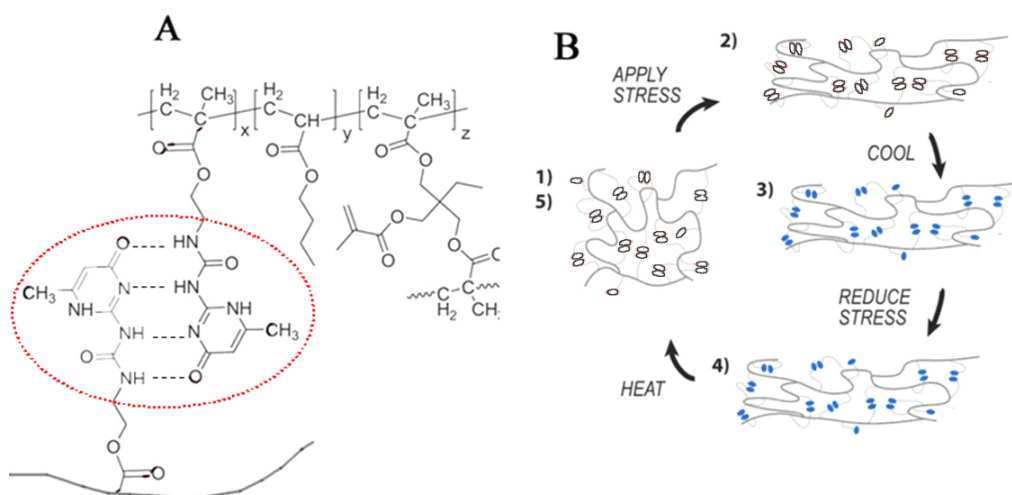


Figure 2.1 (A) lightly crosslinked SMPs containing pendent ureidopyrimidinone side-groups. The moieties in the red circle show the quadruple hydrogen bonding interaction. B) shape memory mechanism of the SMPs with thermo-reversible H-bonding. Colored side-groups represent H-bonding groups in the hot (hollow) and cold (filled) states, and the darker lines represent the lightly crosslinked covalent network. [133]

2.1.4 Two-way shape memory effect based on anisotropic chain conformation change

Many applications of SMPs require reversible two-way shape memory effect otherwise the shape memory behaviour is not reversible without external deformation force. All the above three types of shape memory effect is one-way shape memory effect. Researchers have made great efforts to prepare SMPs with two-way shape memory effect. Ahir [136], Qin and Mather [137] observed two-way shape memory effect in liquid-crystalline polymers. Ahir et al.[138] prepared a self-assembled two-way shape memory fiber of a triblock liquid-

crystal polymer using the telechelic principle of microphase separation in triblock copolymers. The large central block is made of a main-chain nematic polymer which has large spontaneous elongation along the nematic director. The effective crosslinking is established by small terminal blocks formed of terphenyl moieties, which phase separates into semicrystalline micelles acting as multifunctional junction points of the network. The resulting transient network retains the director alignment and shows a significant two-way shape memory effect. Reversible nematic-isotropic transition of the polymer causes contraction at heating and elongation on cooling. Unfortunately, the switching temperature of liquid-crystal polymers is still very high which is above 100°C so that they are not suitable for textile product applications.

2.1.5 Two-way shape memory effect based on cooling-induced crystallization elongation

Chung et al. [139] studied the shape memory effect of a semicrystalline network poly(cyclooctene) (PCO). A set of crosslinked PCO films was prepared with different concentrations of dicumyl peroxide as a crosslinking agent. The cooling-induced crystallization of crosslinked PCO films under tension (not for deformation of a secondary shape) led to significant elongation, and subsequent heating to melt the network caused contracting. This two-way shape memory effect was affected by the crosslinking density of the PCO network and the stress applied to stretch the PCO chains at high temperature. For this two-way shape memory effect, finite external stress was required.

2.1.6 Shape memory effect by in-direction heating

A certain level of electrical conductivity of SMPs can be reached by incorporating electrical conductive ingredients into SMPs. When a current passes through the conductive ingredient network within SMPs, the induced Joule heating may raise the internal temperature to above the switching transition temperature of the polymer to trigger shape recovery [140-144]. The conductive ingredients which have been used as conductive fillers include carbon nanotubes, polypyrrole (PPy) [145-147], carbon black, short carbon fiber [21, 148-153].

Light absorbed by a deformed SMP can also increase SMP temperature to trigger shape recovery [154-156]. To improve light absorbing efficiency, dyes such as indocyanine green and Epolight 4121 [156, 157], carbon blacks and carbon nanotubes may be used in SMPs [33, 34, 140].

By employing ferromagnetic fillers in SMPs, magnetic-responsive SMPs were also prepared. SMPs recovered their original shape as a result of electromagnetic field induced heating [36, 158-165].

2.1.7 Shape memory effect of polymeric gels

Various polymeric gels have been developed, which are responsive to temperature [166], pH values [167], solvents, light intensity/wavelength [168, 169], ionic strength [170], magnetic field [4], electrical field [171], and pressure [172]. Among the stimuli-responsive polymeric gels, temperature and pH-responsive hydrogels are the most extensively studied ones because of their significant applications in physiological, biological and biomedical areas for human use.

Thermal-responsive polymeric hydrogels (TRPGs) are three-dimensional macromolecular gel networks containing a large fraction of water within their structures [173, 174]. TRPGs change their volume significantly in response to temperature change by increasing or decreasing their degree of swelling at below and above a critical temperature respectively which is called the lower critical solution temperature (LCST) [175, 176].

The most widely studied TRPG is poly(N-isopropylacrylamide) (PNIPAAm) hydrogel. PNIPAAm hydrogels have a well-defined LCST in aqueous medium at around 32~34°C which is close to the human body temperature for medical applications [177-180]. At the temperature below the LCST, hydrogen bonding between hydrophilic segments of the polymer chains and water molecules dominates, leading to enhanced dissolution and swelling in water. At the temperature above the LCST, the hydrophobic interaction among hydrophobic segments is high, while the hydrogen bonding is less. The final result yields in the shrinkage of TRPGs due to the hydrophobic interactions. Recently, it was found that PNIPAAm had moderate cytotoxicity [181]. Researchers have developed copolymer P(MEO₂MA-co-OEGMA) composed of 2-(2-methoxyethoxy)ethyl methacrylate (MEO₂MA) and oligo(ethylene glycol) methacrylate (OEGMA) as an ideal substitute of PNIPAAm [182, 183].

In addition to TRPGs, pH-responsive hydrogels (PRPGs) are also widely studied due to their physiological significance. PRPGs such as chitosan [184] and poly(vinyl alcohol) (PVA)/poly(acrylic acid) (PAA) hydrogels [185] usually have weak acid or alkaline groups in them, such as carboxyls or amino respectively [186]. TRPGs and PRPGs have been used in smart textiles [187-

200], tissue scaffolds [201], molecular recognition [202], bio-microelectromechanical system devices [171], gene delivery vectors [203], drug carriers and delivery media [204], artificial muscles [205], chemical valves [171], immobilization of enzymes [206] and cells [207], and bioseparation [208-211].

2.2 Shape memory polyurethanes (SMPUs)

Foremost among SMPs, SMPUs have been mostly studied and commercially applied [16, 70, 212]. SMPU may be synthesized from three starting materials: long chain polyol, diisocyanate, and chain extender. Diisocyanate and chain extender forms the hard segment and the long chain polyol forms the soft segment. Also SMPU may be synthesized with two kinds of long chain polyols coupled with diisocyanate where one polyol with a higher thermal transition acts as the hard segment and another polyol acts as the soft segment [17, 213-215].

The shape memory effect of SMPUs is due to the thermodynamic incompatibility of soft segments (aliphatic polyether or polyester) and hard segment (aromatic diisocyanates and small size diols or diamines). The hard segment phase has a higher thermal transition temperature (T_{perm}), while the soft segment phase has a lower phase transition temperature (T_{trans}) which can either be a glass transition (T_g) or a melting transition (T_m) temperature. When the SMPU is deformed at a temperature (T_{high}) and cooled to a temperature (T_{low}) below T_{trans} , the temporary deformation can be set. If the same polyurethane is reheated up to a temperature above the T_{trans} , the original un-deformed shape recovers due to the entropy elasticity [115, 216-226]. SMPU differentiates itself

from conventional polyurethane by a prominent glass transition (T_g type) or melting transition (T_m type) at around or slightly above ambient temperature [70].

The switching temperature of SMPU films is tailor-able and can be adjusted to around body temperature. SMPU films have a wide range of applications due to their shape memory features, good processability and molecular design flexibility. The good processability and tailor-bale mechanical properties of SMPUs make them suitable for textile finishing and spinning to fabricate smart textiles with self-adaptability to body and environmental temperature.

2.3 SMPUs in film forms

Basing on the melting or glass transitions as the switching temperature of the SMPU films, SMPU films fall into T_m type SMPU and T_g type SMPU. In T_m -type-SMPU films, a high crystallinity of soft phase and a stable hard segment phase are the two conditions for the SMPU films to show good shape memory effect [80]. Kim *et al.* [227] developed a series of T_m type SMPUs with MDI and BD as the hard segment while PCL diols as the hard segment. The T_m of hard phase was found to locate in the range of 200-240°C; and the T_m of soft segment phase was in the range of 44 and 55°C, which was influenced by the hard segment content and the PCL molecular weight. The research of Li *et al.* [228, 229] shows that the SMPUs with high molecular weight PCL diols and high hard segment contents produce the good shape memory properties. Furthermore, a stable hard phase is essential when the deformation temperature is above the T_m of soft segment phase. At a low hard segment content such as 10

wt%, the T_m type SMPU film can not show shape memory effect because no hard segment domains can form as such a low hard segment content.

Many T_g type SMPU films with low soft segment molecular weight and high hard segment contents have also been developed. In general, the T_g value increases with increasing of hard segment contents and decreasing soft segment molecular weight. To get a switching temperature above room temperature, the hard segment content of T_g type SMPU films is usually above 55%. Hayashi et al. [230] first studied the shape memory effect of T_g type SMPU films which were produced by Mitsubishi Heavy Industries.

Lin *et al.* [62, 231] developed PTMG (poly(oxytetramethylene)glycol) based SMPU films with the MDI and BDO as the hard segment.. In the PTMG-250 serial SMPU films, the T_g increased from 16°C to 54°C with increasing hard segment content from 57% to 95%. In the PTMG-650 serial SMPU films, the T_g increased from -13°C to 38°C with increasing hard segment content from 32% to 87%. The similar increasing trend of the T_g was observed on PTMG-1000 based SMP films.

2.4 Phase change materials based on SMPUs

Human body has the most comfortable temperature at every part of skins. When the temperature of the skin differs more than 3.0°C from the ideal temperature, the human body feels uncomfortable [232, 233]. It would be most ideal, if at high temperature the excess heat a person produced could be stored in the clothing system and then release again when he starts to get chilly. Phase

change materials (PCMs) that have been used to regulate temperature fluctuations have this function [234-237].

A great number of organic, inorganic, and polymeric PCMs have latent heat-storage properties [232, 233, 238-245]. In the temperature-regulating clothing system, the phase transition temperature should be in the range of 10-50°C [239, 246-249]. The phase change temperature of several kinds of material is in this interval, such as hydrated inorganic salts, polyhydric alcohol mixture (water solution), PEG, polytetramethylene glycol, aliphatic polyester, linear chain hydrocarbon, hydrocarbon alcohol and hydrocarbon acid [250-253].

PEG is a mostly studied solid-liquid phase change polymeric material. It has a melting temperature from around 3.2°C to 68.7°C and a very high phase change enthalpy depending on its molecular weight [233, 234, 239]. Several research groups [240-242] have made great efforts to prepare solid-solid PCMs, by employing PEG as phase change ingredient and another skeleton forming ingredient to keep the material in a solid state after the melting of PEG.

Zhang et al. [253, 254] prepared fibers of PEG/polypropylene, poly(ethylene terephthalate) and ethylene-vinyl acetate by controlling suitable spinning parameters and component contents. The PCMs prepared via physical blending have a tendency to lose their phase change characteristics after several heating-cooling cycles due to the loss of PEG. Jiang et al. [255] developed a network solid-solid PCM with rigid polymer cellulose diacetate (CDA) serving as a skeleton, and the PEG as a branch chain. However, because of the covalent network structure of the PEG grafted CDA, the material is not fit for fiber preparation. More recently, Li et al. [256] prepared a novel PEG/MDI (4,4-

diphenylmethane diisocyanate)/pentaerythritol crosslinking copolymer via the condensation reaction of PEG with tetrafunctional pentaerythritol isocyanate. The phase transition enthalpy was more than 100 J/g with a transition point at 58.68°C. Unfortunately, this material is prepared by solution polymerization and using DMF as solution, which is harmful for the environment and human body. In addition, the material has the same problem of not fitting for fiber fabrication.

In this project, with PEG as the soft segment of polyurethane, a temperature-regulating fiber is prepared. The shape memory effect of polyurethane arises from the so-called micro-phase-separated heterogeneous structure which is composed of the hard segment phase and soft segment phase. The temperature-regulating fibers also show obvious shape memory effect.

2.5 Multiwalled CNT (MWCNT)/SMPU composites

Conventionally, the shape memory effect of SMPs is induced by directly heating the polymer to a temperature above the switching temperature. It has been demonstrated that the shape recovery of SMPs can be achieved by Joule heating after the SMPs are filled with conductive fillers such as carbon black and carbon nanotubes [144, 257].

Another disadvantage of SMFs compared with SMAs is lower recovery stress though SMFs have the advantages of low cost, good processability, high deformability, high shape recoverability, soft mechanical properties and tailorable switching temperature [67, 258-261]. Furthermore, because a glass transition or melting transition is employed as the “switch”, the mechanical

properties of the SMFs decrease severely at around the switching temperature. One of the immediate methods to improve the recovery stress of SMFs may be by reinforcing SMFs with different kinds of fillers. It has been shown CNTs are excellent nano-fillers of polymer matrix to prepare nanocomposites with advanced properties [64, 262-282].

Many research groups have conducted research on polymer reinforcement by employing CNTs [262-267, 280, 281, 283, 284]. Generally, efforts to improve CNT dispersion in polymer matrix include the use of micro-scale twin-screw extruders, surfactants and the oxidation or chemical modifications of CNT surfaces. Thostenson and Chou [285] utilized a micro-scale twin-screw extruder to obtain the high shear mixing necessary to disentangle MWCNTs and disperse them uniformly in a polystyrene thermoplastic matrix. Hou et al. [286] prepared polyacrylonitrile nanofibers containing a high concentration of MWCNTs. The spinning solution of polyacrylonitrile and MWCNTs in DMF was very stable. They ascribed the high stability of the polyacrylonitrile-MWCNTs-DMF to the high interaction between the molecules of solvent DMF and the MWCNT surface. For conventional elastic CNT/polyurethane systems, Kwon and Kim [287] and Jung et al. [265] improved the compatibility of MWCNTs with elastic polyurethane matrix by treating MWCNTs with 60% nitric acid. Chen and Tao [288] prepared polyurethane composites with aligned single walled CNTs by dispersing CNTs in polyurethane solution with tetrahydrofuran as a solvent. They reported that the solvent-polymer interactions served as a driving force for the macroscopic alignment of the CNTs. There has also been one report on the CNT/SMPU system. Ni et al. [232, 233] distributed CNTs in SMPU solution using an ultrasonic process. The influence of CNTs on the shape fixity and

recovery ratios was studied. The composite showed excellent shape recoverability.

In this project, MWCNTs were incorporated into SMFs by *in-situ* polymerization after MWCNT were treated by a mixture solvent of concentrated sulfuric acid and nitric acid. The electro-active shape memory effect of the MWCNT/SMPU fiber was studied. The influence of MWCNTs on shape recovery stress of the SMF was discussed.

2.6 Biomedical applications of SMPUs

The biomedical applications of SMPs for smart medical devices are of great interest to scientists and engineers. A few smart medical devices have been invented from SMPs by different research groups around the world. Langer and Lendlein et al. [17, 33, 34, 45, 215] used SMPU which is both compatible with the body and biodegradable to produce coronary stents. Such stents can be compressed and fed through a tiny hole in the body into a blocked artery. Then, the warmth of body can trigger the polymer's expansion into its original shape. Instead of requiring a second surgery to remove the material, the polymer would gradually dissolve in the body. Another example is a biodegradable SMP suture developed by MnemoScience [17, 40, 41]. This suture can tie itself into a perfect knot in the body after being applied to wounds. It can be used to seal difficult wounds where access is limited. A third example is a laser or magnetic activated shape memory device for the mechanical removal of blood clots [35-37, 156, 157]. The device can be compressed into a small temporary shape and inserted by minimally invasive surgery into a blood vessel. Upon laser or magnetic activation the device coils into its predetermined (original) corkscrew

shape, which enables the removal of blood clots. A forth biomedical application of the SMPs is aneurysm coils for the treatment of intracranial aneurysm in place of platinum coils [39]. The deployed SMP coils inside aneurysm dome are stable and do not migrate within the cavity compared with conventional platinum coils which have the possibility of re-opening as a result of the bio-inertness of platinum. Also, shape memory foams have been proposed to be used to help overweight patients lose weight. Due to the fact that an implanting foam will inflate at the body temperature in the stomach, the foam provides the patients with a feeling of satiety [91, 92]. Also, SMP foams have been proposed to be used to deliver drugs to treat disorders and diseases in the stomach or intestine [19, 93]. In addition, an orthodontic appliance is invented using SMPs. The shape memory appliance is inserted equally into the marrow cavities of both sections of a broken or incised bone. The SMP for bone fixation can recover the original molded article in the shape of a thick and round bar and comes in close contact with the inner faces of the marrow cavities [42-44].

SMFs and fabrics in the special forms may find promising applications as biomedical materials due to their soft structure and permeability. For biomedical application, it would be ideal if the shape recovery can be triggered by human body temperature. The internal temperature of human bodies is 36.5°C with fluctuation below 1.5°C [289]. The switching temperature of SMPUs is tailor-able from about -50 to above 100°C by varying soft segment and hard segment types and contents. Especially, adjustment of the switching temperature of T_g type SMPUs is more feasible due to the fact that the T_g of SMPUs can be regarded as a mixed glass transition temperature of the hard segment phase and soft segment phase [290]. Therefore, a T_g type SMPU is synthesized with

suitable switching temperature by solution polymerization and a corresponding SMF was fabricated with potential biomedical applications.

The evaluation of animal responses to the fiber is important in determining the fiber capacity for a clinical situation. Specific requirements may differ according to the nature of applications. In this project, the biological evaluations of the prepared fiber are preliminary conducted in terms of cytotoxicity, haemolysis, sensitization and dermal irritant.

CHAPTER 3 EXPERIMENTAL

This chapter includes synthesis of SMPUs, preparation of SMFs and characterization techniques used in the study. T_m type and T_g type SMPUs are synthesized and corresponding SMFs are fabricated. Shape memory hollow fibers and CNT/SMPU fibers are fabricated. SMFs which may have potential biomedical applications are spun. The characterization techniques in the study are described in the chapter.

3.1 Material and equipment

The main raw materials used in this project are tabulated in Table 3.1 with the suppliers' information. The main equipments used in the study are shown in Table 3.2.

Table 3.1 Raw materials used in the synthesis of SMPUs

Chemical	Abbreviation	Supplier
Poly(ϵ -caprolactone)	PCL	Daicel Chemical Industry
4,4-diphenylmethane diisocyanate	MDI	Aldrich Chemical Company
1,4-butanediol	BDO	Acros Organics
N,N-dimethylformamide	DMF	Jax Finechem (NZ) Ltd
Polyethylene glycol	PEG	International Laboratory
Ethylene glycol	EG	Sigma-Aldrich Chemical Company
Poly(butylene adipate)	PBA	Aldrich Chemical Company

Table 3.1 Continued

Polystyrene	PS	Polymer Laboratories (Varian, Inc.)
Multiwalled carbon nanotube	MWCNT	Chengdu Organic Chemicals Co., Ltd of Chinese Academy of Sciences

Table 3.2 The main equipment used in the project

Equipment	Supplier
Cryo-ultramicrotome-Frigocut 2800E	Leica Inc.
Davenport Melt Flow Index	Fareham, UK
Diamond Differential Scanning Calorimeter	Perkin-Elmer Inc.
Diamond Dynamic Mechanical Analyzer	Perkin-Elmer Inc.
Digital camera	Pixera Corporation, Japan
Fourier Transform Infrared Spectroscope-2000	PerkinElmer Inc.
Haake Minijet	Thermo Electron Corporation
Instron 4411	Instron Corporation, USA
Instron 4466	Instron Corporation, USA
Field-emission Scanning Electron Microscope- JEOL JSM-6335F	JEOL Ltd.
JM-500ZGX Vacuum Drying oven	Jinma Electronic Light Technological Research Institute, China

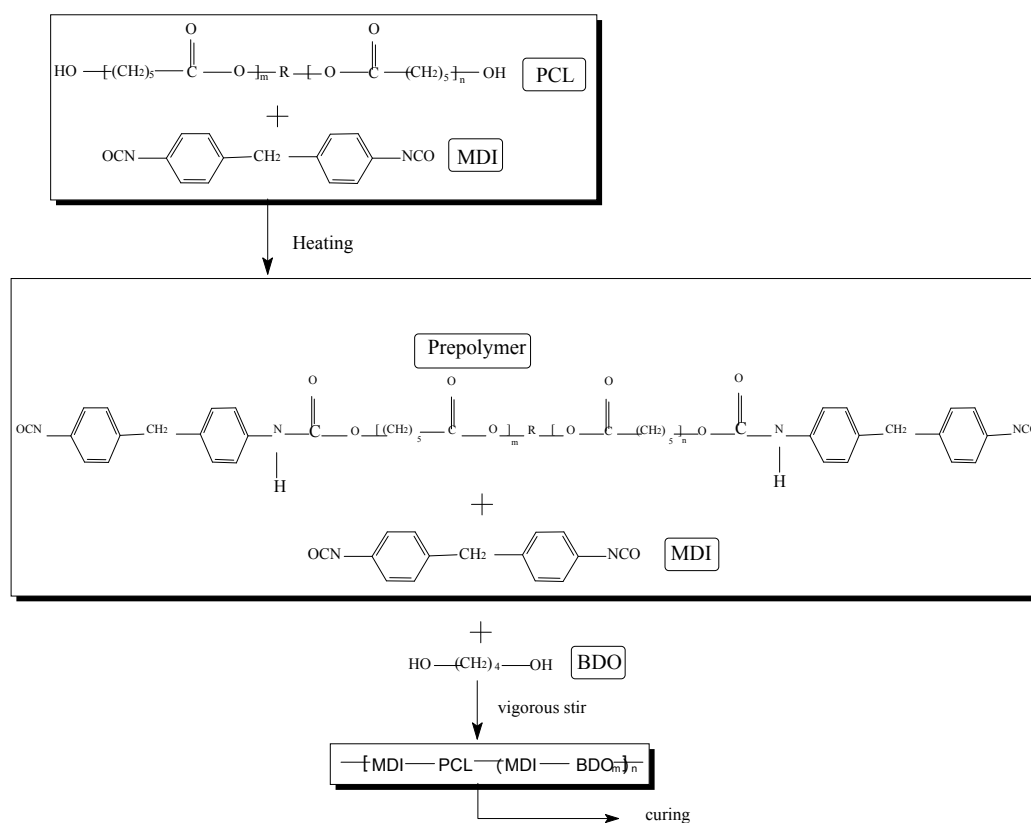
Table 3.2 continued

Scanning Electron Microscopy-Leica Stereoscan 440	Leica Camera AG Corporation
Melt Spinning Equipment	Self-designed
Micro-water Analyzer CHY-8	Donghua University, China
Muffle Furnace	Carbolite Corporation
Polarizing Optical Microscope	Ernst Leitz Wetzlar, Germany
Scanning Probe Microscope	Seiko Instruments Inc.
Single-screw Extruder	Qichang Plastic Processing Machine Company, China
Small Angle X-ray Scatter	Bruker Corporation
Three-roller Drawing Unit	Alex James & Associate, Inc. USA
Tricolab Type Machine (single jersey machine)	Tricolab, France
Twin-screw Extruder	Thermo Electron Corporation
Ultrasonicator	Shanghai Sheng PU Ultrasonic Equipment Factory
Vacuum Oven	Sheldon Manufacturing, Inc.
Waters Gel Permeation Chromatography	Water Corporation
Wet Spinning Equipment	Self-designed
Wide Angle X-ray Diffraction	Philips Corporation

3.2 Preparation of T_m type SMFs

3.2.1 Synthesis of T_m type SMPUs

The polyurethane was synthesized using MDI (4,4'-Diphenylmethane diisocyanate) and BDO (1,4-butanediol) as the hard segment. PCL diol was dried and degassed at 80°C under 1-2 mmHg for 12 hours prior to use. Extra pure grade of MDI was melt at 50°C without further treatment. BDO was dried by molecular sieves beforehand. The polyurethane was prepared by the pre-polymerization technique as shown in Equation 3.1.



Equation 3.1 Illustration for the pre-polymerization of SMPUs

Pre-polymers were prepared by terminating PCL with excessive MDI at both ends [225, 291]. Then the remaining MDI was added. BDO was added during

the last stage. The polyurethane was further cured for 24 hours. To protect against hydrolysis, a carbodiimide (acid acceptor) type antihydrolysis agent was added to SMPUs. To protect against thermal degradation, a phenolic phosphite type stabilizer (reducer of oxidized free radical) was used. The number molecule weight of the prepared SMPU was 127,128 Daltons with a polydispersity index 1.34.

3.2.2 Preparation of SMFs

The PCL-based polyurethane chips were prepared using a single-screw extruder. The chips were dried in a vacuum oven for 12 hours to decrease the relative humidity to below 100 ppm tested using a Micro-water Analyzer before spinning. The SMFs were fabricated using a 20 cm single-screw extruder spinning machine. The spinning temperature was 210°C.

3.2.3 Heat treatments

SMFs underwent heat treatments on a three-roller drawing unit. The schematic representation of the heat treatment process is shown in Figure 3.1. The temperature of the three rollers was the same. Filaments were wound up at a relaxation state without external stress. The specimens were denoted as SMF-X°C, i.e. SMF-65°C, SMF-85°C, SMF-105°C, SMF-125°C, where X was the heat treatment temperature. To make a comparison, the as-spun SMF is designated as SMF-22°C (22°C ambient temperature). After heat treatments, the samples were stored at a constant temperature and humidity laboratory (temperature: 22°C, relative humidity: 61%) for 7 days before the properties were investigated.

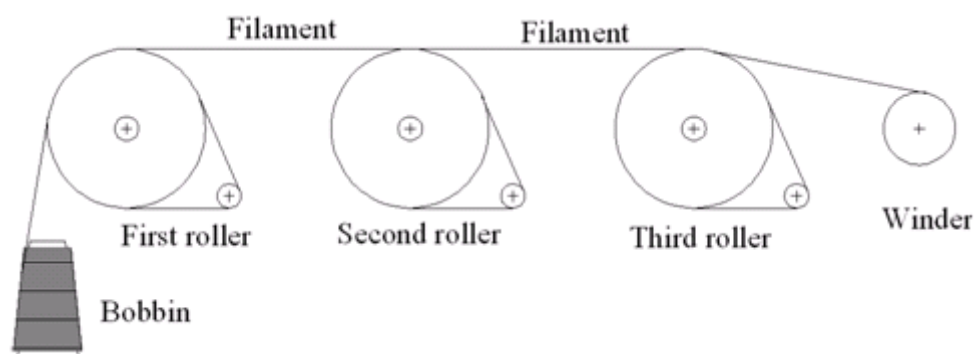


Figure 3.1 The schematic representation of the heat treatment process

3.3 Preparation of T_m type SMPU hollow fibers

3.3.1 Synthesis of T_m type SMPUs

The polyurethane was synthesized using PCL as soft segment, MDI and ethylene glycol (EG) as the hard segment by bulk polymerization. PCL diol was dried and degassed at 70°C under 1–2 mmHg for 12 hours prior to polyurethane synthesis. Extra pure grade of MDI was melt at 50°C without further treatment. EG was dried by molecular sieves beforehand. The polyurethane was prepared by the pre-polymerization technique [70, 117, 226, 292]. Pre-polymers were prepared by terminating PCL with excessive MDI on both ends at 80°C for half an hour. EG was added during the last stage. Then the polyurethane was further cured at 100°C for 24 hours. The obtained polyurethane has an M_n of 1.42×10^5 with a polydispersity index 1.29.

3.3.2 Preparation of SMPU hollow fibers

Before spinning, the polyurethane was dried in an oven to reduce moisture content to less than 100 ppm tested using a Micro-water Analyzer. The smart

hollow monofilament was spun using a laboratory spinning machine. The melt spinning temperature was 210°C. The cross-sectional shape of the nozzle hole in the spinneret is shown in Figure 3.2. The quench temperature was the ambient temperature. The winding speed was 100 m/min. The shape memory hollow fiber is named TRHF (Thermal-responsive hollow fiber).

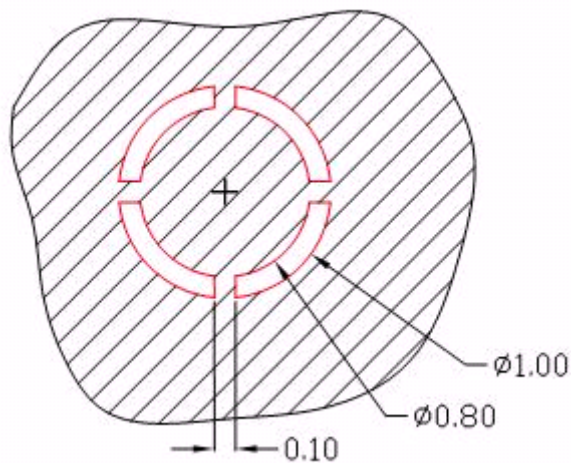


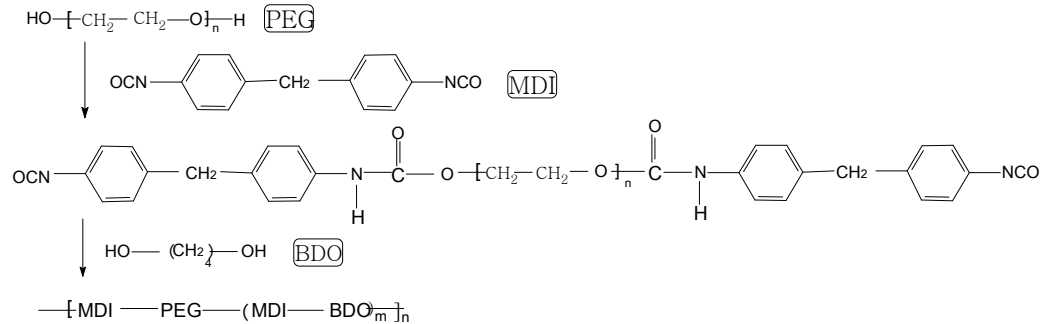
Figure 3.2 Cross-sectional shape of the nozzle hole in the spinneret (unit: mm)

3.4 Preparation of temperature-regulating SMFs

3.4.1 Synthesis of temperature-regulating SMPUs

The PEG-based linear chain polyurethane was synthesized using PEG as the soft segment, MDI and BDO as the hard segment. The polyurethane was prepared by the pre-polymerization technique [225, 291]. Pre-polymers were obtained by terminating PEG with excessive MDI on both ends at 80°C for half an hour. BDO was added at last. The schematic synthesis route is shown in Equation 3.2. Polyurethane chips were prepared using a single extruder. The

obtained polyurethane had an M_n of 1.65×10^5 with the polydispersity index 1.49.



Equation 3.2 Synthetic scheme of the PEG polyurethane

3.4.2 Preparation of temperature-regulating SMFs

Before spinning, the polyurethane was dried in a vacuum oven to reduce polymer moisture content to less than 100 ppm tested using a Micro-water Analyzer. The temperature-regulating fiber was spun using a laboratory spinning machine. The fibers are named TRSMF (temperature-regulating SMF).

3.5 Preparation of MWCNT/SMPU fibers

3.5.1 Modification of MWCNTs

The MWCNTs have an outer diameter of 10-20 nm, inner diameter 5-10 nm, and $\sim 50 \mu\text{m}$ in length. They were used after being treated by a mixed solvent of 70% nitric acid and 98% sulfuric acid (1.0: 2.5 by volume) according to reported literature [287] to improve the interfacial bonding with polyurethane matrix. Figure 3.3 shows the schematic of the surface treatment of the MWCNTs. The mixture solvent with MWCNTs was heated to 140°C and kept for 10 minutes (with mechanical stirring). Then an ultrasonicator with a power

of 100 W and nominal frequency 50 kHz was used to distribute the MWCNT in the mixed solvent for 1 hour. The treated MWCNTs were collected by a glass filter (pore size= 500 nm) after being washed with sufficient distilled water repeatedly. The collected MWCNTs were desiccated in a vacuum oven to remove the residual moisture. they were stored in a desiccator containing phosphorous pentoxide prior to use.

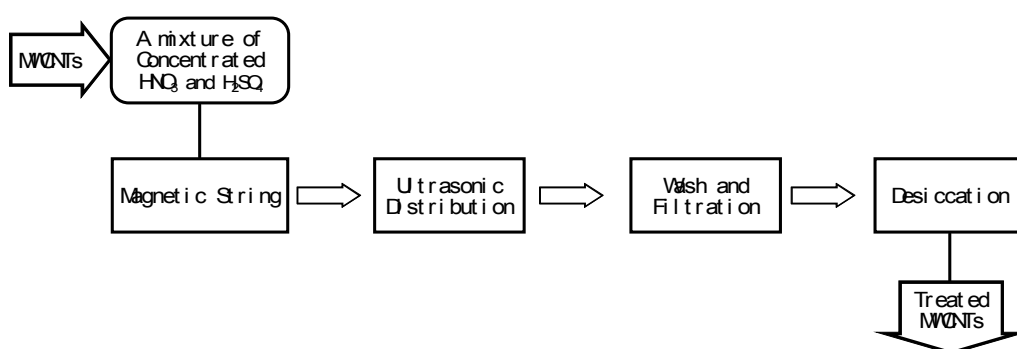


Figure 3.3 Schematic for preparing the MWCNTs

3.5.2 Synthesis of MWCNT/SMPU composites

The SMPUs were synthesized using PCL as the soft segment while MDI and molecular extender BDO as the hard segment. PCL diol was dried and degassed at 80°C under 1-2 mmHg for 12 hours prior to polyurethane synthesis. BDO was dried by molecular sieves beforehand. A calculated amount of modified MWCNTs were pre-distributed in HPLC (High performance liquid chromatography) grade DMF. While keeping the MDI melt at 80°C, it was subject to vigorous stirring for half an hour and ultrasonic vibration for 1 hour. The SMPU was prepared by pre-polymerization. CNT/SMPU chips were prepared using a twin-screw extruder. The obtained polyurethane had a number

average molecular weight of 137,000 Daltons with a polydispersity index of 1.65.

3.5.3 Preparation of MWCNT/SMPU fibers

MWCNT/SMPU monofilaments were spun by using a laboratory melt spinning machine. The composite chips were dried in a vacuum oven at 80°C for 12 hours. A spinneret with a single 0.4mm hole was used.

3.6 Preparation of SMFs for biological evaluation

3.6.1 Synthesis of T_g type SMPUs

DMF was used in the polyurethane synthesis as the solvent. It was dehydrated with 4 Å molecular sieves for two days prior to being used. The polyurethane was synthesized by the pre-polymerization method using PBA (poly(butylene adipate)-600 (Mn) as the soft segment, while MDI and BDO as the hard segment [115, 293]. The solid concentration of the spinning solution in DMF was 25 wt%. The switching temperature of the SMPU was tuned by changing the hard segment phase (MDI+BDO) content.

3.6.2 Preparation of T_g type SMFs

The polyurethane solution was extruded through 30 spinneret capillary holes to prepare SMFs by wet spinning. The polyurethane filaments were wound with at a speed of 20 m/min. In order to release the internal stress caused by the velocity difference among rollers in the drying and winding process, the fibers were subject to saturated water vapor treatment under around 200 kPa for 10 minutes.

3.6.3 Fabrication of shape memory fabrics

A fabric of SMFs was knitted by using a Tricolab type machine. The machine gauge was 25 needles per inch. The course of the fabric was 30 wales per centimeter and the wales are 28 courses per centimeter.

3.7 Preparation of SMPU films

Polyurethane films were prepared by solution casting. Polyurethane was first dissolved in DMF at a solid concentration of 15 wt%. Then the solution was cast into a polytetrafluoroethylene mold (inner dimension: 5×30 mm). In order to make pinhole free films, the solvent was evaporated at 60°C for 12 hours in 50 Pa vacuum and the residual solvent was removed at 80°C for another 12 hours. The thickness of the prepared films was about 0.5 mm.

3.8 Characterization techniques

3.8.1 Molecular weight test

The molecular weight of the SMPU samples was assessed using a Waters gel permeation chromatography (GPC) system equipped with a refractive index detector (Waters 2414 refractive index detector) and a UV detector (Water 2489 Uv/Visible Detector) equipped with a Waters Styragel HR4 (for DMF) column. A Waters 1515 Isocratic HPLC pump was used. The refractive index obtained by the Waters 2414 refractive index detector was employed for data analysis. The solvent used was high performance liquid chromatography DMF. It was ultrasonicated before use to get rid of trifle bubbles which may affect the refractive index. The temperature of the column and refractive index detector was 30°C. The standard calibration curve was obtained by using

narrow distributed polystyrene-medium molecular weight calibration kit provided by Polymer Laboratories. The flow rate was 1.0 mL/min. The concentration of the standard samples and polyurethane samples were prepared in DMF at a concentration of about 0.25-0.1% following the column specification. The number-average (M_n) and weight-average (M_w) were determined and the polydispersity index was calculated for each polymer using a Breeze GPC soft ware.

3.8.2 FTIR spectrometry

The FTIR transmission and reflection spectra were determined by using a Perkin-Elmer spectrometer in the region of 700–4000 cm^{-1} at the ambient temperature. The SMFs were cut into small sects to make KBr tablets. Each sample was scanned 30 times at a resolution of 2 cm^{-1} and the scan signals were averaged. The FTIR spectra of shape memory bulks were obtained by using a Perkin-Elmer universal accessory. To make a comparison, all IR spectra were normalized by using the height of the 1412 cm^{-1} peak, assigned to the C—C stretching mode of the aromatic ring [292, 294, 295].

3.8.3 Melt flow index

The melt flow index (MFI) was tested with a Davenport melt flow indexer MFI-10. Samples were pre-heated in a barrel held at 210°C for 6 minutes. The test was conducted five times and averaged on each polymer melt.

3.8.4 Capillary rheological measurement

Capillary rheological measurements were performed using a Ceast rheologic 5000-twin bore capillary rheometer. The barrel diameter was 15 mm. The die was 1 mm in diameter with a slenderness ratio 30. The preheat time was set as 120 seconds. No correction was applied to the data. The SMPU was dried in a vacuum oven at 100°C for 10 hours to reduce moisture content to less than 100ppm tested using a Micro-water Analyzer.

3.8.5 Mechanical property test

The fiber tenacity was tested with the tensile tester Instron 4411 following the standard ASTM D2256. The sample gauge length between clamps was 20 mm and the stretching speed was 300 mm/min. Fiber cross-section areas were measured from the cross-sectional photos taken by using an optical microscope (X 400 times). Film samples of $60 \times 5 \times 0.5 \text{ mm}^3$ in dimension were cut out from the cast films. The sample gauge length was 20 mm. To make a comparison with the shape memory fiber, the film tensile strength was also measured following the specification of ASTM D-2256, where the stress unit was cN/dtex while not MPa. For fibers, the tensile speed was 10 mm/min and load cell 5 N. For films, the tensile speed was 10 mm/min and load cell 2.5 kN. Measurements on each sample were repeated 10 times to obtain average values.

3.8.6 Thermomechanical cyclic tensile test

Thermomechanical cyclic tensile testing was carried out using a tensile tester Instron 4466 equipped with a temperature controllable chamber. In the experiments, the fibers or films were heated to 70°C (T_{high}) to deform, and

cooled to ambient temperature (22°C) (T_{low}) to fix temporary elongation [14, 70]. Fiber samples were of 20 mm in gauge length.

(1) Drawing at high temperature (70°C) and thermal recovery (70°C)

The programmed thermomechanical cyclic tensile testing process is shown in Figure 3.4. The cyclic tensile testing path is shown in Figure 3.5(a). (1) The sample was first stretched to 100% elongation ratio at 70°C (T_{high}) at a drawing speed of 10 mm/min. (2) Subsequently, cool air was vented passively into the chamber to cool down the sample to 22°C and the temperature was maintained at the temperature for 15 minutes to fix the temporary elongation. (3) Then upper clamp was returned to the original position at a speed of 40 mm/min and the sample shrank from 100% to ϵ_u because of instant elastic recovery. ϵ_u is the strain after unloading at T_{low} . (4) Finally, the sample was heated to 70°C to allow the shape memory recovery with result sample elongation returned to ϵ_p . $\epsilon_p(N)$ is the residual strain after recovering in the N^{th} cycle. (5) After the cycle was completed, a second cycle began.

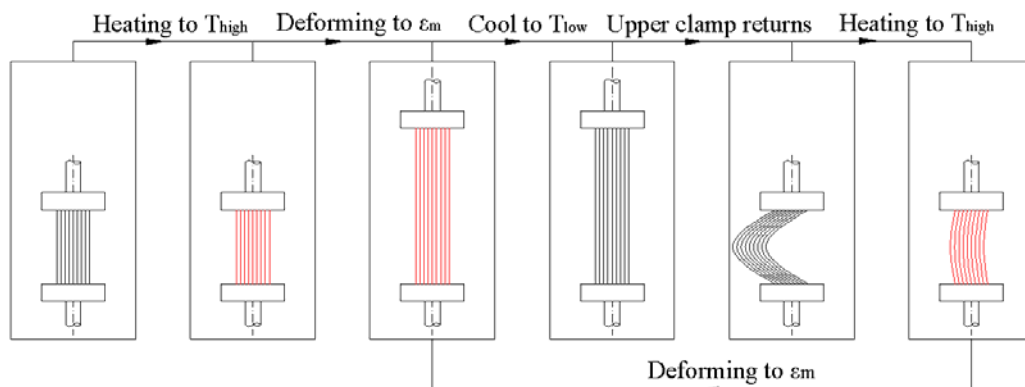


Figure 3.4 The thermomechanical cyclic tensile testing process of SMFs

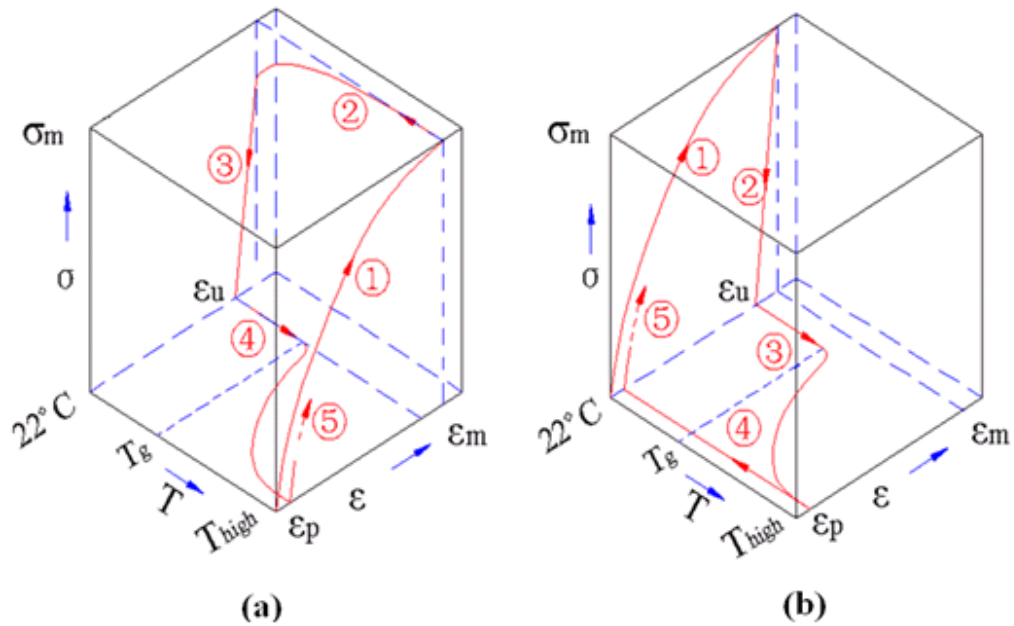


Figure 3.5 (a) Cyclic tensile testing path under drawing at high temperature and thermal recovery; (b) Cyclic tensile testing path under drawing at low temperature and thermal recovery

(2) Drawing at low temperature (22°C) and thermal recovery (70°C)

The cyclic tensile testing path under drawing at high temperature and thermal recovery is shown in Figure 3.5(b). (1) First, fibers were stretched to 100% strain at a speed of 10 mm/min at ambient temperature. (2) Second, the upper clamp was returned to the original position. (3) Third, the fibers were heated to 70°C to recover. (4) Forth, the fibers were cooled to ambient temperature and left for 5 min for heat balance. (5) The second cycle started.

The above cycle was repeated 4 times and the stress-strain were recorded for analysis. The schematic representation of typical stress-strain behaviors are shown in Figure 3.6(a) and (b). ϵ_m is the maximum strain in the cyclic tensile

tests. σ_m is the maximum stress at the maximum strain ϵ_m . ϵ_u is the strain after unloading at T_{low} , and $\epsilon_p(N)$ is the residual strain after recovering in the N^{th} cycle. The ϵ_m value is set at 100% strain for the study. The fixity ratio ($R_f(N)$) and recovery ratio ($R_r(N)$) at the N^{th} cycle and total recovery ratio (R_{r-tot}) after the N^{th} cycle are calculated according to following equations [14, 70].

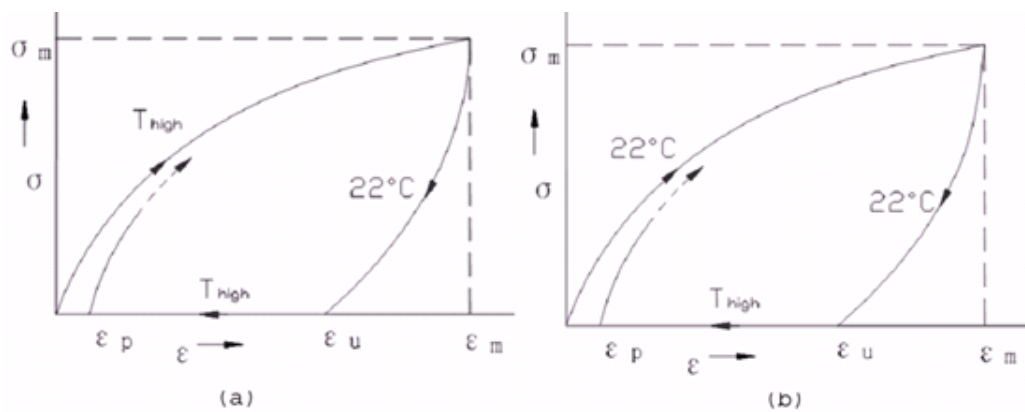


Figure 3.6 (a) Schematic stress-strain curves under drawing at high temperature and thermal recovery; (b) Schematic stress-strain curves under drawing at low temperature and thermal recovery

$$R_f(N) = \epsilon_u(N) / \epsilon_m \times 100\%$$

$$R_r(N) = (\epsilon_m - \epsilon_p(N)) / (\epsilon_m - \epsilon_p(N-1)) \times 100\%$$

$$R_{r-tot} = (\epsilon_m - \epsilon_p(N)) / \epsilon_m \times 100\%$$

3.8.7 Shape memory effect test of SMFs

The shape memory effect test of the SMFs for potentially biomedical applications was performed on an Instron 4466 tensile tester equipped with a self-fabricated temperature-controllable chamber. The schematic cyclic tensile testing path is quite similar with that of conventional shape memory test by drawing at high temperature and thermal recovery as shown in Figure 3.5(a) except that different recovery temperature was used. Since human body's internal temperature is around 36.5°C, the triggering temperature T_{high} was set at 36.5°C. The thermomechanical cycles for measuring the shape memory properties are as follows: (1) The fiber was first stretched to 100% elongation ratio at 36.5°C which is above the switching temperature (glass transition temperature) at a drawing speed of 10 mm/min [70, 226]. (2) Subsequently, cool air was vented passively into the chamber to cool the sample down to 22°C and the temperature was maintained for 15 minutes to fix the temporary elongation. (3) Then the upper clamp was returned to the original position at a speed of 40 mm/min and the membrane shrank from ε_m to ε_u because of instant elastic recovery. (4) Finally, the fiber was heated to 36.5°C to allow the shape memory recovery with result fiber elongation returned to ε_p . (5) After the cycle was completed, a second cycle began. The above cycle was repeated for 5 times.

3.8.8 Shape memory effect test of shape memory fabrics

The shape memory effect of the shape memory fabrics was characterized by bagging using self-fabricated equipment. The shape memory effect of the fabric was not determined by the thermomechanical cyclic tensile testing because the fabric selvedge may be destroyed during the testing process [296]. Bagging a

fabric into a 3D spherical shape can determine the fabric's performance simply by bag shape and height, although bagging a fabric into a 3D spherical shape involves complex deformations including tension, shearing, bending and compression. Figure 3.7 shows the schematic representation of the bagging and shape recovery testing process. A piece of round shape memory fabric with diameter 80 mm was used. The whole process took place in a temperature-controlled chamber. First, the fabric sample was fastened on the top of the circular bottom plate (diameter: 5 cm). Second, the chamber temperature was increased to 36.5°C and the fabric was deformed using the ball at a speed of 150 mm/min to form a crown of 5 cm height on the fabric. Third, fabric and ball temperature was cooled to the ambient temperature and the ball was retreated at a speed of 300 mm/min. After two minutes, the height of the bag was measured. Fourth, the chamber temperature was increased to 36.5°C and the bag height was recorded.

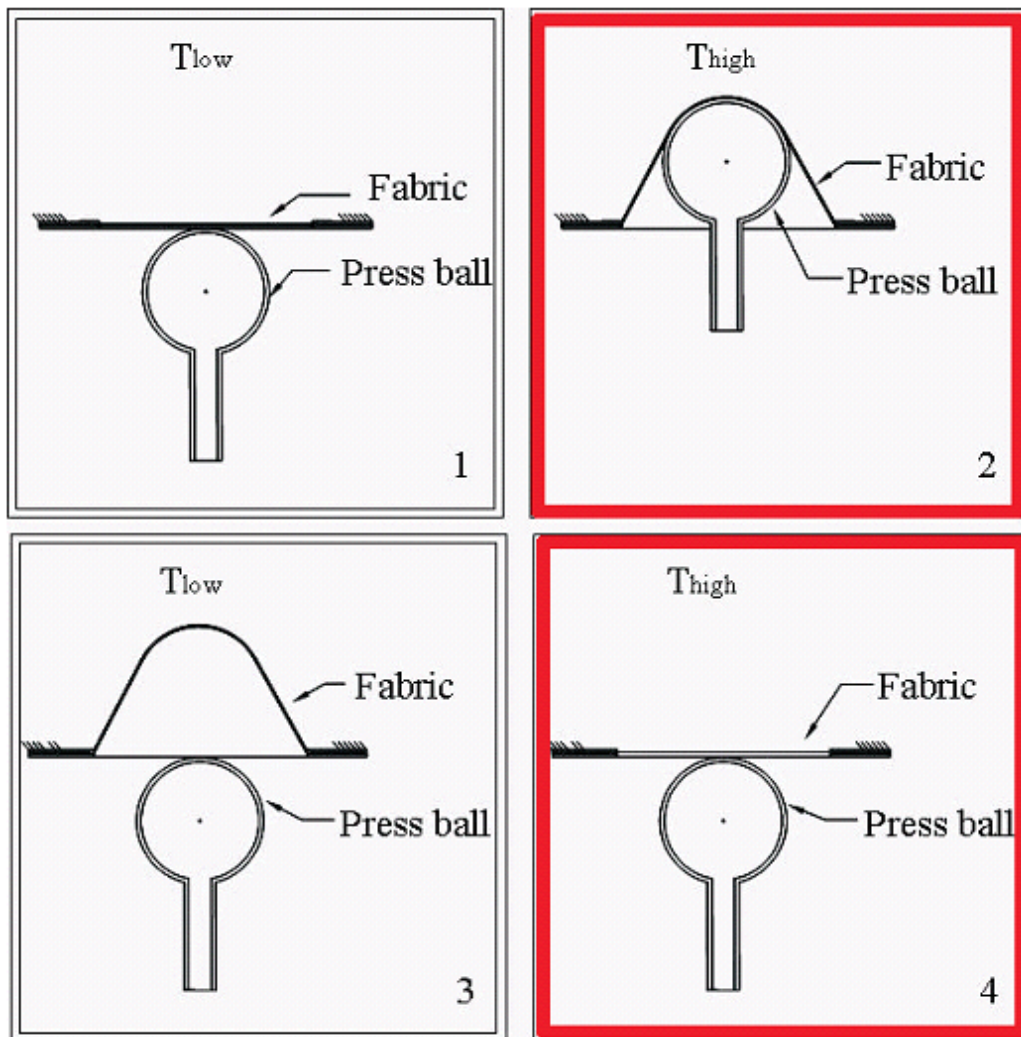


Figure 3.7 The bagging and recovery process of the shape memory fabric

3.8.9 Stress relaxation test

In characterizing shape memory behavior, the deformation is usually conducted at a temperature above the switching transition temperature because at a high temperature, polymer shows lower elastic modulus than that at an ambient temperature. However, in practice, the elongation deformation of SMF usually happens at ambient temperatures such as the wrinkles on cloth. Therefore, it is

very important to understand what degree the stress can be stored in the fiber after deformation at the temperature below the switching transition temperature (cold drawing). The stress relaxation tests were carried out on the Instron 4466. First, the fibers were stretched to 100% strain at a speed of 10 mm/min at an ambient temperature, and then the strain was kept for 15 minutes to record the stress relaxation for analysis. The sample gauge length was 20 mm.

3.8.10 Shape recovery stress test

The shape recovery stress tests were also carried out using the same equipment Instron 4466. First, the sample was stretched to 50% strain at a speed of 10 mm/min at ambient temperature and the strain was maintained for 10 minutes to fix the internal stress. Then the upper clamp was retreated to the position where exactly no force was applied to the sample. After 5 minutes, the temperature was increased to 70°C and the stress change versus time was recorded for analysis. The cN/dtex was also used as the unit of recovery stress because most of the test samples were in fiber forms. The linear density of the rectangular film is obtained similarly as that of the fibers by dividing the film quality by the film length.

3.8.11 Thermal-responsive inner diameter test

The hollow fiber cross-sections were taken using an optical microscope (U-TEX MODEL UT901) equipped with scale. One lattice was corresponding to 0.1 mm. Two kinds of stress were employed to deform the hollow fiber inner diameter; by stretching the hollow fiber in the fiber direction and by pressing the hollow fiber in the fiber transverse direction using forceps under an eye gauge. During

the stretch method, first, the hollow fiber original cross-section image was taken using the optical microscope; second, the hollow fiber was stretched to 200% elongation ratio in 65°C water to change inner diameter; third, the fiber was cooled in water at the ambient temperature to fix the temporary inner diameter and a deformed cross-section image was taken. Finally, the deformed fiber was put into hot water at 65°C again so that the fiber's inner diameter recovered and a recover cross-section image was taken. In the pressing method, first, the hollow fiber original cross-section images were taken using the optical microscope; second, the hollow fiber was pressed into flat in 65°C water to change inner diameter using forceps; third, the fiber was cooled in water at the ambient temperature to fix the temporary cross-section and a deformed cross-section image was taken. After that, the deformed fiber was put into hot water at 65°C again so that the fiber inner cross-section recovered and then an image of the recovery cross-section was taken.

3.8.12 Differential scanning calorimetry

The thermal properties of samples were determined using a DSC instrument with nitrogen as the purged gas. Spinning oil on the fibers was removed with methanol before testing. The heating rate was 10°C/min. When thermal properties of specific fiber was studied, the thermal history of samples was removed. When the influence of heat treatment on the properties of fibers was studied, the thermal history was not removed.

3.8.13 Wide angle X-ray diffraction test

The wide angle X-ray diffraction (XRD) data were recorded at a voltage of 40V, 30mA current with a radiation wavelength of 1.542 Å. Spectra were obtained in a range of Bragg's angle $2\theta = 10^\circ \sim 45^\circ$ with scanning step size 0.02° and time per step 1 second.

3.8.14 Dynamic mechanical analysis

The DMA test was operated in a tensile mode. The heating rate was $2^\circ\text{C}/\text{min}$, the frequency 1 Hz, and the oscillation amplitude $5.0\mu\text{m}$. The test was conducted over the temperature range from -120 to 200°C . The gauge length between the clamps was 15 mm. Modulus was usually calculated by the determined force, the cross-section area and the caused strain employed in testing specimens. If the cross-section area was used in the calculation of stress and modulus, then the units will be GPa or MPa. Melt spun fibers cross-sectional areas could be measured from the cross-sectional photos taken by using an optical microscope (X 400 times). However, for the wet spun fiber, the cross-section area which was not strictly regular was difficult to measure. Then the resulting data about the storage modulus was obtained by using linear density instead of cross-section areas similar to the calculation of fiber initial modulus in ASTM D2256. The unit of the storage modulus was N/dtex.

3.8.15 Atomic force microscopy

The phase separation morphology of the samples was observed using an atomic force microscope in the tapping-mode under an ambient environment ($22\pm 2^\circ\text{C}$,

45±5% RH). To prepare a section of a fiber, a small piece of fiber was first embedded in epoxy resin one day before the test. After the epoxy was completely solidified, the sample was trimmed to the shape of a pyramid, and its tip was cryo-ultramicrotomed with a diamond blade to form an observation section. NANOSENSORS™ PPP-SEIHR AFM probes (Seiko Instruments / high force constant) was used. The silicon cantilever spring constants was 15 N/m, length 225 um and resonance frequency 130 kHz. Height and phase images were recorded simultaneously.

3.8.16 Polarizing optical microscopy

A Leitz wetzlar polarizing optical microscope equipped with a Mettler FP 80 hot stage and a controller were used to observe the crystalline morphology. A digital camera was used to capture images in converging white light with analyzer and polarizer crossed. The fiber cross-section was obtained by using microtome. First, a monofilament was embedded in epoxy resin one day before test. After the epoxy was completely hardened, it was microtomed in the fiber transverse direction with a diamond knife (Micro Star Co.) and a Reichert–Jung Ultracut microtome (at the ambient temperature) .

3.8.17 Scanning electron microscopy

The fiber surface and fracture surface images were taken using a Leica Stereoscan 440 (SEM) Scanning Electron Microscopy operating at 20 kV and a JEOL JSM-6335F field-emission scanning electron microscope operating at 5kV. Composite film surface was etched by using DMF.

3.8.18 Small angle x-ray scattering

SAXS (small angle x-ray scattering) tests of SMFs, Elasthan fibers and shape memory films were conducted on the SAXS equipment Nanostar. The x-ray source was Cu K α and the wavelength was about 0.154 nm. Every sample was scanned in the range of 0.14° ~ 2.8° (2 θ) at a scanning rate of 0.05° min⁻¹.

3.8.19 FTIR dichroism

Among FTIR dichroism [224, 294, 297-299], birefringence [298], SAXS [58], wide-angle X-ray diffraction [300], and sonic modulus methods, FTIR dichroism measurement is one of the most effective methods to study the polyurethane molecular orientation because it can characterize the specific orientation of hard and soft segment phases of polyurethane. The orientation function of SMPU molecules was determined by using a Perkin-Elmer microscopy equipped with a diamond cryogenic Micro-ATR unit and an IR polarizer. The dichroic ratio of specific groups is calculated from relative intensity ratios of the selected bands of the infrared spectra obtained with the polarizer parallel (A_{\parallel}) and perpendicular (A_{\perp}) to the fiber direction. The spectrum dichroic ratio D is defined by the following equation [224, 298, 301, 302]

$$D = \frac{A_{\parallel}}{A_{\perp}}$$

The orientation function of the specific groups is calculated from the dichroic value [297, 298, 303-305]

$$f = \frac{(D_0 + 2)(D - 1)}{(D_0 - 1)(D + 2)}$$

where D_0 is the dichroic value of the perfectly oriented sample which can be calculated with the equation [294, 299, 300, 306]

$$D_0 = 2 \cot^2 \alpha$$

where α is the angle between the transition moment direction and polymer chain axis. In the analysis here, α is assumed to be 0° for backbone vibrations and 90° for vibrations of functional groups perpendicular to the polymer backbone [224, 300, 301, 306].

The orientation function of CH_2 which is a typical group of soft segments is related to the soft segment phase and is used to represent the orientation of soft segment phase. The orientation function of N-H which is a typical group of hard segments is related to the hard segment phase and is used to represent the orientation of the hard segment phase [298, 301]. The infrared spectra of the samples parallel and perpendicular to the fiber direction at the same point were obtained by tuning the polarizer at 0° and 90° respectively. Each sample was scanned for 300 times at a resolution of 2 cm^{-1} and the scan signals were averaged in the region of $750\text{--}4000 \text{ cm}^{-1}$.

3.9 Biological evaluations of SMFs

3.9.1 Cytotoxicity test

The cytotoxicity test was conducted by Intertek Testing Service Hong Kong Ltd following ISO 10993-5:1999, biological evaluation of medical devices: tests for cytotoxicity: in vitro methods. The test article was the shape memory fabrics; the negative control was saline; the positive control was natural latex rubber

sheeting. Three milliliters of L-929 mouse fibroblast cell suspension were placed into wells of six well, multiwell tissue culture plates, to prepare monolayers of cells. Following incubation, the culture medium was aspirated from the monolayers. The medium was replaced with serum-supplemented culture medium containing not more than 2% of agar. The agar layer was thin enough to permit diffusion of any leached chemicals. The test article and the negative and positive controls were placed, in triplicate cultures, so that they were in contact with the solidified agar surface. The test article was applied so that the shape memory fabric surface was in contact with the agar. All cultures were then incubated for not less than 24 hours in a humidified incubator at $37(\pm 1)^{\circ}\text{C}$ and $5(\pm 1)\%$ carbon dioxide. After incubation, an inverted microscope was used to examine each culture.

3.7.2 Haemolysis test

The haemolysis test was conducted by Intertek Testing Service Hong Kong Ltd following ISO 10993-4: 2002, biological evaluation of medical devices: selection of tests for interactions with blood. 15 g of the shape memory fabric was divided into three equal parts. Each part was added into test tubes respectively prior to use. Fresh anticoagulated rabbit blood was prepared by adding 10mL of fresh healthy rabbit heart blood with 0.5mL of 20 g/L potassium oxalate solution. The diluted blood was prepared by diluting 4mL of this rabbit blood with 5mL of 9% sodium chloride injection (SC). Three shape memory fabric tubes were added with 10 ml of SC; three negative control tubes were added with 10mL of SC (SC); three positive control tubes were added with 10ml of purified water. After all the tubes were incubated at $(37\pm 1)^{\circ}\text{C}$ for 30min,

each tube was added with 0.2ml of diluted rabbit blood and mixed gently, then incubated at $(37 \pm 1)^{\circ}\text{C}$ for 60min. The tubes were centrifuged for 5 minutes (2500 rpm), and the absorption of the supernatant fluid was measured at a test wavelength of 545 nm by spectrophotometer.

3.9.3 Sensitization test

The sensitization test was conducted by Intertek Testing Service Hong Kong Ltd with reference to ISO 10993-10: 2002, biological evaluation of medical devices: tests for sensitization. Ten hartley-strain guinea pigs, 341-394 grams, were utilized as the test group. An additional five (3male and 2 female) hartley-strain guinea pigs, 354-408 grams, were utilized as the control group. For induction, each animal in the test group received three, six hours topical applications of the test article, made once per week for three consecutive weeks. The control group animals were similarly dosed but without the test article. Two weeks after the last topical induction application, the challenge application was made. These six hours challenge applications were made to virgin sites on the flank of each animal in the test and control groups. Observations of erythema, edema and other effects were recorded 24 and 48 hours after the challenge applications. The test article, in one inch squares, was moistened with the physiological saline upon dosing.

3.9.4 Dermal irritant test

The dermal irritant test was conducted Intertek Testing Service Hong Kong Ltd with reference to ISO 10993-10:2002, biological evaluation of medical devices: tests for irritation. Three New Zealand white rabbits each received a single

dermal application of 25 mm x 25 mm of the test article on two test sites, both non-abraded. Each animal also had two negative control sites consisting only of gauze moistened with physiological saline. The test sites were semi-occluded for four hours and were observed individually for erythema, edema and other effects 5, 24, 48 and 72 hours after application. Mean score of control was subtracted from the mean score of test article to obtain the primary irritation index. The test article in one inch square was moistened with the physiological saline upon dosing.

CHAPTER 4 STUDIES OF GENERAL SMFs

A T_m type SMPU was synthesized and corresponding SMFs were fabricated. Polyester PCL was chosen as the soft segment instead of polyether because it is reported that PCL-based polyurethanes have comprehensively good properties. Small size diol BDO was selected as molecular extender instead of diamine because the diamines forming urea-urethane groups will increase the processing temperature of the polyurethane too high to be processed in a molten state [307]. The switching temperature of the obtained SMF was the soft segment phase melting temperature which was higher than ambient temperature [62, 63, 65, 308]. The stress-strain behavior and thermal/mechanical properties especially the shape memory effect of the SMF were investigated.

4.1 FTIR analysis

The SMPUs for melt spinning should have high thermal stability and relatively high molecular weight to obtain good mechanical properties. During the polyurethane synthesis, polyester poly(ϵ -caprolactone) PCL was chosen as the soft segment because it was reported that the PCL-based polyurethanes have comprehensively good properties [307]. Small size diol was used as molecular extender instead of diamine because the diamines forming urea-urethane groups increase the processing temperature of the polymer too high to be processed in a molten state.

According to International Chemical Safety Cards (ICSC International Programme on Chemical Safety 0298), inhalation of MDI will cause headache, nausea, shortness of breath, sore throat and contact with skin will cause redness.

The -NCO group of MDI has four characteristic IR peaks: $2260\text{--}2280\text{ cm}^{-1}$ because of asymmetry stretching vibration; $1375\text{--}1395\text{ cm}^{-1}$ because of symmetry stretching vibration; $600\text{--}650\text{ cm}^{-1}$ because of out-plane bending vibration; and $590\text{--}600\text{ cm}^{-1}$ of in-plane bending vibration. The peak at $2260\text{--}2280\text{ cm}^{-1}$ is prominent, which is frequently used to determine the existence of -NCO . The FTIR spectra of MDI and SMPUs at $2000\text{--}2400\text{ cm}^{-1}$ with increasing curing time at 110°C are presented in Figure 4.1. The main IR-band assignment of the SMPU spectra and the domain origin are tabulated in Table 4.1. It can be seen with increasing curing time, the area of the peak at $2260\text{--}2280\text{ cm}^{-1}$ decreases. After 22 hours cure, the peak almost disappears. In following experiments, SMPUs are usually cured for 24 hours at 110°C .

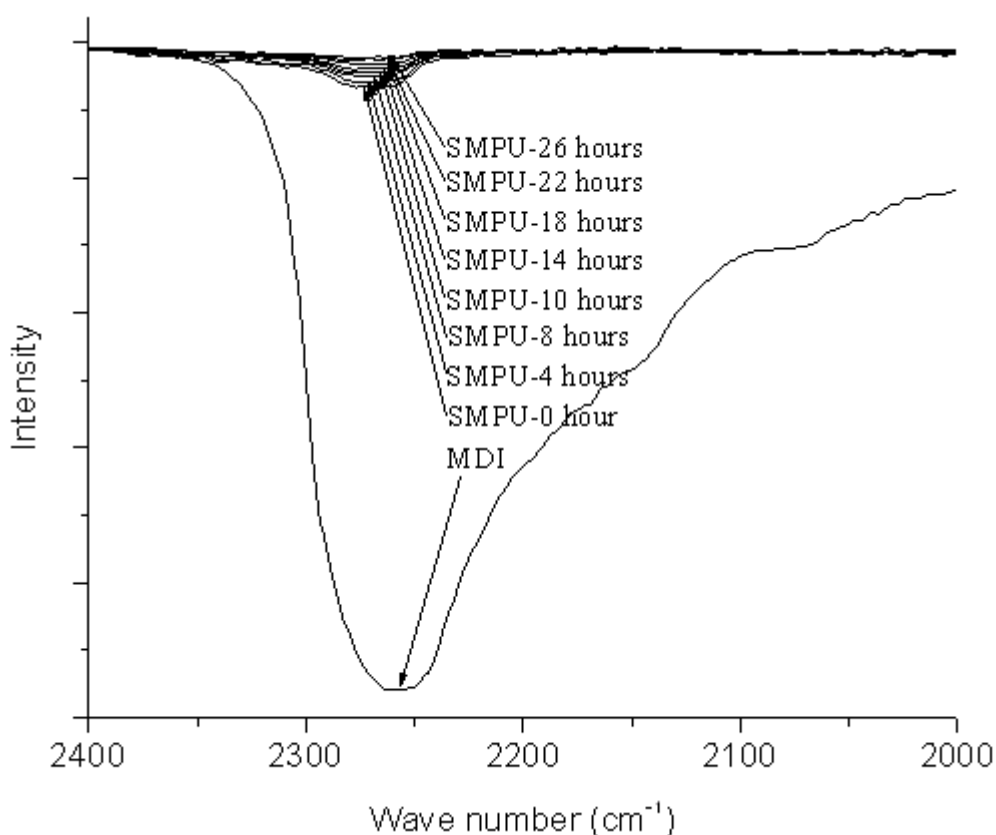


Figure 4.1 The change of -NCO FTIR intensity with increasing curing time

Polyurethanes do not show good thermal stability because of the labile urethane linkages and ester bonds. It is reported that the initial decomposition point of urethane formed by MDI and poly(ethylene adipate) is 227°C [309]. The decomposition of the SMPU yields diisocyanate and polyols. The MDI hard segment undergoes secondary reactions and produces more stable urea and isocyanurate structures [309]. SMPU is also prone to hydrolysis in the presence of very small amounts of moisture, yielding an amine and carbonic acid. The carbonic acid formed is very unstable and is decarboxylated immediately. As a result, the hydrolytic degradation products of a SMPU include amines, alcohols and carbon dioxide. At high temperatures, other types of degradation reactions are also possible. Therefore, to protect against hydrolysis, a carbodiimide (acid acceptor) type antihydrolysis agent was added to SMPUs. Therefore, to protect against thermal degradation, a phenolic phosphite type stabilizer (reducer of oxidized free radical) was used.

Table 4.1 Band assignment and domain origin

Energy (cm ⁻¹)	Assignment	Domain origin
3322	ν (N-H)	Hard
2952	ν (C-H)	Hard/soft
2939	ν (C-H)	Hard/soft
2850	ν (C-H)	Hard/soft
1726, 1702	ν (C=O)	Hard/soft
1612	phenyl ring mode 8a [301]	Hard
1596	phenyl ring mode 8b [301]	Hard
1524	ν (C-N)+ δ (N-H)	Hard
1412	phenyl ring mode 19b	Hard
1358	CH ₂ wag	Soft
1308, 1222	ν (C-N)+ δ (N-H)	Hard
1204	Phenyl ring mode a _g	Hard
1064	ν (C-O-C)	Soft
1018	Phenyl ring mode 18a	Hard

N=stretching, δ =in-plane bending

4.2 Shape recovery of SMP rods

The PCL based SMPU chips prepared by bulk polymerization are shown in Figure 4.2. The shape memory effect of the prepare SMP chips is demonstrated by using the SMP rod extruded from a single screw extruder. The shape recovery process of the SMP rod under thermal stimulation is shown in Figure 4.3. The SMP rod is first stretched (Figure 4.3 (a)) by hands after being extruded from the extruder before cooling down. A temporary length of the SMP rod is thus obtained (Figure 4.3 (b)). Then, the deformed SMP rod is put on a hot plate of about 100°C (Figure 4.3 (c)). The SMP rod recovers its original

length and shape rapidly within 1 minute (Figure 4.3 (c)-(f)).



Figure 4.2 PCL-based SMPU chips

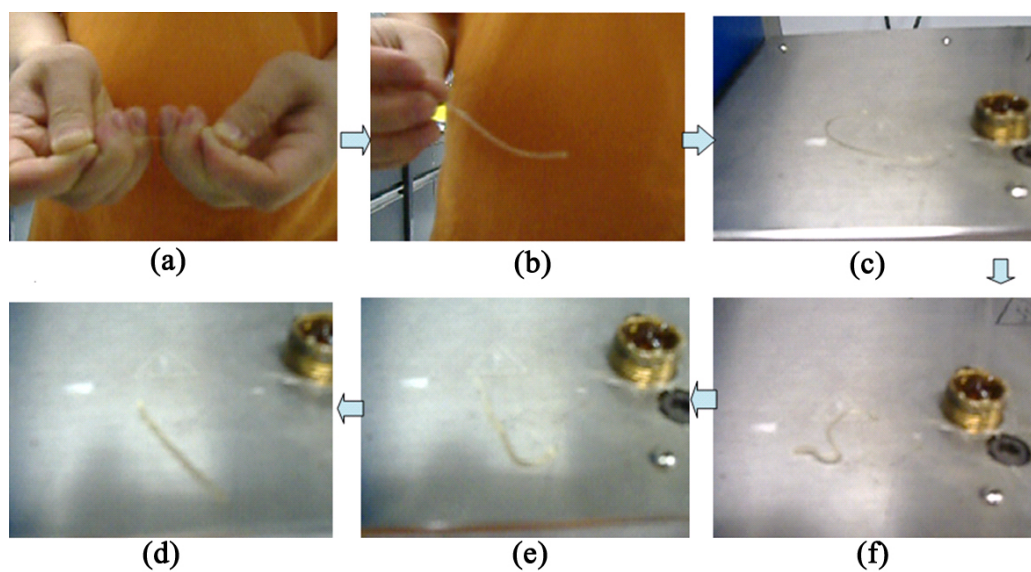


Figure 4.3 The shape recovery of the SMPU rod

4.3 Capillary rheological properties

The apparent shear stress τ , apparent shear rate γ , non-Newton index n and apparent viscosity η are calculated using the following equations.

$$\tau(Pa) = \frac{R\Delta P}{2L};$$

$$\gamma(s^{-1}) = \frac{4Q}{\pi R^3};$$

$$n = \frac{d \lg \tau}{d \lg \gamma};$$

$$\eta = \frac{4n}{3n + 1\gamma}$$

where R is the radius of the capillary, which is equal to 0.1 cm; L is the length of the capillary, which is equal to 3.0 cm in the study; ΔP is the pressure drop, Pa; and Q is the volumetric flow rate, ml/s. The value of melt apparent viscosity is calculated from the ratio of apparent shear stress to apparent shear rate.

The curves of viscosity vs. shear rate of the SMPU at different temperatures are shown in Figure 4.4. The polyurethanes show prominent shear thinning when the shear rate increases from 100 to about 3500 s^{-1} . The shear thinning is due to three reasons. First, the entanglement points of molecules decrease with the disentanglement and slippage of the molecules of the SMPUs; second, the molecule orientation caused by the shear stress decreases the energy required to drive the molecule layer movement; third, the molecules of SMPU degrade to some extent with increasing processing time and shearing speed. It can be seen

that processing temperature has strong affect on the viscoelastic properties of the SMPU. Raising the temperature by 10°C decreases the melt viscosity significantly especially at low temperature.

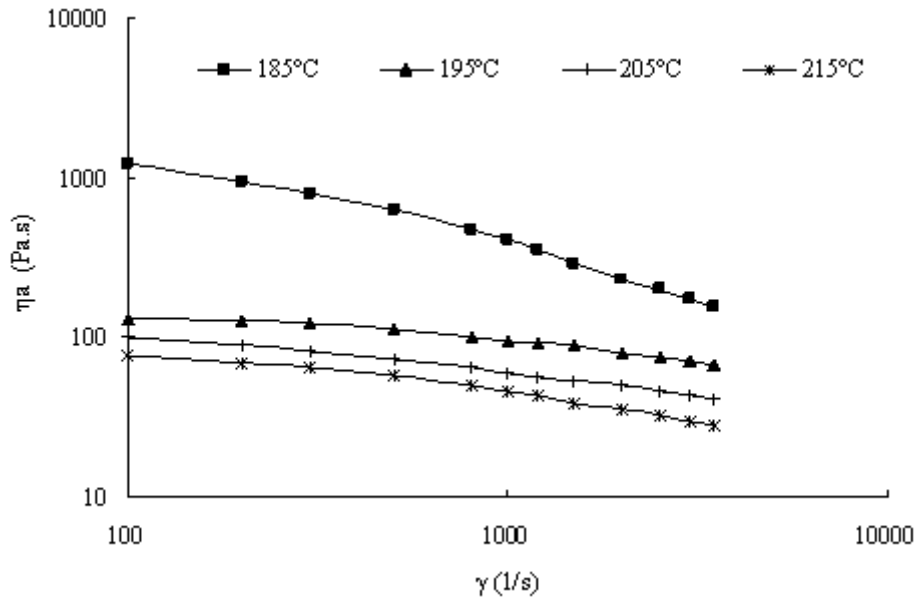


Figure 4.4 The relation between apparent viscosity η_a and shear rate γ at different temperature of the SMPU

The relation between $Lg\sigma$ and $Lg\gamma$ of the SMPU is shown in Figure 4.5 and the calculated non-Newton indexes at different temperatures are tabulated in Table 4.2. Presently no specific definition of the melt spinnability is available. The structural viscosity index ($\Delta\eta$) is employed to roughly evaluate the spinnability of polymer melts.

$$\Delta\eta = -\left[\frac{d \lg \eta}{d r^{1/2}}\right] \times 10^2$$

Where η is the apparent viscosity of polymers; and γ is the shear rate.

For polymer melts with shear thinning properties, in the non-Newtonian area, $\Delta\eta$ is above 0. The bigger the $\Delta\eta$, the worse the melt spinnability becomes. The structural viscosity indexes of the SMPU at different temperatures obtained from Figure 4.6 are shown in Table 4.3. It seems that the best spinning temperature is 195°C.

The spinning experiments of the SMPU were conducted at different temperatures from 195 to 215°C. It was found that at 195°C, the fiber could not be spun because of melt fracture. At 210°C, the SMPU had the best spinnability with a high spinning speed and a low filament breakage rate. During experiments, the influences of soft segment species, molecular weight, soft segment contents and phase separation on the spinnability of SMPUs were also evaluated during the spinning processes. It was found that long soft segment and high soft segment content decreased the spinnability. High phase separation brought bad melt spinnability. The spinnability of polyether-based SMFs is better than that of polyester-based SMFs.

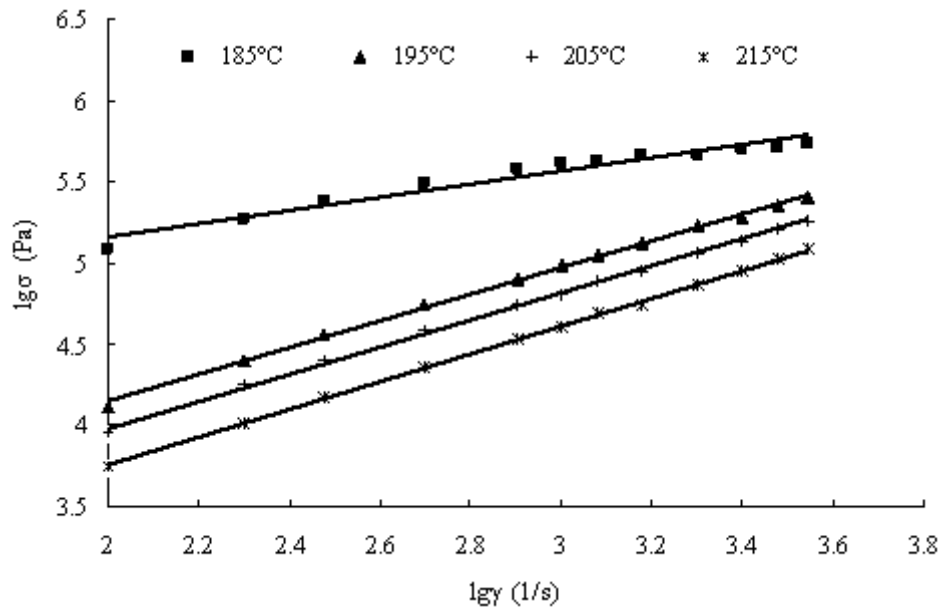


Figure 4.5 The relation between $Lg\sigma$ and Lgy of the SMPU

Table 4.2 The non-Newton index of the SMPU

Temperature	185°C	195°C	205°C	215°C
Non-Newton index	0.402	0.823	0.829	0.858

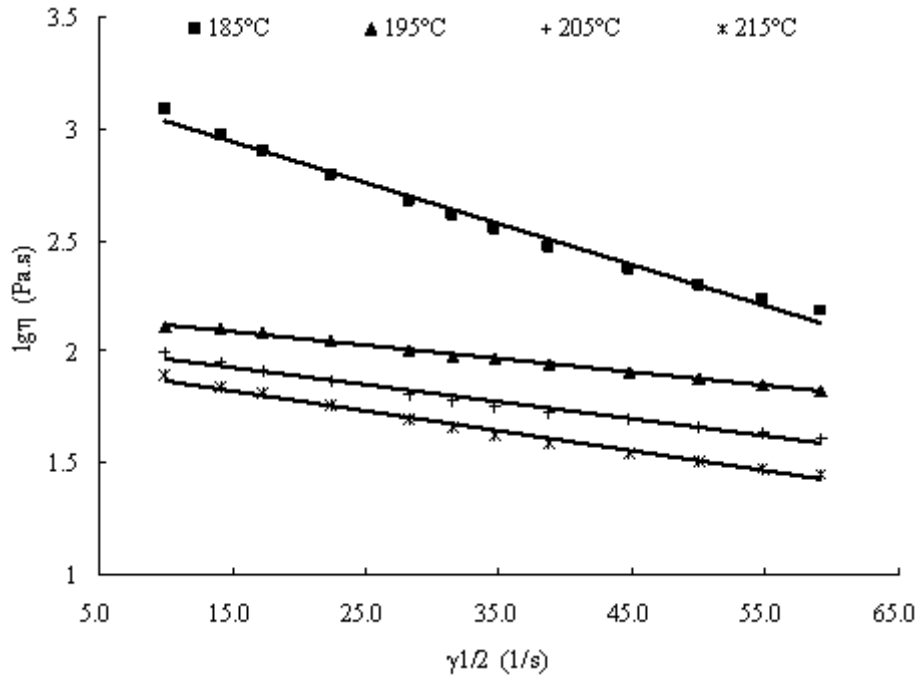


Figure 4.6 The relation between $\lg \eta$ and $\dot{\gamma}^{1/2}$ at different temperature of SMPUs prepared

Table 4.3 The structural viscosity index of the SMPU at different temperatures

Temperature	185°C	195°C	205°C	215°C
Structural viscosity index	1.84	0.60	0.77	0.91

4.4 Morphology of SMFs

From the SMP chips, PCL-based SMFs were fabricated by melt spinning. The prepared SMFs are shown in Figure 4.7.



Figure 4.7 PCL-based SMFs prepared by melt spinning

The SMF cross-section image taken using an optical microscope is shown in Figure 4.8. The SEM surface image of the SMF is shown in Figure 4.9. The cross-section of the SMF is round and the surface is smooth.

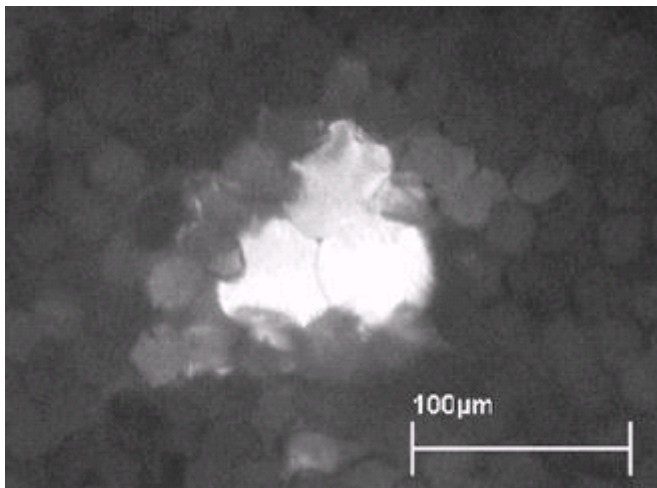


Figure 4.8 The cross-section of the prepared SMF (embedded in nylon filaments)

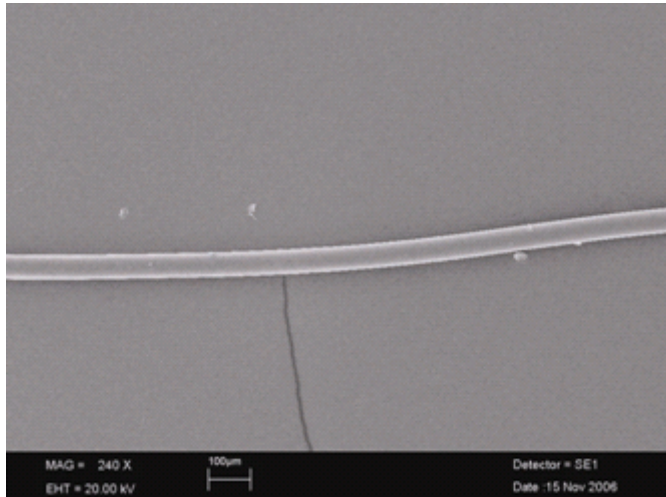


Figure 4.9 The surface image of the prepared SMFs

4.5 Mechanical properties

The prepared SMF has a tenacity of about 1.0 cN/dtex, and the strain at break 562 ~ 600%. The tenacity is acceptable to textile applications in most circumstances. In comparison with most other manmade fibers such as Polyester and Nylon, the mechanical strength of SMF is lower. Polyester and Nylon usually have high tenacity above 3.0 cN/dtex and low breaking elongation ratios. The mechanical properties of Polyester and Nylon fibers are attributed to their higher overall orientation, strong intermolecular bonding in polyamide and the high crystallinity of the molecular chain in polyester [310]. However, for the SMF which shows high shape fixity ratios and shape recovery ratios, the elongation at break is much higher compared with that of Polyester and Nylon. The mechanical properties of SMF can be further improved using the pre-polymer crosslinking method or pre-end-capping method which have been applied in melt spinning of commercialized polyurethane elastic fibers [311].

4.6 Shape memory properties

(1) Drawing at high temperature and thermal recovery cyclic tensile properties

The stress-strain behaviors of the SMF by drawing at high temperature and thermal recovery cyclic tensile testing are shown in Figure 4.10. The data of the fixity ratio, recovery ratio and stress at 100% strain are tabulated in Table 4.4. The SMF has a fixity ratio of more than 84% and recovery ratio up to 95%. The recovery stress at 100% elongation is about 2 times of that of SMPU without molecule orientation [49, 54, 312]. The significant difference between the first thermal cycle and the remaining cycles is partially because of reorganization of fiber molecules involving molecule orientation, crystallization, or weak point broken during elongation. After one cycle, the stress-strain behaviors become very similar. Figure 4.10 suggests that the SMF cannot fix the temporary elongation completely while cooled from T_{high} to ambient temperature. The instant elastic deformation recovers once the external stress is released. It can be deduced that the fixity ratio can be improved by increasing the crystallinity of the soft segments. Also, the SMF can not recover its original length completely because of the molecular slippage and breakage during the fiber cyclic elongation.

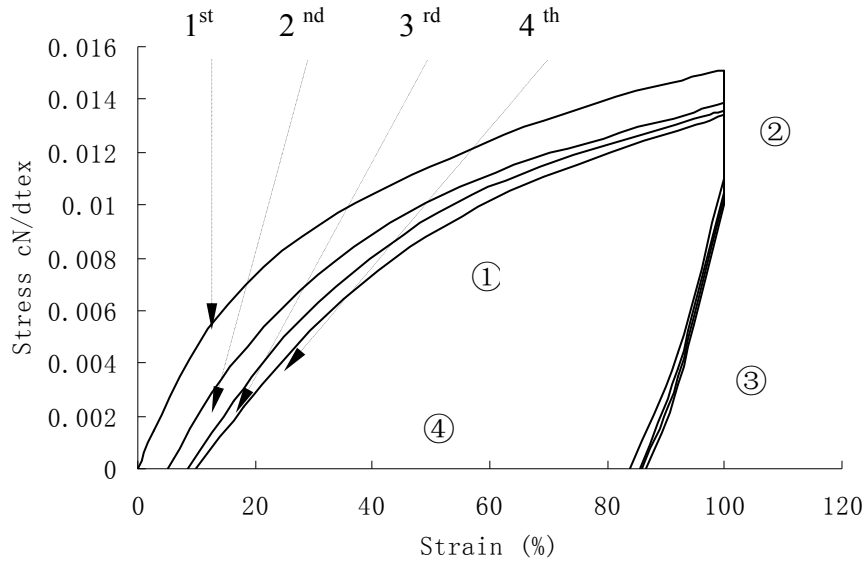


Figure 4.10 Cyclic tensile curves of the SMF under drawing at high temperature and thermal recovery

Table 4.4 Cyclic tensile properties of the SMF under drawing at high temperature and thermal recovery

Cycle No.	$\epsilon_p(N)$	ϵ_u ($R_f(N)$)	Stress at 100% strain(cN/dtex)	$R_{r,tot}(N)$	$R_r(N)$
1	0.0%	84.0%	0.0152	100.00%	
2	5.0%	85.5%	0.0139	95.00%	95.0%
3	8.6%	86.0%	0.0136	91.40%	96.2%
4	10.0%	86.5%	0.0134	90.00%	98.5%

The shape memory mechanism of the SMF can be illustrated as follows. During melt spinning, at a temperature which is higher than T_{perm} , the fiber is extruded from spinneret. Upon cooling to ambient temperature which is below T_{trans} , the fiber is winded up and the permanent fiber shape is cast. The model in Figure 4.11 can be employed to illustrate the shape memory effect of the SMF. In

Figure 4.11, zig-zag represents coiled or folded chains of polyols, black points represent isocyanate groups. In the unstretched state, the fiber has their molecules slightly oriented with some crystallized soft segments. The hard segments are still but have a tendency to adhere each other through strong hydrogen bonding. When the fiber is heated to 70°C which is above the soft segment phase melting temperature (T_{trans}), the soft segments are in a random state. When it is stretched, the soft segments are extended. If the temperature is cooled to below T_{trans} , the soft segments crystallize. As a result, the internal stress is stored in the fiber and associated deformation is fixed temporarily. If the SMF is reheated to above T_{trans} , the soft segments become flexible. Consequently, the soft segments resume to the folded configuration with the release of the internal stress stored among the hard segments. As a result, the SMF recovers its original length.

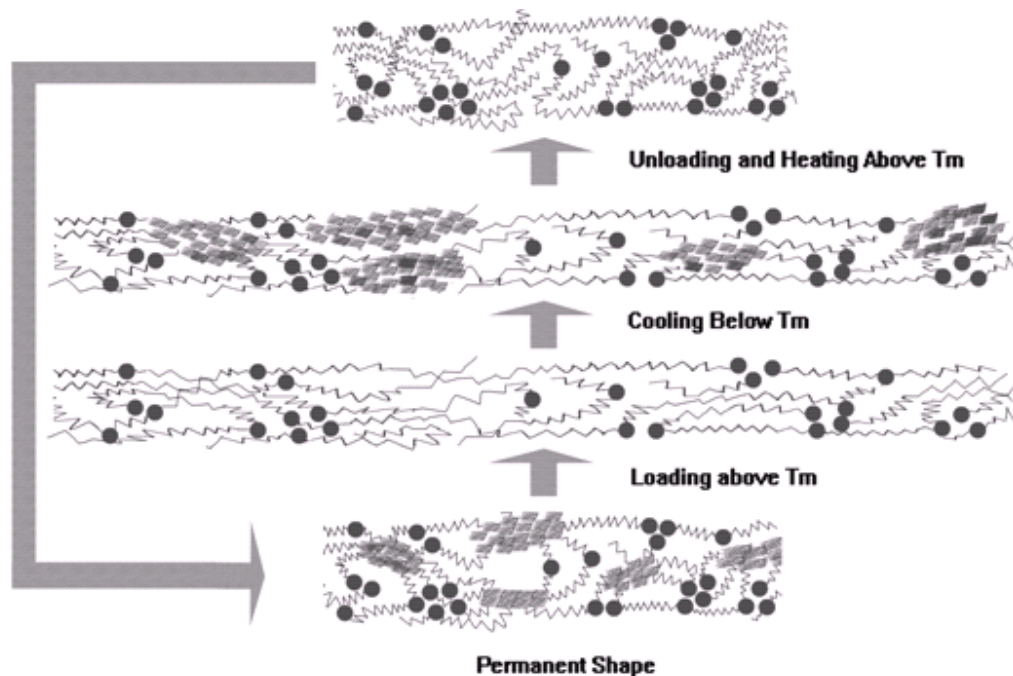


Figure 4.11 The molecular mechanism of the shape memory effect of the SMF

(2) Drawing at low temperature and thermal recovery cyclic tensile properties

When characterizing the shape memory effect of SMPs, the deformation is usually conducted at temperature higher than the switching transition temperature because at the high temperature the deformation is easy to be developed. However, in practice, the deformation in SMFs, such as the creation of crease on the cloth, usually happens at the ambient temperature. Therefore, the drawing at low temperature and thermal recovery testing was conducted to study the shape memory effect in SMFs. The drawing at low temperature and thermal recovery cyclic tensile curves of the SMF are shown in Figure 4.12. The data of fixity ratio, recovery ratio and stress at 100% strain are summarized in Table 4.5. The SMF also has high shape recovery ratios about 95%. The fixity ratios are about 55% which is much lower compared with those of SMF tested by drawing at high temperature and thermal recovery.

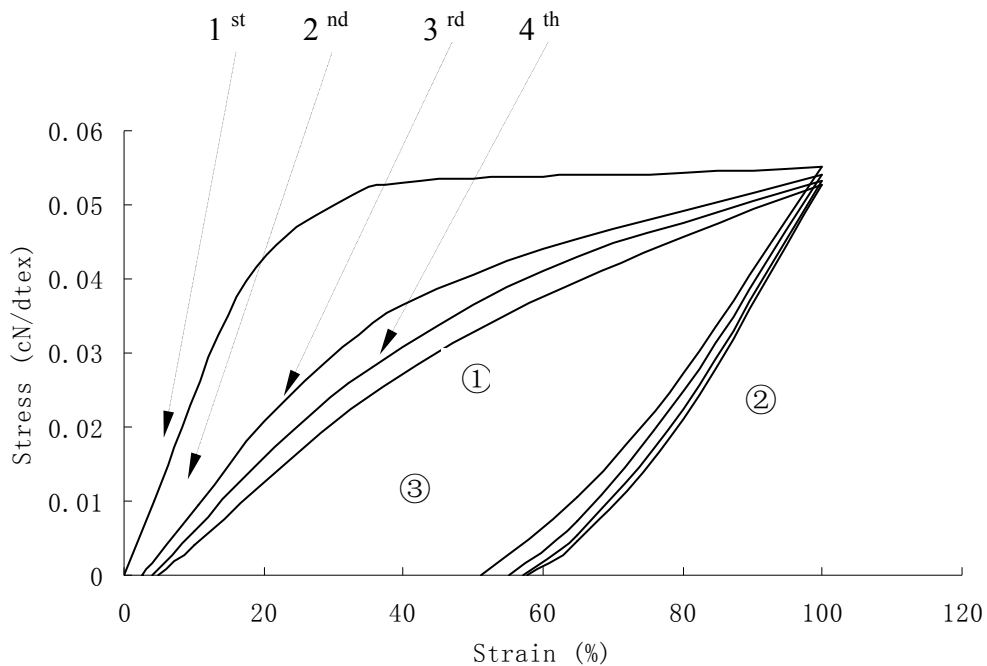


Figure 4.12 Cyclic tensile curves of the SMF under drawing at low temperature and thermal recovery

Table 4.5 Cyclic tensile properties of the SMF under drawing at low temperature and thermal recovery

Cycle No.	ϵ_p (N)	ϵ_u (R _f (N))	Stress at 100% strain(cN/dtex)	R _{r,tot} (N)	R _r (N)
1	0.00%	51.00%	0.0550	100.00%	
2	2.50%	55.00%	0.0540	97.50%	97.5%
3	4.00%	57.00%	0.0533	96.00%	98.5%
4	5.00%	57.50%	0.0527	95.00%	99.0%

4.7 Thermal properties

The DSC results of the SMF are shown in Figure 4.13. The melting temperature and crystalline enthalpy are tabulated in Table 4.6. The soft segments of the SMF show a melting transition at 47°C; the hard segments display a moderate endothermic peak at about 215°C. The crystallinity of the soft segments in the SMF is 14.42%, which is calculated from the enthalpy data ΔH of the crystallization peak using the 140 J/g enthalpy value for fusion of 100% crystalline PCL [292, 313].

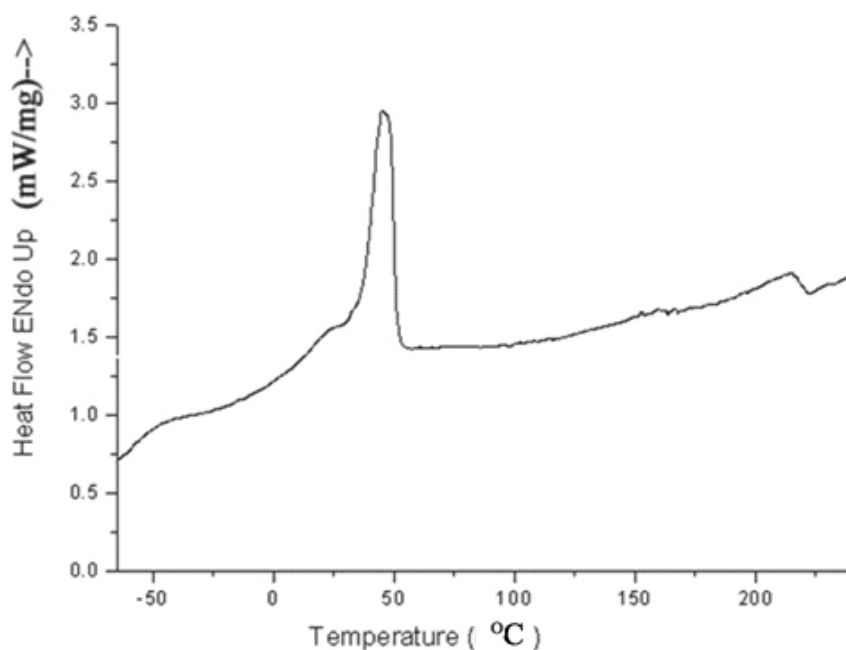


Figure 4.13 DSC analysis of the SMF

Table 4.6 Results of DSC analysis of the SMF

		Value
Soft segment	T_m (°C)	47.02
	ΔH (J/g)	20.19
Hard Segments	Endothermic peak (°C)	214.54
	ΔH (J/g)	1.286

At ambient temperature, the soft segments are partially crystallized. As a result, the fiber is not completely elastic. It can be deduced that the shape memory effect of the SMF can be improved by increasing the soft segment crystallinity; however this is in the expense of the elasticity of the SMF.

4.8 Summary

A SMPU was prepared by using PCL as the soft segment, while MDI and BDO as the hard segment. A corresponding SMF was fabricated by using the SMPU. The switching transition temperature of the SMF was the PCL segment phase melting temperature at 47°C. The mechanical properties, shape memory effect, and thermal properties of the SMF were studied. The prepared SMF had a tenacity of about 1.0 cN/dtex, and strain at break of 562~660%. The fixity ratio reached 84% and the recovery ratio up to 95% under thermal draw and thermal recovery test. During drawing at low temperature and thermal recovery testing, the shape fixity ratios were about 55%. The partially crystallized PCL segment phase provided the SMF with partially elasticity at ambient temperature and the ability to fix the temporary length once the fiber was cooled to ambient temperature. The SMF could recover its original length by reheating the fiber above 47°C at which the crystallized soft segments melt.

CHAPTER 5 STUDIES OF THE HEAT TREATMENT OF SMFs

Heat treatments were applied to the SMFs to eliminate internal stress and structure deficiency. The influences of heat treatments on the fiber thermal properties, crystalline properties, molecule orientation, hydrogen bonding, mechanical properties, dimensional stability, recovery force relaxation, thermomechanical cyclic properties and shape memory behavior were studied.

5.1 Thermal properties

The DSC thermograms of PCL-4000, as-spun SMF and SMFs after heat treatment are presented in Figure 5.1 and the thermal property parameters are tabulated in Table 5.1. The soft segment crystallinity was calculated from the enthalpy data ΔH of the crystallization by using the 140 J/g enthalpy value for fusion of 100% crystalline PCL given by Crescenzi et al. [313, 314]. In the DSC curve of the as-spun SMF, the melting transition peak in the vicinity of 41°C is ascribed to the soft segment melting transition [62, 63]. Due to the impendence of the hard segment, the crystallinity of soft segment PCL decreases and the melting temperature decreases simultaneously in comparison with that of pure PCL. From Figure 5.1 and Table 5.1, it can be seen that the heat treatment has a marked influence on the soft segment phase crystallinity of the SMFs. With increasing heat treatment temperature, the soft segment crystallinity increases from 18.8% of as-spun SMF to 28.4% of SMF-125°C. The melting temperature also increases slightly with increasing heat treatment temperature.

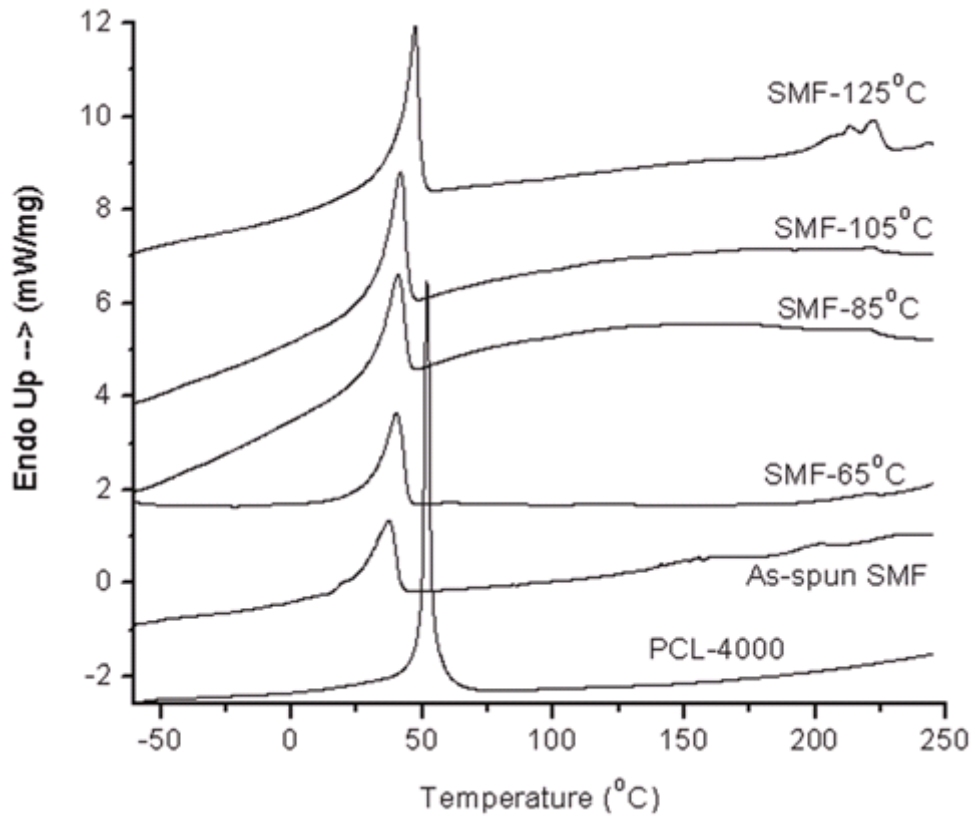


Figure 5.1 DSC thermograms of PCL, as the as-spun SMF and SMFs after heat treatment

Table 5.1 Thermal properties of the PCL, as-spun SMF and SMFs after heat treatment

	Soft Segment		
	T_m (°C)	ΔH (J/g)	Crystallinity (%)
PCL-4000	59.00	53.68	39.8
SMF-125°C	48.58	38.36	28.4
SMF-105°C	46.46	36.85	27.3
SMF-85°C	45.35	34.97	25.9
SMF-65°C	43.64	31.68	23.5
As-spun SMF	41.20	25.34	18.8

From Figure 5.1, it can be seen that the heat treatment, especially high temperature heat treatment, also has an influence on the SMFs hard segment phase. It seems that low temperature heat treatment nearly has no influence on the hard segment phase. However, after 125°C heat treatment, the SMF shows obvious hard segment endothermic peaks which may be related to the relatively short-range ordered hard segments. According to previous reports [315, 316], the glass transition temperature of the hard segment phase in polyurethane locates at around 125°C and the melting point of hard segment phase is in the range of 200–240°C [317]. The above results suggest the high temperature heat treatment benefits for the hard segment aggregation to form a stable hard segment phase.

5.2 Dynamic mechanical properties

The dynamic mechanical properties of SMF-125°C which had the best dimensional stability were evaluated. Due to the severe shrinkage of the other fibers with increasing temperature, the dynamic mechanical properties of the as-spun SMF and SMF- 65°C, SMF- 85°C, SMF- 105°C were not tested. The elastic modulus (E') and loss tangent ($\tan \delta$) of the SMF-125°C over the temperature range from -110 to 190°C are presented in Figure 5.2.

The elastic modulus (E') of the SMF-125°C shows a sharp drop at about -50°C and a second sharp drop at 47°C. The loss tangent peak locating at -50°C is due to the glass transition of the soft segment phase; the sharp increase at around 50°C is related to the melting transition of the soft segment phase [70, 318]. This result is consistent with those obtained from the DSC analysis. At a temperature above soft segments melting transition, the mechanical properties

of the SMF is almost completely contributed by the hard segments phase [319] as can be seen by the plateau region of E' . This also demonstrates the existence of the hard segment rich phase [318]. Upon heating above 175°C, another sharp decrease of E' is observed, indicating that the physical crosslinking sites between hard segments are totally destroyed.

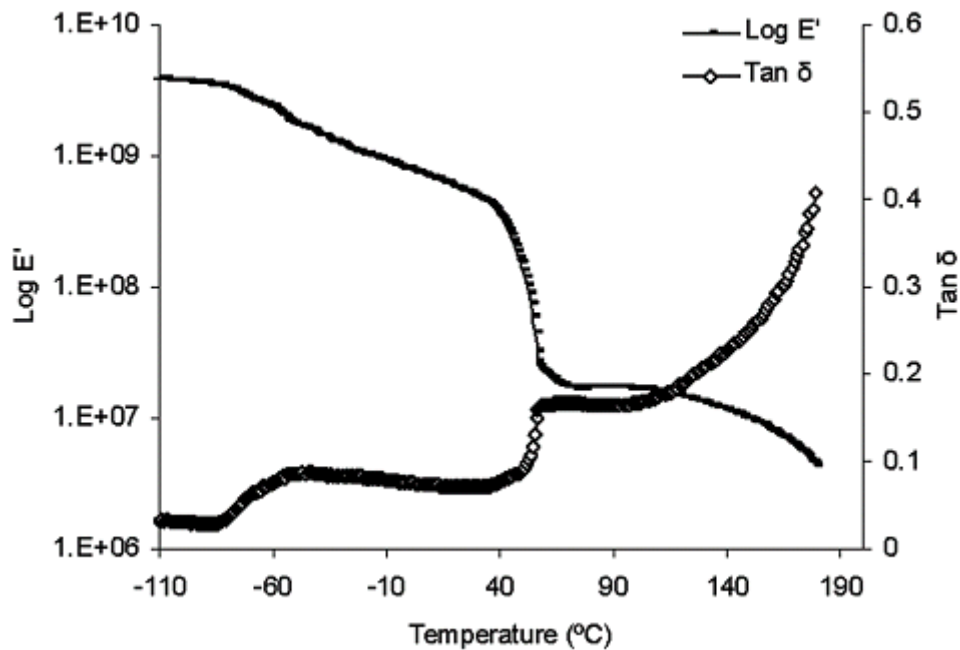


Figure 5.2 The elastic modulus and loss tangent of the SMF-125°C

5.3 Crystalline structures

The crystalline structures and unit cell parameters of pure PCL-4000, as-spun SMF and SMFs after heat treatment at different temperature were studied using XRD. The XRD patterns are shown in Figure 5.3 and the results of lattice parameters are tabulated in Table 5.2. The percent crystallinity (X_c) within the sample was calculated using the method described by Young and Lovell [320].

$$X_c = \left(\frac{\sum_i A_{ci}}{\sum_i A_{ci} + \sum_j A_{aj}} \right) \times 100\%$$

Where the A_c is the area of the X-ray diffraction curve due to scattering from the crystalline phase and A_a is the area of the X-ray diffraction curve due to scattering from amorphous phase.

The average crystallite size was determined coarsely using Debye-Scherrer formula [321, 322]: $L_{(hkl)} = k \lambda / \beta \cos \theta$. Here λ is the applied X-ray wave length $\lambda_{Cu} = 1.542 \text{ \AA}$; θ is diffraction angle, $k = 0.89$, β - FWHM (full width at half maximum) in radians.

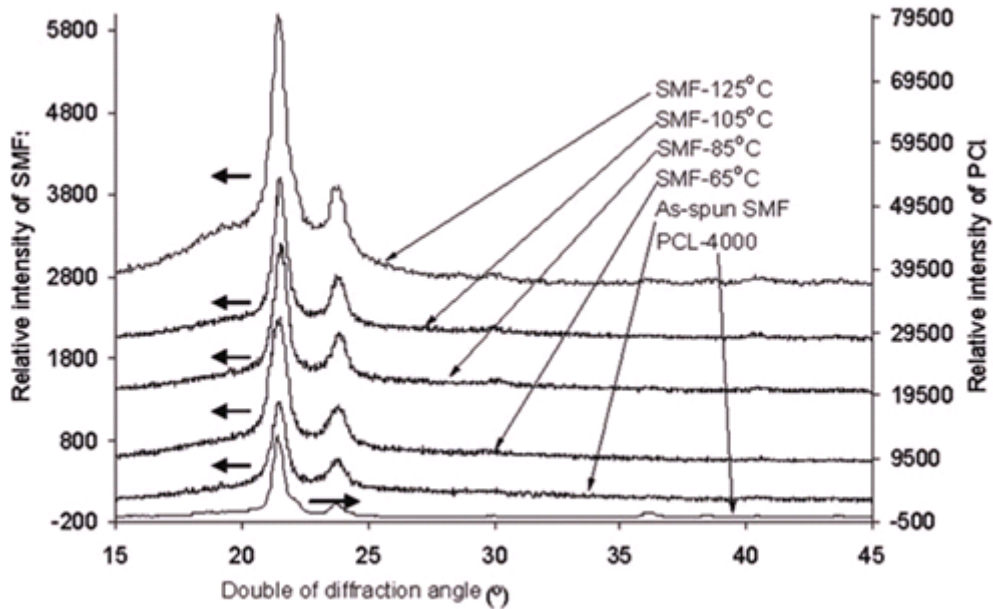


Figure 5.3 Wide-angle X-ray scattering patterns of the PCL, as-spun SMF and SMFs after heat treatment

Table 5.2 The results of peak separation and calculated crystallinity

Sample	Peak position 2 θ (°)	FWHM (°)	Height (count)	Area (count)	Crystallinity
PCL-4000	1	20.61	7.07	732.7	6298.1
	2	21.43	0.44	9280.8	5001.1
	3	22.11	0.37	1171.2	552.7
	4	23.78	0.55	959.9	640.1
	5	29.92	1.27	126.1	194.3
	6	36.15	0.53	591.9	383.0
	7	38.45	0.39	198.5	94.8
	8	41.10	17.04	162.6	3367.8
As-spun SMF	1	21.44	7.19	77.1	6731.6
	2	21.45	0.7	2297.6	1840.2
	3	23.87	0.82	666.0	545.3
	4	28.62	0.58	55.9	39.2
	5	29.97	1.07	78.1	101.2
	6	40.33	19.43	93.7	2212.4
SMF-65°C	1	21.43	6.48	1460.2	1118.9
	2	21.47	0.66	738.5	517.0
	3	23.84	0.73	264.7	185.4
	4	28.39	13.60	1315.3	1106.7
	5	29.87	0.75	20.7	14.5
	6	40.50	0.81	21.9	15.4
SMF-85°C	1	21.21	6.30	191.5	1465.8
	2	21.48	0.63	1145.0	773.8
	3	23.81	0.67	372.9	289.9
	4	27.18	16.75	75.1	1527.7
	5	29.96	0.47	42.2	24.2
	6	40.46	0.71	35.2	24.7
SMF-105°C	1	21.17	6.02	175.0	1280.3
	2	21.5	0.56	1072.1	746.5
	3	23.8	0.66	343.5	274.6
	4	27.27	14.53	73.2	1292.1
	5	30.08	0.74	29.1	26.2
	6	40.63	1.35	19.5	31.9
SMF-125°C	1	20.77	6.49	198.9	1569.7
	2	21.54	0.54	1034.7	873.4
	3	23.78	0.64	303.4	300.6
	4	27.88	14.35	62.7	1092.5
	5	29.89	1.06	16.7	21.6
	6	40.54	0.73	14.5	12.9

Different from the result from the DSC curve of SMF-125°C where a melting endothermic peak appears during the SMF heating scanning, no obvious hard segment crystal diffraction peak is observed in the XRD curve of SMF-125°C. This may be because in the SMF the hard segments is relatively short-range ordered and not well-ordered enough to form crystallites.

The peaks of XRD curves were separated and areas of the X-ray scattering of every amorphous phase broad peak and sharp crystalline phase peak were integrated using a Philips Xpert XRD system soft ware. The peaks separating results and calculated crystallinities are presented in Table 5.2. The crystallinity changing trend with increasing heat treatment temperature are generally consistent with those obtained from DSC analysis. The heat treatment increases the crystallinity and as a result benefits the phase separation [62].

The influence of heat treatments on the unit cell parameters was also studied. From Figure 5.3, it can see that all the PCL-4000, as-spun SMF and SMFs after heat treatment have two prominent diffraction peaks at about 21.5° and 23.80° respectively. The peak at 21.5° can be attributed to the plane (110) diffraction of PCL soft segment. The peak at 23.8° is due to the plane (200) diffraction [323]. The unit cell parameters of the PCL and SMFs are presented in Table 5.3.

Table 5.3 The lattice parameters of the SMFs

Sample	(110)			(200)		
	2 θ	FWHM ($^{\circ}$)	L(hkl)	2 θ	FWHM ($^{\circ}$)	L(hkl)
PCL-4000	21.43	0.44	181.64	23.78	0.55	145.91
As-spun SMF	21.45	0.70	114.18	23.87	0.82	97.88
SMF-65 $^{\circ}$ C	21.47	0.66	121.10	23.84	0.73	109.95
SMF-85 $^{\circ}$ C	21.48	0.63	126.87	23.81	0.67	119.78
SMF-105 $^{\circ}$ C	21.5	0.56	142.74	23.8	0.66	121.60
SMF-125 $^{\circ}$ C	21.54	0.54	148.03	23.78	0.64	125.39

For plane (110), with increasing heat treatment temperature, the average crystallite size increases. For plane (200), with increasing heat treatment temperature, the average crystallite size also increases. In conclusion, the heat treatment increases the soft segment crystallites dimension.

5.4 Hydrogen bonding analysis

It is well known that the hydrogen bonding between functional groups of polyurethanes has remarkably influences on polyurethane properties [292, 324, 325]. To study the hydrogen bonding of polyurethanes, the carbonyl stretching bands is mostly used because the quantitative results based on N-H bands are not reliable [218]. The mole absorptive ratio of hydrogen boned amido and free amido was 4.6:1, while that of hydrogen boned carbonyl group and free carbonyl group is 1.05:1. Therefore, the carbonyl group is employed to study the hydrogen bonding though the hard segment amide band composes the complete hydrogen bonding [292, 324, 326].

The FTIR spectra of pure PCL-4000, as-spun SMF and SMFs after heat treatment from 1800 to 1550 cm^{-1} are tested and the results are shown in Figure 5.4. For the pure PCL where no hydrogen bonded carbonyl group exists, the carbonyl group stretching vibration displays the absorption peak at 1723 cm^{-1} . In the SMFs, the free carbonyl group peak locates at about 1728 cm^{-1} and hydrogen bond carbonyl group peak situates at 1701 cm^{-1} [327]. It can be seen that with increasing heat treatment temperature, the peak intensity of the free carbonyl group decreases and the area of free carbonyl group peak reduces. Simultaneously, the peak intensity of the hydrogen bonded carbonyl group increases and the corresponding area increases with increasing heat treatment temperature. These suggest that with increasing heat treatment temperature, part of the free carbonyl groups transform to hydrogen boned groups.

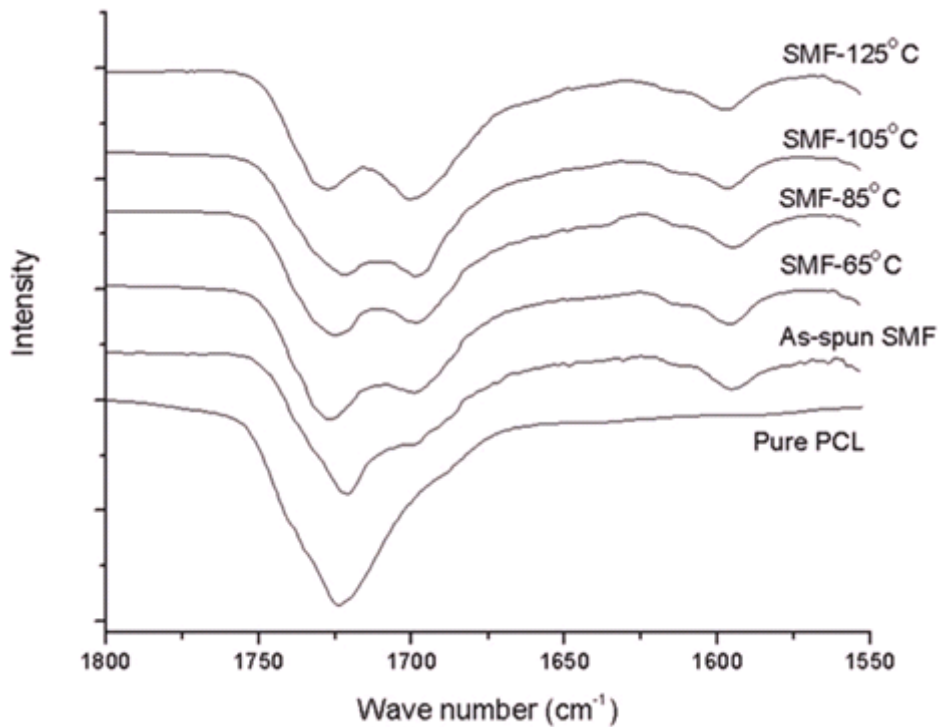


Figure 5.4 Carbonyl absorption in the FTIR spectra of pure PCL-4000 and SMFs as the function of increasing heat treatment temperature

In fact, in the SMFs, two kinds of hydrogen bonding of carbonyl groups co-exist. One is the hydrogen bonding in the hard segments phase between carbonyl group and hydrogen of amido. Another is the hydrogen bonding between carbonyl group in the soft segment and hydrogen of amido in the hard segment. The wave number difference of these two hydrogen bondings is generally so small that they are difficult to separate in the IR spectra [292, 294, 295, 328-330]. According to the results obtained from DSC and XRD analysis, the heat treatment increases the crystallinity and “purity” of soft segment phase, as a result, the hydrogen bonding between carbonyl group in the PCL soft segment and hydrogen of amido in the hard segment decreases [292, 324, 331].

Therefore, it can be concluded that the hydrogen bonding in the hard segment phase increases. This result also indicates that a more stable hard segment phase is formed in the SMF after heat treatment.

5.5 Tenacity

The tenacity of SMFs as a function of heat treatment temperature is shown in Figure 5.5. Heat treatment especially low temperature heat treatment decreases the SMF tenacity. Further increasing heat treatment temperature does not change the tenacity much. These results may be attributed to two aspects: molecule disorientation and phase separation during the heat treatment. Low temperature heat treatment at above the soft segment phase melting temperature decreases the molecular orientation, while at the same time the heat treatment increases the phase separation of the soft segment phase and hard segment phase. Especially, it has been demonstrated that the high temperature heat treatment increases the hard segment phase stability. In a low temperature heat treatment, the soft segment molecule disorientation is dominant; therefore, the fiber tenacity decreases. While with increasing heat treatment temperature at about the hard segment glass transition temperature, most of the soft segment molecules disorientation has finished. At this temperature, the hard segments have more mobility to reorganize to form more stable hard segment domains; as a result, the tenacity of the SMF does not decrease so markedly.

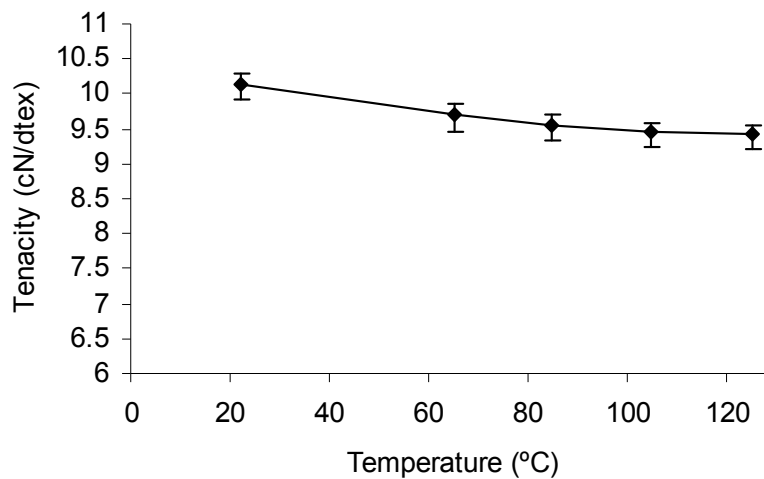


Figure 5.5 Influence of heat treatments on SMF tenacity

5.6 Breaking elongation

The breaking elongation of the SMFs as a function of heat treatment temperature is shown in Figure 5.6. It can be seen the breaking elongation increases after heat treatment especially at below 85°C heat treatment temperature. Continuously increasing heat treatment temperature has little influence on the breaking elongation. During the low temperature heat treatment, the molecules disorient and internal stress is released; therefore, the breaking elongation of the SMF after heat treatment increases. At high temperature heat treatment, the breaking elongation does not change much as most of the internal stress has been released and most of the molecules disorientation has finished at the low temperature.

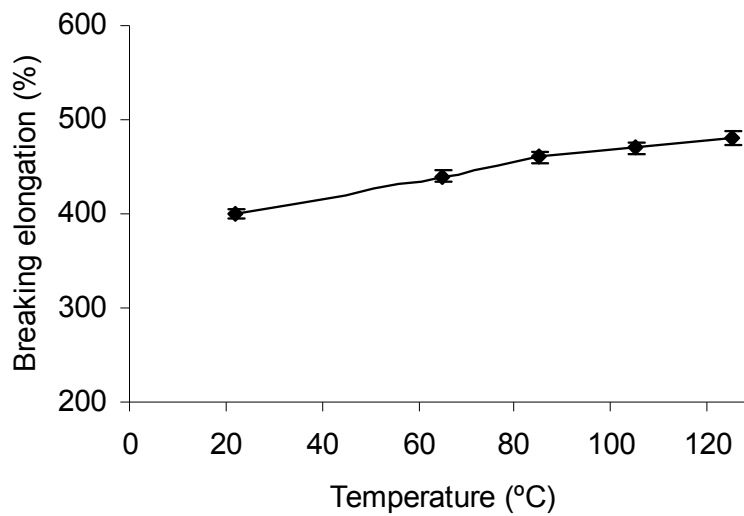


Figure 5.6 Influence of heat treatments on SMF breaking elongation

5.7 Boiling water shrinkage

The results of heat treatment on the SMF boiling water shrinkage are shown in Figure 5.7. It can be seen that with increasing heat treatment temperature, the fiber dimensional stability increases. After 65°C and 85°C treatment which are above the soft segment melting temperature, the soft segments have enough mobility to re-arrange themselves. Continuously increasing heat treatment temperature had hardly any influence on the boiling water shrinkage. However, it can be seen that after 125°C heat treatment, the SMFs still have high boiling water shrinkage. This may be because at the experiment temperature 125°C, the hard segment mobility is not active enough. Even though the heat treatment improves the soft segment dimensional stability and has some influence on the hard segment phase, the hard segment phase does not obtain enough energy to

release the residual stress stored in the hard segment phase. According to previous studies [315, 316], the glass transition temperature of the hard segment phase in polyurethane is located at around 125°C and the melting point of hard segment phase is in the range of 200~240°C [317]. From this point of view, the SMF should be heat treated at a much higher temperature above the hard segment glass transition temperature. Unfortunately, when the heat treatment temperature was higher than 125°C, the SMFs became too soft and tacky because of the melting of the soft segment phase so that the heat treatment could not be conducted. At this temperature, the hydrogen bonding as physical crosslink to restrict the free movement of the soft segments above its melting temperature may begin to be destroyed. Therefore, the SMF becomes too soft and tacky.

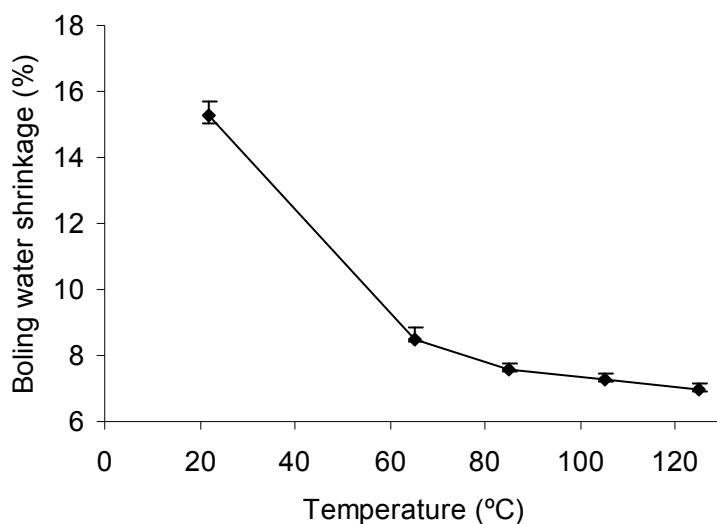


Figure 5.7 Influence of heat treatments on SMF boiling water shrinkage

5.8 Stress relaxation

The influence of heat treatment on the stress decay of SMFs was investigated during deformation because actually the shape recovery driving force of SMFs is the stress stored in the hard segment phase during deformation. The stress decay study is especially important if the SMF is for long term applications. The results of stress relaxation process of various SMFs after stretching to 100% are presented in Figure 5.8. It can be seen the stresses reach the maximum values after 2 minutes. With increasing heat treatment temperature, the maximum stress and plateau stress decrease greatly. This is maybe mainly due to the disorientation of the SMFs with increasing heat treatment temperature. From Figure 5.8, it can be seen that the stress decay speed of SMFs decreases with increasing heat treatment temperature. The stress of SMF-125°C at plateau area nearly has no obvious change in the testing range. These may be ascribed two reasons: First, the heat treatment increases the phase separation as has been established by DSC and XRD analysis; second, the hard segments transferred to well-ordered structures with strongly H-bonding after the high temperature heat treatment. As a result, the stress of the SMF after high temperature heat treatment is more stable at the plateaus area.

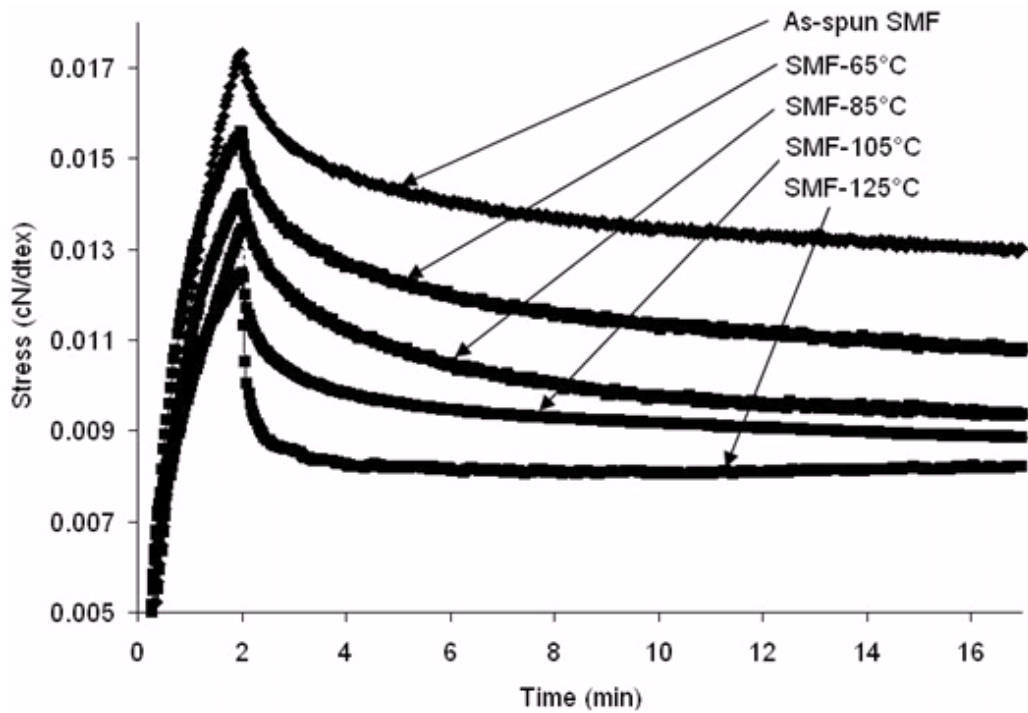


Figure 5.8 Stress relaxation of SMFs

5.9 Shape memory properties

The thermomechanical cyclic tensile curves of the as-spun SMF and SMFs after heat treatment are shown in Figure 5.9. The detailed data of fixity ratios, recovery ratios and maximum stress at 100% strain are tabulated in Table 5.4. After 65°C heat treatment, the recovery ratios of the SMF decrease greatly, while the fixity ratios increase. With increasing heat treatment temperature, both the shape recovery ratios and fixity ratios increase slightly.

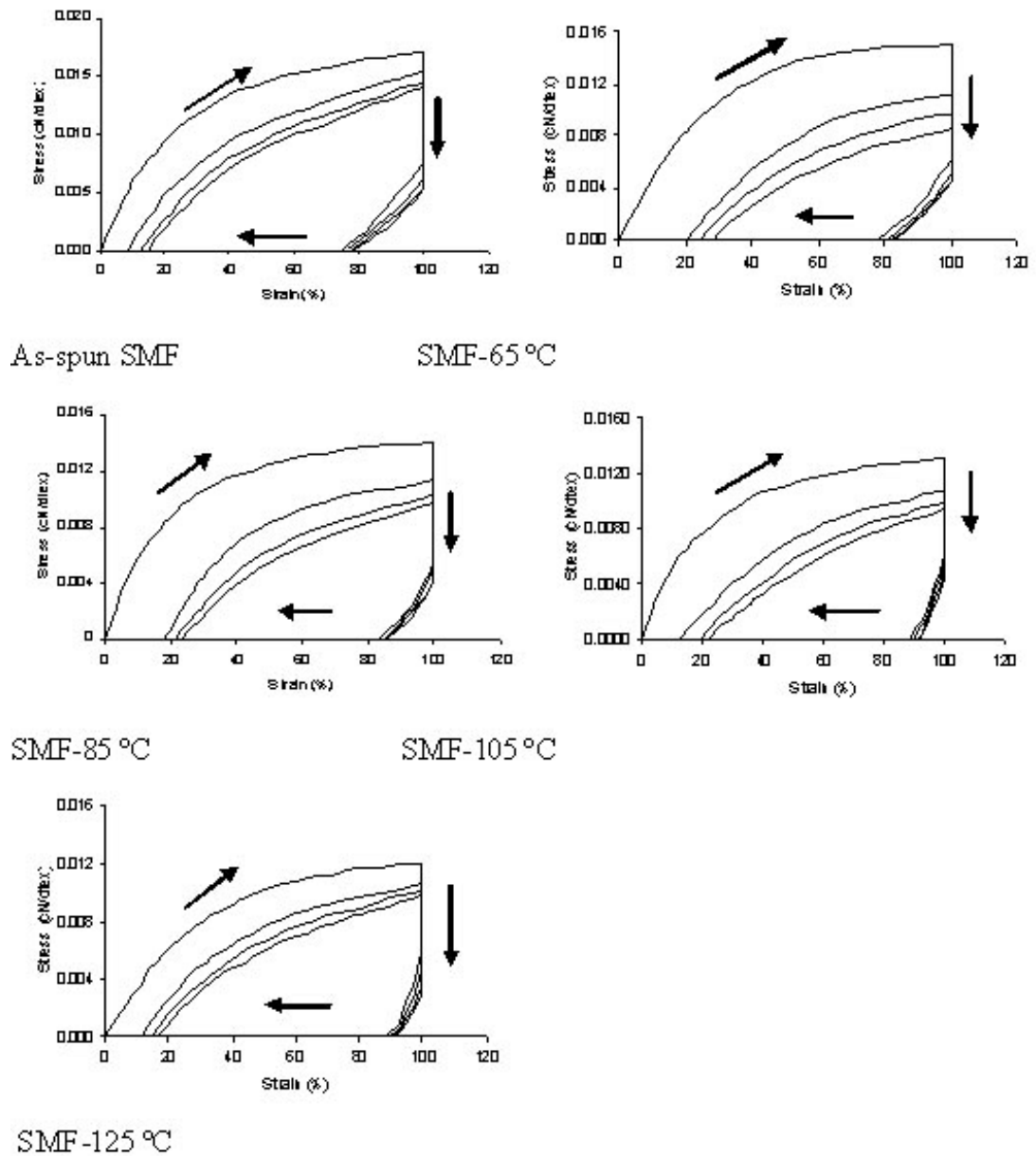


Figure 5.9 Thermomechanical cyclic tensile testing strain-stress curves of the SMFs

Table 5.4 Thermomechanical cyclic tensile testing result of SMFs

Circle No.	$\epsilon_p(N)$	$\epsilon_a [R_d(N)]$	Stress at 100% strain(cN/dtex)	$R_{100}(N)$	$R_d(N)$
As-spun SMF					
1	0.0%	74.2%	0.0170	100.0%	
2	8.5%	76.5%	0.0155	91.5%	91.5%
3	12.4%	77.3%	0.0145	87.6%	95.7%
4	15.0%	78.1%	0.0140	85.0%	97.0%
SMF-65 °C					
1	0.0%	78.0%	0.0158	100.0%	
2	20.8%	81.0%	0.0111	79.2%	79.2%
3	24.6%	82.4%	0.0097	75.4%	95.2%
4	28.0%	83.0%	0.0086	72.0%	95.5%
SMF-85 °C					
1	0.0%	83.0%	0.0140	100.0%	
2	17.8%	84.5%	0.0120	82.2%	82.2%
3	21.1%	85.5%	0.0102	78.9%	96.0%
4	23.6%	85.7%	0.0098	76.4%	96.8%
SMF-105 °C					
1	0.0%	87.8%	0.0120	100.0%	
2	12.6%	88.9%	0.0107	87.4%	87.4%
3	19.0%	90.0%	0.0098	81.0%	92.7%
4	22.1%	90.4%	0.0093	77.9%	96.2%
SMF-125 °C					
1	0.0%	89.0%	0.0120	100.0%	
2	11.0%	90.0%	0.0107	89.0%	89.0%
3	14.5%	90.5%	0.0102	85.5%	96.1%
4	16.2%	91.0%	0.0098	83.8%	98.0%

Generally, it has been widely accepted that in the polyurethane system, the soft segment phase is in charge of shape fixity by freezing the polyurethane molecules after being cooled to a temperature below the switching transition temperature, and the hard segment phase acting as physical crosslinking is responsible for shape recovery by releasing the stress stored during deformation [14, 61, 62, 117, 308]. However, for the SMFs which have molecular orientation and internal stress caused by melt spinning, they will shrink because

of the stress releasing and molecules disorientation during heat treatment. During 65°C heat treatment, the internal stress releases and molecules partially disorient because of the melting of the soft segment phase. Therefore, the recovery ratios decrease and fixity ratios increase after 65°C heat treatment. With increasing heat treatment temperature, as has been established above, the soft segment phase crystallinity and phase separation increase and the hard segment phase stability especially after 125°C is also improved. Therefore, the soft segment has more ability to freeze the polyurethane molecules when cooled from temperature above the switching transition temperature to ambient temperature. In addition, a more stable hydrogen bonded hard segment network is produced after the heat treatment; therefore more deformation energy can be stored in the hard segment phase. Consequently, the SMF has more power to recover the original length if the deformed SMF is heated to a temperature above the switching transition temperature. As a whole, the shape fixity ratios and recovery ratios increase slightly with increasing heat treatment temperature [218].

5.10 Mechanism of the heat treatment

A model shown in Figure 5.10 can be employed to explain the molecule disorientation and phase changes process of the SMFs during heat treatment. In Figure 5.10, the soft segments are shown as thin lines. The hard segments have a tendency to adhere to one another through strong hydrogen bonding to form hard segment phase. The hard segment phase is shown as islands. During melt spinning, at the spinning temperature which is higher than the hard segment melting temperature, the fiber is extruded from a spinneret. Upon being cooled

to the ambient temperature which is below the soft segment melting temperature, the fiber is wound up and the fiber shape is cast. The soft segment phase is partially crystallized and oriented at an ambient temperature and the hard segment phase is also stretched in the fiber axial direction after the spinning process. During the low temperature heat treatment above the soft segment melting temperature, the soft segments disorient and re-organize following the release of the internal stress caused during the spinning process.

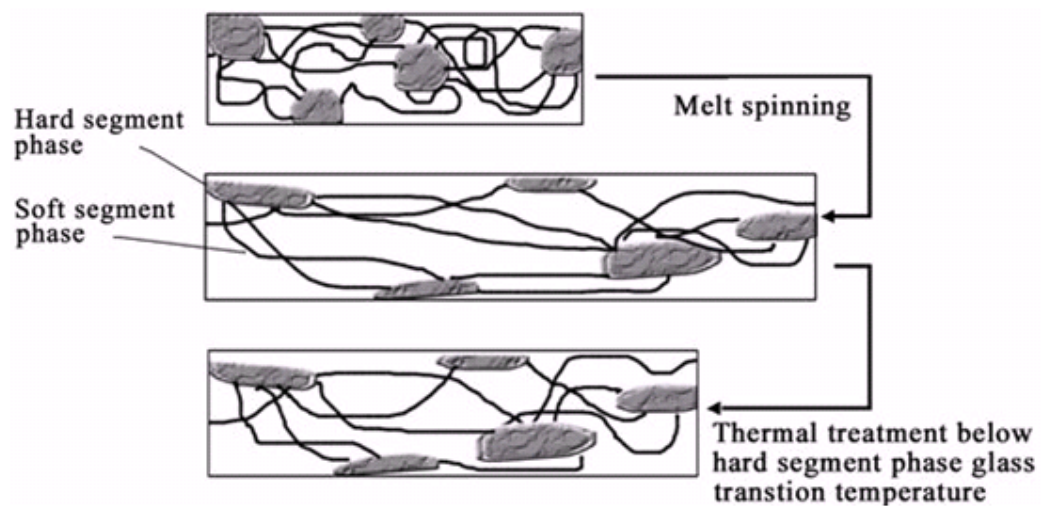


Figure 5.10 Schematic representation of molecular disorientation and phase changes of SMFs induced by heat treatment

At the low temperature which is below the hard segment phase glass transition, the oriented hard segments are intact. Because at the low temperature the hard segments do not have enough mobility to rearrange and release the internal stress, the low temperature heat treatment is not completely effective for the SMF comprehensive properties improvement. Unfortunately, if the heat treatment temperature is continuously increased, the heat treatment cannot be

conducted because the SMFs become too soft and tacky because of the melting transition of the soft segment phase.

5.11 Summary

SMFs underwent heat treatments at different temperature to eliminate internal stress and structure deficiency generated during the melt spinning. The influences of heat treatments on the SMF thermal properties, crystallinity, molecular orientation, hydrogen bonding, mechanical properties, dimensional stability, recovery force relaxation, and shape memory behavior were studied. Several main physical property changes of SMFs after heat treatment were observed.

- (1) Heat treatments increased soft segment crystallinity and phase separation.
- (2) Low temperature heat treatment increased breaking elongation and shape fixity ratios, decreased boiling water shrinkage, tenacity and shape recovery ratios.
- (3) High temperature heat treatment benefited the improvement of hard segment phase stability. The boiling water shrinkage was still very high even after 125°C heat treatment because its' limit effect on the hard segment phase.
- (4) Increasing the heat treatment temperature increased both the shape recovery ratios and fixity ratios because the heat treatment increased both the soft segment phase crystallinity and hard segment phase stability.

The SMF is expected to be treated at a high temperature considering the high glass transition temperature of the hard segment. Unfortunately, the heat

treatment could not be conducted at a temperature above 125°C because at the temperature the SMF became too tacky and soft due to the melting of the soft segment phase.

CHAPTER 6 SMFs WITH THERMAL-RESPONSIVE INNER DIAMETERS

A shape memory hollow fiber with thermal-responsive inner diameters was fabricated. The fiber's thermal, mechanical, and shape memory effect were investigated explicitly. As hollow fibers have many special properties in comparison with cylindrical fibers, the thermal-responsive hollow fiber (TRHF) may find many special applications. First, changes of the hollow fiber inner diameter will affect the physical properties of the products. If this kind of fiber is used in fabrics, the thermal-responsive heat transfer of the fabric will change according to the environment and body temperature. Second, the hollow fiber is proposed for use in the stuffing of pillows, and mattresses which can adjust to body contours for a comfortable feeling. If unloaded, after some time, they recover their original shapes. Furthermore, this kind of hollow fibers may be used in smart filtration, drug controlled release and liquid transportation [120].

6.1 Mechanical properties

The prepared TRHF cross-section image taken using an optical microscope (U-TEX/ELECTRO-MICROSCOPE MODEL UT901) is shown in Figure 6.1. The stress–strain curves of the TRHF derived from 5 experiments are shown in Figure 6.2. The TRHF has a tenacity of about 1.14cN/dtex and breaking elongation 682%. The tenacity is acceptable for textile applications in most circumstances [332].



Figure 6.1 Cross-section image of the prepared hollow fiber

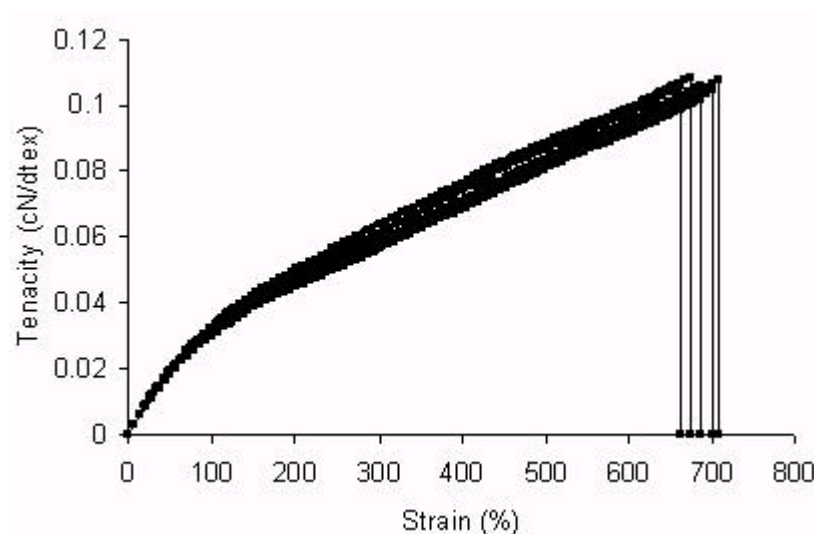


Figure 6.2 Static stress-strain curves of the TRHF

In the TRHF, the high molecular weight PCL provides the fiber with high breaking elongation ratios and the hydrogen bonded hard segment provides it with a high mechanical strength [217, 333]. The TRHF mechanical strength

can be improved through increasing hard segment content or molecular orientation.

6.2 Thermal properties

The DSC curves of the pure PCL and TRHF in the cooling and heating scan are shown in Figure 6.3. The detailed melting temperature, crystallizing temperature, corresponding enthalpy and crystallinity are tabulated in Table 6.1. The thermograms of both pure PCL and TRHF show the exothermic crystallization peak in the cooling scan and the endothermic melting peak in the heating scan. The melting temperature of TRHF is about 41.2°C which is attributed to the PCL soft segment phase transition in the TRHF. The crystallinity of TRHF is much lower in comparison with that of pure PCL. This is because in the polyurethane system, the hard segment intrudes into the well formed PCL phase and interferes with the PCL crystalline behavior. No obvious hard segment phase endothermic peak appears in the TRHF heating scanning. This may be due to the fact that the hard segment content in the TRHF is relatively low, and consequently no well ordered hard segment phase forms. According to previous studies, normally no crystallized structure of hard segment will form if the hard segment content is very low such as below 50 wt% [310]. At the ambient temperature, the soft segment phase is partially crystallized, therefore, the TRHF is not completely elastic as those in elastic polyurethane fibers [298, 334].

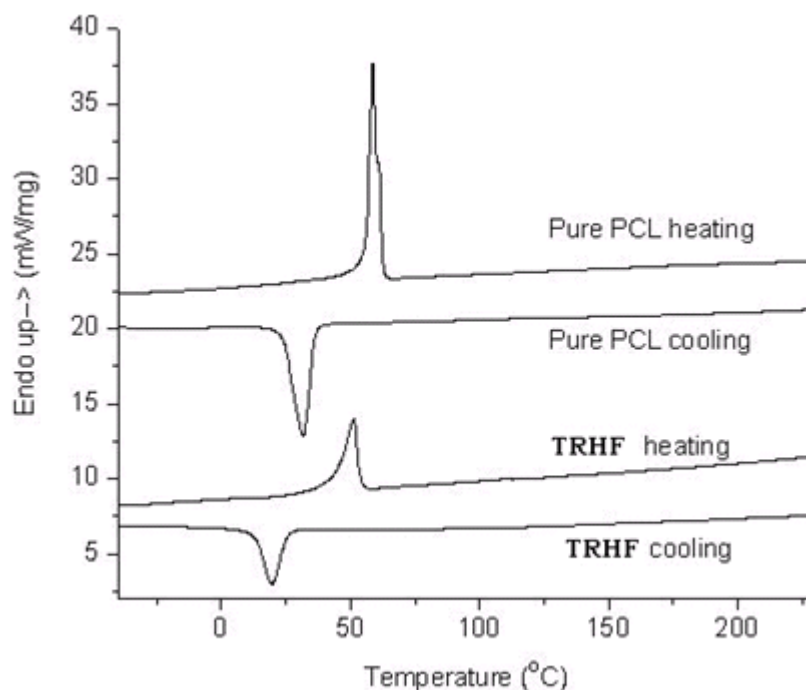


Figure 6.3 The DSC curves of the pure PCL and the TRHF

Table 6.1 Thermal transition temperature and crystallinity of pure PCL and TRHF

		$T_c/T_m(^{\circ}\text{C})$	$\Delta H(\text{J/g})$	Crystallinity(%)
PCL-4000	Cooling	31.6	53.0	37.9
	Heating	58.6	53.2	38.0
TRHF	Cooling	19.6	28.4	20.3
	Heating	41.2	27.9	19.9

T_m is crystal melting temperature, ΔH the heat of fusion. The soft segment crystallinity was calculated from the enthalpy data ΔH of the crystallization by using the 140 J/g enthalpy value for fusion of 100% crystalline PCL given by Crescenzi *et al.* [193, 200].

6.3 Crystalline structures

To further investigate the crystalline properties, the crystalline structures and unit cell parameters of the pure PCL and TRHF were studied using XRD. The XRD patterns are shown in Figure 6.4. The peaks of XRD curves were separated and areas of the X-ray scattering of every amorphous phase broad peak and sharp crystalline phase peak were integrated using the Philips Xpert XRD system software. The degree of crystallinity was calculated using the method described by Young and Lovell et al. [320]. The percent crystallinity (X_c) within the sample was calculated using the equation:

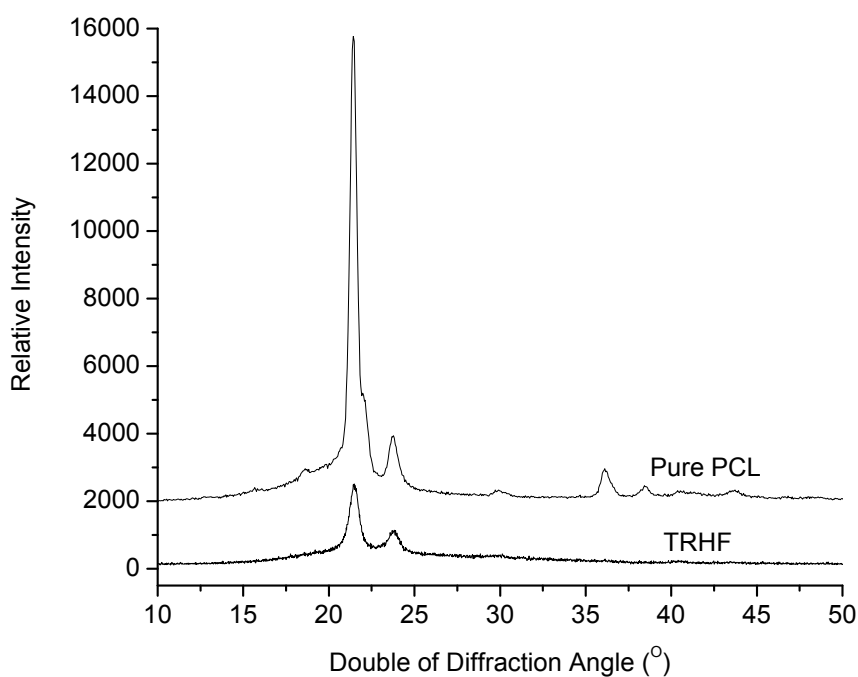


Figure 6.4 XRD patterns of pure PCL and the TRHF

$$X_c = \left(\frac{\sum_i A_{ci}}{\sum_i A_{ci} + \sum_j A_{Aj}} \right) \times 100\%$$

Where the A_c is the area of the X-ray diffraction curve due to scattering from the crystalline phase, and A_a is the area of the X-ray diffraction curve due to scattering from amorphous.

The calculated crystallinities are presented in Table 6.2. The thermal property results are generally consistent with those obtained from DSC analysis. The soft segment phase in the TRHF has high crystallinity even though the PCL crystallization in the TRHF is suppressed by the employed hard segment [62].

The average crystallite size was determined coarsely using Debye-Scherrer formula [321, 322]: $L_{(hkl)} = k \lambda / \beta \cos \theta$. Here λ is the applied X-ray wave length $\lambda_{Cu} = 1.542 \text{ \AA}$, θ is diffraction angle, $k = 0.89$, β - FWHM (full width at half maximum) in radians. From Figure 6.4 it can be seen that both the pure PCL and TRHF have two prominent diffraction peaks. The peaks of TRHF at 21.48° can be attributed to the plane (110) diffraction of PCL. The peak at 23.79° is because of the plane (200) diffraction [323]. The unit cell parameters of TRHF with those of pure PCL as references are presented in Table 6.2. For plane (110), the average crystallite size is lower compared with that in pure PCL. For plane (200), the average crystallites is also smaller in comparison pure PCL.

Table 6.2 The lattice parameters of the TRHF

Sample	Crystallinity	(110)			(200)		
		2 θ	FWHM (°)	L(hkl)	2 θ	FWHM (°)	L(hkl)
PCL	41.53%	21.43	0.44	181.64	23.78	0.55	145.91
TRHF	21.99%	21.48	0.70	114.19	23.79	0.82	97.87

6.4 Shape memory properties

The cyclic strain-stress curves of TRHF obtained by thermomechanical cyclic tensile testing by the 300% elongation mode and 600% elongation mode are shown in Figure 6.5. The significant difference between the first thermal cycle and the remaining cycles is because of reorganization of polyurethane molecules involving molecule orientation, crystallization, and weak point broken during elongation. After the first cycle, the thermomechanical properties become very similar. The detailed shape fixity ratios and recovery ratios are tabulated in Table 6.3. The TRHF has the fixity ratios of more than 80%; and recovery ratios of more than 90% at the 300% maximum elongation mode. The fixity ratio is above 85% and recovery ratio above 90% at the 600% maximum elongation mode. In the first cycle, at the maximum strain, the stress is 0.26 cN/dtex at 300% elongation, and 0.70 cN/dtex at 600% elongation.

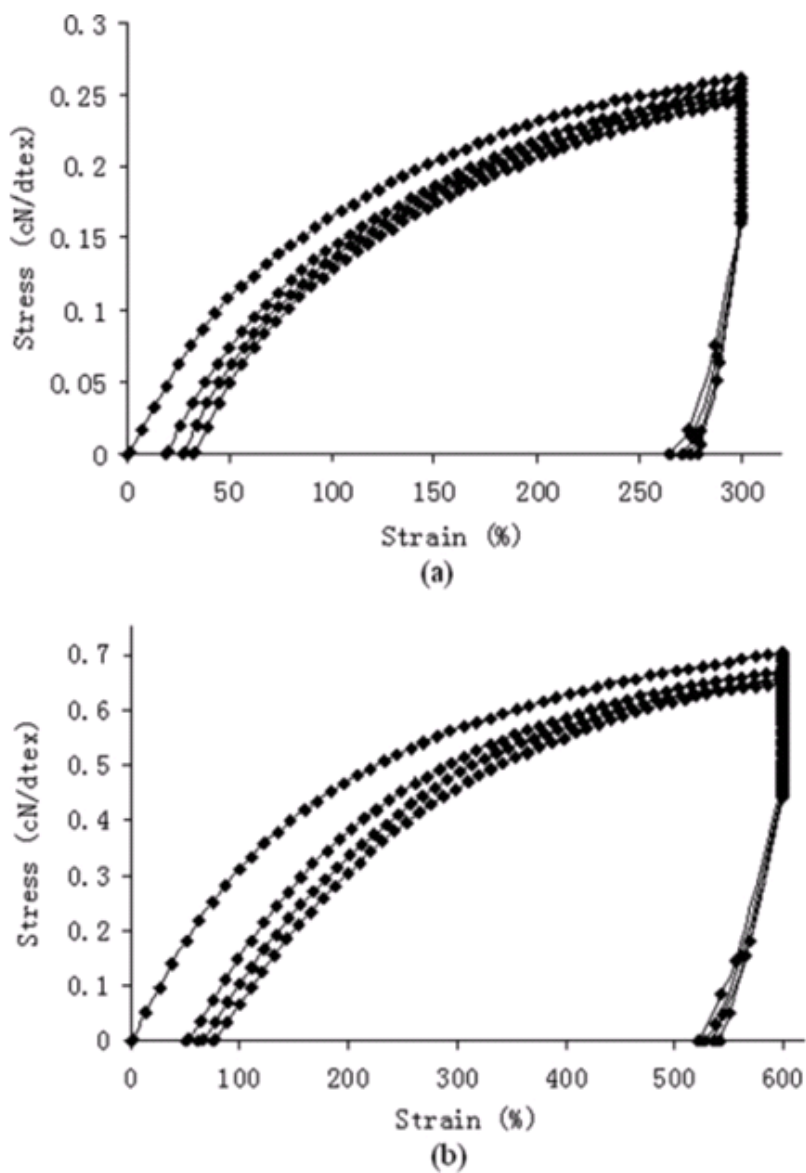


Figure 6.5 The cyclic tensile testing result of the TRHF (a) set maximum elongation 300%, b) set maximum elongation 600%)

Table 6.3 Shape fixity and recovery ratios of TRHF

Circle No.	ϵ_p (N)	ϵ_u (N)	$[R_f(N)]$	Stress at maximum strain(cN/dtex)	$R_{r,tot}(N)$	$R_r(N)$
Set maximum elongation 300%						
1	0.0%	250.0%	83.3%	0.26	100.0%	
2	19.3%	256.0%	85.3%	0.25	93.6%	93.6%
3	27.0%	262.0%	87.3%	0.25	91.0%	97.2%
4	32.3%	264.0%	88.0%	0.25	89.3%	98.1%
Set maximum elongation 600%						
1	0.0%	522.0%	87.0%	0.70	100.0%	
2	51.0%	529.0%	88.2%	0.67	91.5%	91.5%
3	64.0%	536.0%	89.3%	0.66	89.3%	97.6%
4	75.0%	542.0%	90.3%	0.65	87.5%	97.9%

6.5 Thermally-tunable inner diameter

The change of hollow fiber inner diameter will influence the physical properties of its products. Therefore, the thermally tunable cross-section of the hollow fiber was investigated. The images of the original cross-section, deformed cross-section and recovery cross-section of the TRHF are shown in Figure 6.6 and Figure 6.7. In Figure 6.6, the deformation is conducted by longitude stretching. In Figure 6.7, the deformation is carried out by pressing the fiber in the transverse direction. From Figure 6.6, it can be seen that the hollow fiber inner diameter has become smaller after stretching, and the shape is fixed at the ambient temperature (Figure 6.6(b)). After being put in hot water at 65°C, the fiber cross-section recovers its original shape (Figure 6.6(c)). The same result is obtained in Figure 6.7 where deformation is conducted by pressing the fiber in the transverse direction. The deformed flat shape is fixed

(Figure 6.7(b)); and after being heated to 65°C, it recovers its original shape (Figure 6.7(c)).

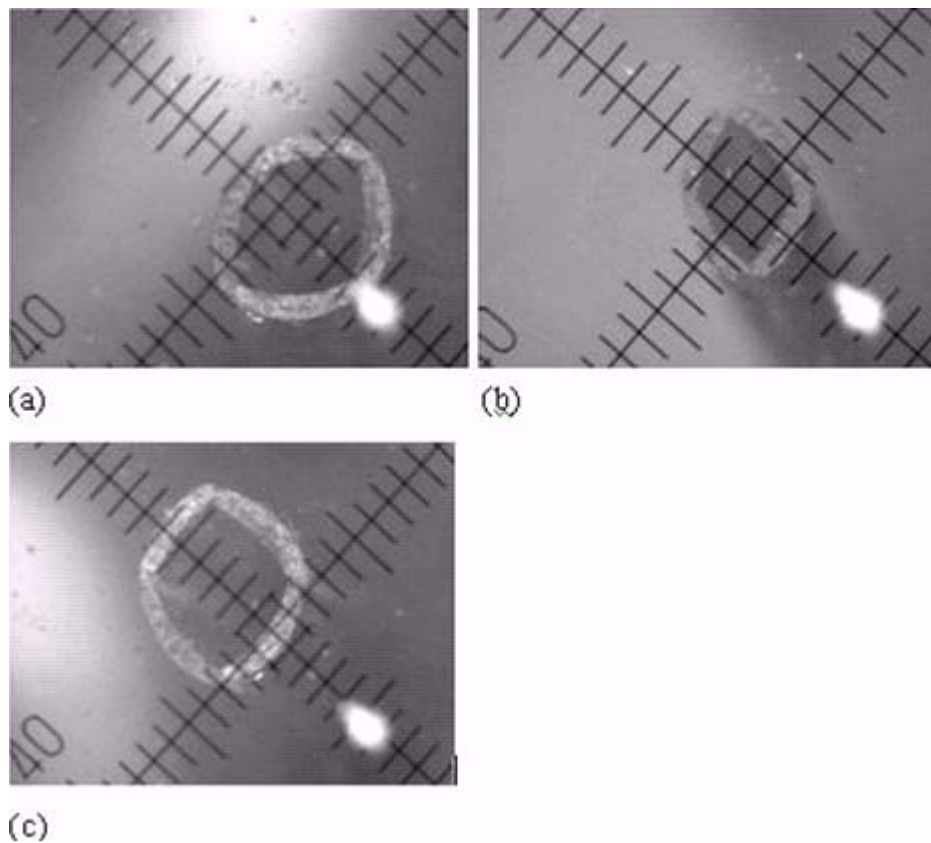


Figure 6.6 Thermally adjustable inner cavity of the TRHF (Deformed by longitude stretching) (a, original shape; b, deformed shape, c, recovered shape)

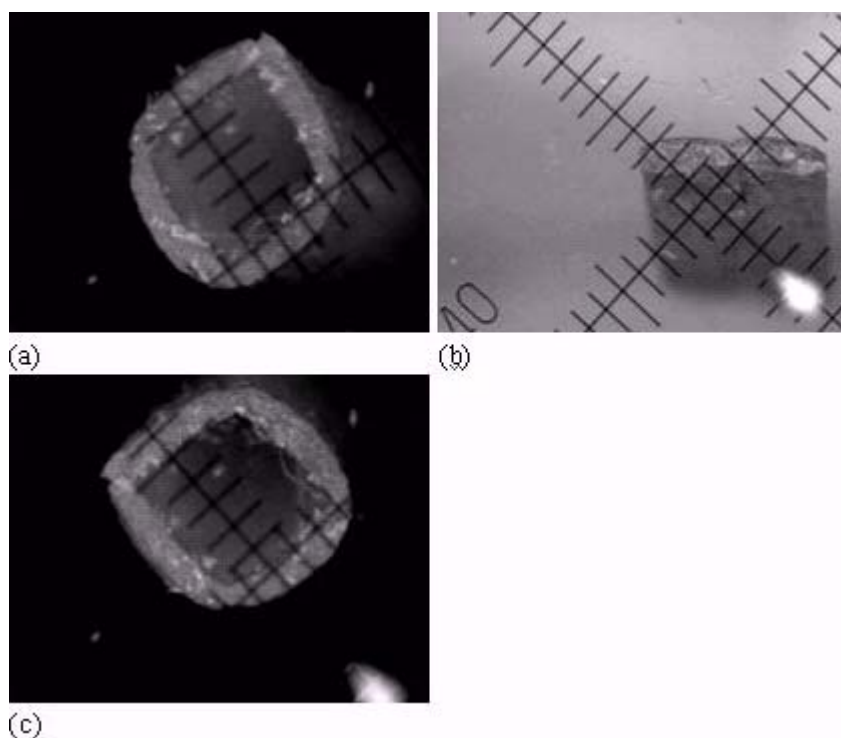


Figure 6.7 Thermally adjustable internal cavity of the TRHF (Deformed by transverse pressing) (a, original shape; b, deformed shape, c, recovered shape)

6.6 Summary

A SMPU was synthesized and a corresponding TRHF was fabricated. The fiber mechanical properties, especially shape memory effect, were characterized by static tensile, thermomechanical cyclic tensile testing. The main properties of the TRHF were as follows.

(1) The hollow fiber switching temperature was the melting temperature of the soft segment phase at about 41°C.

CHAPTER 6 SMFs WITH THERMAL-RESPONSIVE INNER DIAMETER

(2) The hollow fiber had a tenacity of about 1.14 cN/dtex, and strain at break 682%. The shape fixity ratio was above 80% and the recovery ratio above 90%.

(3) The inner diameter of the hollow fiber could be noticeably changed and the deformed fiber cross-section could be well fixed. After being heated above the soft segment phase melting temperature, the hollow fiber inner cavity recovered its original diameter.

(4) The changes of the hollow fiber inner diameter affect the physical properties of the product using the hollow fiber. This fiber may be used in smart textiles for thermal management, or as stuffing of pillows and mattresses which can adjust to body contours. Furthermore, this kind of hollow fibers with thermal-responsive inner diameter may be used in smart filtration, controlled drug-release and liquid transportation.

CHAPTER 7 SMFs WITH TEMPERATURE-REGULATING EFFECTS

A SMF with temperature-regulating effect (TRSMF) was prepared by using PEG as the soft segment. The fiber's phase change behaviors, crystalline morphology and dynamic mechanical properties were investigated using POM, DSC, and DMA. Since SMFs can be used in textiles for novel functions, the SMFs possessing temperature-regulating effect may have more applications. Unfortunately, the spinnability of the fibers was not good due to the significant melting transition of the PEG-based SMPU at low temperature. Furthermore, the degree of supercooling of the fiber was too high and the mechanical properties of the fiber were also not satisfied.

7.1 Mechanical properties

The image of the prepared TRSMF in Figure 7.1 shows that the TRSMF surface is smooth and uniform. The stress-strain curves of the TRSMF derived from the 5 experiments are shown in Figure 7.2. The 100 dtex TRSMF has a tenacity of about 0.7 cN/dtex, and the strain at break 488%. The fiber shows obvious neck-type phenomena which is frequently observed in the static stress-strain curves of crystalline polymers.

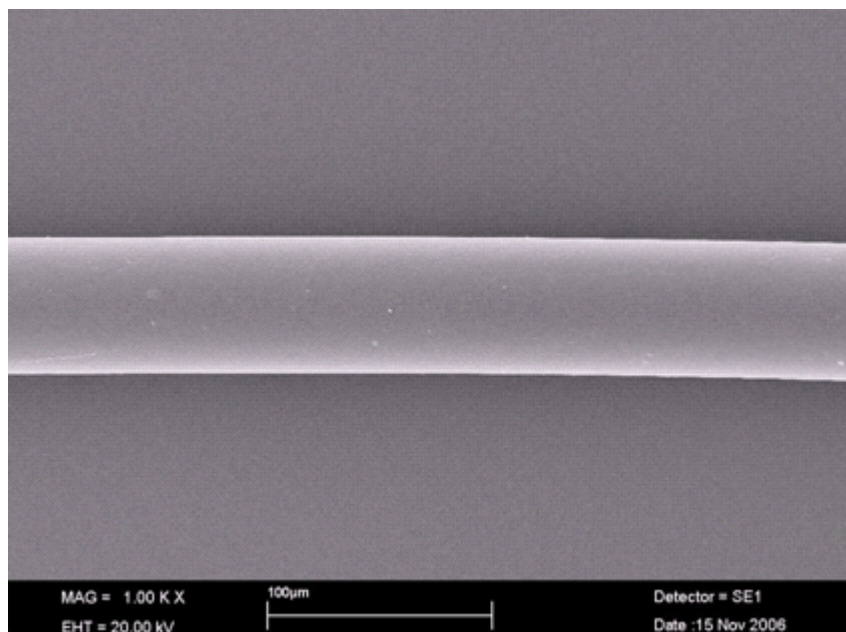


Figure 7.1 SEM surface image of TRSMF

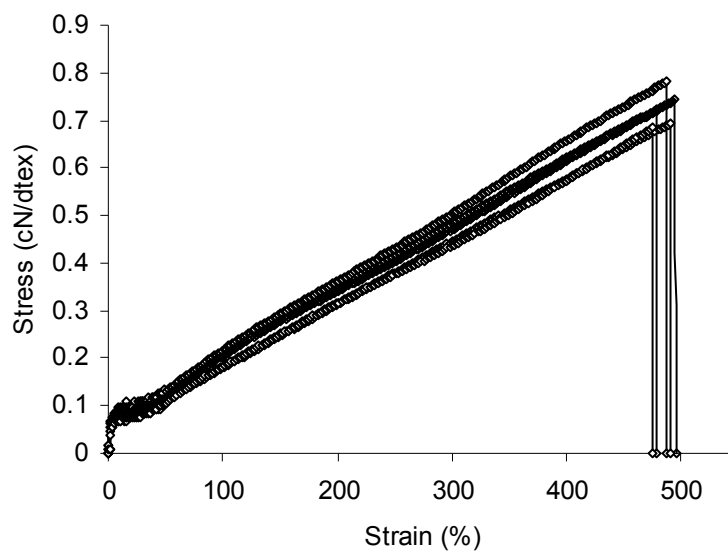


Figure 7.2 Stress-strain curves of the TRSMF

In the TRSMF, the high molecular weight polyol provides the TRSMF with high breaking elongation ratios more than 400% and the hydrogen bonded hard segments contribute to the mechanical strength. The mechanical strength of the TRSMF was very low which was 0.7 cN/dtex only. The fiber mechanical strength can be improved through decreasing the soft segment content; however, this is in the expense of TRSMF heat storage capacity.

7.2 Crystalline structures

The POM images of the pure PEG and TRSMF at the ambient temperature are given in Figure 7.3(a) and (b) respectively. It can be seen that at the ambient temperature, both pure PEG and TRSMF show crystalline cross-extinction patterns which suggest that their crystals are spherulites. The spherulites in TRSMF are much smaller than and not as perfect as those in pure PEG. In Figure 7.3(a), only one spherulite is observed, while in Figure 7.3(b), in the same size area, several crystals exist. In addition, many crystal fragments are observed in the POM image of the TRSMF. This is due to two reasons: first, in the TRSMF, the hard segments intrude into the well formed PEG phase and interfere with the PEG crystalline behavior; second, during the melt spinning process and winding process, the spherulites of PEG phase in TRSMF is stretched and deformed in the fiber longitude direction, which may destroy the spherulites to some extent.

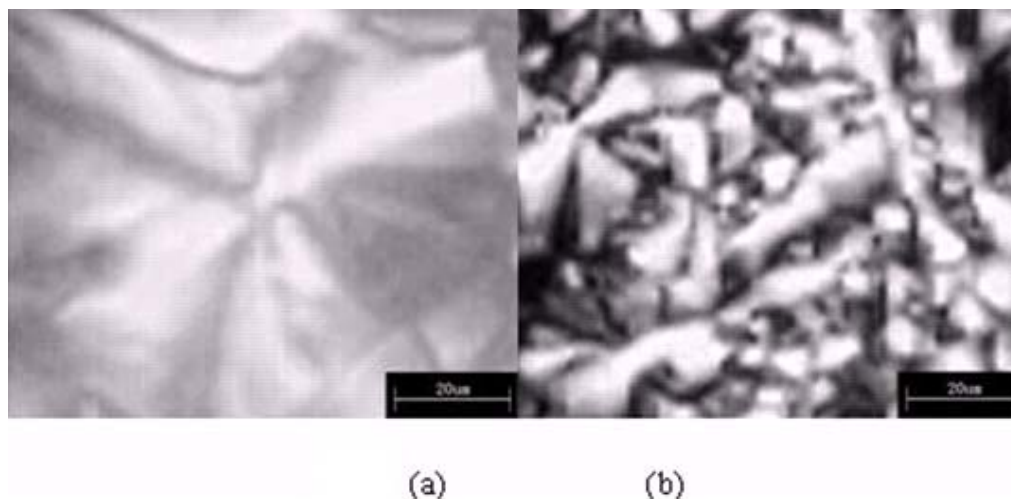
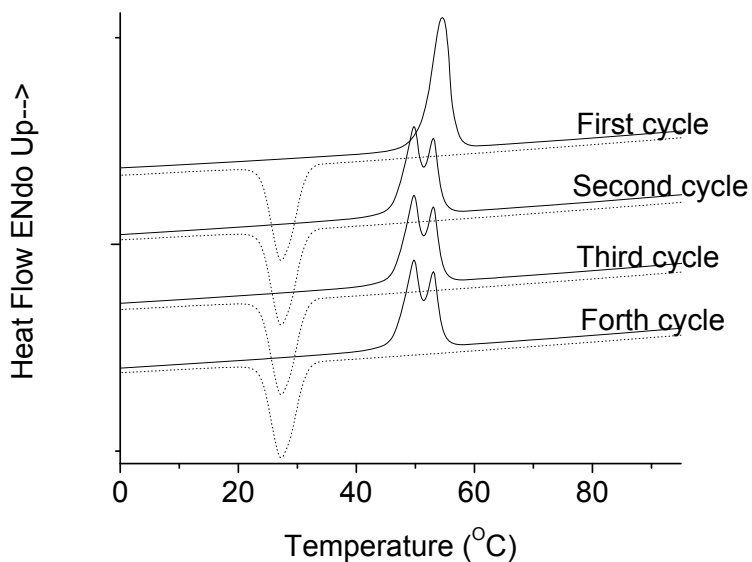


Figure 7.3 POM images of (a) Pure PEG at room, (b) TRSMF at the ambient temperature

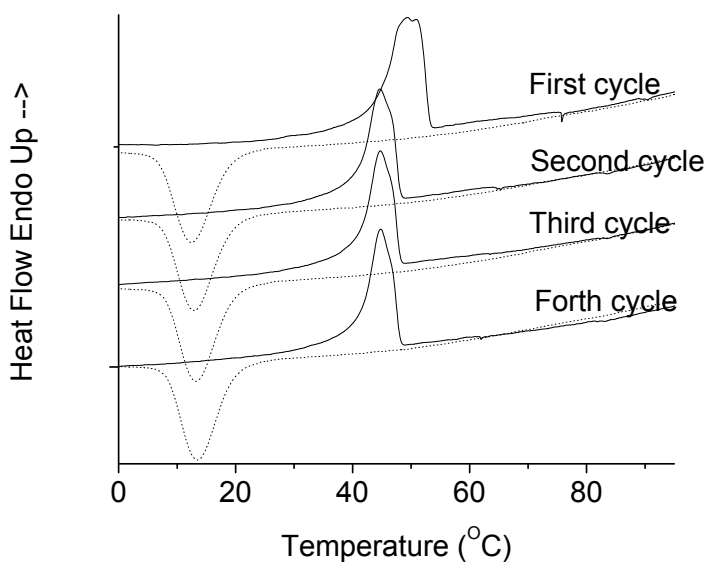
7.3 Thermal properties

The DSC curves of the pure PEG and TRSMF are shown in Figure 7.4(a) and (b). The melting temperature, crystallizing temperature, melting enthalpy and crystalline enthalpy are tabulated in Table 7.1. The DSC results in the first heating scan are different from those in the following cycles. This is attributed to the sample different thermal history. The thermogram curves of the pure PEG show an exothermic crystallization peak at 29.4°C in the cooling scan and endothermic melting peaks in the second heating at 51.7°C and 55.1°C. Similarly, the thermogram curves of TRSMF display an exothermic crystallization peak at 20.7°C in the cooling scan and an endothermic melting peak at 44.7°C in the heating scan. The crystallizing and fusion enthalpy of TRSMF is about 100 J/g. The crystallizing and fusion enthalpy of TRSMF is

comparable with those of most solid-solid PCMs reported previously [255, 256, 335, 336].



(a)



(b)

Figure 7.4 The DSC curves of pure PEG and TRSMF (solid line: heating; dot line cooling) ((a) pure PEG, (b) TRSMF)

Table 7.1 Thermal transition temperature, enthalpy and crystallinity of pure PEG and TRSMF

		T_m & T_c (°C)	ΔH (J/g)	Crystallinity (%)	
PEG-3400	First cycle	Heating	56.6	174.1	88.4
		Cooling	29.3	158.8	80.6
	Second cycle	Heating	51.7/55.1	154.1	78.2
		Cooling	29.4	158.9	80.7
	Third cycle	Heating	51.7/55.1	154.1	78.2
		Cooling	29.5	159.0	80.7
	Forth cycle	Heating	51.7/55.2	155.2	78.8
		Cooling	29.5	160.0	81.2
TRSMF	First cycle	Heating	49.5	105	53.3
		Cooling	20.4	82	41.6
	Second cycle	Heating	44.7	74	37.6
		Cooling	20.9	83	42.1
	Third cycle	Heating	44.7	73	37.1
		Cooling	21.3	85	43.1
	Forth cycle	Heating	44.8	76	38.6
		Cooling	21.5	87	44.2

Note: T_m is the crystal melting temperature, T_c is the crystal crystallizing temperature, ΔH is the fusion and crystallizing heat, The PEG crystallinity is calculated from the enthalpy data, ΔH , of the crystallization by using the 197 J/g enthalpy value for the fusion of 100% crystalline PEG given by literatures[289, 290].

7.4 Shape memory properties

The cyclic strain-stress curves of TRSMF obtained by thermomechanical cyclic tensile testing are shown in Figure 7.5. The TRSMF has a fixity ratio of more than 85.8% and a recovery ratio more than 95.4%. The detailed shape fixity ratios and recovery ratios are tabulated in Table 7.2. At 60°C, in the first cycle, the maximum stress is 0.07 cN/dtex at 100% elongation.

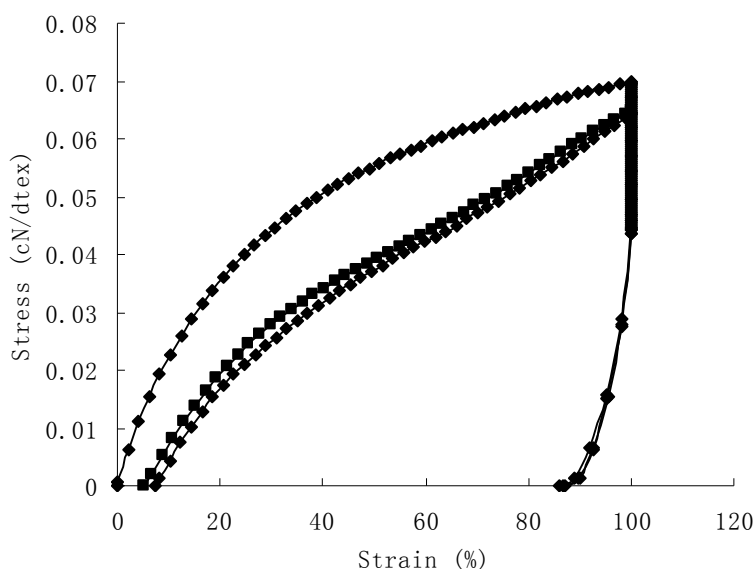


Figure 7.5 The cyclic tensile testing curves of TRSMF

Table 7.2 Detailed shape fixity ratios and recovery ratios of TRSMF

Circle No.	$\epsilon_p(\text{N})$	ϵ_u [$R_f(\text{N})$]	stress at 100% strain(cN/dtex)	$R_{r.tot}(\text{N})$	$R_r(\text{N})$
1	0.0%	85.8%	0.070	100.00%	
2	4.6%	86.7%	0.065	95.40%	95.4%
3	6.6%	87.2%	0.064	93.40%	97.9%

The TRSMF shape memory effect accompanied with phase change effect can be illustrated as follows. In the unstretched state, the PEG phase in the TRSMF has high crystallinity as have been demonstrated by DSC analysis. When the TRSMF is heated from the ambient temperature to 60°C which is above the PEG phase melting temperature (T_{trans}), the fiber absorbs heat energy, and as a result the PEG phase melts and becomes a random state. However, the fiber does not break because of the hard segment ‘physical crosslinks’ which restrict the soft segment phase free movement. When the TRSMF is stretched, the soft segments in the fiber are extended. If the temperature is cooled to below T_{trans} , the latent heat is released and consequently the soft segments crystallize. As a result, the internal stress is stored in the TRSMF and associated deformation is fixed temporally. If the TRSMF is reheated to a temperature above T_{trans} , the soft segment phase absorbs heat energy and becomes flexible and the fiber resumes to the original length as a result of releasing internal stress stored among hard segments. Therefore, the TRSMF show latent heat-storage properties and shape memory effect simultaneously.

7.5 Microstructures

The phase separation microstructure of the SMPU was investigated using atomic force microscopy in a tapping-mode. Atomic force microscopy is a preferred method to examine phase separation structure in polyurethane [337-341] because Transmission Electron Microscopy (TEM) on stained films or element specific TEM [265] has the problem of beam damage or the problem of staining efficacy.

The atomic force microscopy ‘phase’ images were obtained by detecting the phase shift between the actual oscillation of a tip and its drive oscillation. The obtained atomic force microscopy ‘height’ and ‘phase’ images of PEG-based SMPU are shown in Figure 7.6. In phase images obtained by tapping-mode atomic force microscopy, a higher modulus material induces a higher phase offset and it appears lighter as opposed to a softer phase which appears darker. Thus, for the polyurethane system in this investigation, the hard segment phase regions appear lighter while darker regions correspond to the soft polyol phase [340, 342-344]. Ji et al. [56] ever demonstrated the existence of no hard segment domains, interconnected and isolated hard segment domains of SMPU with increasing hard segment content using DSC, thermomechanical analysis and SAXS. Figure 7.6 shows the connected hard segment phase network. This phase structure is like microcapsules with hard segment phase forming hard shells and soft segment phase as cores. In Figure 7.6, the thickness of hard segment phase walls is comparable to the average domain width reported in other: ~9 nm by atomic force microscopy [345] and ~13 nm by TEM [346, 347]. Unfortunately, this phase structure was not observed in the TRSMF.

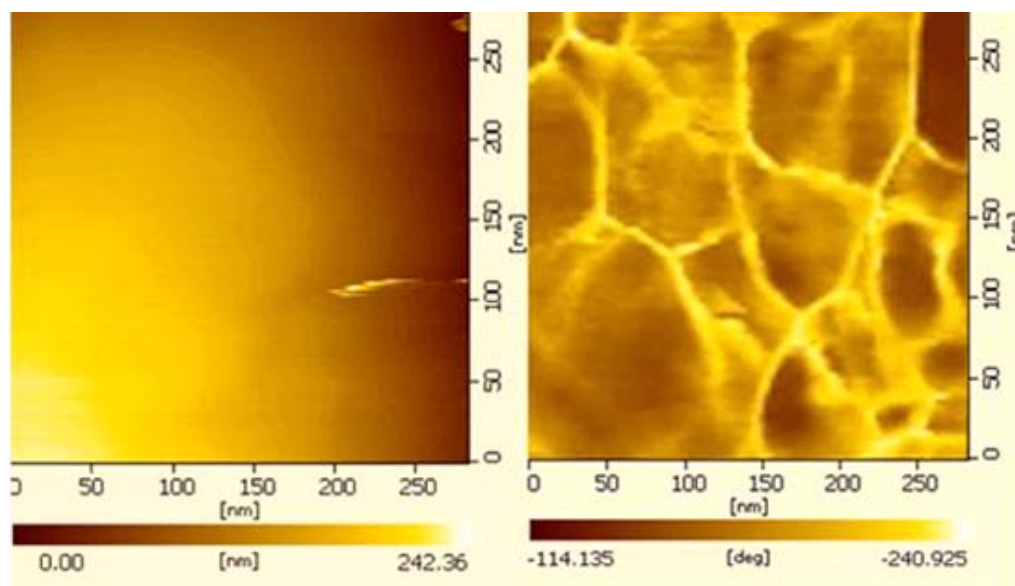


Figure 7.6 AFM images of the bulk polymer (left: height image, right: phase image)

7.6 Summary

A PEG-based thermoplastic SMPU was synthesized and the corresponding fiber was fabricated. The fiber's phase change behaviors, crystalline morphology and microstructures were investigated using POM, DSC and AFM. The prepared 100 dtex fiber had a tenacity of 0.7 cN/dtex and breaking elongation about 488%. The PEG soft segment phase transferring between crystalline and amorphous states resulted in the heat storage and release. At temperature above the PEG phase melting transition, the TRSMF was still solid because the hydrogen bonded hard segments restricted the soft segments free movement. The DSC results indicated that the TRSMF had latent heat storage about 100 J/g. The crystallizing temperature was at 20.9°C and melting

temperature at 44.7°C. The thermomechanical cyclic tensile testing results suggested that the TRSMF had good shape memory effect with the shape fixity ratio more than 85.8% and shape fixity ratio above 95.4%. The disadvantages of the PEG-based SMF as a temperature-regulating fiber were that the degree of the supercooling of the fiber was too high and the mechanical properties of the fiber were not satisfied. Furthermore, due to the significant melt transition at the low temperature, the fiber does not have good spinnability.

CHAPTER 8 SMFs WITH ELECTRO-ACTIVE EFFECT

Conventionally, the thermal-responsive shape recovery of SMPs is induced by directly heating the polymer to a temperature above the switching temperature. MWCNTs were incorporated into SMFs by *in-situ* polymerization to achieve electro-active shape memory effect of the SMF by Joule heating. The influence of MWCNTs on the properties especially shape recovery stress of SMF was studied.

8.1 Spinnability

The SEM images of the SMFs with different MWCNT contents are shown in Figure 8.1. The surface of the MWCNT/SMPU fiber becomes rough and coarse with increasing MWCNT content. When MWCNT content increases from 3 to 5 wt%, the fiber surface becomes very coarse and has bad hand feel. This may be because at a high MWCNT content, some MWCNTs aggregate and are exposed from the fiber surface.

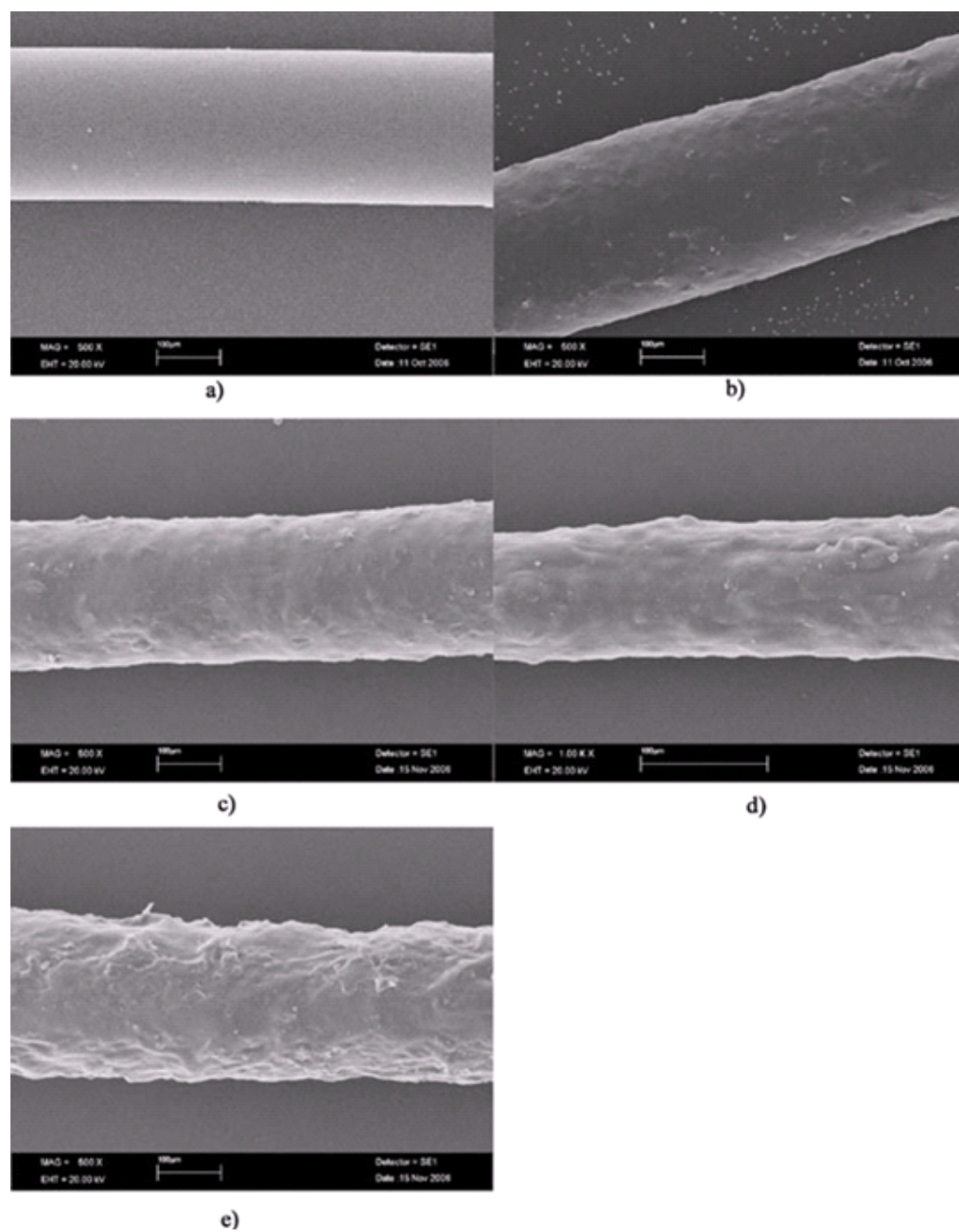


Figure 8.1 Influence of MWCNT on the fiber surface quality; (a): 0 wt%, (b): 1.0 wt%, (c): 3.0 wt%, (d): 5.0 wt%, (e): 7.0 wt% of MWCNT

8.2 Micromorphology

Figure 8.2 shows the SEM image of the MWCNTs used in the study. They were entangled together with long nanosized dimensions. The outer diameter of the MWCNTs was about 10-20 nm. Figure 8.3 the SEM distribution in SMPU films. In MWCNT/SMPU films, many of the MWCNTs are distributed on the film 2-dimensionl plane. Figure 8.4 shows the cross-sectional SEM images of MWCNT/SMPU fibers. In the MWCNT/SMF, most MWCNTs are perpendicular to the fiber cross-section, which suggests that most MWCNTs are preferentially aligned in the fiber axial.

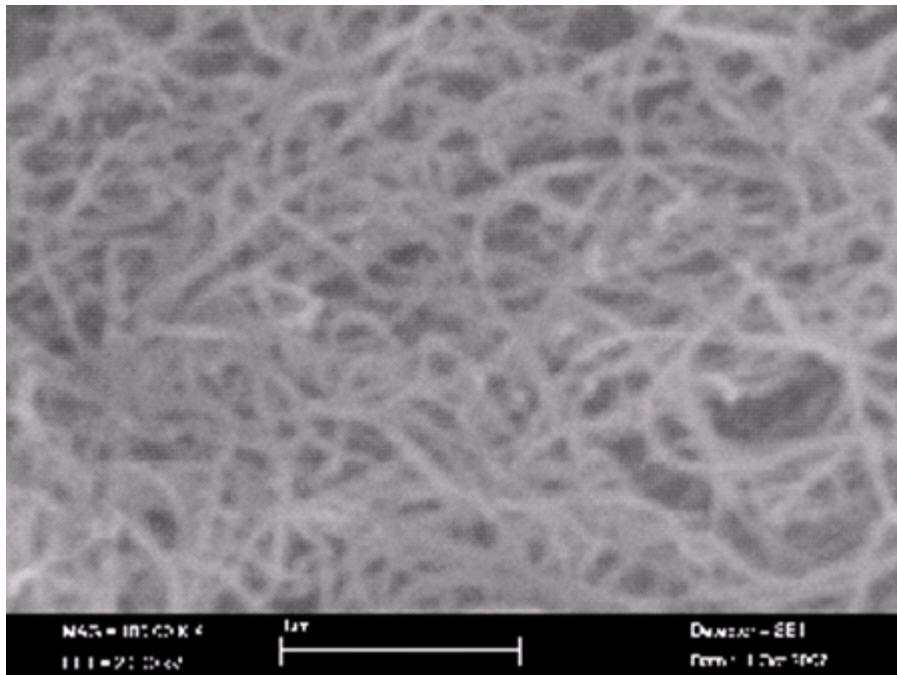


Figure 8.2 SEM images of MWCNT

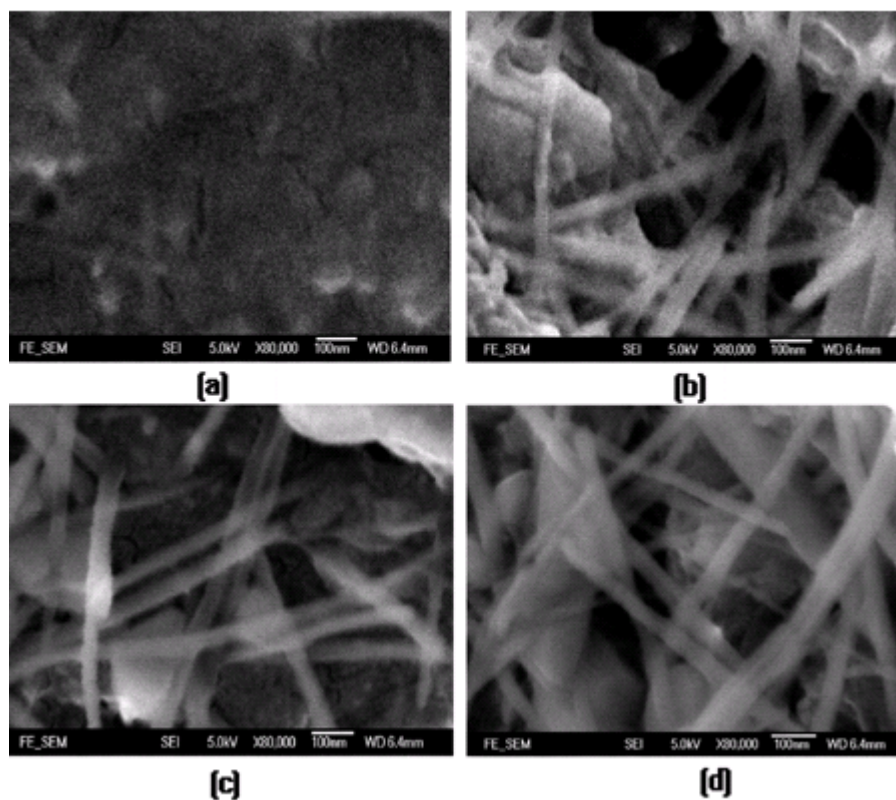


Figure 8.3 In-plane surface images of traditional MWCNT/SMPU films after etching using DMF (a: 0.25 wt% MWCNTs, b: 1.0 wt% MWCNTs, c: 2.0 wt% MWCNTs, d: 3.0 wt% MWCNTs).

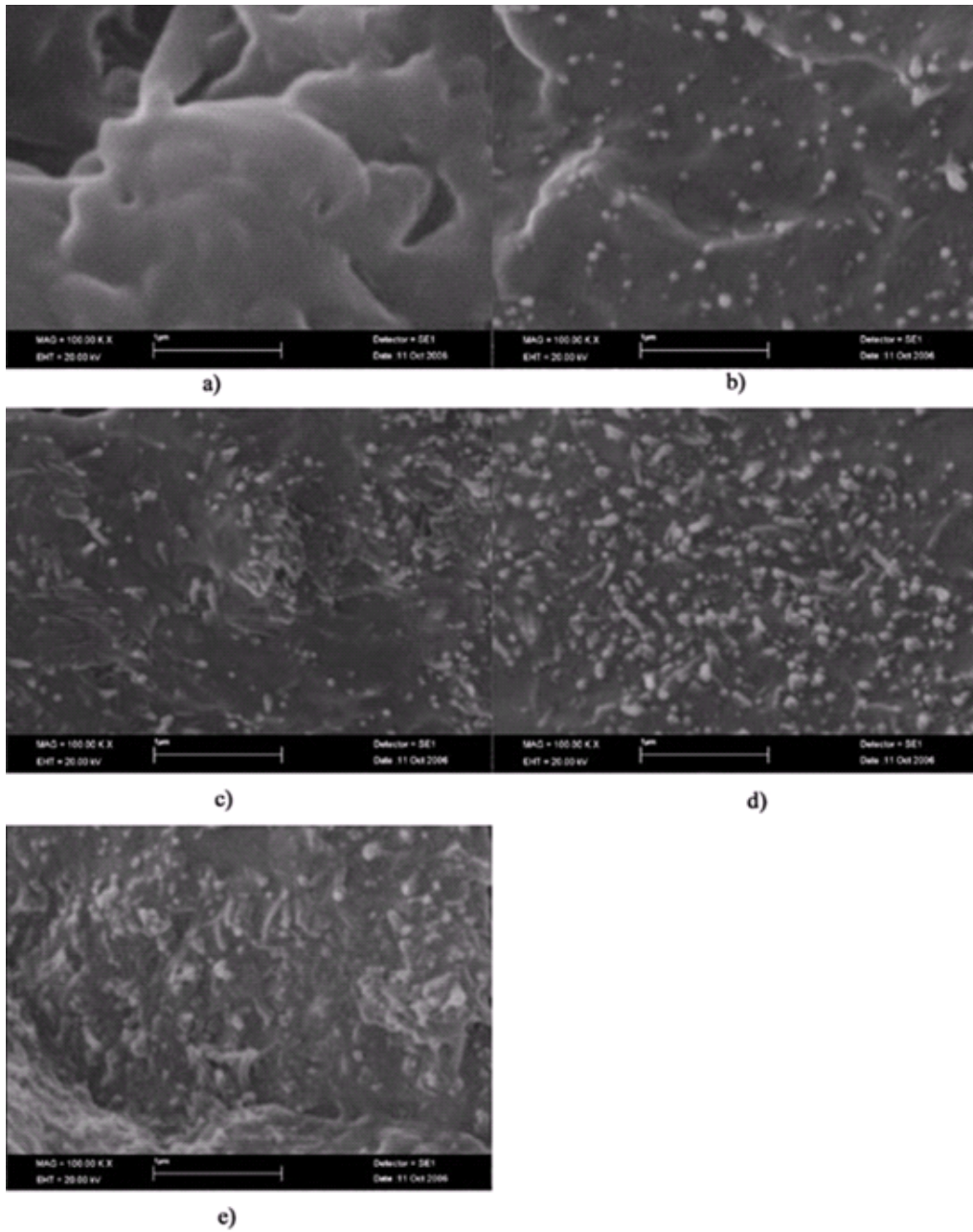


Figure 8.4 SEM images of the fracture surface of the fibers with (a) 0 wt%, (b) 1.0 wt%, (c) 3.0 wt%, (d) 5.0 wt%, (e) 7.0 wt% MWCNT content

Many researchers have developed polymeric composites with aligned CNTs by different methods [283-286, 288, 348-352]. Haggenueller et al. [283]

prepared CNT/poly(methyl methacrylate) fibers with aligned CNTs by solvent casting and melt spinning. Thostenson and Chou [285] utilized a micro-scale twin-screw extruder and post drawing to disentangle and align MWCNTs uniformly in a polystyrene thermoplastic matrix. Cooper et al. [348] developed CNT/poly(methyl methacrylate) composites with aligned CNT by melting blending and extrusion. Miaudet et al. [349] prepared CNT/PVA fibers with aligned CNT by a solution spinning and post drawing method.

Figure 8.4 shows that at 1.0 wt%, the MWCNTs can be distributed homogeneously in the SMPU matrix. At 3.0 wt% MWCNT content, a little aggregation is observed. With continuously increasing MWCNT content, the MWCNT distribution becomes inhomogeneous.

The model in Figure 8.5 can be employed to explain the distribution and alignment effect of the MWCNTs in the SMFs induced by melt extrusion and melt spinning processes. In Figure 8.5, the soft segments of polyester are shown as being coiled or folded on themselves. The schematic section length of the zig-gag line corresponds to one repeating unit within the polyol. The isocyanate is shown as rigid circles. The hard segments are rigid and fixed, having a tendency to adhere to each other through strong hydrogen bonding. The MWCNTs are entangled with polyurethane on a molecular level in the polymer matrix. During *in-situ* polymerization, the treated MWCNTs are pre-distributed in the MDI by the ultrasonic process. The SMPU molecular chains grow on the treated MWCNT surface. As a result, the MWCNT adhere to SMPU matrix, especially to the hard segments (diisocyanates). When the MWCNT/SMPU composites are heated above the T_{trans} , the soft segment

phases are melted. During melt blending, extrusion and spinning process, the higher shear force, and drawing ratio contribute to the improved homogenous distribution and axial alignment of the MWCNTs. This alignment effect is more pronounced as the SMP is composed of soft and hard segments. The hard segment phase fixed by hydrogen bonding may stretch the curled MWCNTs to align axially.

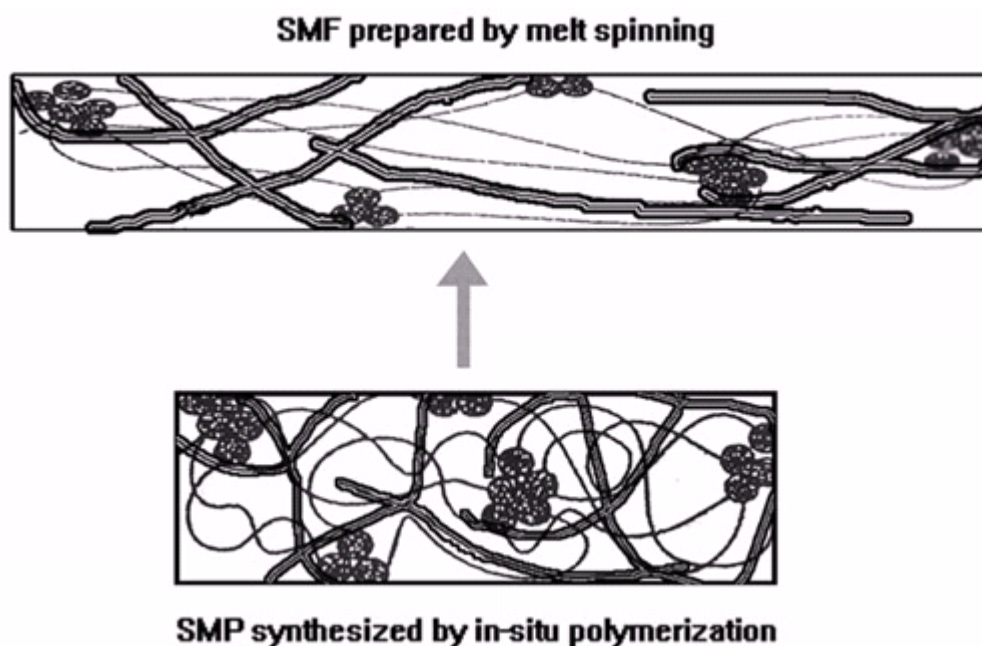


Figure 8.5 Schematic representation of MWCNT alignment in the SMF during blending and spinning (The thin lines represent chains of polyols, the circles represent aggregated hard segment groups, and the thick hollow lines represent MWCNTs.)

8.3 Electro-active shape memory effect

The homogeneously and axially aligned MWCNTs in the SMP matrix can contribute to the conductivity of MWCNT/SMF. However, due to the aggregation of MWCNTs and the difficulty of fabricating MWCNT/SMFs with a high MWCNT content, the MWCNT/SMF conductivity can not reach a very high level. Furthermore, when the MWCNT content reaches 8.0 wt%, the MWCNT/SMF could not be fabricated.

At low MWCNT content, the MWCNT/SMF electrical resistance was too high and no electro-responsive shape memory effect was observed. When the MWCNT content reached 7.0 wt%, the prepared MWCNT/SMF maximum strain was very low and large stretching deformation could not be performed. In this study, MWCNT/SMFs having 6.0 wt% MWCNT content with 90% elongation at break were used. The electro-active shape recovery of the SMPU rod with 6.0 wt% MWCNT content is presented in Figure 8.6 (A – E). The SMPU rod was obtained from the melt extrusion right before pelleting. The temporary shape was obtained by bending the rod in hot water. The ends of the rod are connected with power source by conductive wires. The shape recovery started at 1 second (B); and the speed of recovery increased within the first 10 seconds (C-D), after which the shape recovery speed decreased (D-E). The shape recovery process finished within 1 minute (A-F). When studying the electro-active shape memory effect of MWCNT/SMFs, 20 pieces of fibers were employed together because one fiber's resistance was too high to produce enough heat to heat the sample temperature to above the switching temperature (about 42°C). The fibers original length was 60 mm (the original length in

Figure 8.7 (a)). They were first stretched to 90 mm (50% strain) in a temperature controllable chamber at 60°C. After being cooled to the ambient temperature and gotten rid of external stress, the fibers' length became 80 mm (the length after elongation in Figure 8.7 (b)). Then the MWCNT/SMFs were connected to a power source of 210 V. The fibers began to shrink. Finally, the fibers recovered the original length of about 60 mm.

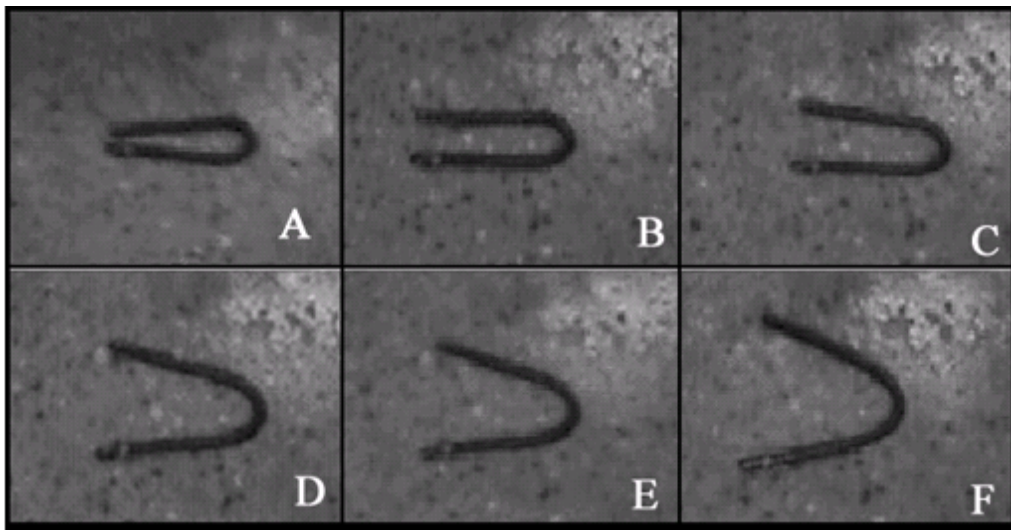


Figure 8.6 The electro-active shape recovery effect of MWCNT/SMFs rod

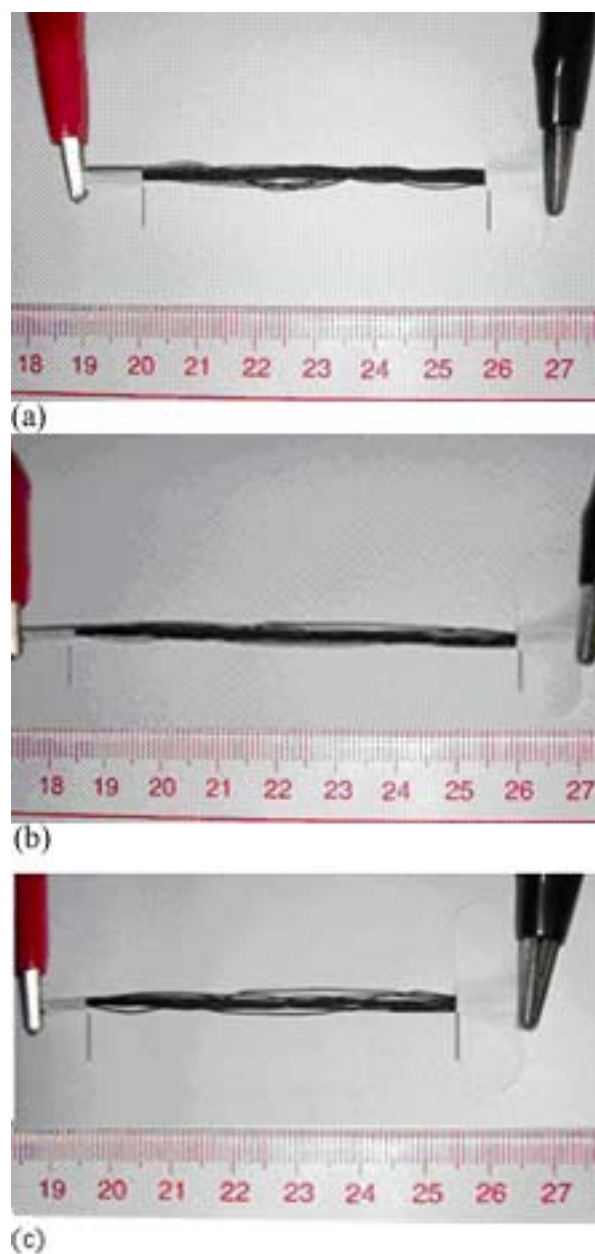


Figure 8.7 The electro-active shape memory effect of MWCNT/SMFs ((a) the original length, (b) the length after elongation, (c) the length after recovery).

8.4 Stress storage properties

The shape recovery driving force of SMFs is the stress stored in the hard segment phase during deformation. If the fiber is heated above the switching

transition temperature, the internal stress stored in the hard segment phase releases and thereby the fiber returns to its original length. Therefore, it is very important to investigate the influence of the MWCNTs on the stress relaxation of the SMF during deformation.

The curves of stress relaxation of MWCNT/SMFs after stretching are presented in Figure 8.8. The MWCNT/SMFs reach the set maximum strain (%) and the stresses reach the maximum values after the 2 minutes. With increasing MWCNT content, the maximum stress increases greatly. Though the stress of MWCNT/SMF at 7.0 wt% MWCNT is lower than that of MWCNT/SMP at 5.0 wt%, it is still much higher than that of pure SMF. This is also the case at the plateau stress. These results indicate that the aligned MWCNTs may help storing the internal elastic energy during deformation.

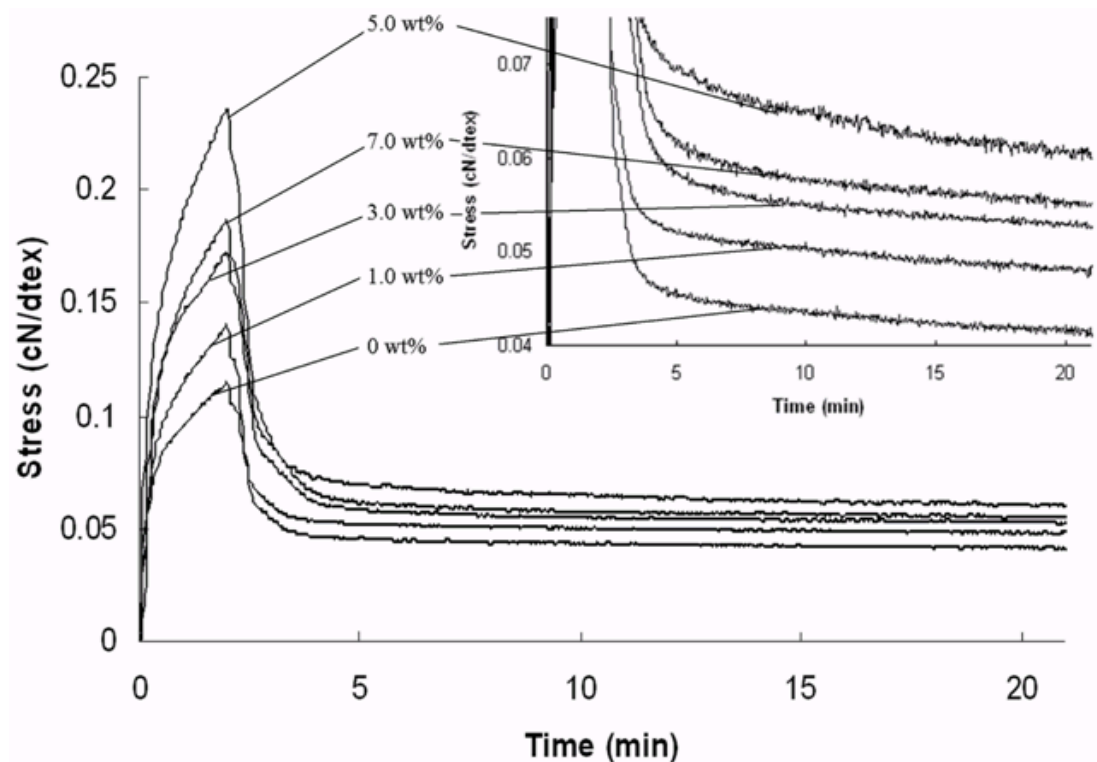


Figure 8.8 Stress relaxation of SMFs with different MWCNT contents (with partial enlarged details)

8.5 Shape recovery stress

The cold drawing shape recovery stress of MWCNT/SMFs at different MWCNT contents is shown in Figure 8.9. The recovery stresses of MWCNT/SMFs at 1.0 wt% and 3.0 wt% MWCNT contents are much higher than that of pure SMF. At 3.0 wt% MWCNT content, the recovery stress of the composite fiber is more than two times of that of pure SMF. For pure SMF, the recovery stress is mainly contributed by the hard segment phase, while for the MWCNT/SMF systems, the aligned MWCNTs having high interaction with hard segment may also contribute to the recovery stress improvement.

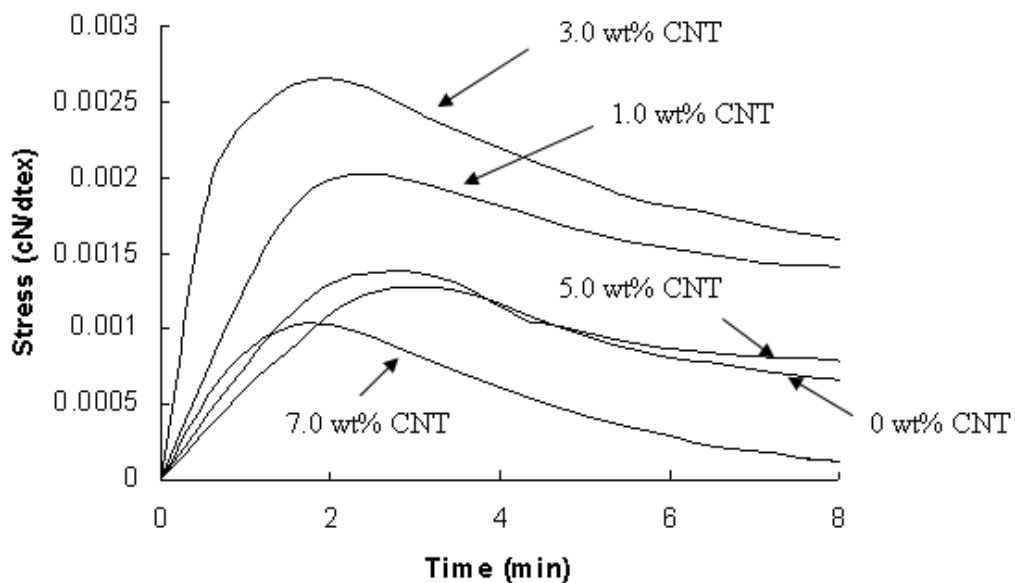


Figure 8.9 Shape recovery stress of MWCNT/SMFs with different MWCNT contents

With continuously increasing the MWCNT content to 5.0 wt%, the shape recovery stress of the composite fiber drops rapidly. This can be ascribed to three reasons. First, with increasing MWCNT content, homogenous distribution is more difficult to be achieved. Second, fiber surface quality becomes poor. Both of these factors deteriorate the mechanical strength of the composite fiber. Third, the fiber recovery degree also decreases at this high level MWCNT content, which may also bring down the recovery stress.

8.6 Summary

MWCNTs were incorporated into SMFs by *in-situ* polymerization and melt spinning. MWCNTs were treated with a mixture of concentrated sulfuric acid and nitric acid to improve their compatibility with SMP matrix prior to use. The spinnability of MWCNT/SMF decreased significantly with increasing the MWCNT content. When the MWCNT content reached 7.0 wt%, the processability of the composite deteriorated and the spinnability was lost. At MWCNT contents below 5.0 wt%, the MWCNTs were distributed homogeneously and aligned axially in the fibers by the melt blending, extrusion, and melt spinning process. At high MWCNT contents, the aligned MWCNT aggregated. By employing a power of 210 V and 20 pieces of 210 denier monofilaments, at 6.0 wt% MWCNT, the electro-active shape memory effect was observed. The recovery force was increased markedly because of the interaction between the MWCNTs and SMPU molecules, especially with hard segments, which helped store the internal elastic energy during loading and shape fixing.

CHAPTER 9 SMFs FOR BIOLOGICAL APPLICATIONS

In comparison with their bulk counterpart, SMFs may have outstanding mechanical properties and shape recovery force because of molecular orientation. In comparison with spandex and polyester fiber, shape memory fabrics may have better capabilities for 3-D textile due to good shape fixity. Furthermore, the fabrics made of shape memory fibers may fit wearers well and bring comforting feeling to wearers resulting from the good deformability and retention properties of SMFs. Therefore, SMFs and fabrics in the special forms may find promising applications as biomedical materials such as wound dressing, scaffolding materials and pressure garments.

For biomedical applications, it would be ideal if the shape recovery can be triggered by human body temperature. The internal temperature of human bodies is 36.5°C with fluctuation below 1.5°C [289]. The T_g type SMPU was used because of the easy adjustment of glass transition temperature (switching temperature) by varying the soft segment length and content. The switching temperature of the SMF was adjusted to a value around body temperature.

The evaluation of animal responses to the fiber is important in determining SMF's capacity for clinical situations. Specific requirements may differ according to the nature of applications. In this study, not focusing on one specific application, the biological evaluations of the prepared fiber were preliminary conducted in terms of cytotoxicity, haemolysis, sensitization and dermal irritant.

9.1 Morphology

The synthesized SMPU solution with a solid concentration 25 wt% is shown in Figure 9.1. The fabricated SMFs are presented in Figure 9.2. Figure 9.3 shows the optical image of the shape memory multifilament surface.



Figure 9.1 PBA-based SMP solution for wet spinning



Figure 9.2 PBA -based SMFs prepared by wet spinning

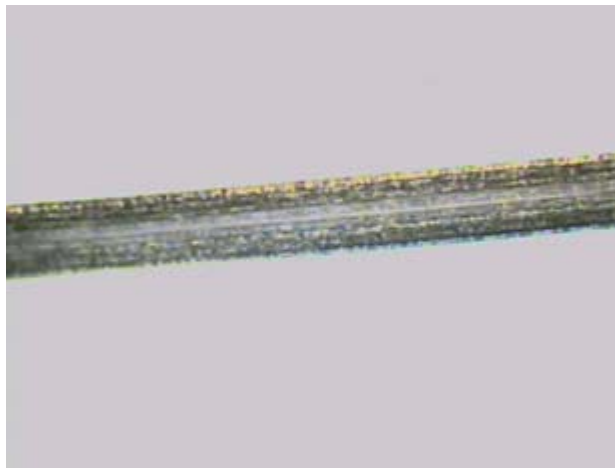


Figure 9.3 The image of the prepared shape memory multifilament

9.2 Thermal properties

The glass transition temperature of the SMF was determined using DSC. As shown in Figure 9.4, the SMF displays an endothermic step change at 35.9°C indicating the glass transition of the soft segment phase. This glass transition at 35.9°C of soft segment phase is employed as the switching temperature of the SMF to fix and unfix the shapes at below and above the thermal transition temperature. The switching temperature is close to body temperature, so that shape changes may be triggered by human bodies. Two hard segment melting transition peaks are observed on the curve at 121.9 and 144.0°C, which indicates that the hard segment phase may crystallize slightly [115].

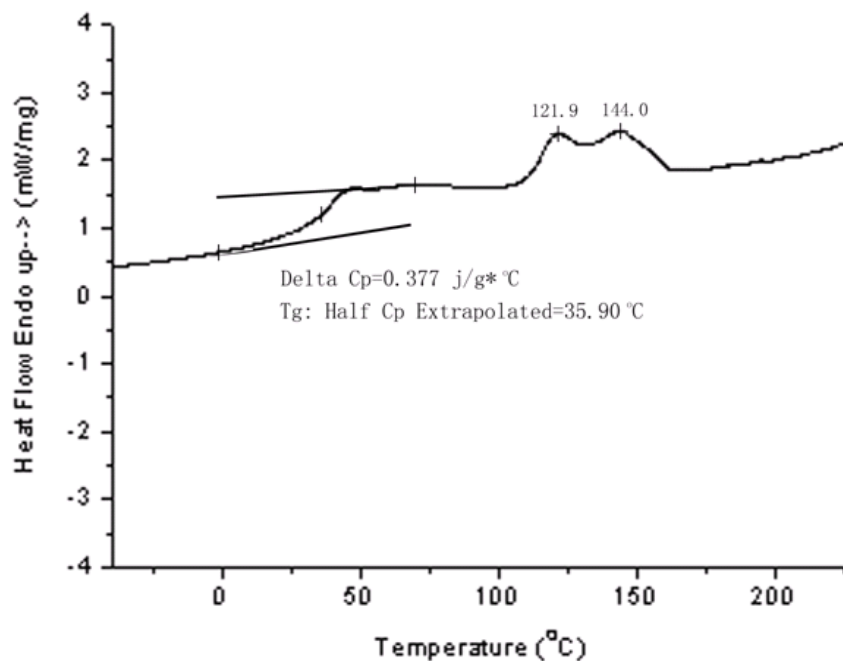


Figure 9.4 The DSC of the SMF

9.3 Molecular orientation

SAXS has been extensively used to study the oriented structures of polymer fibers [353-355]. The SAXS patterns of the SMF and shape memory film are shown in Figure 9.5 and Figure 9.6. The arrow in Figure 9.5 denotes the direction of the fiber axis. The SAXS of the SMPU film was taken in an arbitrary direction. The equatorial streak in Figure 9.5 is contributed by the surface reflection of the fibers. The asymmetric scattering pattern in Figure 9.5 indicates the overall molecular orientation in the SMF caused by the spinning process [355, 356]. Since intrinsically no significant molecular orientation exist in the shape memory film, symmetric scattering pattern is observed in Figure 9.6.

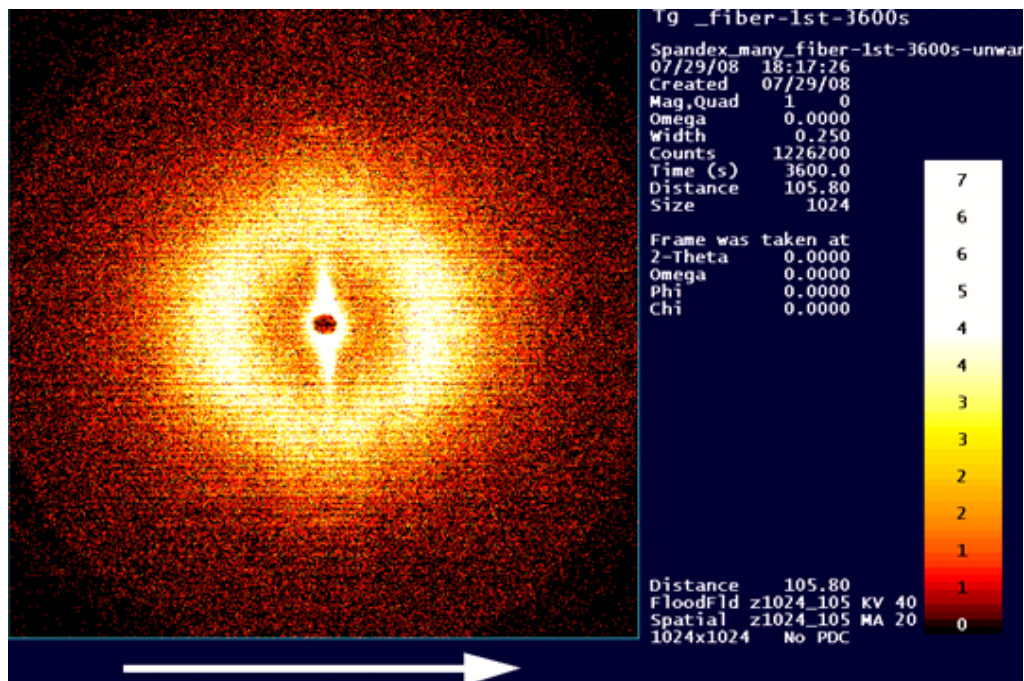


Figure 9.5 The SAXS pattern of the SMF

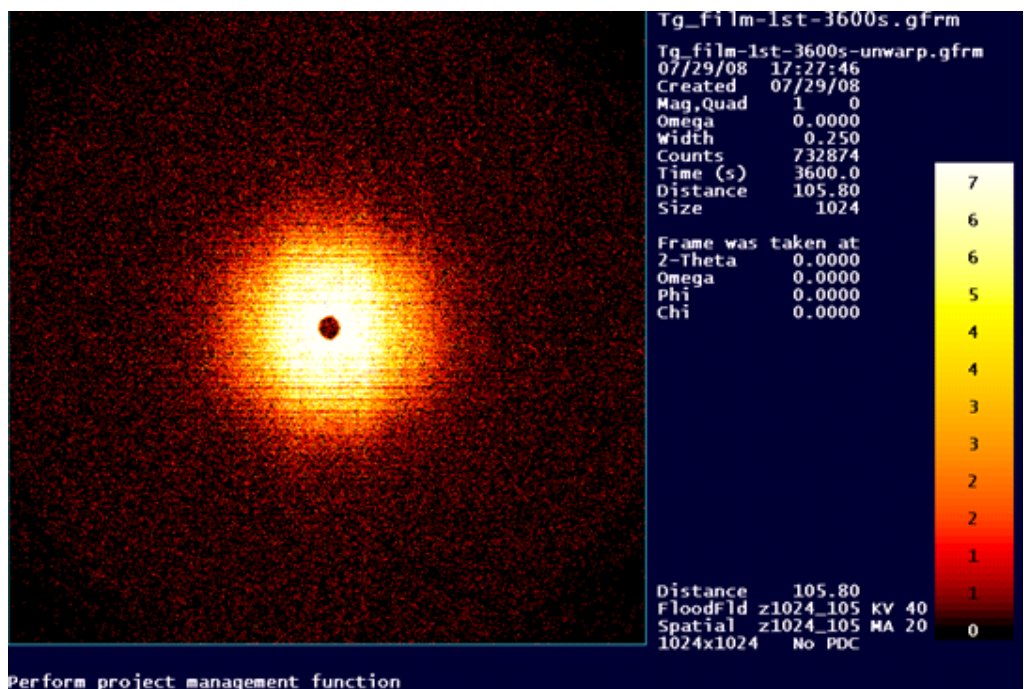


Figure 9.6 The SAXS pattern of the SMPU film

The molecular orientation in the SMF was also studied using FTIR dichroism in comparison with the shape memory film. The infrared spectra of the SMPU film with the polarizer in an arbitrary direction and the direction perpendicular to the arbitrary direction are presented in Figure 9.7. Since the dichroic ratio of specific groups in samples is determined from relative intensity ratios of the selected bands of the infrared spectra obtained with the polarizer parallel (A_{\parallel}) and perpendicular (A_{\perp}) to the fiber direction, if there is no difference between the A_{\parallel} and perpendicular A_{\perp} , there should be no molecular orientation of the specific groups. Figure 9.7 suggest that the shape memory film have no difference between the two spectra at the two directions. This is because intrinsically in the film there is hardly any molecular orientation.

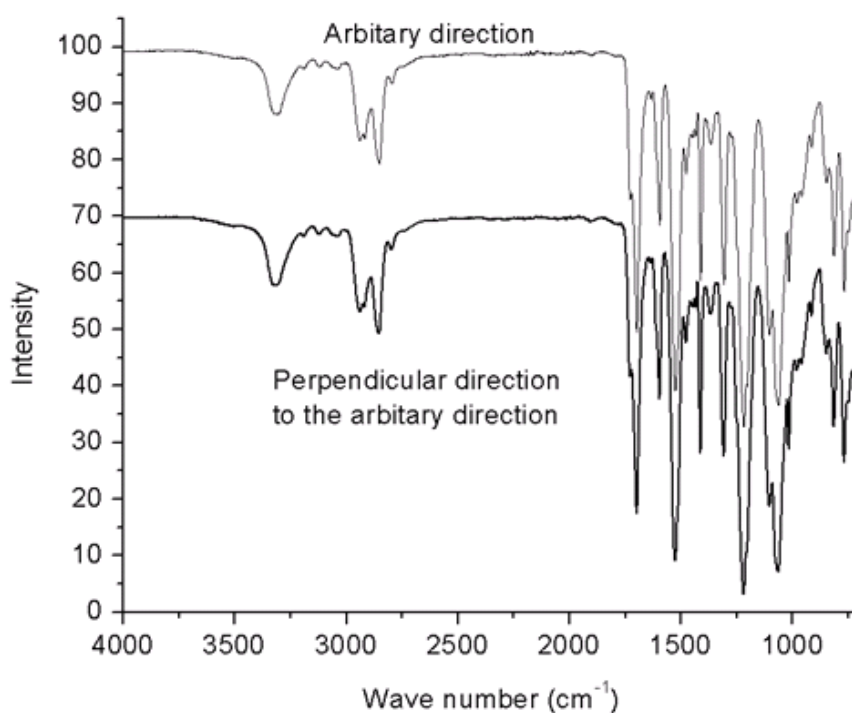


Figure 9.7 The infrared spectra of the shape memory film with the polarizer in an arbitrary direction and the direction perpendicular to the arbitrary direction

As shown in Figure 9.8, the intensity of infrared spectra of the SMFs with the polarization direction parallel and perpendicular to the fiber axis are significantly different. This indicates there is a preferential orientation of hard and soft segments phase in the SMF with respect to the fiber direction [357]. The orientation function magnitude for a perfectly oriented polymer is 1.0. Siesler et al. [357] have calculated that, on the basis of the urethane crystal structure, the highest orientation function to be expected is 0.65. In this study the soft orientation function of SMF calculated by using C-H bond wagging at 1358 cm^{-1} is 0.36, and the hard segment orientation function calculated by using N-H bond stretching vibration at 3322 cm^{-1} is 0.12. The soft segment and hard segment orientation structure also suggest the physical difference between the SMF and Spandex fibers.

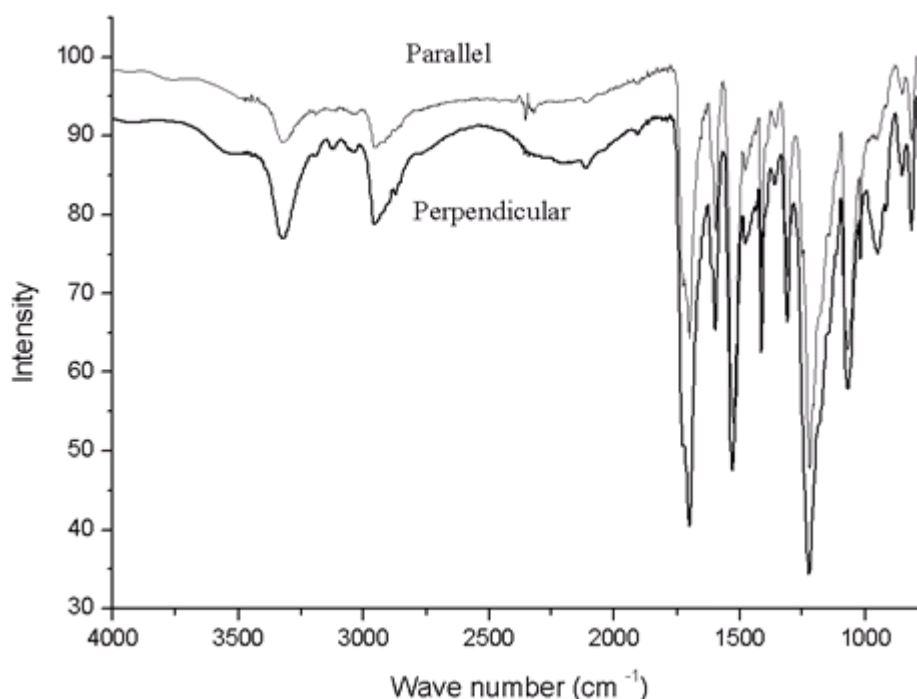


Figure 9.8 The infrared spectra of the SMF with the polarizer parallel and perpendicular to the fiber direction

9.4 Dynamic mechanical properties

The elastic modulus (E') and loss tangent ($\text{Tan } \delta$) of the SMF and SMPU film over the temperature range from -100 to 250°C are shown in Figure 9.9 and Figure 9.10 respectively.

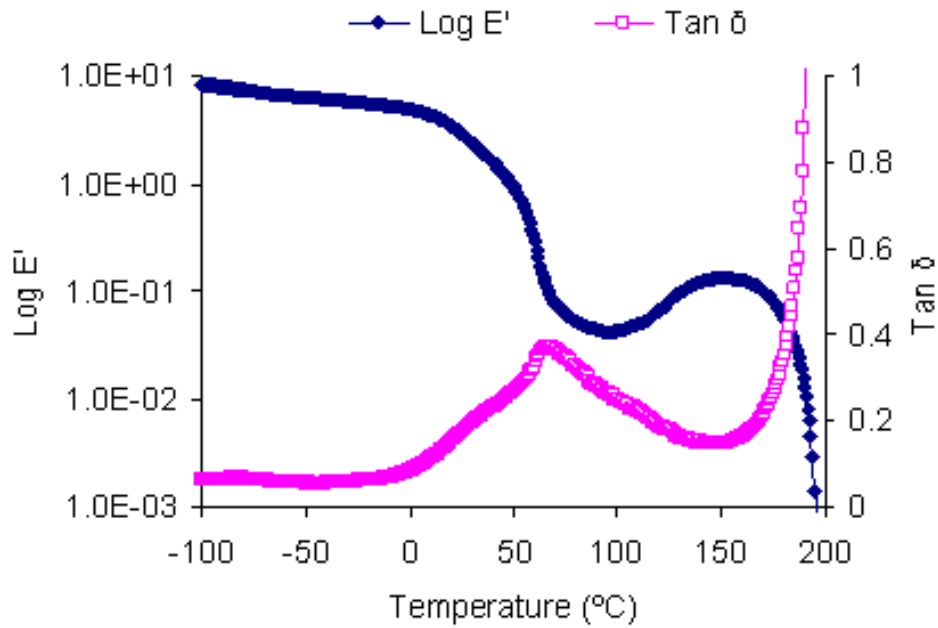


Figure 9.9 The $\text{Log } E'$ - temperature curve and $\text{Tan } \delta$ - temperature curve of the SMF, E' (cN/dtex)

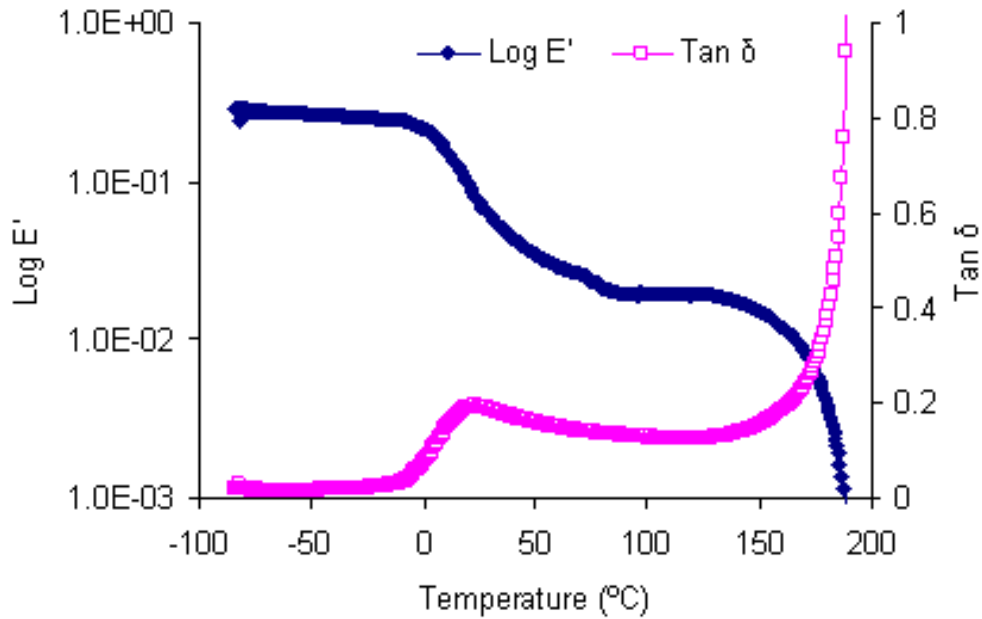


Figure 9.10 The Log E' - temperature curve and $\text{Tan } \delta$ - temperature curve of the SMPU film, E' (cN/dtex)

Figure 9.9 shows that the $\text{Tan } \delta$ peak of the SMF locates at 55°C , which is associated with the glass transition of the SMF. The E' of the SMF shows an increase at above glass transition temperature due to the molecule disorientation of the polyurethane, which may have slightly shifted the glass transition temperature during the temperature scanning. As shown in Figure 9.10, in the E' curve of the shape memory film, the E' increase is not observed at above the glass transition temperature.

9.5 Mechanical properties

The mechanical properties of the SMF are compared with the corresponding shape memory film. Dumb-bell shape specimens of SMPU films were

prepared by injection molding using a HAAKE MiniJet. The SMPU melt was loaded to the melt cavity of the injection molding system immediately after extrusion. The cavity temperature was set at 190°C and the mold temperature was ambient temperature. The dumb-bell shape specimens of SMPU film is shown in Figure 9.11.



Figure 9.11 Dumb-bell shape specimens of SMPU film

The static strain-stress curves of SMFs and films are presented in Figure 9.12. The SMF has an average tenacity of about 1.04 cN/dtex, and a breaking elongation of 76%. The breaking strength of the SMF is about 5 times of that of the SMPU film. Therefore, the SMF and the prepared fabric may be used in the body parts where high stress is required.

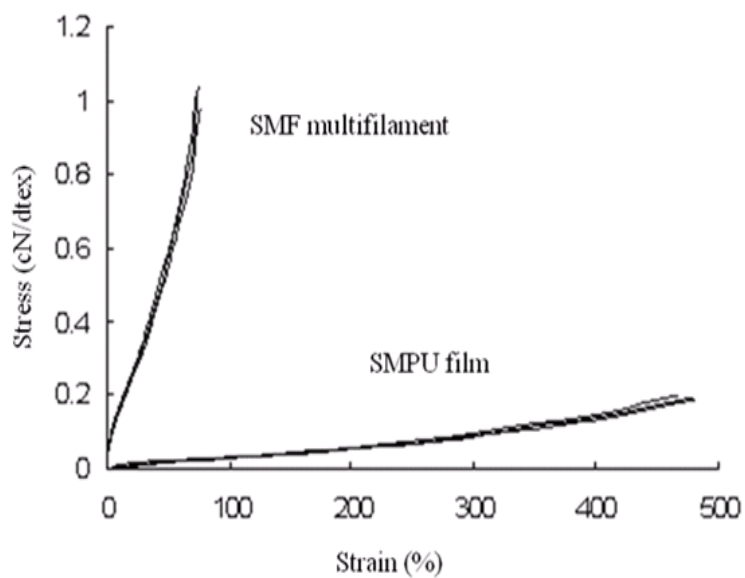


Figure 9.12 The tensile properties of the SMF multifilament and SMPU film

9.6 Shape memory properties

The thermomechanical cyclic tensile testing curves of the SMF are presented in Figure 9.13. The SMF has a fixity ratio of more than 80% and recovery ratio up to 90% in the first cycle.

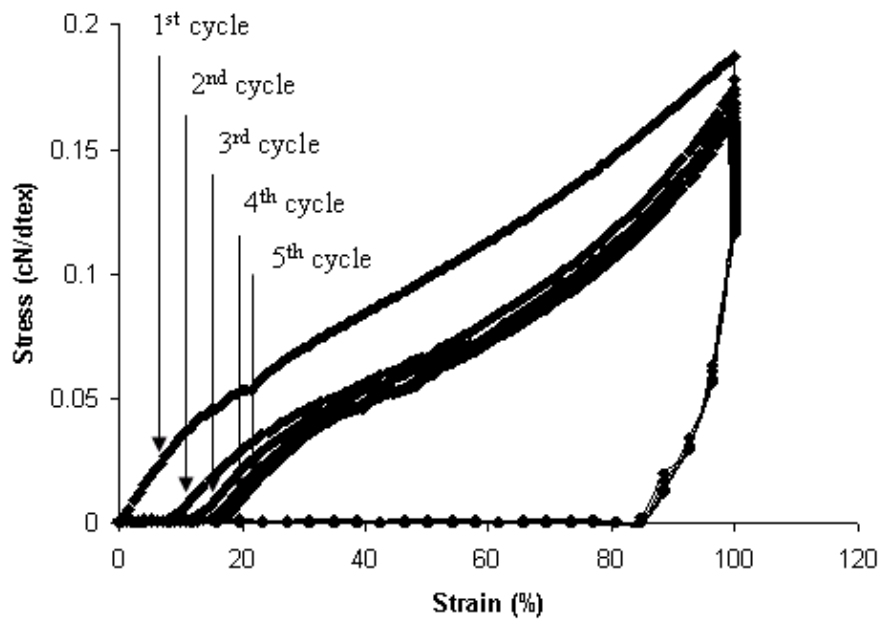
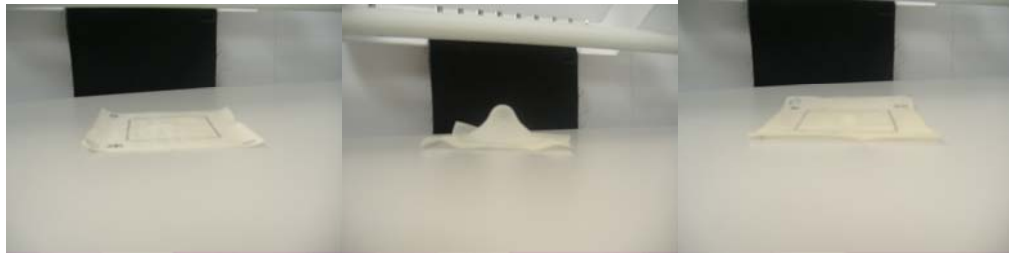


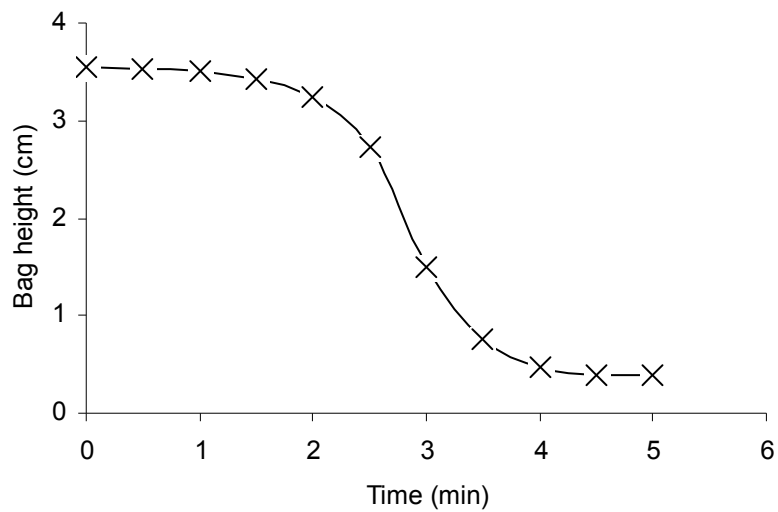
Figure 9.13 The thermomechanical cyclic tensile testing curves of the SMF

Figure 9.14(a) and (b) show the shape memory behavior of the shape memory fabric. A bag is first developed on the shape memory fabric by using an Instron machine at 36.5°C. The bag shape is fixed by cooling the shape memory fabric to a low temperature. With increasing temperature, after about 2 minutes the bag height recovers rapidly to about 0.4 cm. As shown in Figure 9.14(b), the bag does not recover flat completely. This may be partially due to the molecule orientation and weak point broken of the fiber molecules. Also, it may be influenced by the fabric knitting structure. The friction and entanglement between fibers in the fabric may decrease the shape recovery ratio. Changing fabric structures will result in different fabric mechanical properties and different shape memory effects, which may make the shape memory fabric to be suitable for different applications situations.



Original shape Deformed shape Recovery shape

(a)



(b)

Figure 9.14 The bag recovery curve of the shape memory fabric (a: the shapes of the bag during the shape recovery testing process; b: the height change of the bag during the shape recovery as a function of time)

The shape memory behavior of the T_g type SMF may be illustrated using the molecule model shown in Figure 9.15. In Figure 9.15, the soft segments PBA are shown as being coiled or folded on themselves. The schematic section

length of the zig-gag line corresponds to one repeating unit within the PBA. The MDI is shown as a rigid circle. The hard segments have a tendency to adhere to each other through strong hydrogen bonding. During SMF melt spinning at a temperature above T_{perm} , the SMF is fabricated. Upon cooling to the ambient temperature below T_{trans} , the fiber is winded up and the permanent fiber shape is cast. At ambient temperature, in the unstretched state, the fiber has its molecules oriented at a certain extent as a result of the spinning process. When the fiber is heated above T_g , the soft segment phase turns into a “random” state. If it is stretched, the soft segment phase is extended. If the temperature is again cooled to a temperature below T_g , the soft segment phase becomes inflexible. As a result, the internal stress is stored in the hard segment phase and the associated deformation is fixed temporarily. If the SMF is reheated to a temperature above T_g , the soft segment phase becomes flexible. Therefore, the fiber resumes to the folded configuration as a result of releasing the internal stress stored among the hard segments.

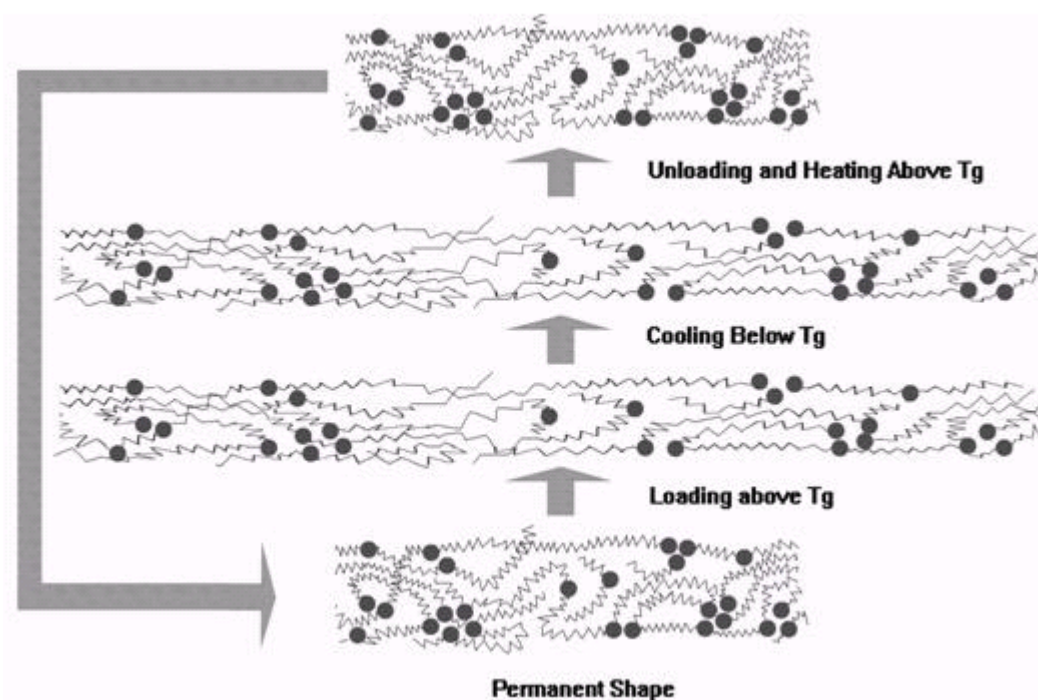


Figure 9.15 The schematic representation of the molecular mechanism of the shape memory effect of the SMF

9.7 Cytotoxicity

The biological reactivity (cellular degeneration and malformation) was described and rated on a scale of 0 to 4 as shown in Table 9.1.

Table 9.1 The biological reactivity rated on a scale of 0 to 4

Grade	Reactivity	Description of reactivity zone
0	None	No detectable zone around or under specimen
1	Slight	Some malformed or degenerated cells under specimen
2	Mild	Zone limited to area under specimen
3	Moderate	Zone extends 0.5 to 1.0 cm beyond specimen Zone extends greater than 1.0 cm beyond specimen but does
4	Severe	not involve entire dish

The responses obtained from the negative and positive controls and the shape memory fabric are shown in Table 9.2. The test system was considered suitable because the observed response corresponds to the labeled biological reactivity grade of the relevant reference standard. The test article met the requirements of the test if none of the cell cultures exposed to the test article exhibit greater than a mild reactivity (grade 2). Based on the test result and under the conditions of the test, the test article met the requirement of the test and was not considered cytotoxic.

Table 9.2 Agar diffusion test results

Article	Reactivity grade @24 hours
Positive control (1 cm ² Latex)	3
Positive control (1 cm ² Latex)	3
Positive control (1 cm ² Latex)	3
Negative control (Physiological saline, 0.1 ml)	0
Negative control (Physiological saline, 0.1 ml)	0
Negative control (Physiological saline, 0.1 ml)	0
Shape memory fabric (1 cm ²)	0
Shape memory fabric (1 cm ²)	1
Shape memory fabric (1 cm ²)	1

9.8 Haemolysis

The haemolysis index was calculated according to the equation below.

$$\text{Haemolysis index (\%)} = \frac{A_{TS} - A_{NC}}{A_{PC} - A_{AC}} \times 100\%$$

A_{TS} : Absorption of test group; A_{PC} : Absorption of positive control group; A_{NC} : Absorption of negative control group.

A mean haemolysis index from the three test samples of 5% or less was considered to be nonhaemolysis. Absorption of negative control solution should be not more than 0.03; absorption of positive control solution should be

0.8±0.3. The absorption data of test and control groups are presented in Table 9.3. The free hemoglobin concentration was measured to determine the haemolysis index of the test article extracts by a spectrophotometrical method. Under the conditions of this study; haemolysis was not observed in the diluted rabbit blood which directly contacted with the test article extracts. Haemolysis index of the test article was 0.35%.

Table 9.3 Haemolytic index

Group	Absorption			Average	Haemolysis index (%)
Test	0.006	0.005	0.008	0.006	
Negative	0.005	0.003	0.002	0.003	0.35%
Positive	0.870	0.850	0.884	0.868	

9.9 Sensitization

The specific rating standard of sensitization is presented in Table 9.4. The guinea pig closed patch sensitization test results of control group (induction: 25 hilltop chamber moist with saline; challenge: 1 square inch test article using a 25 mm hilltop chamber moist with saline) are shown in Table 9.5. The guinea pig closed patch sensitization test results of the test group (dosage: 1 square inch test article using a 25 mm hilltop chamber moist with saline) are given in Table 9.6. Based on the test results, the shape memory fabric was not considered a sensitizer in guinea pigs.

Table 9.4 Scoring criteria for skin reactions

Erythema formation		Edema formation	
No erythema	0	No edema	0
Slight erythema	1	Slight edema	1
Well-defined erythema	2	Well-defined edema	2
Moderate erythema	3	Moderate edema	3
Severe erythema to slight eschar formation	4	Severe edema	4
Total possible erythema score=4		Total possible edema score=4	

Table 9.5 Guinea pig closed patch sensitization test results of control group (induction: 25 hilltop chamber moist with saline; challenge: 1 square inch test article using a 25 mm hilltop chamber moist with saline)

Induction	Time after application	Animal number (sex)				
		1M	2M	3M	4F	5F
1	7 hours	0/0	0/0	0/0	0/0	0/0
	24 hours	0/0	0/0	0/0	0/0	0/0
2	7 hours	0/0	0/0	0/0	0/0	0/0
	24 hours	0/0	0/0	0/0	0/0	0/0
3	7 hours	0/0	0/0	0/0	0/0	0/0
	24 hours	0/0	0/0	0/0	0/0	0/0
Challenge	24 hours	0/0	0/0	0/0	0/0	0/0
	48 hours	0/0	0/0	0/0	0/0	0/0

Table 9.6 Guinea pig closed patch sensitization test results of the test group (dosage: 1 square inch test article using a 25 mm hilltop chamber moist with saline)

Induction	Time after application	Animal number (sex)									
		1M	2M	3M	4M	5M	6F	7F	8F	9F	10F
1	7 hours	0/0	0/0	0/0	0/0	0/0	0/0	0/0	0/0	0/0	0/0
	24 hours	0/0	0/0	0/0	0/0	0/0	0/0	0/0	0/0	0/0	0/0
2	7 hours	0/0	0/0	0/0	0/0	0/0	0/0	0/0	0/0	0/0	0/0
	24 hours	0/0	0/0	0/0	0/0	0/0	0/0	0/0	0/0	0/0	0/0
3	7 hours	0/0	0/0	0/0	0/0	0/0	0/0	0/0	0/0	0/0	0/0
	24 hours	0/0	0/0	0/0	0/0	0/0	0/0	0/0	0/0	0/0	0/0
Challenge	24 hours	0/0	0/0	0/0	0/0	0/0	0/0	0/0	0/0	0/0	0/0
	48 hours	0/0	0/0	0/0	0/0	0/0	0/0	0/0	0/0	0/0	0/0

9.10 Dermal irritation

The scoring criteria for skin reactions are shown in Table 9.7 and the dermal irritation response categories are tabulated in Table 9.8. The primary skin irritation summary of scores for skin irritation (dose = 25 mm x 25 mm (moist with physiological saline)) is shown in Table 9.9. All sites were intact. Based on the test result and under the conditions of the test, the test article met the requirement of the test as per ISO 10993-10: 2002 biological evaluation of medical devices: tests for irritation, and was not considered a primary dermal irritant (negligible dermal irritation response in rabbits).

Table 9.7 Scoring criteria for skin reactions (rabbit)

Erythema formation		Edema formation	
No erythema	0	No edema	0
Slight erythema	1	Slight edema	1
Well-defined erythema	2	Well-defined edema	2
Moderate erythema	3	Moderate edema	3
Severe erythema to slight eschar formation	4	Severe edema	4
Total possible erythema score=4		Total possible edema score=4	

Table 9.8 Dermal irritation response categories in the rabbit

Response category	Mean score
Negligible	0.0 to 0.4
Slight	0.5 to 1.9
Moderate	2.0 to 4.9
Severe	5.0 to 8.0

Table 9.9 Primary skin irritation summary of scores for skin irritation (dose = 25 mm x 25 mm (moist with physiological saline))

Animal (sex)	Initial weight (Kg)	Site	Score ^a			
			5 hours	24 hours	48 hours	72 hours
1 (M)	2.01	T ^b	0/0	0/0	0/0	0/0
		T	0/0	0/0	0/0	0/0
		C ^c	0/0	0/0	0/0	0/0
		C	0/0	0/0	0/0	0/0
2 (F)	2.05	T	0/0	0/0	0/0	0/0
		C	0/0	0/0	0/0	0/0
		C	0/0	0/0	0/0	0/0
		T	0/0	0/0	0/0	0/0
3 (M)	2.09	T	0/0	0/0	0/0	0/0
		C	0/0	0/0	0/0	0/0
		C	0/0	0/0	0/0	0/0

^a scores: erythema/edema

^b T: test article site

^c C: control site

9.11 Summary

A T_g type SMPU was synthesized by solution polymerization and the corresponding fiber and fabric were prepared, which might be used for biomedical applications. The following conclusions are drawn:

- (1) The switching temperature of the prepared fiber was 35.9°C, which was close to body temperature, so that shape change could be triggered at 36.5°C close to body temperature.

(2) The SMF had a recovery ratio of up to 90% and a fixity ratio above 80%. The prepared shape memory fabric showed good shape memory effect demonstrated by bagging recovery.

(3) The SMF had much higher mechanical strength than that of corresponding SMPU films. Therefore, the SMF and the prepared fabric may be used in the body parts where high stress is required.

(4) The biological evaluations of the prepared shape memory fabric were preliminary evaluated in terms of cytotoxicity, haemolysis, sensitization and dermal irritant. Based on the test results, the shape memory fabric was not considered cytotoxic, haemolytic, sensitive and irritant.

CHAPTER 10 CONCLUSIONS AND SUGGESTIONS FOR FUTURE WORK

10.1 Conclusions

10.1.1 Studies of general SMFs

SMPs can rapidly change their shapes in a predefined way from one temporary shape to the original shape under heat stimulation. By using a typical thermal-responsive SMP, SMPU, a T_m type SMF was prepared. PCL was chosen as the soft segment. Small size diol BDO and MDI were used as the soft segment. The shape memory switching temperature was the melting transition of the soft segment phase mainly composed of PCL at 47°C. The prepared SMF had a tenacity of about 1.0 cN/dtex, and strain at break 562~660%. The shape fixity ratio reached 84% and the recovery ratio was up to 95%.

10.1.2 Studies of the heat treatment of SMFs

To eliminate internal stress and structure deficiency of SMFs caused by the melt spinning process, the SMFs were subject to heat treatments. The influences of heat treatments on the properties of SMFs were investigated. It was found that with increasing heat treatment temperature, the soft segment crystallinity, crystallite dimension and micro-phase separation increased; the hydrogen bonding in the hard segment phase increased; molecular orientation decreased. Low temperature heat treatments decreased the shape recovery ratios while increasing the shape fixity ratios and breaking elongation as a result of internal stress releasing and molecules disorientation. High temperature heat treatments increased the hard segment stability, shape

recovery ratios, fixity ratios, recovery stress stability; while decreasing the fiber mechanical strength. Increasing heat treatment temperature resulted in the improvement of both the shape recovery and fixity because it promoted the phase separation. In order to obtain comprehensive outstanding properties, the SMF is expected to be treated at a high temperature because of the high glass transition temperature of hard segments. Unfortunately, the heat treatment could not be conducted at too high a temperature because the SMF became too tacky and soft due to the melting of the soft segment phase.

10.1.3 Studies of SMFs with thermal-responsive inner diameters

As shape memory hollow fiber with a thermal-responsive inner diameter has special properties in comparison with cylindrical fiber, it may have many special applications. In the project, a shape memory hollow fiber with thermal-responsive inner diameters was fabricated and the properties were studied. First, if this kind of shape memory hollow fiber is used in fabrics, the thermal-responsive heat transfer of the fabric will change according to the environment and body temperature. Second, if this kind of fiber is used as the stuffing of pillows and mattresses, the products may adjust to body contours for a comfortable feeling. If unloaded, after some time, they recover their original shapes. Furthermore, this kind of hollow fibers may be used in smart filtration, drug controlled release and liquid transportation in vitro or in vivo. The hollow fiber switching temperature was the melting temperature of the soft segment phase at about 41°C. The tenacity of the hollow fiber was about 1.14 cN/dtex, and breaking elongation 682%. The shape fixity ratio was above 87% and the recovery ratio above 89%. The inner diameter of the hollow fiber could be

noticeably changed and the deformed fiber cross-section could be well fixed. Once heated above the soft segment phase melting temperature, the hollow fiber inner cavity recovered its original diameter.

10.1.4 Studies of SMFs with temperature-regulating effects

PEG is a mostly studied solid-liquid phase change polymeric material. By employing PEG as the soft segment of SMPU, a TRSMF was prepared though the spinnability of the fiber was not good because of the significant low temperature melting transition of the polyurethane. The prepared 100 dtex fiber had a tenacity of 0.7 cN/dtex and the breaking elongation about 488%. The PEG soft segment phase transfer between crystalline and amorphous states resulted in the heat storage and release. The fiber had large latent heat storage capacity about 100 J/g with a crystallizing temperature at 20.9°C and a melting temperature at 44.7°C. Simultaneously, the fiber had shape memory effect with the shape fixity ratio 85.8% and the shape fixity ratio 95.4%. Currently, the degree of supercooling of the fiber was very high and the mechanical properties of the RSMF were not satisfied.

10.1.5 Studies of SMFs with electro-active effect

MWCNTs were incorporated into SMFs by *in-situ* polymerization to achieve electro-active shape memory effect and improve the shape recovery force of SMFs. It was found that the spinnability of MWCNT/SMP decreased significantly with increasing MWCNT content. When the MWCNT content reached 8.0 wt%, the fibers could not be produced because of the poor rheological properties of the composites. The melt blending, extrusion, and

melt spinning processes upon the SMF particularly at low MWCNT content caused the nanotubes to distribute homogenously and preferentially aligned along the drawing direction of the SMF. Employing a power of 210 V, by 20 pieces of 210 denier monofilaments, at 6.0 wt% MWCNTs, electro-active shape memory effect was observed. It was also found that the recovery force was improved which may be because the MWCNT helped store the internal elastic energy during stretching and fixing.

10.1.6 Studies of SMFs for biomedical applications

The medical applications of SMFs for smart medical devices are of great interest due to their combination of tailor-able transition temperature, fast actuation, large deformation, large recovery, and elastic properties. A T_g type SMPU was synthesized by solution polymerization and the corresponding fiber and fabric were prepared by using the SMPU, which might be used for biomedical applications. The switching temperature of the prepared fiber was 35.9°C, which was close to body temperature, so that shape change could be triggered at 36.5°C close to body temperature. The biological evaluations of the prepared shape memory fabric were preliminarily conducted in terms of cytotoxicity, haemolysis, sensitization and dermal irritant. Based on the test results and under the conditions of the test, the shape memory fiber/fabric is not considered cytotoxic, haemolytic, sensitive and irritant.

10.2 Suggestions for future work

10.2.1 Large scale production

The production of the SMPUs and SMFs in the study is on a lab-scale as shown in Figure 10.1. Although the preparation method is feasible in labs, it is time consuming and is significantly different from large scale production. A new flow chart shown in Figure 10.2 is designed, which adapts more to factory production. The synthesis conditions, processing parameters, SMPU and SMF properties need to be studied.

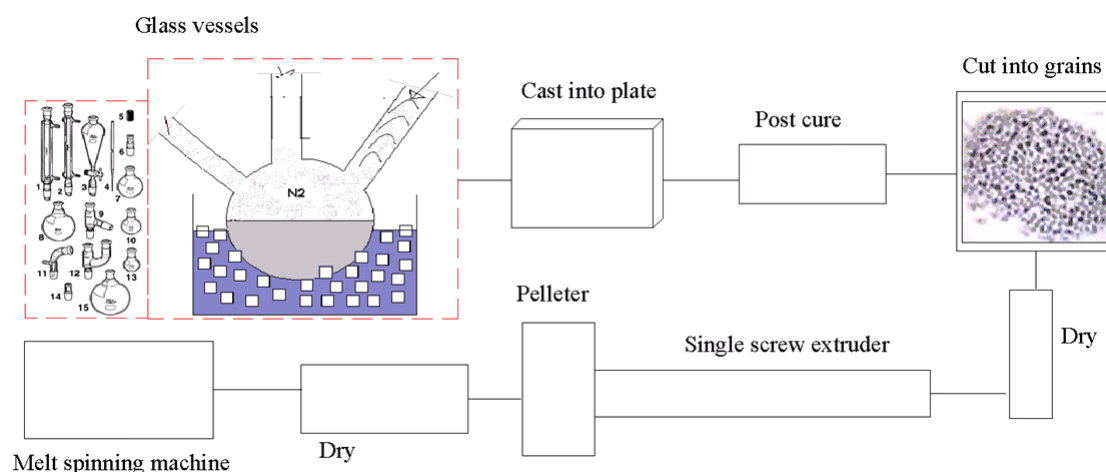


Figure 10.1 The lab-scale flow chart

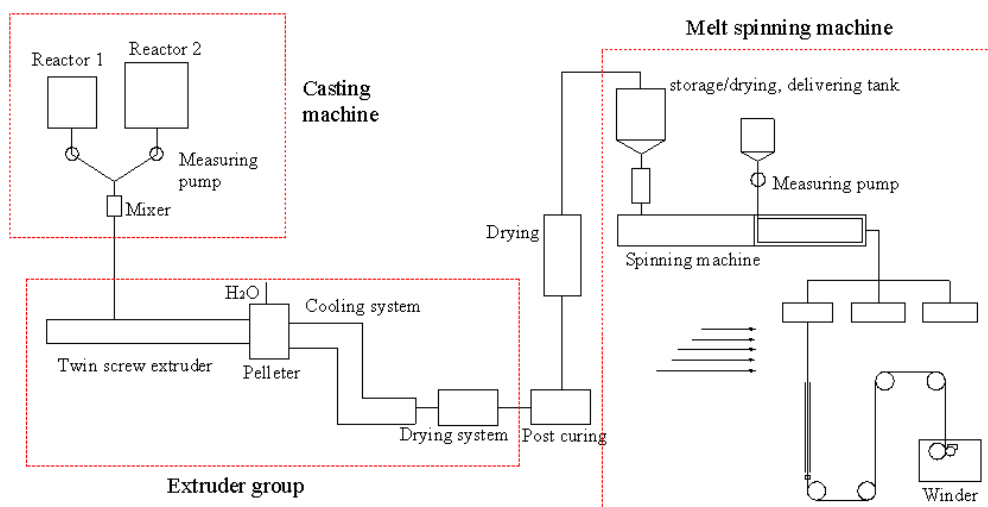


Figure 10.2 The newly designed flow chart

10.2.2 Two-way SMFs

The shape memory effect of the SMFs developed in the project is one-way shape memory effect. This means that the shape change of the shape memory fiber is not reversible and cannot be repeated without using external force. Several technologies have been reported to develop SMPs with two-way shape memory effect. Chung et al. [139] reported a two-way shape memory effect in crosslinked shape memory poly(cyclooctene). Cooling-induced crystallization under a tensile load results in elongation and subsequent heating to melt the network yields contracting (shape recovery). However, a tensile load is necessary for the two-way shape memory effect. Furthermore, the two-way shape memory effect is difficult to control. Ahir et al. [136], Qin and Mather [137] showed two-way shape memory effect through anisotropic chain

conformation change of liquid-crystalline polymers. Unfortunately, anisotropic chain conformation change of the liquid-crystalline polymers requires a temperature of above 100°C which makes the material unsuitable for clothing applications. Furthermore, it is difficult to tailor the shape recovery properties of the SMPs for specific applications.

Hu et al. [358, 359] have achieved two-way shape memory effect on SMP composites by laminating a SMP with an elastic polymer. The two-way shape memory effect was ascribed to the release of elastic strain of SMP layer upon heating, and the recovery of elastic strain induced by the bending force of elastic polymer layer upon cooling. They are also developing bi-component fibers with one component as a SMP and another component as an elastic fiber, and studying the two-way shape memory effect of the conjugate fibers.

10.2.3 Multi-stimuli-responsive SMFs

At present, the SMFs are responsive only to one specific stimulus signal viz. thermal stimulus. By incorporating hydrophilic segments in SMPU, water/moisture active shape memory effect has been achieved [360, 361]. By incorporating conductive particles in SMPs, electro-responsive SMPs have been prepared [362, 363]. By copolymerizing light-responsive azobenzene moiety into the SMPs, light-responsive SMPs have also been developed [364]. In future, SMPs with multi-stimuli-responsive function should be developed by integrating the different stimuli-response materials into one polymer. Therefore, the SMFs may adapt themselves to different environmental

CHAPTER 10 CONCLUSIONS & SUGGESTIONS FOR FUTURE WORK

conditions with varying temperature, light, humidity, electricity signals and pH vaule etc.

Figure 10.3 shows a smart shirt named “Sphere React Shirt” [365] whose rear vents can open up to allow perspiration and heat to escape when the wearer sweats. The vents automatically close at a dry state. It may be very effective to use thermal/moisture-dual responsive shape memory textiles which can change macro-shape or microstructures to achieve such functions for moisture and heat management between skin and fabric. If the wearer begins to feel hot and starts sweating after excessive muscular activity, the windows on the fabric will open to allow heat and sweat to release into the environment. In a cold situation without sweat, the windows close and keep the wearer warm.



Figure 10.3 The backside of Nike “Sphere React Shirt” with a smart vent structure (Reprinted with permission of Nike company) [365]

10.2.4 Medical applications

Shape memory fibers and fabrics in the special forms may find promising applications as biomedical materials due to their soft structures, permeability, and good compatibility with human bodies in comparison with film or bulk counterparts. Furthermore, the SMFs may be used in medical applications where high mechanical strength is required.

Shape memory textiles with volume and shape changes may be used for skin-care products with controllable release of perfume, nutrition, and drug [47]. Shape memory textiles may open new opportunities for smart textiles in the field of medicine and medical areas widening their applications.

REFERENCES

1. Gutowska, A., Bae, Y.H., Jacobs, H., Feijen, J. & Kim, S.W., *Thermosensitive Interpenetrating Polymer Network: Synthesis, Characterisation, and Macromolecular Release*. *Macromolecules*, 1994. **27**: p. 4167-4175.
2. Asaka, K. & Oguro, K., *Bending of Polyelectrolyte Membrane Platinum Composites by Electric Stimuli*. *Journal of Electro - analytical Chemistry*, 2000. **480**: p. 186-198.
3. Jiang, H.Y., Kelch, S. & Lendlein, A., *Polymers Move in Response to Light*. *Advanced Materials*, 2006. **18**: p. 1471-1475.
4. Makhosaxana, X.P., Filipcsei, G. & Zrínyi, M., *Preparation and Responsive Properties of Magnetically Soft Poly(N-isopropylacrylamide) Gels*. *Macromolecules*, 2000. **33**: p. 1716-1719.
5. Yang, B., Huang, W.M., Li, C. & Li, L., *Effects of Moisture on the Thermomechanical Properties of a Polyurethane Shape Memory Polymer*. *Polymer*, 2006. **47**: p. 1348-1356.
6. Hoffman, A.S., *"Smart" Polymers and Smart Hydrogels: Design, Synthesis and Applications*. 2007, The Hong Kong Polytechnic University: Hong Kong. p. 76.
7. Meng, Q. & Hu, J., *A Review of Shape Memory Polymer Composites and Blends*. *Composites Part A*, in press, 2009. **40**: p. 1661-1672.
8. Mather, P.T., Luo, X. & Rousseau, I.A., *Shape Memory Polymer Research*. *Annual Review of Materials Research*, 2009. **39**: p. 445-471.
9. Gunes, I.S. & Jana, S.C., *Shape Memory Polymers and Their Nanocomposites: A Review of Science and Technology of New Multifunctional Materials*. *Journal of Nanoscience and Nanotechnology*, 2008. **8**: p. 1616-1637.
10. Dietsch, B. & Tong, T., *A review: Features and Benefits of Shape Memory Polymers (SMPs)*. *Journal of Advanced Materials*, 2007. **39**: p. 3-12.
11. Tobushi, H., Hoshio, K., Hayashi, S. & Miwa, N., *Shape Memory Composite of SMA and SMP and Its Property*. *Key Engineering Materials*, 2007. **340-341 II**: p. 1187-1192.
12. Hu, J.L., *Shape Memory Polymers and Textiles*. 2007, Cambridge, England: Woodhead Publishing Limited. 15-25.
13. Behl, M. & Lendlein, A., *Shape-memory Polymers*. *Materials Today*, 2007. **10**: p. 20-28.
14. Lendlein, A. & Kelch, S., *Shape-Memory Polymers*. *Angewandte Chemie International Edition*, 2002. **41**: p. 2034-2057.
15. Ratna, D. & Karger-Kocsis, J., *Recent Advances in Shape Memory Polymers and Composites: a Review*. *Journal of Materials Science*, 2008. **43**: p. 254-269.
16. Meng, Q.H., Hu, J.L. & Yeung, L.Y., *An Electro-active Shape Memory Fibre by Incorporating Multi-walled Carbon Nanotubes*. *Smart Materials and Structures*, 2007. **16**: p. 830-836.

REFERENCES

17. Lendlein, A. & Langer, R., *Biodegradable, Elastic Shape-Memory Polymers for Potential Biomedical Applications*. Science, 2002. **96**: p. 1673 - 1676.
18. Metcalfe, A., Desfaits, A.-C., Salazkin, I., L. Yahiab, Sokolowski, W.M. & Raymonda, J., *Cold Hibernated Elastic Memory Foams for Endovascular Interventions*. Biomaterials, 2003. **24**: p. 491-497.
19. Wache, H.M., Tartakowska, D.J., Hentrich, A. & Wagner, M.H., *Development of a Polymer Stent with Shape Memory Effect as a Drug Delivery System*. Journal of Materials Science: Materials in Medicine, 2004. **14**: p. 109-112.
20. Charlesby, A., *Atomic Radiation and Polymers*. 1960: 198, New York: Pergamon Press.
21. Lan, X., Huang, W.M., Liu, N., Phee, S.Y., Leng, J.S. & Du, S.Y. *Improving the Electrical Conductivity by Forming Ni Powder Chains in a Shape-memory Polymer Filled With Carbon Black*. in *Proceedings of SPIE - The International Society for Optical Engineering*, v 6927, *Electroactive Polymer Actuators and Devices (EAPAD) 2008*, 2008, p 692717, San Diego, CA, United States. 2008.
22. Kunzelman, J., Chung, T., Mather, P. & Weder, C., *Shape Memory Polymers with Built-in Threshold Temperature Sensors*. Journal of Materials Chemistry, 2008. **18**: p. 1082-1086.
23. Mondal, S., Hu, J.L. & Zhu, Y., *Free Volume and Water Vapor Permeability of Dense Segmented Polyurethane Membrane*. Journal of Membrane Science, 2006. **280**: p. 427-432.
24. Campbell, D., Maji, A. & F.A.SCE, *Failure Mechanisms and Deployment Accuracy of Elastic-Memory Composites*. Journal of Aerospace Engineering, 2006. **19**: p. 184-193.
25. Eddington, D.T. & Beebe, D.J., *Flow control with hydrogels*. Advanced Drug Delivery Reviews, 2004. **56**(2): p. 199-210.
26. Miyata, T., Uragami, T. & Nakamae, K., *Biomolecule-sensitive hydrogels*. Advanced Drug Delivery Reviews, 2002. **54**(1): p. 79-98.
27. Yang, J.H., Chun, B.C., Chung, Y.C., Cho, J.W. & Cho, B.G., *Vibration Control Ability of Multilayered Composite Material Made of Epoxy Beam and Polyurethane Copolymer with Shape Memory Effect*. Journal of Applied Polymer Science, 2004. **94**: p. 302-307.
28. Xie, T. & Xiao, X., *Self-Peeling Reversible Dry Adhesive System*. Chemistry of Materials, 2008. **20**: p. 2866-2868.
29. Lendlein, A., *Blends of Shape Memory Polymers with Thermoplastic Polymers, PCT, PCT/EP2006/011420*. 2006.
30. Hayashi, S., Tasaka, Y., Hayashi, N. & Akita, Y., *Development of Smart Polymer Materials and its Various Applications*. Mitsubishi Heavy Industries, Ltd. Technical Review, 2004. **41**: p. 1-3.
31. Lendlein, A., Lang, G., Knitz, K., Krause, T., Kalbfleisch, A., Allwohn, J., Burgliaus, J., Sendelhach, G., Beyer, A., Mallinger, D., Uhl, S., Birkel, S., Duchscherer, A., Hasson, T.A.A., Jiang, H.Y., Morsheim, S., Ghazlan, Y., Lang, G., Knitz, K., Krause, T., Kalbfleisch, A., Allwohn, J., Burgliaus, J., Sendelhach, G., Beyer, A., Mallinger, D., Uhl, S., Birkel, S., Duchscherer, A., Hasson, T.A.A., Jiang, H.Y., Morsheim, S. & Ghazlan, Y., *Method for Achieving Shape Memory Effects on Hair*

REFERENCES

- by Combining Shape Memory Polymer with Canonic Active Ingredients*. Nov. 3, 2005: US Patent 2005/0244353 A1.
32. Lendlein, A. & Ridder, U., *Method for Hair Treatment with Shape Memory Polymers*. Apr. 19, 2007: US Patent 2007/0088135 A1.
 33. Langer, R. & Tirrell, D.A., *Designing Materials for Biology and Medicine*. Nature, 2004. **428**: p. 487-492.
 34. Laroche, F.E.F.G., Fiset, M. & Mantovani, D., *Shape Memory Materials for Biomedical Applications*. Advanced Engineering Materials, 2002. **4**: p. 91-104.
 35. Maitland, D.J., Metzger, M.F., Schumann, D., Lee, A. & Wilson, T.S., *Photothermal Properties of Shape Memory Polymer Micro-actuators for Treating Stroke*. Lasers in Surgery and Medicine, 2002. **30**: p. 1-11.
 36. Buckley, P.R., McKinley, G.H., Wilson, T.S., IV, W.S., Benett, W.J., Beringer, J.P., McElfresh, M.W. & Maitland, D.J. *Inductively Heated Shape Memory Polymer for the Magnetic Actuation of Medical Devices*. in *IEEE Transactions on Biomedical Engineering*. 2006: 53.
 37. Schmidt, A.M., *Electromagnetic Activation of Shape Memory Polymer Networks Containing Magnetic Nanoparticles*. Macromolecular Rapid Communications, 2006. **27**: p. 1168-1172.
 38. Small, W., Wilson, T.S., Buckley, P.R., Benett, W.J., Loge, J.M. & Hartman, J., *Prototype Fabrication and Preliminary in Vitro Testing of a Shape Memory Endovascular Thrombectomy Device*. IEEE Transactions on Biomedical Engineering, 2007. **54**: p. 1657-1666.
 39. Hampikian, J.M., Heaton, B.C., Tong, F.C., Zhang, Z. & Wong, C.P., *Mechanical and Radiographic Properties of a Shape Memory Polymer Composite for Intracranial Aneurysm Coils*. Materials Science and Engineering C, 2006. **26**: p. 1373-1379.
 40. *Smart Surgery*. Future Materials (through Textile Technology Index), 2004(1): p. 33-34.
 41. Langer, R.S. & Lendlein, A., *Biodegradable Shape Memory Polymeric Sutures*, World Patent WO 2003088818 A2. 2003.
 42. Yasuo, S., *Shape-memory, Biodegradable and Absorbable Material*, US Patent 19980189973. 1998.
 43. Mather, P.T., Liu, C. & Burstone, C.J., *Shape Memory Polymer Orthodontic Appliances, and Methods of Making and Using the Same*, European Patent EP1844097, World Patent 2006071520, 2006. Dec. 2005.
 44. Liu, C., Mather, P.T. & Burstone, C. *Proceedings of the Annual Technical Conference - Society of Plastics Engineers, 64th, Society of Plastics Engineers, Brookfield, CT, USA, pp. 1356-1360*. 2006.
 45. Sharp, A.A., Panchawagh, H.V., Ortega, A., Artale, R., Richardson-Burns, S., Finch, D.S., Gall, K., Mahajan, R.L. & Restrepo, D., *Toward a Self-deploying Shape Memory Polymer Neuronal Electrode*. Journal of Neural Engineering, 2006. **3**: p. L23-L30.
 46. Ortega, J., Small, W., Wilson, T., Benett, W., Loge, J. & Maitland, D., *A Shape Memory Polymer Dialysis Needle Adapter for the Reduction of Hemodynamic Stress Within Arteriovenous Grafts*. IEEE Transactions on Biomedical Engineering, 2007. **54**: p. 1722-1724.

REFERENCES

47. Wischke, C., Neffe, A.T., Steuer, S. & Lendlein, A., *Evaluation of a Degradable Shape-memory Polymer Network as Matrix for Controlled Drug Release*. *Journal of Controlled Release*, 2009. **138**: p. 243-250.
48. Nagahama, K., Ueda, Y., Ouchi, T. & Ohya, Y., *Biodegradable Shape-Memory Polymers Exhibiting Sharp Thermal Transitions and Controlled Drug Release*. *Biomacromolecules*, 2009. **10**: p. 1789-1794.
49. Hu, J.L., Ji, F.L. & Wong, Y.W., *Dependency of the Shape Memory Properties of a polyurethane upon Thermomechanical Cyclic Conditions*. *Polymer International*, 2005. **54**: p. 600-605.
50. Langer, R.S. & Andreas, L., *Shape memory polymers*. 2002: U.S. Pat. 6,388,043 B1.
51. Liu, C., Qin, H. & Mather, P.T., *Review of Progress in Shape-Memory Polymers*. *Journal of Materials Chemistry*, 2007. **17**: p. 1543-1558.
52. Hu, J.L., Ding, X.M. & Tao, X.M., *Shape Memory Polymers and Their Applications to Smart Textile Products*. *Journal of China Textile University*, 2002. **19**: p. 89-93.
53. Hu, J.L. & Mondal, S., *Structural characterization and mass transfer properties of segmented polyurethane: influence of block length of hydrophilic segments*. *Polymer International*, 2005. **54**: p. 764-771.
54. Hu, J.L., Yang, Z.h., Ji, F.L. & Liu, Y.Q., *Crosslinked Polyurethanes with Shape Memory Properties*. *Polymer International*, 2005. **54**: p. 854-859.
55. Beloshenko, V.A., Varyukhin, V.N. & Voznyak, Y.V., *The Shape Memory Effect in Polymers*. *Russian Chemical Review*, 2005. **74**: p. 265-283.
56. Ji, F.L., Hu, J.L., Li, T.C. & Wong, Y.W., *Morphology and Shape Memory Effect of Segmented Polyurethanes. Part I: With crystalline Reversible Phase*. *Polymer*, 2007. **48**: p. 5133-5145.
57. Zhu, Y., Hu, J.L., Yeung, K.W., Liu, Y.Q. & Liem, H.M., *Influence of Ionic Groups on the Crystallization and Melting Behavior of Segmented Polyurethane Ionomers*. *Journal of Applied Polymer Science*, 2006. **100**: p. 4603-4613.
58. Ji, F.L., Zhu, Y., Hu, J.L., Liu, Y., Yeung, L.Y. & Ye, G.D., *Smart Polymer Fibers with Shape Memory Effect*. *Smart Materials and Structures*, 2006. **15**: p. 1547-1554.
59. Rousseau, I. & Mather, P.T., *Shape Memory Effect Exhibited by Smectic-C Liquid Crystalline Elastomers*. *Journal of the American Chemical Society*, 2003. **125**: p. 15300-15301.
60. Hyashi, S., *Properties and applications of polyurethane*. *International progress in urethanes*, 1993. **6**: p. 90-115.
61. Tobushi, H., Hashimoto, T., N.Ito, Hayashi, S. & Yamada, E., *Shape Fixity and Shape Recovery in a Film of Shape Memory Polymer of Polyurethane Series*. *Journal of Intelligent Material Systems and Structures*, 1998. **9**: p. 127-136.
62. Lin, J.R. & Chen, L.W., *Study on Shape-Memory Behaviour of Polyether-Based Polyurethanes. I. Influence of the Hard-Segment Content*. *Journal of Applied Polymer Science*, 1998. **69**: p. 1563-1574.
63. Lin, J.R. & Chen, L.W., *Study on Shape-Memory Behavior of Polyether-Based Polyurethanes. II. Influence of Soft-Segment*

REFERENCES

- Molecular Weight*. Journal of Applied Polymer Science, 1998. **69**: p. 1575-1586.
64. Wei, Z.G., Sandstrom, R. & Miyazaki, S., *Shape-memory Materials and Hybrid Composites for Smart Systems: Part I Shape-memory Materials*. Journal of Materials Science, 1998. **33**: p. 3743-3762.
65. Yang, J.H., Chun, B.C., Chung, Y.-C. & Cho, J.H., *Comparison of Thermal/mechanical Properties and Shape Memory Effect of Polyurethane Block-copolymers with Planar or Bent Shape of Hard Segment*. Polymer, 2003. **44**: p. 3251-3258.
66. Liang, C. & C. A. Rogers, *One-dimensional Thermomechanical Constitutive Relations for Shape Memory Materials*. Journal of Intelligent Material Systems and Structures, 1997. **8**: p. 285-302.
67. Xie, T. & Rousseau, I.A., *Facile Tailoring of Thermal Transition Temperatures of Epoxy Shape Memory Polymers*. Polymer, 2009. **50**: p. 1852-1856.
68. Zhu, Y., Hu, J., Yeung, K.-w., Choi, K.-f., Liu, Y. & Liem, H., *Effect of Cationic Group Content on Shape Memory Effect in Segmented Polyurethane Cationomer*. Journal of Applied Polymer Science, 2007. **103**: p. 545-556.
69. Hu, J.L. & Mondal, S., *Structural Characterization and Mass Transfer Properties of Segmented Polyurethane: Influence of Block Length of Hydrophilic Segments*. Polymer International, 2005. **54**: p. 764-771.
70. Kim, B.K., Lee, S.Y. & Xu, M., *Polyurethane Having Shape Memory Effect*. Polymer, 1996. **37**: p. 5781-5793.
71. Ratna, D. & Karger-Kocsis, J., *Recent Advances in Shape Memory Polymers and Composites: a Review*. Journal of Materials Science, 2008. **43**: p. 254-269.
72. Rousseau, I.A., *Challenges of Shape Memory Polymers: A Review of the Progress Toward Overcoming SMP's Limitations*. Polymer Engineering & Science, 2008. **48**: p. 2075-2089.
73. Liu, Y., Lv, H., Lan, X., Leng, J. & Du, S., *Review of Electro-Active Shape-Memory Polymer Composite*, doi:10.1016/j.compscitech.2008.08.016. Composites Science and Technology, 2008.
74. Hayashi, S., Tasaka, Y., Hayashi, N. & Akita, Y., *Development of Smart Polymer Materials and its Various Applications*. Mitsubishi Heavy Industries, Ltd. Technical Review Vol.41 No.1, Feb. 2004. **41 No.1**.
75. Kongolo, D., *Luminescent Textiles, WIPO Patent Application WO/2008/148138*. 2008.
76. Lee, S. & Starner, T. *Stop Burdening Your Eyes: a Wearable Electro-Tactile Display*. 12th IEEE International Symposium on Wearable Computers, Pittsburgh, PA, USA. 2008.
77. Studstill, K., *Emotion Sensing Dress Releases Mood Driven Scents*, <http://www.psfk.com/2010/01/emotion-sensing-dress-releases-mood-driven-scents.html>. Date accessed: Feb. 12nd. 2010.
78. Qi, K., Chen, X. & Liu, Y., *Facile Preparation of Anatase/SiO₂ Spherical Nanocomposites and Their Application in Self-cleaning Textiles*. Journal of Materials Chemistry, 2007. **17**: p. 3504-3508.

REFERENCES

79. Hayashi, S. & Dondo, S., *Shape Memory Polymer Yarn*. June 29, 1990: Japan.
80. Russel, A., Hayashi, S. & Yamada, T., *Potential Use of Shape Memory Film in Clothing*. Technical Textiles International (through Textile Technology Index), 1999. **8**(8): p. 17-19.
81. Mondal, S. & Hu, J.L., *Structural Characterization and Mass Transfer Properties of Nonporous Segmented Polyurethane Membrane: Influence of Hydrophilic and Carboxylic Group*. Journal of Membrane Science, 2006. **274**: p. 219-226.
82. Mondal, S. & Hu, J.L., *Structural Characterization and Mass Transfer Properties of Nonporous-segmented Polyurethane Membrane: Influence of the Hydrophilic Segment Content and Soft Segment Melting Temperature*. Journal of Membrane Science, 2006. **276**: p. 16-22.
83. Mondal, S. & Hu, J.L., *A Novel Approach to Excellent UV Protecting Cotton Fabric with Functionalized MWNT containing Water Vapor Permeable PU Coating*. Journal of Applied Polymer Science, 2007. **103**: p. 3370-3376.
84. Mondal, S. & Hu, J.L., *Water Vapor Permeability of Cotton Fabrics Coated with Shape Memory Polyurethane*. Carbohydrate Polymers, 2007. **67**: p. 282-287.
85. Jeong, H.M., Ahn, B.K., Cho, S.M. & Kim, B.K., *Water Vapor Permeability of Shape Memory Polyurethane with Amorphous Reversible Phase*. Journal of Polymer Science: Part B: Polymer Physics, 2000. **38**: p. 3009-3017.
86. Jeong, H.M., Ahn, B.K. & Kim, B.K., *Temperature Sensitive Water Vapour Permeability and Shape Memory Effect of Polyurethane with Crystalline Reversible Phase and Hydrophilic Segments*. Polymer International, 2000. **49**: p. 1714-1721.
87. Chen, W., Zhu, C.Y. & Gu, X.R., *Thermosetting Polyurethanes with Water-Swollen and Shape Memory Properties*. Journal of Applied Polymer Science, 2002. **84**: p. 1504-1512.
88. Mondal, S., *Studies of Structure and Water Vapor Transport Properties of Shape Memory Segmented Polyurethanes for Breathable Textiles*, in *Institute of Textiles and Clothing*. 2005, The Hong Kong Polytechnic University: Hong Kong. p. 273.
89. Tobushi, H., Hayashi, S., Hoshio, K. & Miwa, N., *Influence of Strain-holding Conditions on Shape Recovery and Secondary-shape Forming in Polyurethane-shape Memory Polymer*. Smart Materials and Structures, 2006. **15**: p. 1033-1038.
90. Tobushi, H., Matsui, R., Hayashi, S. & Shimada, D., *The Influence of Shape-holding Conditions on Shape Recovery of Polyurethane-shape Memory Polymer Foams*. Smart Materials and Structures, 2004. **13**: p. 881-887.
91. Lendlein, A. & Langer, R.S., 2004. Self-expanding Device for the Gastrointestinal or Urogenital Area.
92. Marco, D. & Eckhouse, S., *Biodegradable Self-inflating Intragastric Implants for Curbing Appetite*, US Patent Office, Pat. No.0156248. 2006.

REFERENCES

93. Huang, W.M., Lee, C.W. & Teo, H.P., *Thermomechanical Behavior of a Polyurethane Shape Memory Polymer Foam*. Journal of Intelligent Material Systems and Structures, 2006. **17**: p. 753-760.
94. Gefen, A., Megido-Ravid, M., Itzchak, Y. & Arcan, M., *Analysis of Muscular Fatigue and Foot Stability During High-heeled Gait*. Gait Posture, 2002. **15**: p. 56-63.
95. Escamilla, R., Fleisig, G. & Lowry, T., *A Three-dimensional Biomechanical Analysis of the Squat During Varying Stance Widths*. Medicine and Science in Sports and Exercise, 2001. **33**: p. 984-998.
96. Lee, C.-M., Jeong, E.-H. & Freivalds, A., *Biomechanical Effects of Wearing High-heeled Shoes*. International Journal of Industrial Ergonomics, 2001. **28**: p. 321-326.
97. Hsiao, E. & Robinovitch, S., *Biomechanical Influences on Balance Recovery by Stepping*. Journal of Biomechanics, 1999. **32**: p. 1099-1106.
98. Dr. Scholl's® Memory Fit® Work Customizing Insoles, <http://www.drsholls.com/drsholls/productSearch.do?method=doProductDetailsLookup&searchArg=53>, Date accessed: Jan. 15th. 2010.
99. Wan, T. & Stylios, G.K. *Investigating Shape Memories Technologies for SMART Fabrics*. in *2nd International Textile Conference of the North India Section of the Textile Institute, New Delhi, India*. 2004.
100. Stylios, G.K. & Wan, T., *Shape Memory Training for Smart Fabrics*. Transactions of the Institute of Measurement and Control, 2007. **29**: p. 321-336.
101. Hu, J., Chung, S. & Li, Y., *Characterization about the Shape Memory Behaviour of Woven Fabrics*. Transactions of the Institute of Measurement and Control, 2007. **29**: p. 301-319.
102. Liem, H., Yeung, L.Y. & Hu, L., *A Prerequisite for the Effective Transfer of the Shape-memory Effect to Cotton Fibers*. Smart Materials and Structures, 2007. **16**: p. 748-753.
103. Liu, X., Hu, J., Babu, K.M. & Wang, S., *Elasticity and Shape Memory Effect of Shape Memory Fabrics*. Textile Research Journal, 2008. **78**: p. 1048-1056.
104. Hu, J., *Textiles of Shape Memory Polymers*, PCT 2007/070172, in. 25-Jun-2007.
105. Liu, Y.Q., Hu, J.L., Zhu, Y. & Yang, Z.H., *Surface Modification of Cotton fabric by Grafting of Polyurethane*. Carbohydrate Polymers, 2005. **62**: p. 276-280.
106. Li, Y., Chung, S., Chan, L. & Hu, J.L., *Characterization of Shape Memory Fabrics*. Textile Asia, 2004. **35**: p. 32-37.
107. Hu, J., *VCD_Shape Memory Finishing of the Shape Memory Textile Centre in the Hong Kong Polytechnic University*. 2007: Hong Kong.
108. Yeung, L.Y., *Structure and Thermal-Mechanical Properties of Shape Memory Polyurethanes and Textiles*, in *Institute of Textiles and Clothing*. 2010, The Hong Kong Polytechnic University: Hong Kong. p. 230.
109. Meng, Q., *Garment finished by SMPUs, taken in the Shape Memory Textiles Centre*. 2009, The Hong Kong Polytechnic University.

REFERENCES

110. Leenders, M., *Shape Memory Textiles*
<http://www.youtube.com/watch?v=HdRRy7hItgI>. Date accessed: Feb. 16th. 2010.
111. Marks, P., *Shirt rolls up its own sleeves*,
<http://www.newscientist.com/article/dn1073-shirt-rolls-up-its-own-sleeves.html>. Date accessed: Jan. 20th. 2010.
112. Dimainstone, *Skorpions Pioneering Kinetic Couture!*
<http://www.youtube.com/watch?v=8OaAffOyXNU&NR=1>. Date accessed: Jan. 16th. 2010.
113. Hu, J.L., Meng, Q.H., Zhu, Y., Lu, J. & Zhuo, H.T., *Shape Memory Fibers Prepared by Wet, Reaction, Dry, Melt, and Electro Spinning*. 2007: US Patent 11907012.
114. Kaursoin, J. & Agrawal, A.K., *Melt Spun Thermoresponsive Shape Memory Fibers Based on Polyurethanes: Effect of Drawing and Heat-Setting on Fiber Morphology and Properties*. Journal of Applied Polymer Science, 2007. **103**: p. 2172-2182.
115. Zhu, Y., Hu, J.L., Yeung, L.Y., Liu, Y., Ji, F.L. & Yeung, K.W., *Development of Shape Memory Polyurethane Fiber with Complete Shape Recoverability*. Smart Materials and Structures, 2006. **15**: p. 1385-1394.
116. Liu, J., Ma, D.Z. & Li, Z., *FTIR studies on the compatibility of hard-soft segments for polyurethane-imide copolymers with different soft segments*. European Polymer Journal, 2002. **38**: p. 661-665.
117. Kim, B.K. & Lee, S.Y., *Polyurethane Ionomers Having Shape Memory Effects*. Polymer, 1998. **39**: p. 2803-2808.
118. Tang, S.L.P. & Stylios, G.K., *An Overview of Smart Technologies for Clothing Design and Engineering*. International Journal of Clothing Science and Technology, 2006. **18**: p. 108-128.
119. Liu, Y., Chung, A., Hu, J.L. & Lu, J., *Shape Memory Behavior of SMPU Knitted Fabric*. Journal of Zhejiang University SCIENCE A, 2007. **8**: p. 830-834.
120. Ltd, U., *Light Weight Hollow Fibre Thermally Insulating Fabrics for Winter Clothings and Sportswear*. Mar. 1996: Japan.
121. Mother, P.T., Jeon, H.G. & Haddad, T.S., *Strain Recovery in POSS Hybrid Thermoplastics*. Polymer Preprints, 2000. **41**: p. 528-529.
122. Irie, M., *Shape Memory Polymers, in Shape Memory Materials*, ed. K. Olsuka & Wayman, C.M. 1998: Cambridge University Press. 203-219.
123. Zhu, Y., Hu, J., Choi, K.F., Yeung, K.W., Meng, Q. & Chen, S., *Crystallization and Melting Behavior of the Crystalline Soft Segment in a Shape-memory Polyurethane Ionomer*. Journal of Applied Polymer Science, 2008. **107**: p. 599-609.
124. Mondal, S. & Hu, J.L., *Studies of Shape Memory Property on Thermoplastic Segmented Polyurethanes: Influence of PEG 3400*. Journal of Elastomers and Plastics, 2007. **39**: p. 81-91.
125. Abrahamson, E.R., Lake, M.S. & Gall, K., *Shape Memory Mechanics of an Elastic Memory Composite Resin*. Journal of Intelligent Material System and Structures, 2003. **14**: p. 623-632.
126. Lake, M.S. & Beavers, F.L. *The Fundamentals of Designing Deployable Structures with Elastic Memory Composites*. in *Collection of Technical Papers - AIAA/ASME/ASCE/AHS/ASC Structures*,

REFERENCES

- Structural Dynamics and Materials Conference, v 3, 2002, p 2050-2063, Denver, CO, United States. 2002.*
127. Tupper, M., Munshi, N., Beavers, F., Meink, T., Gall, K. & Mikulas, M.J. *Developments in Elastic Memory Composite Materials for Spacecraft Deployable Structures.* in *IEEE Aerospace Conference Proceedings, v 5, 2001, p 52541-52548, Big Sky, MT, United States. 2001.*
 128. Rezanejad, S. & Kokabi, M., *Shape memory and mechanical properties of cross-linked polyethylene/clay nanocomposites.* *European Polymer Journal*, 2007. **43**: p. 2856-2865.
 129. Khonakdar, H.A., Jafari, S.H., Rasouli, S., Morshedian, J. & Abedini, H., *Investigation and Modeling of Temperature Dependence Recovery Behavior of Shape-Memory Crosslinked Polyethylene.* *Macromolecular Theory and Simulations*, 2007. **16**: p. 43-52.
 130. Chen, X., Wudl, F., Mal, A.K., Shen, H. & Nutt, S.R., *New Thermally Remendable Highly Cross-Linked Polymeric Materials.* *Macromolecules*, 2003. **36**: p. 1802-1807.
 131. Chen, X., Dam, M.A., Ono, K., Mal, A., Shen, H., Nutt, S.R., Sheran, K. & Wudl, F., *A Thermally Re-mendable Cross-linked Polymeric Material.* *Science*, 2002. **295**: p. 1698-1702.
 132. Ishida, K. & Yoshie, N., *Two-way Conversion Between Hard and Soft Properties of Semicrystalline Crosslinked Polymer.* *Macromolecules*, 2008. **41**: p. 4753-4757.
 133. Li, J., Viveros, J.A., Wrue, M.H. & Anthamatten, M., *Shape-Memory Effects in Polymer Networks Containing Reversibly Associating Side-groups.* *Advanced Materials*, 2007. **19**: p. 2851-2855.
 134. Zhu, Y., Hu, J. & Liu, Y., *Shape Memory Effect of Thermoplastic Segmented Polyurethanes with Self-complementary Quadruple Hydrogen Bonding in Soft Segments.* *The European Physical Journal E*, 2009. **28**: p. 3-10.
 135. Chen, S., Hu, J., Yuen, C.W. & Chan, L., *Novel Moisture-sensitive Shape Memory Polyurethanes Containing Pyridine Moieties.* *Polymer*, doi: 10.1016/j.polymer.2009.07.031, 2009.
 136. Ahir, S.V., Tajbakhsh, A.R. & Terentjev, E.M., *Self-Assembled Shape-Memory Fibers of Triblock Liquid-Crystal Polymers.* *Advanced Functional Materials*, 2006. **16**: p. 556-560.
 137. Qin, H. & Mather, P.T., *Combined One-Way and Two-Way Shape Memory in a Glass-Forming Nematic Network.* *Macromolecules*, 2009. **42**: p. 273-280.
 138. Ahir, S.V., Tajbakhsh, A.R. & Terentjev, E.M., *Self-Assembled Shape-Memory Fibers of Triblock Liquid-Crystal Polymers.* *Advanced Functional Materials*, 2006. **16**: p. 556-560.
 139. Chung, T., Romo-Urbe, A. & Mather, P.T., *Two-Way Reversible Shape Memory in a Semicrystalline Network.* *Macromolecules*, 2008. **41**: p. 184-192.
 140. Koerner, H., Price, G., Pearce, N.A., Alexander, M. & Vaia, R.A., *Remotely Actuated Polymer Nanocomposites-stress-recovery of Carbon-nanotube-filled Thermalplastic Elastomers.* *Natural Material*, 2004. **3**: p. 115-120.

REFERENCES

141. Goo, N.S., Paik, I.H. & Yoon, K.J., *The Durability of a Conducting Shape Memory Polyurethane Actuator*. Smart Materials and Structures, 2007. **16**: p. N23-N26.
142. Paik, I.H., Goo, N.S., Yoon, K.J., Jung, Y.C. & Cho, J.W., *Electric Resistance Property of a Conducting Shape Memory Polyurethane Actuator*. Key Engineering Materials, 2005. **297-300**: p. 1539-1544.
143. Paik, I.H., Goo, N.S., Jung, Y.C. & Cho, J.W., *Development and Application of Conducting Shape Memory Polyurethane Actuators*. Smart Materials and Structures, 2006. **15**: p. 1476-1482.
144. Cho, J.W., Kim, J.W., Jung, Y.C. & Goo, N.S., *Electroactive Shape-Memory Polyurethane Composites Incorporating Carbon Nanotube*. Macromolecular Rapid Communications, 2005. **26**: p. 412-416.
145. Sahoo, N.G., Jung, Y.C. & Cho, J.W., *Electroactive Shape Memory Effect of Polyurethane Composites Filled with Carbon Nanotubes and Conducting Polymer*. Materials and Manufacturing Processes, 2007. **22**: p. 419-423.
146. Sahoo, N.G., Jung, Y.C., Goo, N.S. & Cho, J.W., *Conducting Shape Memory Polyurethane-polypyrrole Composites for an Electroactive Actuator*. Macromolecular Materials and Engineering, 2005. **290**: p. 1049-1055.
147. Sahoo, N.G., Jung, Y.C., Yoo, H.J. & Cho, J.W., *Influence of Carbon Nanotubes and Polypyrrole on the Thermal, Mechanical and Electroactive Shape-memory Properties of Polyurethane Nanocomposites*. Composites Science and Technology, 2007. **67**: p. 1920-1929.
148. Leng, J., Lu, H., Liu, Y. & Du, S. *Conductive Nanoparticles in Electro Activated Shape Memory Polymer Sensor and Actuator*. in *Proceedings of SPIE - The International Society for Optical Engineering*, v 6931, *Nanosensors and Microsensors for Bio-Systems 2008*, 2008, p 693109, San Diego, CA, United States. 2008.
149. Lv, H., Leng, J. & Du, S. *Electro-induced Shape-memory Polymer Nanocomposite Containing Conductive Particles and Short Fibers*. in *Proceedings of SPIE - The International Society for Optical Engineering*, v 6929, *Behavior and Mechanics of Multifunctional and Composite Materials 2008*, p 69291L, *Behavior and Mechanics of Multifunctional and Composite Materials 2008, Mar 10-13 2008, San Diego, CA, United States*. 2008.
150. Leng, J., Lv, H., Liu, Y. & Du, S., *Electroactivate Shape-memory Polymer Filled With Nanocarbon Particles and Short Carbon Fibers*. Applied Physics Letters, 2007. **91**: p. 144105.
151. Leng, J., Lv, H., Liu, Y. & Du, S., *Synergic Effect of Carbon Black and Short Carbon Fiber on Shape Memory Polymer Actuation by Electricity*. Journal of Applied Physics, 2008. **104**: p. 104917.
152. Leng, J.S., Lan, X., Liu, Y.J., Du, S.Y., Huang, W.M., Liu, N., Phee, S.J. & Yuan, Q., *Electrical Conductivity of Thermoresponsive Shape-memory Polymer with Embedded Micron Sized Ni Powder Chains*. Applied Physics Letters, 2008. **92**: p. 014104-1-3.
153. Leng, J.S., Huang, W.M., Lan, X., Liu, Y.J. & Du, S.Y., *Significantly Reducing Electrical Resistivity by Forming Conductive Ni Chains in a*

REFERENCES

- Polyurethane Shape-memory Polymer/carbon-black Composite*. Applied Physics Letters, 2008. **92**: p. 204101-1-3.
154. Small, W., Buckley, P., Wilson, T., Benett, W. & Hartman, J., *Shape Memory Polymer Stent with Expandable Foam: a New Concept for Endovascular Embolization of Fusiform Aneurysms*. IEEE Transactions on Biomedical Engineering, 2007. **54**: p. 1157-1160.
155. Small, W., Metzger, M., Wilson, T. & Maitland, D., *Laser-activated Shape Memory Polymer Microactuator for Thrombus Removal Following Ischemic Stroke: Preliminary in Vitro Analysis*. IEEE Journal of Selected Topics in Quantum Electronics, 2005. **11**: p. 892-901.
156. Small, W., Wilson, T.S., Benett, W.J., Loge, J.M. & Maitland, D.J., *Laser-activated Shape Memory Polymer Intravascular Thrombectomy Device*. Optics Express, 2005. **13**: p. 8204-8213.
157. Small, W., Metzger, M.F., Wilson, T.S. & Maitland, D.J., *Laser-activated Shape Memory Polymer Microactuator for Thrombus Removal Following Ischemic Stroke: Preliminary in Vitro Analysis*. IEEE Journal of Selected Topics in Quantum Electronics, 2005. **11**: p. 892-901.
158. Mohr, R., Kratz, K., Weigel, T., Lucka-Gabor, M., Moneke, M. & Lendlein, A. *Initiation of Shape-memory Effect by Inductive Heating of Magnetic Nanoparticles in Thermoplastic Polymers*. in *Proceedings of the National Academy of Sciences*, v103, 3540-3545, United States. 2006.
159. Yakacki, C.M., Satarkar, N.S., Gall, K., Likos, R. & Hilt, J.Z., *Shape-Memory Polymer Networks with Fe₃O₄ Nanoparticles for Remote Activation*. Journal of Applied Polymer Science, 2009. **112**: p. 3166-3176.
160. Weigel, T., Mohr, R. & Lendlein, A., *Investigation of Parameters to Achieve Temperatures Required to Initiate the Shape-memory Effect of Magnetic Nanocomposites by Inductive Heating*. Smart Materials and Structures, 2009. **18**: p. 025011 (9pp).
161. Cuevas, J.M., Alonso, J., German, L., Iturrondobeitia, M., Laza, J.M., Vilas, J.L. & Leon, L.M., *Magneto-active Shape Memory Composites by Incorporating Ferromagnetic Microparticles in a Thermo-responsive Polyalkenamer*. Smart Materials and Structures, 2009. **18**: p. 075003.
162. Behl, M. *Shape-Memory Polymers*. in *3rd International Conference on Nanotechnology and Smart Textiles for Industry, Healthcare and Fashion, 19 March 2008, The Royal Society 6-9 Carlton House Terrace, London, SW1Y 5AG, UK*. 2008.
163. Varga, Z., Filipcsei, G. & Zrínyi, M., *Magnetic Field Sensitive Functional Elastomers With Tuneable Elastic Modulus*. Polymer, 2006. **47**: p. 227-233.
164. Razzaq, M.Y., Anhalt, M., Frommann, L. & Weidenfeller, B., *Thermal, Electrical and Magnetic Studies of Magnetite Filled Polyurethane Shape Memory Polymers*. Materials Science and Engineering: A, 2007. **444**: p. 227-235.
165. Razzaq, M.Y., Anhalt, M., Frommann, L. & Weidenfeller, B., *Mechanical Spectroscopy of Magnetite Filled Polyurethane Shape*

REFERENCES

- Memory Polymers*. Materials Science and Engineering: A, 2007. **471**: p. 57-62.
166. Mukae, K., Bae, Y.h., Okano, T. & Kim, S.W., *New Thermo-sensitive Hydrogel. Poly(ethylene oxide-dimethyl siloxane-ethylene oxide)/poly(N-isopropyl acrylamide) interpenetrating polymer networks I. Synthesis and characterization*. Polymer Journal, 1990. **22**: p. 206-217.
167. Brannon-Peppas, L. & Peppas, N.A., *Equilibrium swelling behavior of pH-sensitive hydrogels*. Chemical Engineering Science, 1991. **46**: p. 715-722.
168. He, H., Li, L. & Lee, L.J., *Photopolymerization and Structure Formation of Methacrylic Acid Based Hydrogels: The effect of Light Intensity*. Reactive and Functional Polymers, 2008. **68**: p. 103-113.
169. Stromberg, N. & Hulth, S., *A Fluorescence Ratiometric Detection Scheme for Ammonium Ions Based on the Solvent Sensitive Dye MC 540*. Sensors and Actuators B: Chemical, 2003. **90**: p. 308-318.
170. Rodriguez, R., Alvarez-Lorenzo, C. & Concheiro, A., *Cationic Cellulose Hydrogels: Kinetics of the Cross-linking Process and Characterization as pH-/ion-sensitive Drug Delivery Systems*. Journal of Controlled Release, 2003. **86**: p. 253-265.
171. Eddington, D.T. & Beebe, D.J., *Flow control with hydrogels*. Advanced Drug Delivery Reviews, 2004. **56**: p. 199-210.
172. Meyvis, T.K.L., Stubbe, B.G., Steenbergen, M.J.V., Hennink, W.E., Smedt, S.C.D. & Demeester, J., *A Comparison Between the Use of Dynamic Mechanical Analysis and Oscillatory Shear Rheometry for the Characterisation of Hydrogels*. International Journal of Pharmaceutics, 2002. **244**: p. 163-168.
173. Osada, Y. & Matsuda, A., *Shape Memory in Hydrogels*. Nature, 1995. **376**: p. 219-220.
174. Huang, G., Gao, J., Hu, Z., St. John, J.V., Ponder, B.C. & Moro, D., *Controlled Drug Release from Hydrogel Nanoparticle Networks*. Journal of Controlled Release, 2004. **94**: p. 303-311.
175. Qiu, Y. & Park, K., *Environment-sensitive Hydrogels for Drug Delivery*. Advanced Drug Delivery Reviews, 2001. **53**: p. 321-339.
176. Kopecek, J., *Smart and Genetically Engineered Biomaterials and Drug Delivery Systems*. European Journal of Pharmaceutical Sciences, 2003. **20**: p. 1-16.
177. Pan, Y.V., Wesley, R.A., Luginbuhl, R., Dento, D.D. & Ratner, B.D., *Plasma Polymerized N-isopropylacrylamide: Synthesis and Characterization of a Smart Thermally Responsive Coating*. Biomacromolecules, 2001. **2**: p. 32-36.
178. Gupta, K.C. & Sahoo, S., *Graft Copolymerization of Acrylonitrile and Ethyl Methacrylate Comonomers on Cellulose Using Ceric Ions*. Biomacromolecules, 2001. **2**: p. 239-247.
179. Suzuki, Y., Tomonaga, K., Kumazaki, M. & Nishio, I., *Change in Phase Transition Behavior of an NIPA Gel Induced by Solvent Composition: Hydrophobic Effect*. Polymer Gels and Networks, 1996. **4**: p. 129-142.

REFERENCES

180. Chen, G. & Hoffman, A.S., *Graft Copolymers That Exhibit Temperature-induced Phase Transitions Over a Wide Range of pH*. *Nature*, 1995. **373**: p. 49-52.
181. Vihola, H., Laukkanen, A., Valtola, L., Tenhu, H. & Hirvonen, J., *Cytotoxicity of Thermosensitive Polymers Poly(N-isopropylacrylamide), Poly(N-vinylcaprolactam) and Amphiphilically Modified Poly(N-vinylcaprolactam)*. *Biomaterials*, 2005. **26**: p. 3055-3064.
182. Jonas, A.M., Glinel, K., Oren, R., Nysten, B. & Huck, W.T.S., *Thermo-Responsive Polymer Brushes with Tunable Collapse Temperatures in the Physiological Range*. *Macromolecules*, 2007. **40**: p. 4403-4405.
183. Lutz, J.-F., Akdemir, O. & Hoth, A., *Point by Point Comparison of Two Thermosensitive Polymers Exhibiting a Similar LCST: Is the Age of Poly(NIPAM) Over?* *Journal of the American Chemical Society*, 2006. **128**: p. 13046-13047.
184. Jovic, D., *Smart Textile Materials by Surface Modification with Biopolymeric Systems*. *Research Journal of Textile and Apparel*, 2008. **12**: p. 58-65.
185. Gann, M.J.M., Higginbotham, C.L., Geever, L.M. & Nugent, M.J.D., *The Synthesis of Novel pH-sensitive Poly(vinyl alcohol) Composite Hydrogels Using a Freeze/thaw Process for Biomedical Applications*. *International Journal of Pharmaceutics*, 2009. **372**: p. 154-161.
186. Hoffman, A.S., Stayton, P.S., Bulmus, V., Chen, G., Chen, J., Cheung, C., Chilkoti, A., Ding, Z., Dong, L., Fong, R., Lackey, C.A., Long, C.J., Miura, M., Morris, J.E. & Murthy, N., *Really Smart Bioconjugates of Smart Polymers and Receptor Proteins*. *Journal of Biomedical Materials Research*, 2000. **52**: p. 577-586.
187. Liu, B. & Hu, J., *The Application of Temperature-Sensitive Hydrogels to Textiles: A Review of Chinese and Japanese Investigations*. *Fiber and Textiles in Eastern Europe*, 2005. **13**: p. 45-49.
188. Jovic, D., Tourrette, A., Glampedaki, P. & Warmoeskerken, M.M.C.G., *Application of Temperature and pH Responsive Microhydrogels for Functional Finishing of Cotton Fabric*. *Materials Technology*, 2009. **24**: p. 14-23.
189. Tourrette, A., Geyter, N.D., Jovic, D., Morent, R., Warmoeskerken, M.M.C.G. & Leys, C., *Incorporation of Poly(N-isopropylacrylamide)/chitosan Microgel onto Plasma Functionalized Cotton Fibre Surface*. *Colloids and Surfaces A: Physicochemical and Engineering Aspects*, 2009. **352**: p. 126-135.
190. Mano, J.F., *Stimuli-Responsive Polymeric Systems for Biomedical Applications*. *Advanced Engineering Materials*, 2008. **10**: p. 515-527.
191. Liu, B., Hu, J. & Meng, Q., *Nonwoven supported Temperature-sensitive Poly(N-isopropylacrylamide)/Polyurethane Copolymer Hydrogel with Antibacterial Activity*. *Journal of Biomedical Materials Research: Part B - Applied Biomaterials*, in press, 2009. **89B**: p. 1-8.
192. Rybicki, E., Filipowska, B., Kozicki, M., Jeziorski, A. & Jakubic, J. *New Generation Therapeutic Dressings on the Basis of Surface Modified Textiles, 5th International Scientific Conference Medtex "Textiles for Medicine", LoDz-Arturowek, Poland*. 2005.

REFERENCES

193. Ribeiro, M., Espiga, A., Silva, D., Baptista, P., Henriques, J., Ferreira, C., Silva, J., Borges, J., Pires, E., Chaves, P. & Correia, I., *Development of a New Chitosan Hydrogel for Wound Dressing*. *Wound Repair and Regeneration*, 2009. **17**: p. 817-824.
194. Cornelius, V.J., Majcen, N., Snowden, M.J., Mitchell, J.C. & Voncina, B., *Preparation of SMART Wound Dressings Based on Colloidal Microgels and Textile Fibres*. *Smart Materials IV*. Edited by Voelcker, Nicolas H., *Proceedings of the SPIE*, 2007. **6413**.
195. Schneider, L., Korber, A., Grabbe, S. & Dissemond, J., *Influence of pH on wound-healing: a new perspective for wound-therapy?* *Archives of Dermatological Research*, 2007. **9**: p. 413-420.
196. Mokry, M., Gal, P., Vidinsky, B., Kusnir, J., Dubayova, K., Mozes, S. & J.Sabo, *In Vivo Monitoring the Changes of Interstitial pH and FAD/NADH Ratio by Fluorescence Spectroscopy in Healing Skin Wounds*. *Photochemistry and Photobiology*, 2006. **82**: p. 793-797.
197. Pasche, S., Angeloni, S., Ischer, R., Liley, M., Luprano, J. & Voirin, G., *Wearable Biosensors for Monitoring Wound Healing*. *Advances in Science and Technology*, 2008. **57**: p. 80-87.
198. Crespy, D. & Rossi, R.M., *Temperature-responsive Polymers with LCST in the Physiological Range and Their Applications in Textiles*. *Polymer International*, 2007. **56**: p. 1461-1468.
199. Hu, J., Zeng, F. & Li, P., *Methods of Manufacturing Deodorants, and Deodorants Resulting Thereof*, *US Patent Office, Pat. No 2005/0232880*. 2005.
200. Shi, F., Song, Y., Niu, J., Xia, X., Wang, Z. & Zhang, X., *Facile Method To Fabricate a Large-Scale Superhydrophobic Surface by Galvanic Cell Reaction*. *Chemistry of Materials*, 2006. **18**: p. 1365-1368.
201. Khan, F., Tare, R.S., Oreffo, R.O.C. & Bradley, M., *Versatile Biocompatible Polymer Hydrogels: Scaffolds for Cell Growth*. *Angewandte Chemie International Edition*, 2009. **48**: p. 978 - 982.
202. Ju, X., Chu, L., Liu, L., Mi, P. & Lee, Y.M., *A Novel Thermoresponsive Hydrogel with Ion-Recognition Property through Supramolecular Host-Guest Complexation*. *The Journal of Physical Chemistry*, 2009. **112**: p. 1112-1118.
203. Lin, C.-C. & Metters, A.T., *Hydrogels in Controlled Release Formulations: Network Design and Mathematical Modeling*. *Advanced Drug Delivery Reviews*, 2006. **58**: p. 1379-1408.
204. Coughlan, D., Quilty, F. & Corrigan, O., *Effect of Drug Physicochemical Properties on Swelling/deswelling Kinetics and Pulsatile Drug Release from Thermoresponsive Poly(N-isopropylacrylamide) Hydrogels*. *Journal of Controlled Release*, 2004. **98**: p. 97-114.
205. Ueoka, Y., Gong, J. & Osada, Y., *Chemomechanical Polymer Gel with Fish-like Motion*. *Journal of Intelligent Material Systems and Structures*, 1997. **8**: p. 465-471.
206. Helander, I.M., Latva-Kala, K. & Lounatmaa, K., *Permeabilizing action of polyethyleneimine on Salmonella typhimurium involves disruption of the outer membrane and interactions with lipopolysaccharide*. *Microbiology*, 1998. **144**: p. 385-390.

REFERENCES

207. Jen, A.C., Wake, M.C. & G.Mikos, A., *Review: Hydrogels for Cell Immobilization*. Biotechnology and Bioengineering, 1996. **50**: p. 357-364.
208. Lee, C.F., Wen, C.J., Lin, C.L. & Chiu, W.Y., *Morphology and Temperature Responsiveness-Swelling Relationship of Poly(N-isopropylamide-chitosan) Copolymers and Their Application to Drug Release*. Journal of Polymer Science Part A: Polymer Chemistry, 2004. **42**: p. 3029-3037.
209. Kiritoshi, Y. & Ishihara, K., *Synthesis of Hydrophilic Cross-Linker Having Phosphorylcholine-Like Linkage for Improvement of Hydrogel Properties*. Polymer, 2004. **45**: p. 7499-7504.
210. Hoffman, A.S., *Hydrogels for Biomedical Applications*. Advanced Drug Delivery Reviews, 2002. **54**: p. 3-12.
211. Anca, M.Y., Bayramoglu, G., Anca, B., Yalcum, E., Ito, K. & Yagci, Y., *Novel Hydrogel Membrane Based on Copoly(hydroxyethyl methacrylate/p-vinylbenzyl-poly(ethylene oxide)) for Biomedical Applications: Properties and Drug Release Characteristics*. Macromolecular Bioscience, 2005. **5**: p. 983-992.
212. Meng, Q.H., Hu, J.L. & Zhu, Y., *Shape-Memory Polyurethane/Multiwalled Carbon Nanotube Fibers*. Journal of Applied Polymer Science, 2007. **106**: p. 837-848.
213. Kelch, S., Steuer, S., Schmidt, A.M. & Lendlein, A., *Shape-Memory Polymer Networks from Oligo[ϵ -hydroxycaproate]-co-glycolate]dimethacrylates and Butyl Acrylate with Adjustable Hydrolytic Degradation Rate*. Biomacromolecules, 2007. **8**: p. 1018-1027.
214. Alteheld, A., Feng, Y., Kelch, S. & Lendlein, A., *Biodegradable, Amorphous Copolyester-Urethane Networks Having Shape Memory Properties*. Angewandte Chemie International Edition, 2005. **44**: p. 1188-1192.
215. Lendlein, A., Schmidt, A.M. & Langer, R. *AB-polymer Networks Based on Oligo(ϵ -caprolactone) Segments Showing Shape-memory Properties*. in *Proceedings of the National Academy of Sciences*. 2001. USA.
216. Ciardelli, G., Rechichi, A., Sartori, S., Acunto, M.D., Caporale, A., Peggion, E., Vozzi, G. & Giusti, P., *Bioactive Polyurethanes in Clinical Applications*. Polymer Advance Technology, 2006. **17**: p. 786-789.
217. Fourné, F., *Synthetic Fibers Machines and Equipment, Manufacture, Properties*. 1999, Munich: Hanser Publishers. 128-130.
218. Zhu, Y., Hu, J.L., Yeung, L.Y., Lu, J., Meng, Q.H., Chen, S.J. & Yeung, K.W., *Effect of Steaming on Shape Memory Polyurethane Fibers with Various Hard Segment Contents*. Smart Materials and Structures, 2007. **16**: p. 969-981.
219. Langer, R.S. & Andreas, L., *Shape Memory Polymers*. May 14, 2002: U.S. Patent. 6,388,043.
220. Zhu, Y., Hu, J.L., Yeung, K.W., Choi, K.F., Liu, Y.Q. & Liem, H.M., *Effect of Cationic Group Content on Shape Memory Effect in Segmented Polyurethane Cationomer*. Journal of Applied Polymer Science, 2007. **103**: p. 545-556.

REFERENCES

221. Ni, Q.Q., Zhang, C.S., Fu, Y.Q., Dai, G.Z. & Kimura, T., *Shape Memory Effect and Mechanical Properties of Carbon Nanotube/Shape Memory Polymer Nanocomposites*. Composite Structures, 2006.
222. Mondal, S. & Hu, J.L., *Structural Characterization and Mass Transfer Properties of Polyurethane Block Copolymer: Influence of Mixed Soft Segment Block and Crystal Melting Temperature*. Polymer International, 2006. **55**: p. 1013-1020.
223. Korley, L.T.J., Pate, B.D., Thomas, E.L. & Hammond, P.T., *Effect of the Degree of Soft and Hard Segment Ordering on the Morphology and Mechanical Behavior of Semicrystalline Segmented Polyurethanes*. Polymer, 2006. **47**: p. 3073-3082.
224. Melnig, V., Apostu, M.O., Turaa, V. & Ciobanu, C., *Optimization of Polyurethane Membranes Morphology and Structure Studies*. Journal of Membrane Science, 2005. **267**: p. 58-67.
225. Cherubini, *Polymeric Orthotic Devices*. 1995: US Patent 5,415,623.
226. Zhu, Y., Hu, J.L., Yeung, K.w., Fan, H.J. & Liu, Y.Q., *Shape Memory Effect of PU Ionomers with Ionic Groups on Hard-segments*. Chinese Journal of Polymer Science, 2006. **24**: p. 173-186.
227. Kim, B.K., Lee, S.Y. & Xu, M., *Polyurethanes having shape memory effects*. Polymer, 1996. **37**: p. 5781.
228. Li, F., Hou, J., Zhu, W., Zhang, X., Xu, M., Luo, X., Ma, D. & Kim, B.K., *Crystallinity and morphology of segmented polyurethanes with different soft-segment length*. J. Appl. Polym. Sci., 1996. **62**: p. 631.
229. Li, F., Zhang, X., Hou, J., Xu, M., Luo, X., Ma, D. & Kim, B.K., *Studies on thermally stimulated shape memory effect of segmented polyurethanes*. J. Appl. Polym. Sci., 1997. **64**: p. 1511.
230. Tobushi, H., Hara, H., Yamada, E. & Hayashi, S., *Thermomechanical properties in a thin film of shape memory polymer of polyurethane series*. Smart Mater. Struct., 1996. **5**: p. 483.
231. Lin, J.R. & Chen, L.W., *Study on shape-memory behavior of polyether-based polyurethane. I. Influence of the hard-segment content*. J. Appl. Polym. Sci., 1998. **69**: p. 1563.
232. Tao, X.M., *Smart Fibres, Fabrics and Clothing*. Vol. 3. 2001: Woodhead Publishing Limited. 34-36.
233. Mattila, H.R., *Intelligent Textiles and Clothing*, ed. H.R. Mattila. Vol. 3. 2006: Woodhead Publishing Limited. 98-99.
234. Son, C., Moreshouse, H.L. & Jeffrey, H., *An Experimental Investigation of Solid-state Phase-change Materials for Solar Thermal Storage*. Journal of Solar Energy Engineering, 1991. **113**: p. 244-249.
235. Langer, R., *New methods of drug delivery*. Science, 1990. **249**: p. 1527-1533.
236. Veronese, M., Monfardini, C., Caliceti, P., Schiavon, O., Scrawen, M.D. & Beer, D., *Improvement of pharmacokinetic, immunological and stability properties of asparaginase by conjugation to linear and branched monomethoxy poly(ethylene glycol)*. Journal of Controlled Release, 1996. **40**: p. 199-209.
237. Han, D. & Hubbell, J., *Synthesis of polymer network scaffolds from - lactide and poly(ethylene glycol) and their interaction with cells*. Macromolecules. **30**: p. 6077-6083.

REFERENCES

238. Dincer, I. & Rosen, M.A., *Thermal energy storage, Systems and Applications.*, John Wiley & Sons, Chichester (England), ISBN: 978-0-471-49573-4. 2002.
239. Bryant, Y.G. *Melt Spun Fibers Containing Microencapsulated Phase Change Material.* in *Advances in Heat and Mass Transfer in Biotechnology - (The ASME International Mechanical Engineering Congress and Exposition)*, Nashville, TN, USA. Nov 14-Nov 19 1999.
240. He, Q. & Zhang, W., *A Study on Latent Heat Storage Exchangers with the High-temperature Phase-change Material.* International Journal of Energy Research, 2001. **25**: p. 331-341.
241. Liang, X. & Guo, Y.Q., *Crystalline-amorphous Phase Transition of a Poly (ethylene glycol)/cellulose Blend.* Macromolecules, 1995. **28**: p. 6551-6555.
242. Ye, H. & Ge, X., *Preparation of Polyethylene-paraffin Compound as a Form-stable Solid-liquid Phase Change Material.* Solar Energy Materials & Solar Cells, 2000. **64**: p. 37-44.
243. Zalba, B., Marin, J.M., Cabeza, L.F. & Mehling, H., *Review on Thermal Energy Storage With Phase Change: Materials, Heat Transfer Analysis and Applications.* Applied Thermal Engineering, 2003: p. 251-283.
244. Wang, X.W., Lu, E.R., Lin, W.X. & Wang, C.Z., *Micromechanism of Heat Storage in a Binary System of Two Kinds of Polyalcohols As a Solid-solid Phase Change Material.* Energy Conversion and Management, 2000. **41**: p. 135-144.
245. US-Department-of-Energy, *A Consumer's Guide to Energy Efficiency and Renewable Energy*, http://www.eere.energy.gov/consumer/your_home/. Date accessed: Dec. 11st. 2009.
246. Pause, B., *Development of Heat and Cold Insulating Membrane Structures with Phase Change Material.* Journal of Coated Fabrics, 1995. **25**: p. 59-68.
247. Pause, B., *Development of Heat and Cold Insulating Membrane Structures with Phase Change Material.* Journal of Industrial Textiles, 1995. **25**: p. 59-68.
248. Colvin, D.P. *Protective Clothing Containing Encapsulated Phase Change Materials.* in *Proceedings of the 1998 ASME International Mechanical Engineering Congress and Exposition.* Nov 15-20 1998. Anaheim, CA, USA.
249. Colvin, D.P. *Enhanced Thermal Management Using Encapsulated Phase Change Materials an Overview.* in *Advances in Heat and Mass Transfer in Biotechnology - (The ASME International Mechanical Engineering Congress and Exposition)*. Nov 14-Nov 19 1999. Nashville, TN, USA.
250. Vigo, T.L. & Frost, C.M., *Temperature-adaptable Hollow Fibers Containing Polyethylene Glycols.* Journal of Coated Fabrics, 1983. **12**: p. 243-245.
251. Vigo, T.L. & Frost, C.M., *Temperature-adaptable fabrics.* Textile Research Journal, 1985. **55**: p. 737-743.

REFERENCES

252. Bruno, J.S. & Vigo, T.L., *Thermal Properties of Insolubilized Polyacetals Derived From Non-formaldehyde Crosslinking Agents*. *Thermochimica Acta*, 1994. **243**: p. 155-159.
253. Zhang, X.X., Wang, X.C. & Hu, L., *Spinning and Properties of PP/PEG Composite Fibers for Heat Storing and Thermoregulated*. *Journal of Tianjin Institute Textiles Science and Technology*, 1999. **18**: p. 1-3.
254. Zhang, X.X., Zhang, H. & Niu, J.J., *Thermoregulated Fiber and Its Products*. April 10, 2004: China Patent ZL 00105837.1.
255. Jiang, Y., Ding, E. & Li, G., *Study on Transition Characteristics of PEG/CDA Solid-solid Phase Change Materials*. *Polymer*, 2002. **43**: p. 117-122.
256. Li, W.D. & Ding, E.Y., *Preparation and Characterization of Cross-linking PEG/MDI/PE Copolymer as Solid-Solid Phase Change Heat Storage Material*. *Solar Energy Materials & Solar Cells*, 2007. **91**: p. 764-768.
257. HilmarKoerner, G.P., Nathan A. Pearce, Max Alexander and Richard A. Vaia, *Remotely Actuated Polymer Nanocomposites- stress-recovery of Carbon- nanotube- filed Thermalplastic Elastmers*. *Natural Material*, 2004. **3**: p. 115-120.
258. Zhang, H., Wang, H., Zhong, W. & Du, Q., *A Novel Type of Shape Memory Polymer Blend and the Shape Memory Mechanism*. *Polymer*, 2009. **50**: p. 1596-1601.
259. Zhang, S., Yu, Z., Govender, T., Luo, H. & Li, B., *A Novel Supramolecular Shape Memory Material Based on Partial α -CD-PEG Inclusion Complex*. *Polymer*, 2008. **49**: p. 3205-3210.
260. Buckley, C.P., Prisacariu, C. & Caraculacu, A., *Novel Triol-crosslinked Polyurethanes and Their Thermorheological Characterization as Shape-Memory Materials*. *Polymer*, 2007. **48**: p. 1388-1396.
261. Zhang, W., Chen, L. & Zhang, Y., *Surprising Shape-memory Effect of Polylactide Resulted from Toughening by Polyamide Elastomer*. *Polymer*, 2009. **50**: p. 1311-1315.
262. Huang, H.M., Liu, I.C., Y.U.Chang, C. & Tsai, H.C., *Preparing a Polystyrene-functionalized Multiple-walled Carbon Nanotubes via Covalently Linking Acyl Chloride Functionalities with Living Polystyryllithium*. *Journal of Polymer Science Part A: Polymer Chemistry*, 2004. **42**: p. 5802-5810.
263. Biercuk, M.J., Llaguno, M.C., Radosavljevic, M., Hyun, J.K., Johnson, A.T. & Fischer, J.E., *Carbon Nanotube Composites for Thermal Management*. *Applied Physics Letters*, 2002. **80**: p. 2767-2769.
264. Zhang, W.D., Shen, L., Phang, I.Y. & Liu, T., *Carbon Nanotubes Reinforced Nylon-6 Composite Prepared by Simple Melt-compounding*. *Macromolecules*, 2004. **37**: p. 256-259.
265. Jung, Y.C., Sahoo, N.G. & Cho, J.W., *Polymeric Nanocomposites of Polyurethane Block Copolymers and Functionalized Muti-Walled Carbon Nanotubes as Crosslinkers*. *Macromolecular Rapid Communications*, 2006. **27**: p. 126-131.
266. Rahul, S., Bin, Z., Daniel, P., Mikhail, I., Hui, H. & James, L., *Preparation of Single-walled Carbonnanotube Reinforced Polystyrene*

REFERENCES

- and Polyurethane Nanofibers and Membranes by Electrospinning*. Nano Letters, 2004. **4**: p. 459-464.
267. Cadek, M., Coleman, J., Ryan, K., Nicolosi, V., Bister, G. & Fonseca, A., *Reinforcement of Polymers with Carbon Nanotubes: The Role of Nanotube Surface Area*. Nano Letters, 2004. **4**: p. 353-356.
268. Ounaies, Z., C. Park, Wise, K.E., Siochi, E.J. & Harrison, J.S., *Electrical Properties of Single Wall Carbon Nanotube Reinforced Polyimide Composites*. Composites Science and Technology, 2003. **63**: p. 1637-1646.
269. Cadek M, C.J., Ryan KP, Nicolosi V, Bister G, Fonseca A, *Reinforcement of Polymers with Carbon Nanotubes: The Role of Nanotube Surface Area*. Nano Letters, 2004. **4**: p. 353–356.
270. Coopera Carole A, R.D., Lipsb David A, Mayerb Joerg, Wagnera HD, *Distribution and Alignment of Carbon Nanotubes and Nanofibrils in a Polymer Matrix*. Composites Science Technology, 2002. **62**: p. 1105–1112.
271. Lau Kin-Tak, H.D., *The Revolutionary Creation of New Advanced Material-carbon Nanotube Composite*. Composites Part B, 2002. **33**: p. 263–277.
272. Lau Kin-Tak, H.D., *Effectiveness of Using Carbon Nanotubes as Nano-reinforcements for Advanced Composite Structures*. Carbon, 2002. **40**: p. 1605-1606.
273. Gong Xiaoyi, L.J., Baskaran Suresh, Voise Roger D, Young James S., *Surfactant-assisted Processing of Carbon Nanotube/polymer Composites*. Chemistry of Materials, 2000. **12**: p. 1049–1052.
274. Sholz, *Water Soluble Films Used in Synthetic Casting Tapes*. 2000: US Patent 6,077,240.
275. Lourie O, W.H., *Evidence of stress transfer and formation of fracture clusters in carbon nanotube-based composites*. Composites Science and Technology, 1999. **59**: p. 975-977.
276. Zhang Wei De, S.L., Phang In Yee, Liu Tianxi, *Carbon Nanotubes Reinforced Nylon-6 Composite Prepared by Simple Melt-compounding*. Macromolecules, 2004. **37**: p. 256–259.
277. Haggemueller R, G.H., Rinzler AG, Fischer JE, Winey KI, *Aligned Single-wall Carbon Nanotubes Composites by Melt Processing Methods*. Chemical Physics Letters, 2000. **330**: p. 219-225.
278. Thostenson ET, R.Z., Chou Tsu-Wei, *Advances in the Science and Technology of Carbon Nanotubes and Their Composites: a Review*. Composites Science Technology, 2001. **61**: p. 899–912.
279. Gommans HH, A.J., Tashiro H, Park J, Magnuson J, Rinzler AG, *Fibers of Aligned Single-walled Carbon Nanotubes: Polarized Raman Pectroscopy*. Journal of Applied Physics, 2000. **88**: p. 2509-2514.
280. Andrews, R. & Weisenberger, M.C., *Carbon nanotube polymer composites*. Current Opinion in Solid State and Materials Science, 2004. **8**: p. 31-37.
281. Demczyk, B.G., Wang, Y.M., Cumings, J., Hetman, M., Han, W., Zettl, A. & Ritchie, R.O., *Direct Mechanical Measurement of the Tensile Strength and Elastic Modulus of Multiwalled Carbon Nanotubes*. Materials Science and Engineering A, 2002. **334**: p. 173-178.

REFERENCES

282. Jia, Z.J., Wang, Z.Y., Xu, C.I., Liang, J., Wei, B.Q., Wu, D.H. & Zhu, S., *Study on poly(methyl methacrylate)/carbon nanotube composites*. Materials Science & Engineering, A: Structural Materials: Properties, Microstructure and Processing, 1999. **271**: p. 395-400.
283. Haggemueller, R., Gommans, H.H., A. G, R., Fischer, J.E. & Winey, K.I., *Aligned Single-wall Carbon Nanotubes Composites by Melt Processing Methods*. Chemical Physics Letters, 2000. **330**: p. 219-225.
284. Gommans, H.H., Alldredge, J.W., Tashiro, H., Park, J., Magnuson, J. & Rinzler, A.G., *Fibers of Aligned Single-walled Carbon Nanotubes: Polarized Raman Pectroscopy*. Journal of Applied Physics, 2000. **88**: p. 2509-2514.
285. Thostenson, E.T. & Chou, T.W., *Aligned multi-walled Carbon Nanotube-reinforced Composites: Processing and Mechanical Characterization*. Journal of Physics D: Applied Physics, 2002. **35**: p. L77-L80.
286. Hou, H.Q., Ge, J.J., Zeng, J., Li, Q., Reneker, D.H., Greiner, A. & Cheng, S.Z.D., *Electrospun Polyacrylonitrile Nanofibers Containing a High Concentration of Well-Aligned Multiwall Carbon Nanotubes*. Chemistry of Materials, 2005. **17**: p. 967-973.
287. Kwon, J. & Kim, H., *Comparison of the Properties of Waterborne Polyurethane/Multiwalled Carbon Nanotube and Acid-Treated Multiwalled Carbon Nanotube Composites Prepared by In Situ Polymerization*. Journal of Polymer Science Part A: Polymer Chemistry, 2005. **43**: p. 973-3985.
288. Chen, W. & Tao, X.M., *Self-Organizing Alignment of Carbon Nanotubes in Thermoplastic Polyurethane*. Macromolecular Rapid Communications, 2005. **26**: p. 1763-1767.
289. Storey, R.F. & Hickey, T.P., *Degradable Polyurethane Networks Based on D, L - lactide, Glycolide, ϵ -caprolactone, and Trimethylene Carbonate Homopolyester and Copolyester Triols*. Polymer, 1994. **35**: p. 830-838.
290. Gorna, K. & Gogolewski, S., *Biodegradable Polyurethanes for Implants. II. In Vitro Degradation and Calcification of Materials from Poly(ϵ -caprolactone)-Poly(ethylene oxide) Diols and Various Chain Extenders*. Journal of Biomedical Materials Research, 2002. **60**: p. 592-606.
291. Zhang, Z.R., *Shape Memory Bone Fixing Splint*. 2004: China Patent CN20020150720.
292. Luo, N., Wang, D.N. & Ying, S.K., *Crystallinity of Hard and Hydrogen Bonding Segments in Segmented Poly(urethane urea) Copolymers*. Polymer, 1996. **37**: p. 3577-3583.
293. Zhu, Y., Hu, J., Lap-Yan Yeung, Lu, J., Meng, Q., Chen, S. & Yeung, K.-W., *Effect of Steaming on Shape Memory Polyurethane Fibers with Various Hard Segment Contents*. Smart Materials and Structures, 2007. **16**: p. 969-981.
294. Seymour, R.W., Jr., A.E.A. & Cooper, S.L., *Segmental Orientation Studies of Block Polymers. I. Hydrogen-Bonded Polyurethanes*. Macromolecules, 1973. **6**: p. 896-902.

REFERENCES

295. Luo, N., Wang, D.N. & Ying, S.K., *Hydrogen-Bonding Properties of Segmented Polyether Poly(urethane urea) Copolymer*. *Macromolecules*, 1997. **30**: p. 4405-4409.
296. Zhang, X., Li, Y., Yeung, K.W. & Yao, M., *Fabric Bagging Part I: Subjective Perception and Psychophysical Mechanism*. *Textile Research Journal*, 1999. **69**: p. 511-518.
297. Nair, B.R., Gregoriou, V.G. & Hammond, P.T., *FT-IR Studies of Side Chain Liquid Crystalline Thermoplastic Elastomers*. *Polymer*, 2000. **41**: p. 2961-2970.
298. Lee, H.S., Ko, J.H., Song, K.S. & Choi, K.H., *Segmental and Chain Orientational Behavior of Spandex Fibers*. *Journal of Polymer Science Part B: Polymer Physics*, 1997. **35**: p. 1821 - 1832.
299. Estes, G.M., Seymour, R.W. & Cooper, S.L., *Infrared Studies of Segmented Polyurethane Elastomers. II. Infrared Dichroism*. *Macromolecules*, 1971. **4**: p. 452-457.
300. Dai, X.H., Xu, J., Guo, X.L., Lu, Y.L., Shen, D.Y., Ning Zhao, Luo, X.D. & Zhang, X.L., *Study on Structure and Orientation Action of Polyurethane Nanocomposites*. *Macromolecules*, 2004. **37**: p. 5615-5623.
301. Schoonover, J.R., Thompson, D.G., Osborn, J.C., Orlor, E.B., Wroblewski, D.A., Marsh, A.L., Wang, H. & Palmer, R.A., *Infrared linear Dichroism Study of a Hydrolytically Degraded Poly(ester urethane)*. *Polymer Degradation and Stability*, 2001. **74**: p. 87-96.
302. Siesler, H.W. & Holland-Moritz, K., *Infrared and Raman Spectroscopy of Polymers*, Marcel Dekker Inc., New York. 1980.
303. Graff, D.K., Wang, H., Palmer, R.A. & Schoonover, J.R., *Static and Dynamic FT-IR Linear Dichroism Studies of Plasticization Effects in a Polyurethane Elastomer*. *Macromolecules*, 1999. **32**: p. 7147-7155.
304. Rabek, J.F., *Experimental Methods in Polymer Chemistry*, John Wiley & Sons, Wiley, New York. 1980.
305. Griffiths, P.R. & Haseth, J.A.d., *Fourier Transform Infrared Spectroscopy*, Wiley, New York. 1986.
306. Wang, C.B. & Cooper, S.L., *Morphology and Properties of Segmented Polyether Polyurethaneureas*. *Macromolecules*, 1983. **16**: p. 775-786.
307. Fourne, R., *Compact Melt Spinning Process for the Flexible Production of Elastic Yarns*. *Chemical Fibers International*, 1999. **49**: p. 124-125.
308. Li, F.K., Zhang, X., Hou, J.A., Xu, M., Luo, X.L., Ma, D.Z. & Kim, B.K., *Studies on Thermally Stimulated Shape Memory Effect of Segmented Polyurethanes*. *Journal of Applied Polymer Science*, 1996. **64**: p. 1511-1516.
309. Krol, P., *Linear polyurethanes: synthesis methods, chemical structures, properties and applications*. 2008, Leiden; Boston: VSP.
310. Yao, M., Zhou, J., Huang, S., Shao, L., An, R. & Fan, D., *Textile Materials 2nd ed*. 1990: Peking: Textile Industry Publishing House.
311. Yoshihaya, N., Ishihara, H. & Yamada, T., *Relationship Between Segment Structures and Elastic Properties of Segmented Poly(Urethane-urea) Elastic Fibers*. *Polymer Engineering and Science*, 2003. **43**: p. 1740-1746.

REFERENCES

312. Ping, P., Wang, W., Chen, X. & Jing, X., *Poly(E-caprolactone) Polyurethane and Its Shape-Memory Property*. *Biomacromolecules*, 2005. **6**: p. 587-592.
313. Crescenzi, V., Manzini, G., Calzolari, G. & Borri, C., *Thermodynamics of Fusion of Poly- β -propiolactone and Poly- ϵ -caprolactone. Comparative Analysis of the Melting of Aliphatic Polylactone and Polyester Chains*. *European Polymer Journal*, 1972. **8**: p. 449-463.
314. Luo, N., Wang, D. & Ying, S., *Crystallinity of Hard and Hydrogen Bonding Segments in Segmented Poly(urethane urea) Copolymers*. *Polymer*, 1996. **37**: p. 3577-3583.
315. Jr., C.G.S., Koleske, J.V. & Critchfield, F.E., *Thermoplastic urethane elastomers. II. Effects of variations in hard-segment concentration (p)*. *Journal of Applied Polymer Science*, 1975. **19**: p. 2503-2513.
316. Jr., C.G.S., Koleske, J.V. & Critchfield, F.E., *Thermoplastic urethane elastomers. I. Effects of soft-segment variations*. *Journal of Applied Polymer Science*, 1975. **19**: p. 2493-2502.
317. Briber, R.M. & Thomas, E.L., *The Investigation of Two Crystal Forms in MDI/BDO Based. Polyurethanes*. *Journal of Macromolecular Science-Physics*, 1983. **22**: p. 509-526.
318. Chen, S.A. & Chan, W.C., *Polyurethane Cationomers. I. Structure-property Relationships*. *Journal of Polymer Science Part B: Polymer Physics*, 2003. **28**: p. 1499-1514.
319. LaShanda T. Jams Korley, B.D.P., edwin L. THomas, Paula T. Hammond, *Effect of the Degree of Soft and Hard Segment Ordering on the Morphology and Mechanical Behavior of Semicrystalline Segmented Polyurethanes*. *Polymer*, 2006. **47**: p. 3073-3082.
320. Young, R.J. & Lovell, P.A., *Introduction to Polymers(2nd edn)*. 1991, Chapman & Hall, London.
321. Patterson, A.L., *The Scherrer Formula for X-Ray Particle Size Determination*. *Physical Review*, 1939. **56**: p. 978-982.
322. Mo Z S, L.K., Moon YB, Kobayashi M, Heeger A J, Wudl F., *X-ray Scattering from Polythiophene: Crystallinity and Crystallographic Structure*. *macromolecules*, 1985. **18**: p. 1972~1977.
323. Marchessault, H.B.a.R.H., *Crystal structure of. Poly- ϵ -caprolactone*. *Acta Crystallogr: B*, 1970. **26**: p. 1923-1927.
324. Coleman, M.M., Skrovanek, D.J., Hu, J.B. & Painter, P.C., *Hydrogen Bonding in Polymer Blends. 1. FTIR Studies of Urethane-ether Blends*. *Macromolecules*, 1988. **21**: p. 59-65.
325. Frisch, K.C. & Reegen, S.L., *Hydrogen Bonding in Urethanes*. *Advances in Urethane Science and Technology*, 1978. **6**: p. 1-28.
326. Senich, G.A. & MacKnight, W.J., *Fourier Transform Infrared Thermal Analysis of a Segmentd Polyurethane*. *Macromolecules*, 1980. **13**: p. 106-110.
327. Xiao, F.F., Shen, D.Y., Zhang, X., Hu, S.R. & Xu, M., *Studies on the Morphology of Blends of Poly(vinyl chloride) and Segmented Polyurethane*. *Polymer*, 1987. **28**: p. 2335-2345.
328. Sung, C.S.P. & Schneider, N.S., *Temperature Dependence of Hydrogen Bonding in Toluene Diisocyanate Based Polyurethanes*. *Macromolecules*, 1977. **10**: p. 452-458.

REFERENCES

329. Coleman, M.M., Lee, K.H., Skrovanek, D.J. & Painter, P.C., *Hydrogen Bonding in Polymers. 4. Infrared Temperature Studies of a Simple Polyurethane*. *Macromolecules*, 1986. **19**: p. 2149-2157.
330. Harthcock, M.A., *Probing the Complex Hydrogen Bonding Structure of Urethane Block Copolymers and Various Acid Containing Copolymers Using Spectroscopy*. *Polymer*, 1989. **30**: p. 1234-1242.
331. Zhu, Y., Hu, J.L., Yeung, K.w., Fan, H.J. & Liu, Y.Q., *Shape Memory Effect of PU Ionomers with Ionic Groups on Hard-segments*. *Chinese Journal of Polymer Science*, 2006. **24**: p. 173-186.
332. Mark, H.F., Atlas, S.M. & Cernia, E., *Man-Made Fibers Science and Technology VOLUME 3*. 1968: John Wiley & Sons, Inc.
333. Bhat, G., Chand, S. & Yakopson, S., *Thermal Properties of Elastic Fibers*. *Thermochimica Acta*, 2001. **367-368**: p. 161-164.
334. Fabricius, M., Gries, T. & Wulforth, B., *Elastane Fibers (Spandex)*. *Chemical Fibers International*, 1995. **45**: p. 1995.
335. Vigo, T.L. & Bruno, J.S., *Improvement of Various Properties of Fiber Surfaces Containing Crosslinked Polyethylene Glycols*. *Journal of Applied Polymer Science*, 1989. **37**: p. 371-379.
336. Hu, J., Yu, H., Chen, Y.M. & Zhu, M., *Study on Phase-Change Characteristics of PET-PEG Copolymers*. *Journal of Macromolecular Science, Part B: Physics*, 2006. **45**: p. 615-621.
337. Aneja, A. & Wilkes, G.L., *On the Issue of Urea Phase Connectivity in Formulations Based on Molded Flexible Polyurethane Foams*. *Journal of Applied Polymer Science*, 2002. **85**: p. 2956 - 2967.
338. Garrett, J.T., Siedlecki, C.A. & Runt, J., *Microdomain Morphology of Poly(urethane urea) Multiblock Copolymers*. *Macromolecules*, 2001. **34**: p. 7066-7070.
339. McLean, R.S. & Sauer, B.B., *Tapping-Mode AFM Studies Using Phase Detection for Resolution of Nanophases in Segmented Polyurethanes and Other Block Copolymers*. *Macromolecules*, 1997. **30**: p. 8314-8317.
340. Aneja, A. & Wilkes, G.L., *Hard segment connectivity in low molecular weight model 'trisegment' polyurethanes based on monols*. *Polymer* 45, 2004. **45**: p. 927-935.
341. Aneja, A. & Wilkes, G.L., *On the Issue of Urea Phase Connectivity in Formulations Based on Molded Flexible Polyurethane Foams*. *Journal of Applied Polymer Science*, 2002. **85**: p. 2956-2967.
342. Kaushiva, B.D., McCartney, S.R., Rossmly, G.R. & Wilkes, G.L., *Surfactant Level Influences on Structure and Properties of Flexible Slabstock Polyurethane Foams*. *Polymer*, 2000. **41**: p. 285-310.
343. Aneja, A. & Wilkes, G.L., *A Systematic Series of 'model' PTMO Based Segmented Polyurethanes Reinvestigated using Atomic Force Microscopy*. *Polymer*, 2003. **44**: p. 7221-7228.
344. Fuchs, A., Zhang, Q., Elkins, J., Gordaninejad, F. & Evrensel, C., *Development and Characterization of Magnetorheological Elastomers*. *Journal of Applied Polymer Science*, 2007. **105**: p. 2497-2508.
345. Sauer, B.B., McLean, R.S. & Thomas, R.R., *Nanometer Resolution of Crystalline Morphology Using Scanning Probe Microscopy*. *Polymer International*, 2000. **49**: p. 449-452.

REFERENCES

346. Taylor, J.E., Laity, P.R., Wong, S.S., Norris, K., Khunkamchoo, P., Cable, M., Andrews, G., Johnson, A.F. & Cameron, R.E., *Examination of Hard Segment and Soft Segment Phase Separation in Polyurethane Medical Materials by Electron Microscopy Techniques*. *Microscopy and Microanalysis*, 2006. **12**: p. 1-5.
347. Li, C. & Cooper, S.L., *Direct Observation of the Micromorphology of Polyether Polyurethanes Using High Voltage Electron Microscopy*. *Polymer*, 1990. **31**: p. 3-7.
348. Cooper, C.A., Ravich, D., Lips, D., Mayer, J. & Wagner, H.D., *Distribution and Alignment of Carbon nanotubes and Nanofibrils in a Polymer Matrix*. *Composites Science and Technology*, 2002. **62**: p. 1105-1112.
349. Miaudet, P., Badaire, S., Maugey, M., Derré, A., Pichot, V., Launois, P., Poulin, P. & Zakri, C., *Hot-Drawing of Single and Multiwall Carbon Nanotube Fibers for High Toughness and Alignment*. *Nano Letters*, 2005. **5**: p. 2212-2215.
350. Hwang, J., Gommans, H.H., Ugawa, A., Tashiro, H., Haggemueller, R., Winey, K.I., Fischer, J.E., Tanner, D.B. & Rinzler, A.G., *Polarized Spectroscopy of Aligned Single-wall Carbon Nanotubes*. *Physical Review B*, 2000. **62**: p. 310-313.
351. Zamora-Ledezma, C., Blanc, C. & Anglaret, E., *Orientalional Order of Single-wall Carbon Nanotubes in Stretch-aligned Photoluminescent Composite Films*. *Physical Review B (Condensed Matter and Materials Physics)*, 2009. **80**: p. 113407.
352. Borca-Tasciuc, T., Mazumder, M., Son, Y., Pal, S.K., Schadler, L.S. & Ajayan, P.M., *Anisotropic Thermal Diffusivity Characterization of Aligned Carbon Nanotube-polymer Composites*. *Journal of Nanoscience and Nanotechnology*, 2007. **7**: p. 1581-158.
353. Wu, J. & Schultz, J.M., *In-Situ Simultaneous Synchrotron Small- and Wide-Angle X-ray Scattering Measurement of Poly(vinylidene fluoride) Fibers under Deformation*. *Macromolecules*, 2000. **33**: p. 4765-1777.
354. Kolb, R., Seifert, S., Stribeck, N. & Zachmann, H.G., *Simultaneous Measurements of Small- and Wide-angle X-ray Scattering During Low Speed Spinning of Poly(propylene) Using Synchrotron Radiation*. *Polymer*, 2000. **41**: p. 1497-1505.
355. Chu, B., Cunniff, P.M. & Phillips, R.A., *Studies of the Mesophase Development in Polymeric Fibers During Deformation by Synchrotron SAXS/WAXD*. *Journal of Materials Science*, 2001. **36**: p. 3071-3077.
356. Laity, P.R., Taylor, J.E., Wong, S.S., Khunkamchoo, P., Norris, K., Cable, M., Andrews, G.T., Johnson, A.F. & Cameron, R.E., *A review of Small-angle Scattering Models for Random Segmented Poly(ether-urethane) Copolymers*. *Polymer*, 2004. **45**: p. 7273-7291.
357. Siesler, H.W., *Rheo-optical Fourier Transform IR Spectroscopy of Polyurethane Elastomers - 1. Principle of the Method and Measurements at Ambient Temperature*. *Polymer Bulletin*, 1983. **9**: p. 382-389.
358. Chen, S., Hu, J. & Zhuo, H., *Properties and mechanism of two-way shape memory polyurethane composites*. *Composites Science and Technology*, 2010. **70**: p. 1437-1443.

REFERENCES

359. Chen, S., Hu, J., Zhuo, H. & Zhu, Y., *Two-way Shape Memory Effect in Polymer Laminates*. Materials Letters, 2008. **62**: p. 4088-4090.
360. Chen, S., Hu, J., Yuen, C. & Chan, L., *Novel Moisture-sensitive Shape Memory Polyurethanes Containing Pyridine Moieties*. Polymer, 2009. **50**: p. 4424-4428.
361. Huang, W.M. & Yang, B., *Water-driven Programmable Polyurethane Shape Memory Polymer: Demonstration and Mechanism*. Applied Physics Letters, 2005. **86**: p. 114105.
362. Meng, Q. & Hu, J.L., *A Brief Review of Stimulus-active Polymers Responsive to Thermal, Light, Magnetic, Electric, and Water/solvent Stimuli*. Journal of Intelligent Material Systems and Structures, in press, 2010.
363. Leng, J., Lan, X., Liu, Y. & Du, S., *Electroactive Thermoset Shape Memory Polymer Nanocomposite Filled with Nanocarbon Powders*. Smart Materials and Structures, 2009. **18**: p. 074003.
364. Lendlein, A., Jiang, H., Junger, O. & Langer, R., *Light-induced Shape-memory Polymers*. Nature, 2005. **434**: p. 879-882.
365. Nike, *Featured technology, Nike Sphere React Cool*, http://store.nike.com/?country=US&lang_locale=en_US&l=shop,pdp,ctr-inline/cid-100701/pid-240998#l=shop,pdp,ctr-inline/cid-100701/pid-240998. Date accessed: Nov. 17th. 2009.